Universidade do Minho
Escola de Engenharia

André Manuel de Oliveira Mota

Continuous fermentation of alcohol-free beer - bioreactor hydrodynamics and yeast physiology

June of 2012

Continuous fermentation of alcohol-free beer - bioreactor hydrodynamics and yeast physiology
André Manuel de Oliveira Mota
UMinho | 2012

Universidade do Minho
Escola de Engenharia

André Manuel de Oliveira Mota

Continuous fermentation of alcohol-free beer - bioreactor hydrodynamics and yeast physiology

Doctoral Dissertation for PhD degree in Biological and Chemical Engineering

Supervisor of the thesis:
Professor Doutor José António Couto Teixeira

June of 2012

“If I have seen further it is by standing on ye sholders of Giants”

Isaac Newton

à avó Mota

à Nuria

The accomplishment of this thesis was financially supported by a PhD scholarship from Fundação para a Ciência e Tecnologia (Ref.: SFRH/BD/37082/2007), inserted in the Programa Potencial Humano Quadro de Referência Estratégico Nacional (POPH – QREN) - Tipologia 4.1 - Formação Avançada. The POPH-QREN is co-financed by Fundo Social Europeu (FSE) and by Ministério da Ciência, Tecnologia e Ensino Superior (MCTES).

Abstract

In this study, the continuous production with immobilized cells of beer without alcohol was investigated. Apart from the evaluation of the various parameters affecting the quality of the continuous production of alcohol-free beer, a detailed study on the hydrodynamics of three-phase bioreactors was also done.

One of the major costs associated with continuous fermentations is the carrier cost where the yeast is immobilized. Two carriers that are byproducts of the brewing industry and agriculture (corn cobs and spent grains) were considered and applied in two different types of bioreactors: gas-lift and fixed-bed, using small and large particles, respectively.

The presence of solid particles in three-phase systems can influence the course of the fermentation, as the hydrodynamics of the system may be modified. Thus, in this work the influence of spent grains in regime transition on a bubble column was studied. In the presence of spent grains, the limits where the homogeneous regime prevails are smaller than without solids. The effect is similar to liquids with low viscosity. Different configurations of gas-lift bioreactors were also evaluated and the configuration with better global hydrodynamic properties for the continuous fermentation of alcohol-free beer was selected. Having this done, the local hydrodynamic properties of the three-phase system were characterized using advanced techniques such as optical fibers, traditionally applied in two-phase systems. Local studies indicated that the hydrodynamic characteristics are more affected by the fermentation metabolites (*e.g.* ethanol) than the solids.

The gas-lift reactor configuration was demonstrated to be the one that allowed for the obtention of a better quality beer. For this system were also tested the influence of the composition of the gas-phase in the formation of aroma and flavour compounds, as well as the influence of a long-term fermentation on the physiology of immobilized yeast. The results indicated that the use of nitrogen in the gas phase exhibits an

interesting potential in terms of mixing and maintenance of anaerobic conditions essential in a continuous fermentation. Finally strategies for maintaining and monitoring the physiology of the immobilized yeast have been suggested. Among these are the regular addition of fresh carrier (spent grains) and control of the number bud scars resulting from the yeast cell division.

In the continuous production of alcohol-free beer, several knowledge areas are involved and its interaction is of fundamental importance. It starts with the selection of the best carrier and yeast strain. Then, the bioreactor design based on the interaction between its hydrodynamic properties and the fermentation performance. In this work the complex relation between these different fields allowed the acquisition of new knowledge that will be useful in the future.

Keywords: alcohol-free beer, continuous fermentation, bioreactors, hydrodynamics, spent grains, immobilization.

Resumo

Neste trabalho, foi estudada a produção de cerveja sem álcool em contínuo, utilizando leveduras imobilizadas. O trabalho englobou diferentes áreas, como: o estudo da hidrodinâmica de bioreactores trifásicos, e o estudo de diversos parâmetros que afectam a qualidade da fermentação contínua de cerveja sem álcool.

Um dos principais custos associados à fermentação continua é o custo dos suportes onde se imobilizam as leveduras. Assim foram estudados dois suportes que são subprodutos da industria agrícola e cervejeira (espigas de milho e "spent grains"). De acordo com os resultados obtidos, os suportes, de diferentes dimensões, foram aplicados a dois tipos de bioreactores - "gás-lift" (partÍculas menores) e leito fixo (partículas maiores).

A presença de partículas sólidas em sistemas trifásicos pode influenciar o decurso de uma fermentação. Assim neste trabalho foi estudada a influência dos "spent grains" na transição de regime em coluna de bolhas. O estudo teve como objectivo simular uma parte do reactor gas-lift (tubo ascendente) e entender os mecanismos físicos que ai ocorrem. Na presença dos "spent grains" os caudais aos quais o regime homogéneo prevalece são menores, efeito similar a líquidos com baixa viscosidade. Seguidamente a influência dos "spent grains" foi estudada para diferentes configurações de bioreactores gas-lift. No fim foi seleccionada a configuração que apresentava propriedades hidrodinâmicas globais que melhor se adaptam as características de uma fermentação continua de cerveja sem álcool. Feita a selecção do bioreactor estudou-se as propriedades hidrodinâmicas locais do sistema trifásico. Para tal recorreu-se a técnicas mais refinadas (fibras ópticas), normalmente utilizadas em sistemas bifásicos. Assim foi necessário desenvolver um método para a utilização destas técnicas em sistemas trifásicos que pode ser também aplicada a sistemas com elevada densidade celular. Os estudos locais indicaram que as características hidrodinâmicas são mais afectadas pelos subprodutos da fermentação do que pelos sólidos.

Foram também realizadas experiências que permitiram estudar a influência de diversos parâmetros (tipo de bioreactor, estirpe de levedura, suporte) na fermentação continua. Entre os parâmetros estudados o produto final que apresentava melhor qualidade foi obtido utilizando um bioreactor gás-lift com leveduras imobilizadas em "spent grains". Neste sistema foram ainda testados a influência do tipo da fase gasosa na formação de compostos do aroma e sabor, assim como a influência de uma fermentação continua de longa duração na fisiologia das leveduras imobilizadas. Os resultados indicaram que o azoto apresenta um potencial interessante na manutenção das condições de mistura e de anaerobiose essenciais numa fermentação contínua. Finalmente estratégias para a manutenção e controlo da fisiologia das leveduras imobilizadas foram sugeridas. Entre elas encontram-se: a adição regular de suporte fresco ("spent grains") e o controlo das cicatrizes das leveduras resultantes da sua divisão celular.

Na produção continua de cerveja sem álcool interagem diversas areas do conhecimento. Este estudo inicia-se pela seleção do melhor suporte e estirpe de levedura. Posteriormente passa-se ao desenvolvimento de um bioreactor que é baseado na interação entre as suas propriedades hidrodinâmicas e a qualidade da fermentação. Ao longo deste trabalho a complexa relação entre diferentes áreas do conhecimento permitiu a aquisição de novos conhecimentos que poderão ser úteis no futuro.

Palavras-chave: cerveja sem álcool, fermentação contínua, bioreactores, hidrodinâmica, spent grains, imobilização

Ackowledgments

My first ackowledgment are to my two supervisors professors José António Teixeira and António Augusto Vicente, who believed in my scientific abilities and whom invited me to this project. I also thank to Fundação para a Ciência e Tecnologia that financially supported this study during 48 months through a PhD scholarship (SFRH/BD/37082/2007). I also have to ackowledge all my foreing supervisors: Tomas Brániyk (Institute of Chemical Technology in Prague, Czech Republic), Philippe Sechet and Alain Cartellier (Laboratoire des Ecoulements Géophysiques et Industriels de l'Université de Grenoble in Grenoble, France); for their unique scientific support that was essencial to me.

My second akowledgements are to all my laboratory colegues (from Portugal, to Czech Republic and France), who had, during my PhD studying years, supported me. Also for solving a lot of my technical probems during the last years I sincerely thank to the wonderful engineering-technicians (Rudolf Young, Manuel Santos, Madalena Vieira, Jean-Marc) in all three institutions I have worked.

I also have to ackowledge my friends for their friendship and support. And the last but not the least, I thank to my dearest family (grandparents, oncles, aunts and cousins). Especially to my parents (Teresa and Paulo), my sister and my grandmother (Nilza Mota), who taught me to love science.

To you all, this thesis is in part, from you. Thank you all.

List of Publications

Conference proceeddings

Immobilization of Yeast Cells on Corn Cob Particles: A Preliminary Study. **André Mota**, Daniel P. Silva, Tomáš Brányik, António A. Vicente, José A. Teixeira. VII Brazilian Meeting on Chemistry of Food and Beverages. São Paulo, 6th December **2008**

Influence of Different Pre-Treatment Methods on The Immobilization Of Brewer's Yeast on Corn Cob Particles. **Mota, A.,** Teixeira, J., SIPAL – VII International Symposium on the production of Alcohol and Yeasts, México, 25th June **2009**

Measurement of local gas-phase properties using an optical probe in a three-phase systems. **Mota, A.**, Vicente, A. A., Teixeira, J. A., Sechet, P., Cartellier, A. Poster in conference GLS10, Braga, June (2011)

Articles in Journals

Formation of flavour active compounds during continuous alcohol-free beer production: The influence of yeast strain, reactor configuration and carrier type. **Mota A.**, Novak P., Macieira F., Vicente A., Teixeira J., Smogrovicová D., Brányik T. Journal of the American Society of Brewing Chemists, 69(1), 1-7, **2011**.

Effect of spent grains on flow regime transition in bubble column. **A. Mota**., António A. Vicente., José A. Teixeira. Chemical Engineering Science, 66, 3350-3357, **2011.**

CFD simulation and experimental measurement of gas holdup and liquid interstitial velocity in internal loop airlift reactor. Simcik, M., **Mota, A**., Ruzicka, M. C., Vicente, A. A., Teixeira, J. A. Chemical Engineering Science. 66: pp. 3268-3279, **2011**.

Hydrodynamic Properties of a Three-Phase Internal Gas-Lift Reactor with an Enlarged Degasing Zone Using Spent Grains as solid-phase. **Mota, A**., Simcik, M., Ruzicka, M. C.,Vicente, A. A., Teixeira, J. A.. (Work accepted for oral presentation in GLS11 Seul 2013. It is going to be submitted in a special issue of Chemical Engineering Science).

Table of Contents

List of Figures

List of Tables

Nomenclature

Symbol	Description	Unit
a	Coefficient of Darwinian drift	-
A	Cross section area	m^2
a	Acceleration (vector)	m/s^2
A_{lb}	Lateral area of reactor bottoms	m^2
A_{600}	Absorvance at 600 nm	-
C_D	Drag coefficient	-
ch	Chord length	mm
C	Phase-distribution parameter	-
d_{12}	Distance between two points	mm
D	Distance/diameter	m
d_{eq}	Equivalent diameter	m
D	Axial dispersion coefficient	m^2/s
d	Bubble (equivalent) diameter	m
ΔP_T	Total Friction loss	Pa
ΔPf	Friction loss	Pa
e	Phase hold-up	-
Eo	Eotwos number	-
f	Drag function	-
g	Acceleration due to gravity	m/s^2
G	Turbulent kinetic energy production	$J/(m^3s)$
H	Distance/height	m or mm
H_1	Column height (Water Column nr 1)	mm
H_2	Column height (Water Column nr 2)	mm
h_D	Dispersion height	m
j	Drift flux	$m^3/(m^2\ s)$
K	Momentum transfer coefficient	$kg/(m^3s^1)$
Kf	Friction loss coefficient	-
k	Turbulent kinetic energy	m^2/s^2
L	Characteristic length	m
M	Force one phase is acting on other phase	N/m^3
N	Number of tanks	-

Nomenclature

Symbol	Description	Unit
OTR_{TOTAL}	Total Oxygen Transfer Rate	mg/(L.h)
OTR_{OS}	Supply Oxygen Transfer Rate	mg/(L.h)
OTR_{DO}	Dissolved Oxygen Transfer Rate	mg/(L.h)
p	Pressure	Pa
P_L	Pressure difference	Pa
Pe	Peclet number	-
Q_G	Gas Flow rate	L/min
Q_L	Liquid flow rate	L/h
Re	Reynolds number	-
t	Time	min or s
T_G	Gas residence time in optical probe	μs
T_M	Gas mounting time in optical probe	μs
t_m	Mixing time	s
u	Mean bubble rise speed	m/s
u_0	Terminal bubble speed	m/s
U	Superficial velocity	m/s
u	Instantaneous velocity (vector)	m/s
U_{bt}	Bubble terminal velocity	m/s
V	Volume	L
V_{slp}	Volume of sample	L
v	Linear velocity	m/s
v'	Velocity – fluctuating part	m/s
v_{dr}	Drift velocity	m/s
V	Interstitial velocity	m/s
V_R	Reactor working volume	L
V_D	Dead zones volume	L
X_{TGV}	Values from TGV method	-
X_{INJ}	Values from new injection method	-

Greek symbols

Symbol	Description	Unit
ε/α	Phase volume fraction(Hold-up)	-
ρ	Fluid density	kg/m^3
δ	Solid load	% (vol./vol.)
μ	Molecular dynamic viscosity	mPa·s
θ	Adimensional time	-
τ	Mean residence time	min
θ_D	Adimensional time with dead volumes	-
τ_D	Mean residence time with dead volumes	min
μ_t	Turbulent dynamic viscosity	Pa·s
ν_t	Turbulent kinematic viscosity	m^2/s
σ	Surface tension	N/m
τ	Particle relaxation time	s

Sub/superscript

DC	Dry Carrier
G	Gas-phase
L	Liquid-phase
S	Solid-phase
H	Pseudohomogeneous-phase
theo	Theorical
exp	Experimental
c	Critical
C	Columns
bb	Bottom
r	Riser
d	Downcomer/Disperse phase
c	Continuous phase
D	Drag (force)
i,k	Index of a phase
m	Mixture property
TD	Turbulent dispersion (force)
B	Bubble

Abbreviations

AFB	Alcohol-free beer
AATases	Acyltransferases
AL	Aldehydes
AST	Automatic statistics tool
BC	Bubble columns
CFD	Computional fluid dynamics
CCP	Cold contact process
Cc	Corncobs
CSTR	Continuous stirred tank reactor
d_{SG}	Dry spent grains
ES	Esters
FAN	Free amino nitrogen
g-l	"gas – liquid"
g-l-s	"gas – liquid – solid"
HA	Higher alcohols
HoR	Homogeneous regime
HeR	Heterogeneous regime
HSC	High speed camera
iGLR	Internal-loop gas-lift reactor
ICT	Immobilized cell technology
ILV	Isoleucine, leucine and valine
iBio	Immobilized biomass ($g_{Biomass}/g_{Dry\ Carrier}$)
IEC	Ion exchange capacity (meq/g)
LAB	Low-alcohol beer
MIA	Manual image analysis
O.D.	Optical density
OA	Organic acids
OTR	Oxygen transfer rate
OP	Optical probe
PBR	Packed-bed reactor
PFR	Plug Flow Reactor
Rpm	Rotations per minute
SG	Spent grains
SMM	Synthetic mineral medium
TGV	Treatment for gaseous velocity
WAI	Water adsortion index
w_{SG}	Wet spent grains

I. Chapter I – Motivation and Outline

I.1 Thesis Motivation

I.1.1 Alcohol-free beer: definition, history and market

The excess of alcohol consumption contributed more than any other factor to the occurrence of domestic, labour and driving accidents, violence, abuses, mental incapacity and even death. Ethanol is absorbed by diffusion and distributed through all human body tissues by the blood. (Ferreira and Willoughby, 2008). It has been also mentioned that moderate alcohol consumption has better long-term effects on human health, even than no consumption (Brányik et al., 2012; Ferreira and Willoughby, 2008). The main reasons are due to the presence of phenolic compounds (high antioxidant capacity), essential vitamins and minerals (magnesium) (Bamforth, 2002; Brányik et al., 2012). These compounds are also present in alcohol-free beers, although at a lower quantity (Bartolomé et al., 2000), with the main advantage of not having the perverse effects of excessive alcohol consumption (Brányik et al., 2012; Ferreira and Willoughby, 2008).

From a simple point of view, beer can be classified according to its alcohol content, but there is no consensus on this. According to the European Union (EU) directive 98/33/CEE beer is a beverage described by the EU code NC 2203 with an alcohol content superior to 0.5% (vol./vol.) (CCE, 1992; CE, 2005). in most of the countries, generally alcohol-free beer (AFB) or “no alcohol beer” (or “dealcoholized beer”) contains less than 0.5% (vol./vol.) of alcohol, while “low alcohol” beers (LAB) may contain up to 1.2% (vol./vol.) and beers containing between 1.2% (vol./vol.) and 3.0% (vol./vol.) are considered to be “reduced in alcohol” (Lewis and Young, 1995). In some countries, due to cultural and religious rules, AFBs cannot exceed 0.05% (vol./vol.) (Brányik, et al., 2012). The terminology used in this thesis will be the one used in EU legislation, where an AFB contains less than 0.5% (vol./vol.) of ethanol (CCE, 1992).

Historically, AFB production increased during a period (1920-1933) between the two World Wars, especially in the United States due to the National Prohibition Act, also called: “Dry Law”. This law forbid the production, importation and exportation of intoxicant liquors (beverages with more than 0.5% (vol./vol.) of ethanol) to and from the United States of America. For the brewing industry in the United States of America, this law was the driving force that led to the increase of AFBs production and the development of new production methods. Naturally, when the Dry Law was abolished in 1933, AFBs production declined.

In the past two decades the highly competitive markets in brewing industry, allied to the global trend for a healthier life style without alcohol, restricting driving and labour laws and religious issues led to the development and increased consumption of AFB (Brányik et al., 2012; C. MARM, 2011). The production of AFBs is still a grain in the desert of the global beer production. Over the last five years the average sales of AFBs increased by 50% only in Europe. Actually Spain, the largest consumer country of low alcohol beverages, sold 9.5% of AFBs in 2010 (C. MARM, 2011). On the other hand in Germany, which has the biggest beer market, the average sales of AFBs are between 4% and 5% of total beer consumption (Brányik et al., 2012). This has been attributed to EU legislation that restricts alcohol consumption in many daily activities (schools, working, driving) or in some countries in sports events (eg. Stadiums of football).

In 2006 the beer Portuguese market represented 1.5% of the Portuguese gross domestic product generating over 1.5 thousands of millions Euros (APVC, 2006). Portuguese beer consumption has been decreasing over the last five years (**Figure I-1**). In average a Portuguese inhabitant consumes per year 60.6 L of beer (APVC, 2011). In the last five years, the consumption of AFBs in Portugal follows a trend of consumption similar to regular beers. AFBs market share is very low and varies between 2.5% to 3.3% of global Portuguese beer consumption. This market share is similar to the one found in other EU

countries, with the exception of Spain (APVC, 2011; Brányik et al., 2012; C. MARM, 2011).

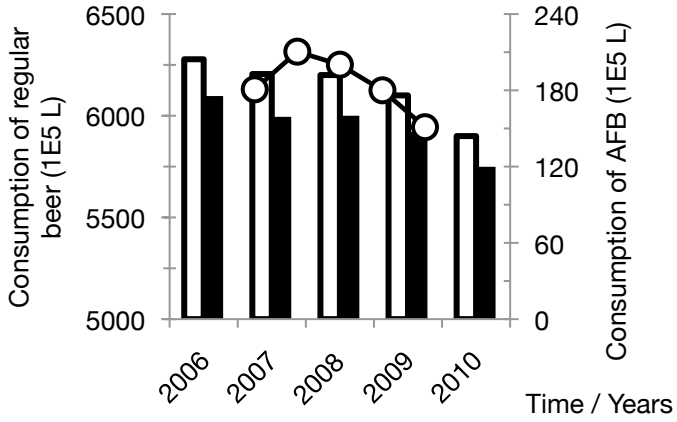

Figure I-1. Beer market in Portugal in the last Five Years. Legend: □: Total Beer Consumption; ■: Regular Beer Consumption; -○-: Alcohol-free Beer Consume. (Data from http://www.apcv.pt/asp/ in 15th December 2011)

A few years ago there were high expectations in the increasing market of AFBs, but the sales did not increase as much as initially predicted. It was expected that the need of a healthier lifestyle and restricting civil laws would drive the consumption from regular beer to AFB. Although the AFB market share in Portugal has been constant, the decrease on AFB consumption indicates a shifting on drinking habits by the Portuguese population. In **Figure I-1** it is suggested that the consumer of AFB in Portugal has a similar profile than a consumer of regular beer. Reasons for this are variable and include: medical indications, obligation due to driving and operating heavy machines, even moral positions about alcohol abuse (www.Ibesa.pt, access 20/04/2010).

In order to contribute for a healthier lifestyle in EU countries and considering the competitive beer market new AFB production methods that reduce production costs and increase AFB quality are worth of research and development.

I.2 Research Aims

The main objective of this thesis was to develop a lab-scale technology for continuous AFB production that would overcome the existing methods in terms of volumetric productivity and would be comparable in terms of product quality. The partial goals to be achieved are:

→ Selection of an economically affordable carrier material for yeast cells immobilization.

→ Evaluate the importance of reactor type, yeast strain and carrier type in a continuous limited primary fermentation of AFBs.

→ Study the consequences of the immobilized biomass ageing on product quality and propose a strategy to minimise its adverse effects

→ Study the influence of carrier properties in three-phase system (gas-liquid-solid) hydrodynamics and understand how that can influence bioreactor performance.

→ Develop, based on global hydrodynamic studies, the bioreactor design for the specific requirements of the limited primary fermentation process with cell immobilized on a cellulose-base carrier.

→ Understand the local hydrodynamics of the designed bioreactor induced by the carrier particles and study the influence of the limited fermentation in local hydrodynamics.

I.3 Thesis Outline

This thesis is subdivided in eight (8) chapters were the work is present and discussed. Each chapter, with the exception of Chapter II and chapter IX, is divided in: Introduction, Material and Methods, Results and Discussion and Conclusions. In the first part of this thesis is related with carrier selection (Chapter III), the second part with the three-phase bioreactor hydrodynamics (Chapter IV to VII), while a third part (Chapter VIII) with continuous fermentation of AFB.

In Chapter II several methods of AFB production are described, both in batch and continuous mode, at laboratory and industrial scale as well as important information about beer quality and flavour.

In Chapter III the selection between two cellulose-based carriers for yeast cells immobilization is investigated. In addition the methods for improving immobilization are studied.

In Chapter IV the fundamental study of spent grains particles' influence in three-phase Bubble Columns (BC) is reported.

In Chapter V the global three-phase internal-loop gas-lift reactor (iGLR) hydrodynamics are studied and the best reactor configuration for continuous AFB is selected.

In chapter VI CFD simulation for *g-l* system in iGLR is performed in order to explain better the phenomena that occurs in this type of reactor.

In Chapter VII the local three-phase GLR hydrodynamics are studied under fermentation conditions and a method for measuring local gas properties in three-phase systems is proposed.

In Chapter VIII the study of different systems for continuous limited AFB primary fermentation are described. Beer quality and flavour compounds formation at different conditions, as well as strategies for long-term fermentation are proposed.

In Chapter IX the general conclusions and suggestions for future work are described.

I.4 References

APVC, Associação Portuguesa de Produtores de Cerveja (**2006**). Indústria cervejeira nacional contribui para 1,5% do PIB. Orient, pp. 1-2.

APVC, Associação Portuguesa de Produtores de Cerveja (**2011**). Relatórios Anuais do Mercado cervejeiro em Protugal (in portuguese). Retrieved December 15th, 2011, from http://www.apcv.pt/asp/

Bamforth, C. W. (**2002**). Nutritional aspects of beer – a review. *Nutrition Research*, 22(1), 227–237.

Brányik, T., Silva, D.P., Baszczyňski, M., Lehnert, R., and Almeida e Silva, J.B. (**2012**). A review of methods of low alcohol and alcohol-free beer production. *Journal of Food Engineering*, 108(4), 493-506.

MARM, Convenio MARM - Cerveceros de España (**2011**). Informe socioeconóomico del sector de la cerveza en España (in Spanish). *Report* (p. 36).

CCE, C. C. E. (**1992**). Directiva 92/83/CEE do Conselho relativa àa harmonização da estrutura dos impostos especiais sobre o consumo de álcool e bebidas álcoólicas (in Protuguese). *Directiva 92/83/CEE do Conselho*.

CE, C. E. (**2005**). Regulamento (CE) N.o 1967/2005 Da Comissão relativo à classificação de certas mercadorias na Nomenclatura Combinada. (in Portuguese). *Jornal Oficial da Comissão Europeia*, 10-12.

Ferreira, M. P. and Willoughby, D. (**2008**). Alcohol consumption: the good, the bad, and the indifferent. *Applied Physiology, Nutrition and Metabolism*, 33(1), 12-20.

Lewis, M. J. and Young, T. W. (**1995**). Brewing. (M. J. Lewis and T. W. Young, Eds.). London: Chapman and Hall.

www.Ibesa.pt. (**2010**). Cerveja sem álcool. Retrieved April 20, 2010, from www.ibesa.pt

II. Chapter II – Alcohol-free Beer

II.1 Methods to Produce Alcohol-free Beer

AFB has been industrial produced since the beginning of XX century and different technologies have been developed over the last century, particularly over the last thirty years. Beer with low alcohol content can be produced by: (1) using additional techniques to remove the alcohol; (2) traditional methods for restricted ethanol formation; (3) continuous fermentation (Brányik et al., 2005; Brányik et al., 2012; Lehnert et al., 2009; Lewis and Young, 1995).

II.1.1 Techniques to remove alcohol from regular beer

These methods require an investment in additional brewing equipment. The techniques that are being used to remove the alcohol from regular beers are either thermal-based (vacuum evaporation or distillation) or membrane-based (dialysis; reverse osmosis) (Lewis and Young, 1995).

II.1.1.1 Thermal-based process

Vacuum evaporation is typically a three-stage process. In the first stage, pre-heated beer (35 ºC) passes under vacuum trough a plate evaporator heated at 50 ºC where the beer is degassed and the volatile compounds are liberated. The beer steam goes to a vacuum column where is separated in two: AFB and an alcohol-rich condensate. The aroma compounds are recovered from degassed CO_2 (by water or AFB) and re-added to the previously obtained AFB. The devices used for vacuum evaporation should be able to remove efficiently ethanol at short residence times. The main vacuum evaporators used are thin film evaporators, which can operate by gravity or using a mechanical device promoting a rotational movement. The main advantage of using vacuum evaporation methods over atmospheric evaporation is the better beer taste preservation. The thermal process allow: (1) to remove completely the alcohol from beer (≤ 0.05% (vol./vol.)); (2) the commercialization of

by-products (alcohol for vinegar production); (3) continuous and automatic operation with short start-up periods; and (4) flexibility (adapted to several beer compositions and volumes – from 200 L to 40 000 L). However, the purchase of these systems requires (1) significant investment; (2) high running costs (energy consumption); (3) thermal damage (loss of volatiles) of beer. Besides these removal steps, at the end, the resulting LAB has to be diluted with oxygen-free water and carbonated (Brányik et al., 2012; Lewis and Young, 1995).

II.1.1.2 Membrane processes

All the membrane processes have less thermal impact on AFB quality. They can operate automatically and are flexible, but at the same time they require significant capital and running costs.

The driving force in dialysis is the concentration gradient between beer and dialysing medium, which normally operates in counter-flow. Briefly, beer (1 °C to 6 °C) passes trough a dialyser where small molecules (as ethanol) pass trough a selective membrane into the dialysate. However, some aspects must be taken in account as the dialysate pressure to avoid CO_2 influence. The dialysate is then dealcoholized in a vacuum distillation column. The process efficiency depends mainly on the membrane's composition (cellulose or synthetic) and arrangement (hollow fibers), beer flow rate and composition of the dialysate. As the membranes are not ethanol selective, other important flavour beer compounds are removed, which can be overcome by the introduction of these in the dialysate to reduce the flavour compounds losses.

In reverse osmosis, the used membrane is more selective than the one normally used in dialysis. Reserve osmosis principle takes in account that water and ethanol permeate more than other beer compounds. Beer passes trough the surface of a membrane at high pressure (40 bar) and the most permeable substances cross the membrane. This method concentrates beer and the transfer of ethanol also increases. Then pure or demineralised water is added (diafiltration)

while ethanol still passes the membrane until the final ethanol concentration is achieved. In reverse osmosis no heat is applied, however membrane cost and the high operation pressures required are main disadvantages. Generally, reserve osmosis AFBs have significant losses of volatile compounds (70% to 80% of higher alcohols, 80% to 90% of esters) (Brányik et al., 2012; Lewis and Young, 1995). The majority of industrial applications are thermal/membrane based, sometimes even a mix of both, but usually brewing industries hide or patent their process to avoid being used by other companies (Bartolomé et al., 2000).

II.1.2 Traditional methods to restrict ethanol formation

Traditional methods to restrict ethanol formation mainly use smaller brewing operations that allow producing AFB. These operations include changes in mashing, arrested or limited fermentation and utilization of special yeast (Brányik et al., 2012; Lewis and Young, 1995).

II.1.2.1 Change in mashing

Mashing is one stage of beer wort production, where the degradation of starch to fermentable sugars and soluble dextrins occurs. So the mashing step has a huge influence in the final concentration of sugars in the wort, thus in final beer ethanol content. If changes are operated in this process the fermentable sugar concentration can be altered. The changes that can be operated during mashing to reduce wort sugars concentration are: the application of high temperatures (75 ºC-80 ºC) that deactivates β-amylase; the cold water malt extraction (<60 ºC), which extract malt flavour compounds without increasing wort gravity; spent grains re-mashing (extrusion or acid hydrolysis; and the utilization of grains deficient in β –amylase (Brányik et al., 2012; Lewis and Young, 1995).

II.1.2.2 Limited or arrested fermentation

Modifications in normal primary beer fermentation to produce AFBs are probably the most usually methods applied in industry. These alterations are made by arrest or limit of the fermentation and allow brewing industries to work with traditional equipment. The main objective is to keep a low ethanol content. Arrested fermentation is obtained by removing yeast before excessive attenuation occurs (rapid cooling or filtration), followed by maturation for 10 days at low temperatures (0 ºC to 1 ºC) prior to new filtration, carbonation, stabilization and sterilization. Limited fermentation methods are done by creating conditions that limit the yeast metabolism. Among these, the cold contact process (CCP), which is done using a low gravity wort fermented at low temperatures (0 ºC to 1 ºC), has a good potential and high volatile compounds are produced. Low aldehyde reduction is achieved leading to strong influence of worty off-flavours in the produced AFB (Perpète and Collin, 1999a, 1999b).

When AFBs are produced by these methods, to improve its quality some operations should be taken in account: (1) adding of dark/pale caramel malt (contributes to final flavour); (2) dilution of wort before boiling (reduces bitterness, increases esters and higher alcohols); (3) decrease wort pH (low temperature attenuation per se is not capable to do that) (Narziss et al., 1992).

II.1.2.3 Special yeasts utilization

The use of special yeast, capable of performing a limited fermentation consists on using their low or zero ability to produce ethanol. Special yeast can be obtained by the selection of a proper microbial strain as *S. lugwigii* unable to ferment maltose - the main wort sugar (Narziss et al., 1992). Other methods include the development of new yeast strains by forcing modification of brewing yeast by random mutation using ultraviolet irradiation (Narvátil et al., 2001) or by using genetic engineering techniques that intentionally delete genes from yeast cells (Selecky et al., 2008). Normally the

intentionally deleted genes are involved in the synthesis of enzymes present in the tricarboxylic acid's (TCA) cycle. Among these, the usual deleted genes are: CIT1, ACO1, FUM1, MDH1, IDH1 IDH2, KGD1, KGD2, and LPD1 (Przybyla-Zawislak et al., 1999; Repetto and Tzagoloff, 1990; Selecky et al., 2008). The development of new yeast strains is normally done in haploid/diploid laboratory strains and not in industrial yeast strains, which not only are alloploids as also have important industrial characteristics (fermentation rate, flavour formation, flocculation). The ideal yeast strain is a hybrid between this genetically modified strains and industrial strains, carrying all-important characteristics for industrial AFB production. In addition, the genetic development and application of yeast strains has legal obstacles and generates concerns in the consumers. Nowadays, no brewing industries will take the risk of using genetically modified yeast strains to produce an AFB.

II.1.2.4 Continuous fermentation

Continuous fermentation of beer and AFB has been, since the last decades, one of the most studied areas in several brewing research groups from different universities across the globe (Lehnert et al., 2009; Mensour et al., 1997; Perpète and Collin, 1999a; Selecky et al., 2008; Van Iersel et al, 1995; Virkajarvi, 2001). The implementation of continuous methods in brewing industry has been driven by the potential economical advantages. Some examples at industrial scale are known (see Section II.2.7). However, unbalanced flavour issues have not yet been totally overcome, leading to the necessity of further investigation for the application of continuous processes (Brányik, et al., 2008; Mensour et al., 1997; Virkajarvi and Linko, 1999; Willaert and Nedovic, 2006).

II.2 Continuous Beer Production

Nowadays in beer industry the traditional batch process of beer fermentation and maturation still prevails over the continuous processes. Considering that are several different types of beers, in traditional batch systems the primary beer fermentation takes place for 5 to 10 days while maturation takes 1 to 3 weeks (Brányik et al., 2008; Mensour et al., 1997). The most successful continuous fermentation systems developed are based on immobilized cell technology (ICT), but despite its advantages they are still not being fully applied at industrial scale (Brányik et al., 2005; Mensouret al., 1997; Pilkington et al., 1998).

The main advantage offered by these systems when compared with traditional fermentation and maturation, is the potential time savings by reducing the production time, which is reflected in economical advantages. By using continuous systems the beer production time has been reduced from a week-base (2 to 4 weeks) to a daily-base (2 to 5 days) (Brányik et al., 2006, 2005; Dömény et al., 1998; Van Iersel et al., 1995; Virkajarvi, 2001). Continuous beer production gives the possibility of not only using short fermentation times and reduce downtimes (filling, cleaning and stand by), but also reduce the investment capital costs, operation costs and space requirements (Brányik et al., 2005; Mensour et al., 1997; Pilkington et al., 1998). The investment costs were estimated to vary between 15% and 100% of the batch process (Brányik et al., 2005; Mensour et al., 1997; Pajunen et al., 1991; Virkajarvi, 2001) and depend mostly on the carrier cost. Operating cost can be both 70% lower and 80% higher than in batch system, depending on the applied technology, estimated annual production and comprehensiveness of the economic study. Moreover, the area requirements are expected to be smaller than for traditional technology (Pajunen et al., 1991). On the other side, there are many reasons that sentenced continuous fermentation to failure (Brányik et al., 2005; Mensour et al., 1997; Pilkington et al., 1998; Willaert and Nedovic, 2006): engineering problems (operation conditions, process

hygiene); unbalanced flavour (cell physiology, ageing); contamination; tradition.

Nowadays the main objective in the area of continuous beer fermentation investigation is to reduce significantly the production times and, at the same time, ensure a uniform high quality beer. It is useless for brewing industry to produce beer in continuous without the same characteristics of the traditional beer drinked by the regular consumers. Beer making is one of the oldest biotechnology process known by men, and consequently tradition aspects have to be taken into account (Lewis and Young, 1995). Tradition is an additional obstacle to be solved by scientific community and consists in demonstrating the advantages of continuously beer technology to the brewing engineers/masters. These advantages must be initially based in economic aspect, but should go beyond. They should allow the production of different beer types only by changing the wort composition and operation parameters without the necessity of new start-up of the bioreactor.

II.2.1 Continuous beer fermentation using cell immobilization systems

According to Mensour et al. (1997), systems using immobilized yeast cells for continuously beer production have been proposed for more than 30 years (Mensour et al., 1997). Narziss and Hellich (1971, 1972) cited by Virkajarvi and Linko (1999) were pioneers in the use of immobilizing yeast for beer fermentation. Their simple bioreactor consists in a packed-bed formed by kieselguhr and yeast in a kieselguhr filter through which wort flows. However the bioreactor's lifetime was only 7–10 days before clogging.

Since then, ICT have been applied and successfully developed for continuous beer and AFB production. Some of then have been applied at industrial scale both on maturation and primary fermentation (Brányik et al., 2005; Mensour et al., 1997; Pilkington et al., 1998). So it is not

surprising that over the last decades, different reactors designs, as well as several immobilized methods, were proposed for continuous primary fermentation and maturation (or secondary fermentation) by several scientific groups and brewing industries.

Table II-1. Examples of carrier types and operation systems used for continuous beer fermentation and/or maturation by immobilized brewing yeast

Carrier material	Reactor type	Process	References
Ca-alginate	Packed-bed	Maturation	(Dömény et al., 1998; Smogrovicová *and* Dömény, 1999)
κ-carrageenan	Packed-bed	Maturation	(Dömény et al., 1998),
κ -carrageenan	Gas-lift	Primary Fermentation	(Smogrovicová *and* Dömény, 1999)
Porous glass (Siran)	Packed-bed ;	Primary Fermentation	(Virkajärvi *and* Kronlöf, 1998)
Gluten pellets	Gas-lift	Maturation	(Šmogrovičová et al., 1999)
Spent grains	Gas-lift	Primary Fermentation	(Brányik et al., 2006)
Corncobs	Packed-bed	Maturation	(Brányik et al., 2006)
PVA particles	Gas-lift	Primary fermentation	(Bezbradica et al., 2007)
Spent grains	Gas-lift	Primary fermentation	(Lehnert et al., 2009)

Carrier cost is one of the main investment costs when beer is produced in a continuous mode. Several types of carriers have been tested to immobilize brewing yeast (Brányik et al., 2005; Pilkington et al., 1998). The carrier type depends on the process to be applied: primary fermentation or maturation. Not only different immobilization methods are implied, but also different reactors designs operating at different conditions (see **Table II-1**). In the last 15 years, the cellulose-base carriers have gained importance mainly due to their good immobilization capacities, high availability and low cost (Brányik et al., 2001). More information about this subject is available in Chapter III.

II.2.2 Immobilization and physiological changes on yeast

Since the early attempts to develop a continuous process for beer production the changes in immobilized cells metabolism have been postulated as the main reason for unbalanced flavour of final beer (Brányik et al., 2005; Mensour et al., 1997; Virkajarvi and Linko, 1999).

It has been reported that immobilized cells induce different physiological responses when compared with free cell systems. These changes are mainly in metabolic functions (substrate uptake, products formation, enzymes expression and/or activity). Most probably they occur due to the different micro-environmental conditions that result from cell-immobilization (Junter et al., 2002; Shen et al., 2003).

These changes can be due to: increased levels of DNA, production of structural carbohydrates and glycogen (Brányik et al., 2005; Doran and Bailey, 1986), increase saturation of fatty acids content, modifications of gene expression levels, cell wall and membrane composition (Shen et al., 2003; Verbelen et al., 2006). This last one has important impact on several enzymes, SENSO proteins, transporters and membrane fluidity that play an important role on ethanol tolerance (Qun et al., 2002) sugar uptake and amino acids metabolism. It is expected that yeast physiological changes affect final beer flavour. However, it is difficult to describe the direct effects of immobilization due to the complexity of the different immobilizations systems, which can induce one or more change in yeast metabolism. Nevertheless, several reasons have been proposed for the modifications that occur in yeast cell as a consequence of immobilization. The main reasons are (1) the continuous mode of reactor operation; (2) internal and external mass transfer limitation; (3) specific environment; (4) ageing of immobilized cells (Brányik et al., 2005; Masschelein et al., 1994; Verbelen et al., 2006).

II.2.2.1 Continuous mode of reactor operation

When the traditional beer fermentations are carried out in batch process, the yeast regulates and adjusts its metabolism during the fermentation with respect to the changes in the medium composition. This does not happen in steady-state immobilized cells systems where the cells are not exposed to significant alterations in reaction environment (Masschelein et al., 1994). In a continuous process, the yeast cells do not make any distinction between lag, exponential and stationary growth phases, because the medium composition is almost constant over the time. This is the biggest difference between continuous and batch processes. In order to minimize it, continuous beer fermentation systems usually consist in two (or more) fermentations vessels (combining agitated vessels and plug-flow like reactors) to achieve the correct beer balance and flavour (Bezbradica et al., 2007; Brányik et al., 2006; Mensour et al., 1997; Smogrovicová and Domény, 1999; Virkajärvi and Kronlöf, 1999; Yamauchi et al., 1995).

II.2.2.2 Internal and external mass transfer limitations

There are two types of mass transfer mechanisms that can limit the continuous beer fermentation where ICT is applied: the internal and external mass transfer. The external mass transfer depends largely on the applied reactor, its design and regime of operation.

The internal mass transfer limitations are related mainly with material diffusion inside the biofilm and/or inside the carrier (e.g. alginate) where cells are entrapped. These limitations are, when compared with free-cells systems, the most usual justification to the often-observed decrease in immobilized cells growth rate (Masschelein et al., 1994) or the variation in specific compound productivities (Taipa et al., 1993). Moreover these limitations create a specific micro-environment on the immobilized cells. External and internal mass transfer barriers do not have a deep impact in the surface of porous and non-porous carriers. If there is a low biofilm thickness, an almost direct contact of immobilized cells with the bulk liquid occurs and therefore no significant mass

transfer limitations occur and consequently there is not a developement of a specific microenvironment. (Brányik et al., 2005).

II.2.2.3 Specific environment

The activity of the immobilized cells around/inside the solid matrix is influenced by the developed microenvironment. There are numerous effects of immobilization on cell physiology reported in literature (Brányik et al., 2005). The reported physiological changes of immobilized yeast include changed metabolic functions such as substrate uptake (Shen et al., 2004), product formation and altered enzyme expression and activity (Iersel et al., 2000). Some authors agree that the enhanced metabolic activity can be attributed also to the surface sensing responses in immobilized cells but the reasons are not yet clearly explained. Among all changes in immobilized yeast, the increase of ethanol content (Qun et al., 2002), modifications at DNA (Doran and Bailey, 1986) level and changes in cells properties are the most important.

II.2.2.4 Ageing

Ageing is the predetermined transition of an individual cell from the youth to old age that finally culminates in death. The Hayflick limit is the maximum lifespan potential of a cell (as *Saccharomyces cerevisiae*). Empirically, it corresponds to the number of divisions which one cell is capable of (between 10 to 30 divisions). Death in yeast cells may occur via two different ways: necrosis and senescence (Powell et al., 2000).

According to Monch et al. (1995) cited by Powel et al. (2000), necrosis is defined as the accumulation of irreparable damage in intracellular components compromising cell integrity and leading to autolysis. On the other side, senescence is the predetermined cessation of life as a result of a genetically controlled progression from youth to old age (Powell et al., 2000). The origin of necrosis is diverse and depends on environmental factors (stress conditions; deletion or disruption of genes; accumulation of DNA damage) (Maskell etl al.,

2003), while senescence starts when no more cell division occurs (Powell et al., 2000; Sinclair et al., 1998). Senescence can be related with the yeast cell cycle/division. The knowledge about yeast cell cycle is very important on brewing industry because after the primary fermentation the yeast cells are collected and re-used. This knowledge allows the optimization of the number of reusing by predicting the formation of biomass on the next step.

Table II-2. Cellular changes accompanying senescence (adapted from Powell et al., 2000)

Characteristic	Change
Cell size	Increase
Surface wrinkle	Increase
Bud scar number	Increase
Cell wall chitin	Increase
Specific gene expression	Altered
Protein synthesis	Decrease
Generation time	Increase

During a normal fermentation the percentage of old cells, which have lower metabolic activity, increases, resulting in irreversible modifications on cell appearance (Barker et Smart, 1996; Maskell et al., 2003). These morphological and physiological changes can act as biomarkers in the determination of cell age or for fermentation control, especially in continuous fermentations with immobilized yeast cells (Barker and Smart, 1996; Maskell et al., 2003).

There are several ageing and senescence mechanisms that have been proposed, such as (Powell et al., 2000; Sinclair et al., 1998a, 1998b):

- the relation between surface- to-volume ratio and the increasing numbers of bud scars (reduction of the surface area for budding and nutrient exchange),

- the gradual loss of telomeric sequences (responsible for ensuring that a complete replication occurs),

- cytoplasm senescent factors (accumulation of toxic compunds),

- genetic factors.

Among all of these, genetic control of ageing has gained the biggest importance over the last ten years (Kennedy et al., 1995; Powell et al., 2000). Consequently, a number of genes that may influence longevity in yeast have already been identified and are listed below (**Table II-3**).

Table II-3. Genes associated with longevity in *Saccharomyces cerevisiae* (adapted from Powell, 2000)

Gene	Function	Observations
LAG1	Unknown	Expressed in young cells
LAG2	Unknown	
RAS	Nutritional status	Related with longevity
SIR4	Gene silencing	Silence AGE stress responsea
AGE	Stress response	

[a]Kenedy et al, 1995

In brewing industry, the term ageing has been incorrectly used, because yeast age is measured chronologically by the number of times a population is reused in successive fermentations. After finishing the prymary beer fermentation the cylindro-conical tank is cooled to promote sedimentation. Cells are deposited in the conical part of the tank, the oldest fraction being located in the bottom and the youngest cells in the top. The flocculation potential of yeast cells is regulated by cell wall properties that change throughout the cell life span (Powell et al., 2003). A rough cell surface topography promotes cell-to-cell adhesion during the onset of flocculation. Although sedimentation capacity is strain-specific, cell size may trigger an important roll in flocculation acting as a nucleation point (Barker and Smart, 1996; Powell et al., 2003).

In theory, continuous fermentation processes with immobilized yeast that has a low Hayflick limit (maximum number of possible cell divisions) is not recommended (Brányik et al., 2005). The main reason is that long periods of continuous fermentation are desirable from the economic point of view and yeast with low Hayflick limit would not support long fermentation runs (Virkajärvi and Kronlöf, 1999; Virkajarvi, 2001). It is known that aged brewing yeast changes their flocculation characteristics (Soares and Mota, 1996) and fermentation performance (Powell et al., 2003). In addition, mutations in brewing yeast leading to

alterations at morphological/biochemical level during fermentation can occur. In a pratical point of view it would important to know: (1) the influence of the different immobilization methods on ageing of brewing yeast and (2) the effect of senescence on cell vitality and fermentation performance (Brányik et al., 2005).

II.2.3 Industrial applications

Continuous primary fermentation and maturation of beer has been a field of interest for brewing since the 1970s. Applications for continuous beer primary fermentation and/or maturation have been implemented at large scale – Cultor Ltd and Tuchenhagen; Kirin Brewery; Meura Delta; Labatt Brewing Company (Mensour et al., 1997).

The Cultor Ltd and Tuchenhagen system process was developed in the early 1990's by a consortium. They developed two processes: (1) accelerated maturation (diacetyl reduction) and (2) continuous AFB. The carrier used was DEAE-cellulose (Spezyme® GDC) in a downflow Packed-bed reactor (PBR). The maturation system has been operational since 1992 at industrial scale (1E8 L) in the Sinebrychoff Brewery in Kerava (Finland), where it is used alongside with traditional maturation process (GEA Process Engineering, 2008; Mensour et al., 1997). Nowadays, this system (Immocon maturation) is available and sold by GEA divison from Tuchenhagen.

The Kirin Brewery Co., Ltd (Japan) system was eventually the first industrial system involving continuous primary beer fermentation and maturation. It is a multi-stage system composed by BC reactor and two PBR (main fermentation) and a third PBR (maturation). Overall, the continuous production of beer takes place within three to five days. The initial 20 L system was scaled-up to 500 L and then to 10 000 L. However some unexpected drawbacks (higher capital and operating costs) condemned to failure the 10 000 L installation (Mensour et al., 1997).

Meura Delta has developed a multi-stage bioreactor system for the production of alcohol-free and regular beer. Yeast cells are immobilized by adsorption on the internal surface of the silicon carbide rods. Based on the success, Meura Delta is trying to implement their design to industrial scale. Little scale-up problems are expected, because the system has a modular design (Mensour et al., 1997; Meura, 2007).

The Labatt Breweries (Canada) in association with the Department of Chemical and Biochemical Engineering at the University of Western Ontario, proposed a continuous beer fermentation system using immobilized yeast cells in κ-carrageenan. Additionally they developed a continuous bead production process (Decamps et al., 2004) based on static mixers. A draft tube gas-lift bioreactor with a degassing zone was applied for the primary fermentation of beer. Labbat Brewery was the first in using a gas-Lift bioreactor for continuous beer production. Moreover the experimental work allows not only research groups to be familiarised with the ICT but also how it could be applied in continuous beer production. Before this application the major problem was related with the production of poor flavour profile mainly due to low free amino nitrogen (FAN) uptake from immobilized cells. Labatt Brewery, with the implementation of a gas-lift bioreactor (good mixing profiles) with a draft tube and small sized immobilisation beads (±1 mm in diameter) managed to reduce significantly mass transfers limitations. Consequently the FAN uptake was better and a final product of acceptable quality was produced. The valuable experience and knowledge gained through the preliminary immobilized cell work at Labatt, provided a solid foundation which is now used to develop this technology into an industrially feasible venture (Mensour et al., 1997).

II.3 Continuous Alcohol-free Beer Production

As reported before, AFBs are mainly produced, at industrial scale, by arrested or limited fermentation (as CCP). Fermenting an AFB is technically simple and resembles secondary fermentation. The continuous production of AFB is based on the limited fermentation strategy. The proposed AFB continuous fermentation systems generally consist of one-stage bioreactor and are similar to the previously reported continuous maturation systems (low temperature, low wort gravity and short contact time). The main aim is to remove the worty flavour without a high alcohol concentration (or only very low amounts of alcohol) in the beer (Brányik et al., 2012; Virkajarvi and Linko, 1999).

Considering that the most successfully applied systems in industry are for maturation of beer (see section II.2.3), the continuous production of AFB has a big potential application due its high productivities when compared with the existing methods. In fact, the still low number of AFBs consumers and absence of a long tradition in its production/consumption (Branyik et al., 2012) can lead to an easier implementation of continuous AFBs production systems at industrial scale. In addition, some applications managed a good reduction of aldehydes by the bioreactor design only (physical mechanism). AFBs are known by their worty off-flavours and aldehydes have been reported as the reason for this character (Perpète and Collin, 1999a).

Many research groups have been developing and optimizing different continuous AFBs systems. The main differences are in reactor design, immobilization method and carrier used. The main reactors used are Packed-bed like reactors (Van Iersel et al., 1995). However and considering the good mixing and aldehyde reduction properties (by stripping) of iGLR, this reactor has also gained importance for continuous AFBs production (Lehnert et al., 2009).

II.3.1 Industrial applications

Although several systems have been proposed and implemented over the last years for continuous AFBs production the methods used in industry are not known by the majority of the scientific community. The main conclusion to be taken is that the proposed continuous fermentation systems have not yet been successfully applied in industrial continuous AFB production. The main reasons that are pointed are the need of industry to acquire special equipment (bioreactor and additional equipment for running it continuously) and to apply additional techniques (immobilization methods) and materials (carrier) not common in brewing industry (Brányik et al., 2012; Mensour et al., 1997; Pilkington et al., 1998). Another possible conclusion may be related with the importance of continuous systems using immobilized cells on continuous AFBs production that may lead brewing companies to hide their progress in this particular field. As referred before only one industrial application for continuous AFBs is known - the Cultor Ltd and Tuchenhagen system. In fact, it is not a pure AFB but a LAB. Considering the similarities between AFB and LAB, some details of this indutrial application will be described below.

The system developed by the Cultor Ltd and Tuchenhagen consortium to produce continuously AFB using immobilized cells in a PBR, when compared to the classical arrested batch fermentation, was found to produce a better tasting LAB with an improved product consistency. The Bavaria BV (Netherlands) is using this system for the continuous production of 15 000 m^3 of LAB per year. It is already one of Bavaria's best selling LAB. A personal communication from Heikki Lommi (business manager of Cultor Technology) cited by Mensour et al. (1997) indicated that other companies (Faxe in Denmark, Ottakringer in Austria), have also purchased this technology and are presently producing continuously AFB. In recent years the GEA group togheter with Tuchenhagen developed the Immocon system for continuously AFB production. They claim that many breweries are using their method,

such as Sinebrychoff Brewery in Kerava – Finland (GEA Process Engineering, 2008; Mensour et al., 1997).

II.3.2 Future trends and challenges

Regular AFBs are known by the worty off-flavour and lack of body. Considering that even the most common industrial approaches cannot solve these issues, and that continuous fermentations technology development has been raising fast this can be a promising field of study in the future. Many studies have to be made to achieve not only the production of a well-balanced AFB, but also in the scale-up issues of the used bioreactors. Thus, it is important to:

- understand better the physiological changes of immobilized yeast;
- control ageing issues in a long-term fermentation;
- understand the interaction between hydrodynamic aspects (k_La; mixing profiles, channelling) and yeast metabolism for each proposed system.

II.4 Beer Quality and Flavour: Origin and Influence

The two distinct aspects to beer quality are the nature or kind and the degree of excellence. There are many quality parameters in beer – flavour, colour, clarity, degree of degradation, presence (or not) of foam, pH and alcohol content are the most important.

Flavour, according to the EBC-ASBC definition, is the combination of olfactory and gustatory attributes perceived during tasting. It includes tactile, thermal, pain and kinesthetic effects. The most important aspects of flavour are mouth-feel, taste and odor (Briggs et al, 2004). Mouth-feel is defined as the tactile perception at the lining of the mouth (tongue and teeth) and is involved in the perception of smoothness, astringency (drying), temperature and CO_2 sensation. Taste is sensed by tongue where four (4) flavours (sweet, salt, sour and bitter) are recognized, while the aroma is sensed by the olfactory

system (Briggs et al., 2004; Lewis and Young, 1995). The predominant influences on beer flavour are derived from hop bitterness and aroma, malt components and fermentation (Lewis and Young, 1995)

There are several compounds that contribute to beer flavour. Each compound has different thresholds, i.e., perception of a substance that is present in a concentration that can just be identified. In the next table (**Table II-4**) are summarized the main beer flavour compounds. **Table II-4** compares the values presented in literature for regular beers and AFBs to continuous and batch production modes.

From **Table II-4**, it is possible to observe that continuous process has similar values to the traditional batch for higher alcohols and esters. The main problem occurs in total VDK's concentration. VDK's amount for regular beers produced in continuous is usually higher than by batch process and than the threshold values (Brányik et al., 2006; Pajunen et al. (2001) in Willaert and Nedovic, 2006). However this does not occur in continuous AFB mainly due to the operational parameters (8 ºC) that limit the fermentation and yeast metabolism. Consequently the formation of all main flavour compounds is lower. Among them VDK's concentration in continuous AFB is similar to the batch process (Lehnert et al., 2008). Some authors (Perpète and Collin, 1999b) considered that, due to AFB low alcohol content, their flavour compounds threshold should be compared with the falvour threshold compound in water and not in beer as is normally done. Being so, in **Table II-4** the threshold in water and beer are displayed for different flavour compounds.

Table II-4. Beer major Flavour compounds in continuous and batch systems for regular (A and B) and AFB (C)

Class	Compound / mg/L or μg/L*	Continuous system			Batch process			Threshold in water (E) / (mg/L)	Threshold in beer (D) / (mg/L)	Flavour in Beer (D)
		A	B	C	A	B	C			
Alcohol	Ethanol	38500	-	3900	44200	-	< 3900	990	14000	Alcohol, strong
Higher Alcohols (HA)	Propanol	16.1	24.9	1.6	17.5	10	2		800	Alcohol
	IsoButanol	8.3	8.4	1.6	12.5	8.2	1.8	0.59	200	Alcohol
	Amyl-Alcohol (2-Methyl-butanol)	55.8	-	8.6	70	-	7.65	1.2	65	Alcohol, Banana, Sweetish, Aromatic
	Isoamyl alcohol (3-Methyl-butanol)	-	47.0	-	-	51	-	0.22	70	Alcohol, Banana, Sweetish, Aromatic
	TOTAL HA	**80.2**	**80.3**	**11.8**	**100**	**69.2**	**11.45**		-	-
Esters (ES)	Ethyl acetate	11.3	26.4	0.58	17.2	21.5	0.78		33	Solvent, Fruity, Sweetish
	Isoamyl acetate	-	1.00	-	-	1.5	-		1.2-1.6	Banana, Apple, Solvent, Estery
	Ethyl Caproate	-	0.2	0.01	-	0.4	0.01		0.21-0.23	Apple, Fruty, Sweetish, Aniseed, Estery
	Ethyl Caprylate	-	0.6	0.22	-	1.4	0.01		0.9	Apple, Sweetish, Fruty
	Amyl Acetates	0.2	-	0.02	1.2	-	0.06		1.2 **	-
	Total ES	**11.5**	**28.2**	**0.83**	**18.4**	**24.8**	**0.86**		-	-

Legend: A – Brányik et al. (2006): Spent Grains (Regular beer); B – Pajunen et al (2001) in Willaert *and* Nedovic (2006): Aspen wood chips (average values of Regular beer); C – Lehnert et al (2008): Spent Grains (AFB); D – Meilgaard (1975); E - Czerny et al. (2008).

* – Values in μg/L ** — Value from Lehnert et al (2008). *** – from Perpète *and* Collin (1999b)

Table II-4. (continuation)

Class	Compound / (mg/L or µg/L*)	Continuous system			Batch process			Threshold in water (E) / (mg/L)	Threshold in beer (D) / (mg/L)	Flavour in Beer (D)
		A	B	C	A	B	C			
Vicinal Diketones (VDK's)	Diacetyl (2,3 - Butanedione)	-	0.25	-	-	-	-		0.15	Diacetyl, butter scotch
	2,3-Pentanedione	-	0.15	-	-	-	-		0.9	Diacetyl, Fruity
	Total VDK's	**0.29**	**0.4**	**0.06**	**0.03**	**-**	**0.05**		-	-
Aldehydes	Acetaldehyde	13.1	-	8.5	8	-	6.9	0.025	10	Green leaves, Fruty, Worty
	Hexanal*	-	-	0.2	-	-	0.2	2.4	0.35	Bitter, Vinous, aldehyde
	2-Methyl propanal*	-	-	1.7	-	-	0.3	0.49	1***	-
	3-Methyl butanal *	-	-	8.7	-	-	1.6	0.5	0.6***	Malty, Chocolate, Almond***
	Methional	-	-	-	-	-	-	-	-	-
	Furfural*	-	-	1.5	-	-	2.7	8000	150	Paper, husk

Legend: A – Brányik et al. (2006): Spent Grains (Regular beer); B – Pajunen et al (2001) in Willaert *and* Nedovic (2006): Aspen wood chips (average values of Regular beer); C – Lehnert et al (2008): Spent Grains (AFB); D – Meilgaard (1975); E - Czerny et al. (2008).

* – Values in µg/L ** — Value from Lehnert et al (2008). *** – from Perpète *and* Collin (1999b)

II.4.1 Higher alcohols

Higher alcohols (HA) are alcohols that have more carbon atoms than ethanol (Lewis and Young, 1995) and contribute to beer flavour due to their alcoholic or solvent-like aroma causing a warm mouth-feel. They are formed during main fermentation and can be divided in aliphatic and aromatic. The main aliphatic HA are: n-propanol, isobutanol (2 methylpropanol), amyl and isoamyl alcohols, while the main aromatic HA are: 2-phenylethanol, tyrosol and tryptophol, being the latter undesirable (Brányik et al., 2008; Willaert and Nedovic, 2006; Meilgaard, 1975).

The HA are formed from the α-keto-acids pool. These acids are decarboxylated to aldehydes and further reduced (by alcohol dehydrogenase) to HA. The α-keto-acids are synthesized trough two pathways: the anabolic and catabolic routes. In the anabolic route, the α-keto-acids formation arises in the amino acid synthesis from carbohydrate metabolism. In he catabolic route, α-keto-acids are synthesized by the uptake of wort amino acids from yeast cells (Brányik et al., 2008; Willaert and Nedovic, 2006). The final concentration of HA is determined by the uptake of the corresponding amino acid and carbohydrate utilization rate and its formation is related with FAN uptake (Brányik et al., 2008; Masschelein et al., 1994; Willaert and Nedovic, 2006). The contribution of anabolic or catabolic pathway is unclear and varies for each alcohol. It is reported that this contribution is influenced by wort amino acid composition, fermentation stage and yeast strain. Moreover, HA can also be originated from the reduction of ketones and aldehydes present in wort. (Brányik et al., 2002).

Regarding **Table II-4** and having in mind the high taste threshold of these compounds, the gap between HA formation during continuous and traditional beer fermentations does not represent the most serious flavour problem (Brányik et al., 2008; Smogrovicová and Domény, 1999). Yet, an increased propanol yield followed by decreased i-butanol

and isoamyl alcohol formation was noticeable in some of the continuous systems (Brányik et al., 2008; Willaert and Nedovic, 2006).

Generally, immobilized cells systems by entrapment are related with low HA formation, mainly due to mass transfer limitations that leads to poor immobilized cell growth and low FAN uptake by the immobilized cells. On the other hand, continuous fermentation using immobilized cells systems by adsorption (spent grains, wood chips) have high FAN uptake, as well as good immobilized cell growth, which, naturally, leads to good formation of HA (Brányik et al., 2008; Masschelein et al., 1994; Smogrovicová and Domény, 1999; Willaert and Nedovic, 2006).

In continuous systems, it is possible to control the formation of HA by choosing an appropriate yeast strain, wort composition, fermentation conditions (CO_2, Temperature, wort velocity), immobilization method (adsorption or entrapment) and reactor design (Yamauchi et al., 1995). HA formation is related with yeast growth intensity. Therefore solutions to increase their formation are mainly solutions that increase yeast cells growth, such as: the increase fo aeration and temperature and the reduce of dissolved CO_2. The HA productions is extremely important as they are related with the production of esters (Brányik et al., 2008; Smogrovicová and Domény, 1999; Willaert and Nedovic, 2006).

II.4.1.1 Higher alcohols production in continuous AFBs

It has been reported that in AFBs due to limited fermentation or alcohol removal techniques the concentration of HA is low (Branyik et al., 2012). Moreover, the concentration of undesirable HA such as tyrosol and tryptophol is also low (Bartolomé et al., 2000). As told before (section II.1), continuous AFB production is normally obtained by limiting yeast growth intensity. Consequently, the concentration of HA is normally very low compared with continuous regular beers production (see **Table II-4**). However, when compared with commercial AFBs the values are similar. Lehnert et al (2008) proved that the increasing of dissolved oxygen in the reactor increases the HA production. It was

sustained that increasing dissolved oxygen, it increases carbohydrate and amino acid metabolism and consequently the α-keto-acids and HA production. Only at high oxygen transfer rates (≥10 mg/L/h) the amount of HA was higher than in the commercial AFBs (Lehnert et al., 2008).

II.4.2 Esters

Esters (ES) represent the largest group of flavour active compounds in beers. Their great importance in flavour is attributed to its low threshold that confers a fruity aroma in beers. Esters are synthesized by the reaction between an alcohol and an acyl-CoA molecule, which is catalyzed by alcohol acyltransferases (AATases). Several other esterases have been reported. Although ester formation in yeast has been very studied over the past years (Verstrepen et al., 2003), the knowledge about the physiological role of these compounds is rather unclear (Brányik et al., 2008; Willaert and Nedovic, 2006). The ES can be divided into two main groups: (1) acetate esters such as ethyl acetate (most common because is derived from ethanol), isoamyl acetate and phenylethyl acetate; and (2) the so-called ethyl or medium chain fatty acid esters e.g. ethyl caproate and ethyl caprylate (Brányik et al., 2008; Willaert and Nedovic, 2006). ES production in batch systems occurs during yeast growth (60%) and stationary phase (40%) (Willaert and Nedovic, 2006). Two factors are important on the rate of ester formation: the availability of the two substrates (acetyl/acyl-CoA and alcohols), and the activity of enzymes (AATases). Ester formation is highly dependent on the yeast strain used and on certain fermentation parameters such as temperature, pitching rate, top pressure and aeration (Calderbank and Hammond, 1994; Van Iersel et al., 1999; Verstrepen and Klis, 2006; Willaert and Nedovic, 2006). Higher wort aeration affects esters synthesis, because fatty acids from wort reduce the availability of acyl-CoA (used for yeast growth and membrane lipid synthesis) (Brányik et al., 2008; Lehnert et al., 2008; Lewis and Young, 1995). Some studies reported that the main factor controlling ester biosynthesis is the expression level of the ATF1 gene, which codes for

AATase. The expression of ATF1 gene is repressed both by oxygen and unsaturated fatty acids (Van Iersel et al., 1999; Verstrepen et al., 2003; Willaert and Nedovic, 2006).

When studing the ES production in continuous and traditional system, the overall tendency indicates reduced ester formation in continuous systems (Brányik et al., 2008). The lack of ES in continuous systems is believed to happen due to the low cellular metabolic activities in these systems (Willaert and Nedovic, 2006). This tendency might be due to incorrect aeration (lack of knowledge of k_La), yeast strain and cell physiology, process design (e.g. type of immobilization) (Brányik et al., 2008), ageing and/or genetic drift (especially in immobilized systems) (Sato et al., 2001), wort composition (specific gravity, lipid and FAN content) and process conditions (temperature, pH, agitation) (Dufour et al., 2003). However, some reports showed higher ES production in continuous immobilized cells systems (Van Iersel et al., 1999; Willaert and Nedovic, 2006). The theoretical explanation relates the ES increase with the low mass transfer and dissolved oxygen. This decrease reduces the immobilized yeast cells growth intensity and an increase in the availability of acyl-CoA for ES synthesis instead of fatty-acids formation occurs (Willaert and Nedovic, 2006). Shen et al, (2003) found a significant reduction (35%) of the amount of total fatty acids in immobilized yeast cells, which allowed the acyl-CoAs to be channelled for esters production (Shen et al., 2003). Moreover low fatty acids will have a less repressive effect on ATF1 gene considered one of main genes in coding ES formation (Shen et al., 2003).

II.4.2.1 Esters production in continuous AFBs

By analysing the commercial beers present in **Table II-4**, it is possible to observe that ES production in AFBs can be up to 30 times less than in regular beers. Moreover, to produce continuously AFBs low temperatures are normally applied (0 ºC to 12 ºC), which limit yeast growth, and also ES production. Van Iersel and his collaborators (1999)

observed better ES production at high temperatures (12 ºC) and low oxygen content. They also observed that the increase in ES content was related with a decreased of fatty acid content associated with an increase of enzyme activity (Van Iersel et al., 1999). Lehnert et al (2008) reported a dual effect from oxygen in ES production. They showed that increase in oxygen concentration leads to increase of HA content in AFBs, which is a substrate on ES production. However, per se, this increase on substrate concentration was not enough and was counter-balanced by low enzyme activity due to oxygen concentration, overall leading to no ES increase (Lehnert et al., 2008). Increasing oxygen transfer rate, the yeast cell uses different metabolic pathways that are related with cell division and not with ES production. Esters synthesis is a complex process involving many factors and is difficult to control. In order to solve this problem, mutants and genetically modified yeast might be a promising instrument to control flavour issues in continuous process (Verstrepen et al., 2001, 2003).

Reactor design may influence ES concentration in the final product, mainly in GLR where stripping of ES by the gas-phase may occur and lead to low ES concentration. Experiments proved that the physical removal of ES by stripping is reduced (below 30%) at dilution rates up to 0.3 h^{-1}. The exception was the ethyl caprylate (losses between 30% and 80%) (Macieira, 2008).

II.4.3 Organic acids

Organic acids (OA) in beer are derived from wort and yeast metabolism. The short carbon skeleton organic acids secreted by yeasts are derived from: (1) the incomplete turnover of TCA cycle and (2) the amino acids catabolism. OA reduce the pH during fermentation conferring a “sour” taste. In addition they provide an increase of microbial stability on the final product (Brányik et al., 2008; Selecky et al., 2008). It can be stated that the OA concentration in continuously systems should be such that does not influence beer flavour but keeps

a good microbial protection. There are few studies about OA formation during continuous beer production. The ones available report little difference in the total organic acid concentration. The control on OA concentration in continuous beer fermentation is similar to HA and is based on the regulation of cell growth and subtrate consumption rate. (Brányik et al., 2008, Smogrovicová and Domény, 1999; Yamauchi et al., 1995.)

II.4.3.1 Organic acids production in continuous AFBs

Working with TCA gene deficient yeast strains, Selecky et al. (2008) were able to produce AFBs with high saccharide concentration with low nitrogen utilization. But the low ethanol was compensated by a high OA formation mainly succinate, fumarate, lactic and malate. The observed high levels of lactic acid (144 mg/L to 495 mg/L) were considered important because it confers good protection against contamination and masks unacceptable worty off-flavours typical from AFBs (Selecky et al, 2008).

II.4.4 Aldehydes

Beer aldehydes arise mainly during wort production (mashing, boiling) and partially are formed during fermentation by yeast(Bartolomé et al., 2000). Aldehydes are very important due to their low threshold, which is hundred times less than the other compounds (see **Table II-4**). They contribute largely to the worty off-flavour detected particularly in low-alcohol beer produced by limited fermentation (Perpéte and Collin, 1999a, 1999b). Several aldehydes present in wort have been identified as responsible for worty off flavour in beers (3 methyl butanal, 2-methyl butanal, hexanal, heptanal).

Beers made by continuous fermentation show a slightly increased acetaldehyde content when comparing to conventional beers (Brányik et al., 2004; Mensour et al., 1997). Usually this is due to the fact that the majority of continuous systems show excess cell growth and/or over-

aeration. Acetaldehyde content has to be controlled either by proper oxygen supply (Brányik et al., 2006) or by prolonged maturation (Kronlöf and Linko, 1992). Higher rates of aldehyde reduction were observed at higher temperatures, but residence time appeared to be a major factor in determining residual aldehyde levels (Debourg et al., 1994; Van Iersel et al., 1995). It is also reported that the enzymatic mechanisms involved in aldehyde reduction capacity were not negatively affected (Debourg et al., 1995) or improved (Van Iersel et al., 2000) by influence of the immobilization method. Immobilized cells, due to higher glucose flux showed both higher aldehydes reduction and higher activity of alcohol dehydrogenase, comparing to free cell systems (Van Iersel et al., 2000).

II.4.4.1 Aldehydes production in continuous AFBs

As indicated before, in AFBs the presence of aldehydes is crucial for a balanced final beer flavour. In AFBs the flavour thresholds are believed to be more near water thresholds than in beer, mainly due to their low alcohol content (Perpète and Collin, 1999b). Wort aldehydes during batch fermentations are reduced relatively swiftly, but as continuous AFBs are normally limited fermentations some concerns arise. Among these, 2- and 3-methylbutanal, hydroxymethylfurfural (Bartolomé and al., 2000) and methional (Perpète and Collin, 1999) arise mainly from wort preparation (mashing).

Perpète and Collin (1999b) studied the aldehyde reduction in CCP using a PBR. After 8 h they found that aldehyde reduction is almost complete and it is influenced by temperature (85% at 28 °C and 60% at 0 °C), pitching rate and wort composition (binding effect of proteins). In a later article, the same authors found that methional (3-methylthiopropionaldehyde) was the key compound responsible for the worty, unpleasant, flavour of AFBs (Perpète and Collin, 1999b). This aldehyde derives from the reaction between methionine with glucose or maltose and has a high boiling point. So this compound has low losses during brewing process. Moreover, it is very hard to detect and has a

very low threshold: 1.7 ppb in water (Perpète and Collin, 1999b) and 250 ppb in beer (Meilgaard, 1975).

Acetaldehyde is also one of the important aldehydes found in beers because it is a precursor of many other compounds (HA, ethanol etc). Its formation is related with fermentation intensity. Therefore the acetaldehyde concentration increases with the increase of the oxygen transfer rate. As its formation is essential, acetaldehyde reduction is lower, however its reduction is generally higher than 85% and the final concentration is similar to the threshold in regular beers (10 mg/L, see **Table II-4**) (Lehnert et al., 2008). Nevertheless, if the final acetaldehyde concentrations obtained in continuous AFBs are compared with the threshold in water (0.025 mg/L) as suggested by some authors, and then its flavour influence can be relevant. Some studies have been made to measure the loss of aldehydes by stripping (physical mechanism)) in an iGLR and it was found that in this type of reactors, at lower dilution rates (below 0.2 h^{-1}), the aldehyde removal (by stripping) was good and higher than 65% (Macieira, 2008). During several continuously AFB fermentations using spent grains as carrier and different strains, it was always obtained an aldehyde reduction above the batch process (85% vs 65%) and no influence on the gas-phase (pure CO_2 vs Air/CO_2 mixture) was noted (Macieira, 2008).

II.4.5 Vicinal diketones

Among the ketones present in beer, the two vicinal diketones (VDK's): diacetyl (2,3-butanedione) and 2,3-pentanedione are those that are of extreme importance on beer off-flavour. Diacetyl is the most flavour-active, because it has a very low taste threshold of approximately 0.15 mg/L (Meilgaard, 1975). They are responsible for an unclean, sweetish taste in beer, which turns into a buttery off-flavour if in higher concentration (Willaert and Nedovic, 2006).

VDK's are produced during main fermentation from yeast metabolites (α-acetolactate and α-ketobutyrate) that are secreted into the green-

beer. These are produced as intermediates in the biosynthesis of the amino acids (isoleucine, leucine and valine – ILV pathway) (Lewis and Young, 1995; Willaert and Nedovic, 2006). During maturation phase, diacetyl is re-assimilated and reduced by yeast to acetoin and 2,3-butanediol, compounds with relatively high flavour thresholds (Meilgaard, 1975). The amount of diacetyl formed is related with the intercellular valine's concentration, but at high concentrations of valine there is an inhibitory effect on the enzyme responsible for α-acetolactate production (Petersen et al, 2004). Generally fermentation conditions that promote yeast growth are related with high production of α-acetolactate, thus high diacetyl concentrations (Willaert and Nedovic, 2006).

In most continuous beer fermentation produced using ICT, the amount of total diacetyl tends to be higher when comparing with traditional systems (Brányik et al, 2005; Willaert and Nedovic, 2006). Several explanations for this trend are: (1) change of cell physiology induced by the immobilization (increasing the expression of acetohydroxy acid synthetase gene); (2) alteration of amino acid (ILV pathway changes) metabolism in immobilized cells; (3) enhanced anabolic formation of amino acid precursors due to rapid yeast growth (Brányik et al, 2005).

In order to control and/or avoid the excessive VDK's formation during immobilized continuous fermentation, the control strategies include: (1) addition of α-acetolactate decarboxylase; (2) using of genetically modified brewer's yeast (encoding α-acetolactate decarboxylase); (3) control of operation conditions (Brányik et al, 2006; Godtfredsen et al, 1984; Kronlof and Linko, 1992; Yamauchi et al., 1995). Considering enzyme costs and the usual reluctance of consumers to the use of genetically modified organisms in food industry, other options should be used. These consist mainly in limiting the growth of immobilized yeast, process changes, and selection of an appropriate yeast strain. However control through growth regulation is difficult and was found to be ineffective (Brányik et al, 2006; Yamauchi et al., 1995). The main

reason because high diacetyl amounts are found in continuous maturated beer is due to the short times normally used in continuous maturation. Yamauchi et al (1995) suggested a strategy to reduce diacetyl effectively. This was obtained by applying an intermediate heat treatment between the primary and secondary fermentation (maturation). The heating was made under anaerobic conditions at 90 °C for 10 min prior to maturation. The main drawback was the necessity of implementing an aditional centrifugation step (to remove biomass) before heating treatment (Yamauchi et al., 1995).

II.4.5.1 Vicinal diketones production in continuous AFBs

As the temperatures used in continuous AFB production are normally low and the VDK's concentration depends on the yeast growth intensity normally the values of VDK's are below threshold for regular beers (**Table II-4**). At low temperatures the α-acetolactate production is lower and most of it is balanced to ILV pathway. Working at low temperature and low dissolved oxygen concentrations will decrease the VDK's production (Van Iersel, 1999).

II.5 References

Barker, M. G., and Smart, K. A. (**1996**). Morphological changes associated with the cellular aging of a brewing yeast strain. *Journal of the American Society of Brewing Chemists*, 54(2), 121–126.

Bartolomé, B., Pena-Neira, A. and Gómez-Cordovés, C. (**2000**). Phenolics and related substances in alcohol-free beers. *European Food Research and Technology*, 210(6), 419–423.

Bezbradica, D., Obradovic, B., Leskosek-Cukalovic, I., Bugarski, B., and Nedovic, V. (**2007**). Immobilization of yeast cells in PVA particles for beer fermentation. *Process Biochemistry*, 42(9), 1348-1351.

Briggs, D. E., Boulton, C. A., Brookes, P. A., and Stevens, R. (**2004**). Brewing Science and practice (p. 2547). Cambridge: Woodhead Publishing Limited.

Brányik, Tomás, Vicente, A. A., Machado Cruz, J. M., and Teixeira, J. A. (**2001**). Spent grains–a new support for brewing yeast immobilisation. *Biotechnology Letters*, 23(13), 1073–1078. Springer.

Brányik, T., Vicente, A. A., Dostálek, P., and Teixeira, J. A. (**2005**). Continuous beer fermentation using immobilized yeast cell bioreactor systems. *Biotechnology progress*, 21(3), 653-63.

Brányik, T., Silva, D. P., Vicente, A. A., Lehnert, R., Silva, J. B. A., Dostálek, P., and Teixeira, J. A. (**2006**). Continuous immobilized yeast reactor system for complete beer fermentation using spent grains and corncobs as carrier materials. *Journal of industrial microbiology and biotechnology*, 33(12), 1010-8.

Brányik, T., Vicente, A. A., Dostálek, P., and Teixeira, J. A. (**2008**). A review of flavour formation in continuous beer fermentations. *Journal of the Institute of Brewing*, 114(1), 3-13.

Brányik, T., Silva, D. P., Baszczyňski, M., Lehnert, R., and Almeida e Silva, J. B. (**2012**). A review of methods of low alcohol and alcohol-free beer production. *Journal of Food Engineering*, 108(4), 493-506.

Calderbank, J., and Hammond, J. (**1994**). Influence of higher alcohol availability on ester formation by yeast. *Journal of the American Society of Brewing Chemists*, 52(2), 84-90.

Czerny, M., Christlbauer, M., Christlbauer, M., Fischer, A., Granvogl, M., Hammer, M., Hartl, C., Hernandez, N. M. and Schieberle, P. (**2008**). Re-investigation on odour thresholds of key food aroma compounds and development of an aroma language based on odour qualities of defined aqueous odorant solutions. *European Food Research and Technology*, 228(2), 265-273.

Dufour, J.-P., Malcorps, P., And Silcock, P. (**2003**). Control of Ester Synthesis During Brewery Fermentation. In K. Smart (Ed.), *Brewing yeast fermentation performance* (2nd ed., pp. 213-233). Oxford: Blackwell Science.

Decamps, C., Norton, S., Poncelet, D., and Neufeld, R. J. (**2004**). Continuous pilot plant-scale immobilization of yeast in κ-carrageenan gel beads. *AIChE Journal*, 50(7), 1599-1605.

Doran, P. M., and Bailey, J. E. (**1986**). Effects of immobilization on growth, fermentation properties, and macromolecular composition of Saccharomyces cerevisiae attached to gelatin. *Biotechnology and Bioengineering*, 28, 73-87.

Dömény, Zoltan, Smogrovicová, D., Gemeiner, P., Sturdík, E., Pátková, J., and Malovíková, A. (**1998**). Continuous secondary fermentation using immobilized yeast. *Biotechnology Letters*, 20(11), 1041–1045.

GEA Process Engineering. (**2008**). Immocon - Rapid and continuous maturation of beer by means of immobilized yeast.

Junter, G. A., Coquet, L., Vilain, S., and Jouenne, T. (**2002**). Immobilized-cell physiology: current data and the potentialities of proteomics. *Enzyme and Microbial Technology*, 31(3), 201–212.

Kennedy, B. K., Austriaco, N. R., Zhang, J., and Guarente, L. (**1995**). Mutation in the Silencing Gene SIR4 Can Delay Aging in S. cerevisiae. *Cell*, 80, 485-496.

Lehnert, R., Kurec, M., Brányik, T., and Teixeira, J. A. (**2008**). Effect of Oxygen Supply on Flavour Formation During Continuous Alcohol-free Beer Production: A Model Study. *Journal of American Society of Brewing Chemist*, 66(4), 233-238.

Lehnert, R., Novák, P., Macieira, F., Kurec, M., Teixeira, J. A., and Brányik, T. (**2009**). Optimisation of Lab-Scale Continuous Alcohol-Free Beer Production. Czech. *Journal of Food Science*, 27(4), 267-275.

Lewis, M. J., and Young, T. W. (**1995**). *Brewing*. (M. J. Lewis and T. W. Young, Eds.). London: Chapman and Hall.

Macieira, F. F. (**2008**). Continuous fermentation of real alcohol-free beer. Master Thesis, University of Minho, Braga

Maskell, D., Kennedy, A., Hodgson, J., and Smart, K. (**2003**). Chronological and replicative lifespan of polyploid (syn. S. pastorianus). *FEMS Yeast Research*, 3(2), 201-209.

Masschelein, C. A., Ryder, D. S., and Simon, J.-P. (**1994**). Immobilized Cell Technology in Beer Production. *Critical Reviews in Biotechnology*, 14(2), 155-177.

Meilgaard, M. C. (**1975**). Flavour chemestry of beer: Part II: Flavour and Threshold of 239 aroma volatiles. *MBAA Technical Quarterly*, 12(3), 151-168.

Mensour, N. A., Margaritis, A., Briens, C. L., Pilkington, P. H., and Russell, I. (**1997**). New developemnts in the Brewing Industry using immobilized yeast cell biorector systems. *Journal of Institute of Brewing*, 103, 363-370.

Meura. (**2007**). The Meurabrew : the brewhouse of the future. Brochure. Retrieved at 12 th of December in 2010, from the website: http://www.meura.com/uploads/pdf/Meurabrew Paper.pdf

Monch, D., Krugwer, E., and Stahl, U. (**1995**). Effects of stress on brewery yeasts. *Monatsschr Brau*, 48, 288-299.

Narvátil, M., Dömény, Z., Šturdík, E., Šmogrovicová, D., and Gemeiner, P. (**2001**). Production of non-alcoholic beer using free and immobilized cells of Saccharomyces cerevisiae deficient in the tricarboxylic acid cycle. *Biotechnology and Applied Biochemistry*, 35(2), 133-140.

Narziss, L., Miedaner, H., Kern, E., and Leibhard, M. (**1992**). Technology and composition of non-alcoholic beers. Processes using arrested fermentation. *Brauwelt International*, 4, 396-410.

Nelson, J., and Griffin, E. G. (**1916**). Adsortion of invertase. *Journal of the American Chemical Society*, 38(5), 1109–1115.

Pajunen, E., Gronqvist, A., and Ranta, B. (**1991**). Immobilized Yeast Reactor Application in Continuous Secondary Fermentation in Industrial Scale Operation. *Proceedings of the European Brewing Convention Congress*, Lisbon (pp. 361-368). Lisbon: IRL Press: Oxford.

Pajunen, E., Tapani, K., Berg, H., Ranta, B., Bergin, J., and Lommi, H. (**2001**). Controlled beer fermentation with continuous on-stage immobilized yeast reactor. *28th EBC Congress*, Chapter 49 (pp. 1-12).

Perpète, Philippe, and Collin, S. (**1999a**). Fate of the worty favours in a cold contact fermentation. *Food Chemistry*, 66, 359-363.

Perpète, P, and Collin, S. (**1999b**). Contribution of 3-methylthiopropionaldehyde to the worty flavour of alcohol-free beers. *Journal of agricultural and food chemistry*, 47(6), 2374-8.

Pilkington, P., Margaritis, A., Mensour, N., and Russell, I. (**1998**). Fundamentals of immobilized yeast cells for continuous beer fermentation: a review. *Journal of the Institute of Brewing*, 104(1), 19–31. London: Harrison and Sons, 1904-.

Powell, C. D., Zandycke, S. M. V., Quain, D. E., and Smart, K. A. (**2000**). Replicative ageing and senescence in Saccharomyces cerevisiae and the impact on brewing fermentations. *Microbiology*, 146, 1023-1034.

Powell, C., Quain, D., and Smart, K. (**2003**). The impact of brewing yeast cell age on fermentation performance, attenuation and flocculation. *FEMS Yeast Research*, 3(2), 149-157.

Przybyla-Zawislak, B., Gadde, D. M., Ducharme, K., and McCammon, M. T. (**1999**). Genetic and biochemical interactions involving tricarboxylic acid cycle (TCA) function using a collection of mutants defective in all TCA cycle genes. *Genetics*, 152(1), 153.

Qun, J., Shanjing, Y., and Lehe, M. (**2002**). Tolerance of immobilized baker ' s yeast in organic solvents. *Enzyme and Microbial Technology*, 30, 721-725.

Repetto, B., and Tzagoloff, a. (**1990**). Structure and regulation of KGD2, the structural gene for yeast dihydrolipoyl transsuccinylase. *Molecular and cellular biology*, 10(8), 4221-32.

Sato, M., Watari, J., and Shinotsuka, K. (**2001**). Genetic instability in flocculation of bottom-fermenting yeast. *Journal of American Society of Brewing Chemist*, 59(3), 130-134.

Sato, T., and Tosa, T. (**1999**). Enzymes, Immobilization methods. In M. C. Flickinger and S. W. Drew (Eds.), Encyclopedia of Bioprocess Technology: Fermentation, Biocatalysis and Bioseparation (1st ed., pp. 1062-1064). New York: New York: John Wiley and Sons, Inc.

Selecky, R., Smogrovicova, D., and Sulo, P. (**2008**). Beer with Reduced Ethanol Content Produced Using Saccharomyces cerevisiae Yeasts Deficient in Various Tricarboxylic Acid Cycle Enzymes. *Journal Of The Institute Of Brewing*, 114(2), 97-101.

Shen, H., Moonjai, N., Verstrepen, K., and Delvaux, F. (**2003**). Impact of attachment immobilization on yeast physiology and fermentation performance. *Journal of the American Society of Brewing Chemists*, 61(2), 79–87.

Sinclair, D a, Mills, K., and Guarente, L. (**1998a**). Molecular mechanisms of yeast aging. *Trends in biochemical sciences*, 23(4), 131-4.

Sinclair, David, Mills, K., and Guarente, L. (**1998b**). Aging in Saccharomyces. *Annual Reviews in Mibrobiology*, 52, 533-60.

Smogrovicová, D., and Domény, Z. (**1999**). Beer volatile by-product formation at different fermentation temperature using immobilized yeasts. *Process Biochemistry*, 34(8), 785-794.

Soares, E. V., and Mota, M. (**1996**). Flocculation onset, growth phase, and genealogical age in Saccharomyces cerevisiae. *Canadian Journal of Microbiology*, 42(6), 539-547.

Taipa, M. A., Cabral, J. M. S., and Santos, H. (**1993**). Comparison of glucose fermentation by suspended and gel-entrapped yeast cells: An in vivo nuclear magnetic resonance study. *Biotechnology and Bioengineering*, 41, 647-653.

Virkajärvi, I., And Kronlöf, J. (**1999**). Long-term stability of immobilized yeast columns in primary fermentation. *Journal of the American Society of Brewing Chemists*, 56(2), 70-75.

Van Iersel, M. F. M., Meersman, E., Swinkels, W., Abee, T., and Rombouts, F. M. (**1995**). Continuous production of non-alcohol beer by immobilized yeast at low temperature. *Journal of Industrial Microbiology and Biotechnology*, 14(6), 495–501.

Van Iersel, M. F. M., Van Dieren, B., Rombouts, F. M., and Abee, T. (**1999**). Flavour formation and cell physiology during the production of alcohol-free beer with immobilized Saccharomyces cerevisiae. *Enzyme and Microbial Technology*, 24(7), 407–411.

Verbelen, P. J., De Schutter, D. P., Delvaux, F., Verstrepen, K. J., and Delvaux, F. R. (**2006**). Immobilized yeast cell systems for continuous fermentation applications. *Biotechnology letters*, 28(19), 1515–1525.

Verstrepen, K J, Derdelinckx, G., Delvaux, F. R., Winderickx, J., Thevelein, J. M., Bauer, F. F., and Pretorius, I. S. (**2001**). Late fermentation expression of FLO1 in Saccharomyces cerevisiae. *Journal of American Society of Brewing Chemist*s, 59(2), 69-76.

Verstrepen, Kevin J, and Klis, F. M. (**2006**). Flocculation, adhesion and biofilm formation in yeasts. *Molecular microbiology*, 60(1), 5-15.

Verstrepen, Kevin J, Derdelinckx, G., Dufour, J.-P., Winderickx, J., Thevelein, J. M., Pretorius, I. S., and Delvaux, F. R. (**2003**). Flavour-active esters: adding fruitiness to beer. *Journal of bioscience and bioengineering*, 96(2), 110-8.

Virkajarvi, I. (**2001**). Feasibility of continuous main fermentation of beer using immobilized yeast. Vtt Publications. Technical Research Centre Of Finland Espoo.

Virkajarvi, I., and Linko, M. (**1999**). Immobilization: A revolution in traditional brewing. *Naturwissenschaften*, 86(3), 112–122.

Willaert, R., and Nedovic, V. (**2006**). Review Primary beer fermentation by immobilized yeast – a review on flavour formation and control strategies. *Journal of Chemical Technology and Biotechnology*, 81, 1353-1367.

Yamauchi, Y., Okamoto, T., Murayama, H., Nagara, A., Kashihara, T., Yoshida, M., Yasui, T., et al. (**1995**). Rapid Fermentation of Beer Using an Immobilized Yeast Multistage Bioreactor System. *Applied Biochemistry And Biotechnology*, 53.

III. Chapter III – Selection of the Best Immobilization Carrier for Brewing Yeast Cells

III.1 Objectives

When implementing a continuous fermentation system using ICT it is necessary to consider some aspects such as: carrier properties, immobilization mechanism and the reactor configuration. One of the main problems when continuous primary beer fermentations are performed is the time that takes for bioreactor start-up (7 to 15 days) i.e., the time that is necessary for the bioreactor to have enough immobilized biomass (iBio) that allows working at high dilution rates (Brányik et al., 2001). If the initial amount of cells adsorbed to the carrier is increased, the start-up time will be reduced. Adsorption depends on many factors and occurs naturally in yeast cells and is more than a simple and physical mechanism. It is a dynamic process until the equilibrium between cell-carrier attachment and detachment processes is reached.

In this chapter the main objective was to study the influence of carrier type (spent grains and corncobs) and of their degree of derivatization on the initial adsorption of yeast cells. In addition, for corncobs it was studied the influence of their size, as well as the influence of different pre-treatment methods and the degree of derivatization on: (1) ion exchange and (2) corncobs adsorption capacity.

III.2 Introduction

III.2.1 Immobilization of biocatalysts: history and application

Bioprocesses using immobilized biocatalysts (enzymes/cells) have been receiving increasing worldwide attention because of their benefits of low environmental pollution and economical utilization of natural resources and energy (Sato and Tosa, 1999). The pioneer work of Nelson and Griffin (1916) in the early XX century was the first demonstration of immobilized biocatalysts (Nelson and Griffin, 1916). At the present, immobilized biocatalysts have contributed to a wide variety

of fields in industry like the production of energy by biological process or production of useful compounds (Sato and Tosa, 1999). Over the last forty years, many biotechnology processes based in immobilized cells systems have been studied. Particularly an increase in the development of immobilized cells systems occurred since the early 1980s (Junter and Jouenne, 2004). These systems can occur naturally by spontaneous adsorption or artificially by entrapment and attachment techniques.

Cell immobilization can be defined as the physical confinement of a microorganism in a certain defined region of space with retention of its catalytic activities, which can be used in repetitive or continuous processes (Junter and Jouenne, 2004). Cell immobilization methods were originally adapted from those earlier applied into enzyme immobilization. The main advantage from using cells instead of enzymes is to avoid the extraction/purification steps. These steps reduce enzyme activity, stability and cost. Actually immobilized cells systems are applied in many different fields, such as the biosynthesis and bioconversions of several products (enzymes, antibiotics, amino acids, OA, alcohols and polysaccharides); environmental processes (biofertilization, bioremediation); food processing (beer, wine, lactose hydrolysis); biosensors (amino acids cholesterol, toxicity tests, metals) (Junter and Jouenne, 2004).

III.2.2 Continuous high cell density systems

The major advantage of using immobilized cells systems over conventional (suspended cells) cultures is that it allows working with high cell density systems and turns easy the application of continuous processes. The main advantages and disadvantages of continuous processes using ICT over suspended cells cultures are summarized in **Table III-1** (Gama et al., 2003; Kourkoutas et al., 2004; Sato and Tosa, 1999; Verbelen et al., 2006; Virkajarvi and Linko, 1999).

The most important advantage indicated in **Table III-1** is the high reactions rates obtained (due to high dilution rates used) in continuous

processes using ICT. The economic benefits are the driving force for the recent increase of continuous biotechnology processes. Although some disadvantages can be observed, immobilized cells systems are a key technology used to perform efficient continuous bioprocesses (Gama et al., 2003; Sato and Tosa, 1999; Verbelen et al., 2006).

Table III-1. Continuous biotechnology processes using ICT: main characteristics

Advantages	Disadvantages
High cell concentration in bioreactor	By-products formation
Higher reaction rates	Low permeation to substrates
Biocatalytic regeneragion activity	Higher nutrients and energy requirement
Utilization of high dilution rates without washout	Risk of product contamination by cells leaked from carriers
Improve product consistency	Low production due to mass transfer limitation
Increased cell activity during storage	Ageing of cells in a long-term fermentation (months)
Reusability of the biocatalyst	Hygienization and contamination
Higher specific product yields	
Controlled microenvironment	
Maintaining of catalytic activity	
Easier downstream processing	

III.2.3 Immobilization methods

The selection of the appropriate immobilization method is necessary and has a crucial role in the final performance of the immobilized cells system. Therefore it is very important to know the different immobilization methods. They can be divided into five categories: carrier – binding (eg. Cells attached to a surface); cross – binding (eg.: agents that induce cell flocculation); entrapment (eg.: Cells inside a porous matrix); mechanical containment behind a barrier (eg.: microencapsulation) and combined methods. Each method has its merits and faults. This is why the choice of an appropriate method is so important and should take into account the purpose of immobilization,

cells characteristics, type of reaction and reactor design (Brányik et al., 2004; Sato and Tosa, 1999; Verbelen et al., 2006; Kobayashi et al., 1998)

The carrier-binding method is based on the attachment of biocatalysts to water-insoluble carrier surface through a covalent/ionic bond, physical adsorption and biospecific binding. The covalent-binding method is usually applied to immobilized enzymes, due to the toxicity of the agents needed for formation of covalent bonds, and the difficulty in finding the ideal conditions for cell immobilization. The cell surface has some reactive components (proteins, saccharides), which can be used for covalent bonding between cells and a modified or activated carrier. Physical adsorption is usually preferred in ICT for the production of alcohol beverages over the use of inducers that may interfere with the process. The adsorption occurs naturally by the attachement of cells to carriers and it is sensitive to environmental factors such as: pH, ionic strength, concentration of reactants and temperature. The phenomena involved are primarily based on Van der Waals forces, ionic and hydrogen bonds, hydrophobic interactions between cell surface and the carrier (Brányik et al., 2004; Sato and Tosa, 1999; Verbelen et al., 2006; Kobayashi et al., 1998).

The cross-linked method uses bi- or multifunctional reagents but not carriers as the previous method. Reagents are used to link cells with each other and cell pellets are formed. Among these reagents, glutaraldehyde, toluene diisocyanate and hexamethylene diisocyanate are commonly used. A particularly case of cross-linked may occurs in yeast cells: flocculation. Yeast flocculation is characterized by cell-cell aggregation. It is a reversible and calcium dependent process in which cells adhere to form flocs/pellets. It involves proteins that selectively bind mannose residues present on the cell walls of yeast cells (Brányik et al., 2005; Kobayashi et al., 1998; Kourkoutas et al., 2004; Verbelen et al., 2006).

In the entrapment method, the cells are placed within a confined matrix. The entrapment of cells can be done by natural diffusion of cells

into a porous matrix or the porous matrix is synthesized around cells (Ca-alginate, agar etc). This is a very popular method for cell immobilization but has some disadvantages: (1) low mass transfer rates and (2) low renewable capacity of carrier (Gama et al., 2003; Sato and Tosa, 1999; Verbelen et al., 2006).

Mechanical containment of cells behind a barrier is achieved by using microporous membrane filters, cell entrapment in microcapsule, or by cell immobilization in the interaction surface of two immiscible liquids. Containment of cells using microporous membrane might be used in continuous processes, but membrane-clogging issues can arise.

Sometimes different mechanisms of cell immobilization inside a reactor may occur. For instance, yeast cells immobilization can occur by natural adhesion inside carrier cavities and at same time yeast flocculation/sedimentation of cells can be also present (Brányik et al., 2004; Verbelen et al., 2006). Therefore, it is very important not only to select but also to understand all immobilization mechanisms involved in the studied system. Thus, to perform a continuous fermentation where high cell density system is present all these concerns about cell immobilization type, techniques and methods should be considered.

III.2.4 Carrier properties and specific characteristics

When immobilized cells systems are applied is very important to choose the correct carrier/surface where cells can be immobilized. The carrier should be: cheap; inert, i.e., should not have any influence on the process; regenerable i.e., able to be used several times; applicable at large scale; stable (mechanical, thermal, chemical and biological); and food grade (on food industry applications). In addition, the carrier should have a big surface area, with functional groups allowing high cells loads without affecting cell activity and with minimal mass transfer limitations (Brányik et al., 2005; Kobayashi et al., 1998; Kourkoutas et al., 2004; Verbelen et al., 2006).

There are different carriers that can be used for immobilization of cells such as: porous glass (Virkajarvi et Pohjala, 2000); Ca-alginate (Dömény et al., 1998); PVA particles (Bezbradica et al., 2007); spent grains (Brányik et al., 2001); and wood chips (Virkajarvi et Linko, 1999). Recently cellulose-based carriers have been used for cell immobilization thanks to their advantageous properties as: high cell loading, high availability and thermal stability (Fujii et al., 1999). In the case of spent grains, the immobilization mechanism consists of mechanical retention in pores and cavities, hydrophobic forces that lead to a stable cell-carrier adhesion, and flocculation-like cell-cell interactions (Brányik et al., 2005) are involved as well.

III.2.5 Spent grains and corncobs: cellulose-based carriers

In this thesis only two carriers were used: spent grains (SG) and corncobs (Cc). In this particularly chapter we evaluate the capacity of Cc and SG as a carrier for yeast cell immobilization.

III.2.5.1 Corncobs

Corncobs are cellulose-based material that makes them a suitable material for immobilization. It is cheap and available in a large amount. According to the Food and Agriculture Organization of the United Nations (FAO, 2008), the annual production of corn cobs worldwide is about 695x109 kg, meaning that for every 100 kg of corn grain approximately 18 kg of corn cobs are produced (Torre et al., 2008).

III.2.5.2 Spent grains

Spent grains are the most produced brewing by-product and represents about 85% (wt./wt.) of total by-products generated by brewing industry. On average SG represents 31% (wt./wt.) of the original malt weight, and are produce approximately 20 kg per 100 L of beer. SG are available at low or no cost throughout the year, because beer is not a seasonal product like wine. So SG are produced

continuously in large quantities. SG consist of the husk–pericarp–seed coat layers that cover the original barley grain, being rich in cellulose and non-cellulosic polysaccharides, lignin, some proteins and lipids. The chemical composition of SG varies according to: barley variety, harvest, malting and mashing conditions, region, quality and type of adjuncts added. In general, SG are considered as a lignocellulose material rich in protein and fibre. (Mussatto et al., 2006)

When SG are discarded from brewing industry (also called barley spent grains) they have an 80% (wt./wt.) content in water. As a result it has a low biological stability (≈ 30 days storage). Among the several processes to increase the shelf-life of SG, drying is the most succeeded one. Drying not only increases SG shelf-life, but also reduces their weight and consequently transportations costs (Mussatto et al., 2006). Due to SG properties (protein and fiber content), it can be used for several applications such as food ingredient for human (high protein flour); animal nutrition (cattle feed); energy production (biogas); charcoal production; brick component; paper manufacture; adsorbent (volatile organic compounds, cadmium, lead, chromium). SG have also applications in biotechnology processes as: substrate for cultivation of microorganisms and enzyme production; carrier in brewing (pre-treated); source of added-value products.

Table III-2. Chemical composition of SG. (from Mussatto et al., 2006)

Component	% (dry weight)
Cellulose	16.8 – 25.4
Arabinoxylan	21.8 – 28.4
Lignin	11.9 – 27.8
Protein	15.2 – 24.0
Lipid	0.0 – 10.6
Ash	2.4 – 4.6

Among all described applications, SG can be used as carrier in continuous brewing primary fermentation (Brányik, et al., 2001; Brányik et al., 2002). SG obtained by Brányik et al (2001) after pre-treated with HCl and NaOH (acid/base treatment) are considered to have ideal

conditions for yeast cells immobilization. The advantages of SG as carrier are: high yeast loading capacity without requiring chemical modification, regenerable (using NaOH solution), inert under fermentation conditions, highly available, cheap (not requiring significant treatments) (Brányik et al., 2001). The process is very laborious and has a low yield (10% from raw dry SG), which is considered a main disadvantage of pre-treated SG (Brányik et al., 2001). Considering raw SG water content and acid/base method yield, for each 100 kg of raw SG leaving brewing industry only 2 kg of treated SG can be obtained. However it is suggested that for industrial applications only NaOH treatment (base treatment) can be applied to clean the raw SG (Brányik et al., 2001).

Brányik et al. (2004) performed an extensive study of SG physicochemical properties. It showed that SG are wettable, hydrophobic particles, with surface negative charged. The same authors found that base-treated SG were less wettable and then more hydrophobic than acid/based-treated SG (Brányik et al., 2004).

III.2.6 Chemical modification of carriers

The chemical modification of the carrier surface can increase cell immobilization, through intensification of the binding between cell surface and carrier (Brányik et al., 2001; Fujii et al., 1999). Several products can be used to increased cell immobilization in surfaces, as: diethylaminoethyl (DEAE) (Al-adhami et al, 2002; Brányik et al., 2001; Fujii et al., 1999), 2-diethylamino-ethylchloride hydrochloride (DEC) (Antrim and Harris, 1991), polyethylenimine (D'Souza and Melo, 2001; D'Souza et al, 1986; Melo et D'Souza, 1999), poly(styrene-ran-sulfonic acid)(Fujii et al., 1999), polystyrene fibers (Yoshioka et Shimamutra, 1986) and polyethyleneimine cellulose (PEIC) (Fujii et al., 1999). SG and Cc are cellulose-based materials that can be derivatized in order to increase their ion exchange capacity (IEC), *i.e.*, to increase the attractiveness of its surface for cell adhesion.

DEC solution has been successfully tested by Antrim and Harris for derivatization of cellulose (1991). The derivatization method used has been originally proposed in the field of enzyme immobilization. It is a process for increasing adsorption capacity of granular cellulosic ion exchange composites in order to improve the product concentration (Antrim and Harris, 1991). Considering that the outer membrane of yeast cells is full of proteins, it is believed that this method can be applied for cell immobilization, as other methods for enzyme immobilization were before (Junter and Jouenne, 2004).

III.3 Material and Methods

III.3.1 Determination of corncobs chemical composition

After being dried at 40 ºC in an oven for 12 h, the Cc were cut into small pieces (1-3 cm in length), milled in a knives' mill to pass through a 0.4 mm screen for the determination of their chemical composition. Two grams of milled Cc were treated with 10 mL of 72% (vol./vol.) H_2SO_4 under stirring at 45 °C for 7 min. The mixture was autoclaved for 30 min at 1.05 bar for the complete hydrolysis of oligomers. After filtration through a Sep-Pak C18 cartridge (aromatic compounds removal), the hydrolysate was analyzed in a MetaCarb 67H column at 45 °C using a Shimadzu chromatograph with refractive-index detector. The mobile phase was 0.005 mol/L H_2SO_4 at 0.6 mL/min flow rate. Sugar concentrations, reported as glucan and xylan, were determined from calibration curves obtained with pure compounds. Lignin was determined by gravimetric analysis (Rocha, 2000).

III.3.2 Carrier particles for immobilization

For immobilization experiments the Cc were cut into three different sizes: (1) cylinders (± 0.6 cm high), (2) the same cylinders were cut into ¼ of cylinders and (3) milled material (d < 0.05 cm). The main characteristics of the particles are depicted in the **Table III-3**.

Table III-3. Main size characteristics of the corn cob and SG particles used for immobilization experiments

Carrier Particle	Diameter / cm	Height / cm	Volume / cm^3
Cylinders (Cc1)	2.22 ± 1.8	0.60 ± 0.02	2.34 ± 0.4
1/4 Cylinder (Cc2)	1.13 ± 0.1	0.60 ± 0.02	0.60 ± 0.1
Milled (Cc3)	0.1 and 0.05	---	$5.24x10^{-4}$ and $6.54x10^{-5}$
SG	0.3 and 0.1	---	---

III.3.3 Derivatization method

Ten grams of carrier (Cc or SG) were placed into an Erlenmeyer flask with 285 mL of deionized water. The suspension was stirred and heated at 40 °C and then 86 g of Na_2SO_4 and 12 g of NaOH were added. Subsequently 20 g of DEC solution (25, 50, and 75% (wt./vol.)) were added at 40 °C during two hours (2 h) period. The mixture was then stirred for 30 min at 40 °C. It was followed by new addition of 10 g of NaOH and 20 g of DEC solution (25, 50, and 75% (wt./vol.)) at 40 °C for a two hours (2 h) period. The final mixture was stirred for 30 min at 60 °C. The mixture was cooled and the pH adjusted to 6.5 using 30% (vol./vol.) H_2SO_4 solution. The derivatized carrier was washed with distilled water and dried at 60 °C.

III.3.4 Pre-treatment of carriers

III.3.4.1 SG preparation

The hydrolysis of residual starchy endosperm and embryo of the barley kernel present in the raw SG was done according to the method proposed by Brányik et al (2001). Raw SG (100 g) were mixed in 1500 mL of 0.35 M (3% (vol./vol.)) HCl solution for 2.5 h at 60 °C. The mixture was cooled and washed with water. The remaining solids (mainly the husks of the barley grain), were partially delignified by shaking (120 rpm) in 500 mL of 0.5 M NaOH at 30 °C for 24 h. After being washed several times with water until neutral pH and dried, the carrier (± 10 $g_{DRY\ BASE}$) was ready to be used. The preparation procedure gives 10% (wt./wt.) yield from dry SG. The drying steps applied in the preparation procedure were necessary only in order to quantify the yields (Brányik et al., 2001).

III.3.4.2 Cc pre-treatment A

Dry Cc (20 g) were added to 300 mL of 1% (v/v) of HCl for 1 h at 60 °C. Then the Cc were washed with distilled water and was added

1% (w/v) of NaOH. The mixture was stirred for 5 h at 120 rpm. The carrier was then cleaned again with distilled water until neutral pH and dried at 40 ºC. This pre-treatment was performed to three Cc conformations (see **Table III-3**). This method provides a yield of 80%, 50% and 20% of Cc1, Cc2, and Cc3 particles respectively.

III.3.4.3 Cc pre-treatment B

Dry Cc (20 g) were added to 2000 mL of distilled water and autoclave for 15 min at 121 ºC (1.05 bar). After cooling the carrier was washed with distilled water and added to 300 mL of 1% (wt./vol.) of NaOH (0.25 M) for 1 h at 120 rpm. Then Cc were cleaned with distilled water until neutral pH. This pre-treatment was performed to three Cc conformations (see **Table III-3**). This method provides a yield of 80%, 50% and 20% of Cc1, Cc2, and Cc3 particles respectively.

III.3.5 Conditions tested

Table III-4 presents all the different conditions made to select the best carrier for yeast cells immobilization.

Table III-4. All conditions (Derivatizations/Pretreatments) used for adhesion tests

Method/Carrier	Cc1	Cc2	Cc3	SG*
0% (wt./vol.) DEC	√	√	√	√√
25% (wt./vol.) DEC	√	√	√	√
50% (wt./vol.) DEC	√	√	√	√√
75% (wt./vol.) DEC	√	√	√	√
Cc Pre-Treatment: A	√√	√√	√√	-
Cc Pre-Treatment: B	√√	√√	√√	-
Cc Method: A + 50% (wt./vol.) DEC	√√	√√	√√	-
Cc Method: B + 50% (wt./vol.) DEC	√√	√√	√√	-

√ - Adhesion test only.
√√ - Adhesion test and Immobilization test with yeast growth.
* All SG used were pre-treated accordingly Brányik et al. (2001).

III.3.6 Medium and microorganisms

Yeast cells used in this chapter were *Saccharomyces cerevisiae* CCMI 890 (Culture collection of industrial microorganism of INETI, Lisbon, Portugal). The medium composition used throughout this chapter is presented in **Table III-5**.

Table III-5. Medium Composition

Component	Concentration / (g/L)
Glucose	20
Yeast Extract	1
MgSO4.7H2O; 5	0.4
KH2PO4	5
NH4SO4	2

III.3.7 Adsorption tests

Growth medium was inoculated and incubated for 12 h at 30 ºC and 150 rpm. The medium was then centrifuged and the supernatant was discarded. The pellet was re-suspended in 200 mL of distilled water and the optical density (O.D.) was measured at 600 nm ($O.D._0$) using a Tecan Sunrise 96 well Microplate Reader (Tecan Group Ltd., Männedorf, Switzerland). The cellular suspension was added to 3 g of carrier and samples of cell suspension were taken every 5 min ($O.D._i$) until O.D. stabilization – Method A (**Figure III-1**). After O.D. stabilization the carrier was gently separated from solution, washed and the amount of attached biomass was determined by dry weight method proposed by Brányik et al (2002b) – Method B. The amount of immobilized biomass (iBio in mg_{BIO}/g_{DC}) by method A was determined from **Eq. III-1**:

$$iBio = \frac{W_{Free\ Bio(i)} - W_{Free\ Bio(0)}}{W_{Carrier\ (Dry\ Base)}} \qquad \textbf{Eq. III-1}$$

Where $W_{Free\ Bio\ (i)}$ is the weight of free biomass at time=0,..,I determined from O.D. vs $C_{Biomass}$ (g/L) calibration curve.

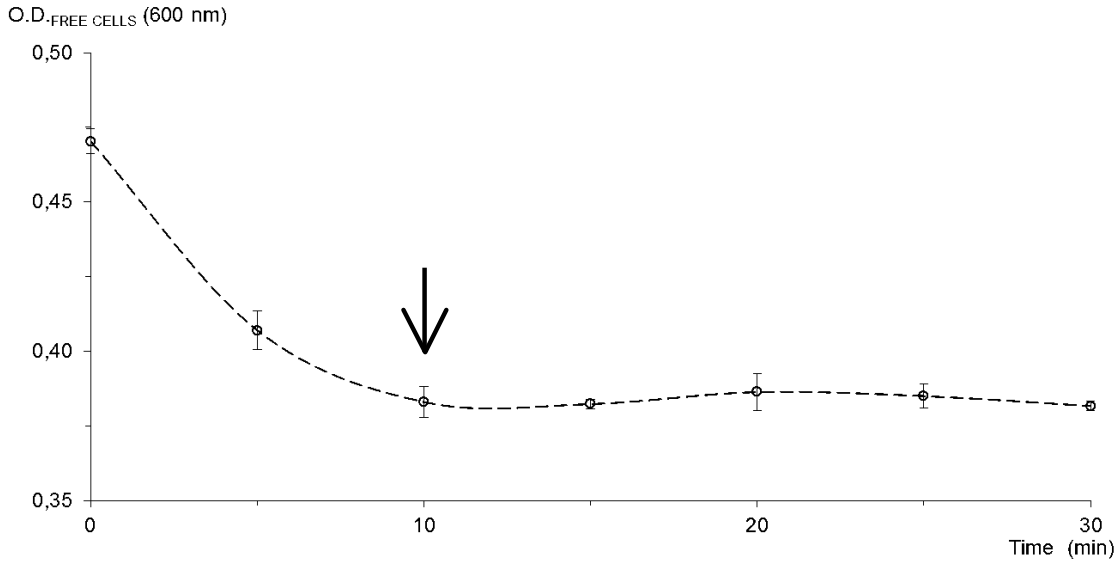

Figure III-1. Evolution of optical density of free cells during immobilization time, obtained for Cc2 particles derivatized with 50% (w/w) DEC solution.

III.3.8 Immobilization with yeast growth test

An Erlenmeyer flask containing 180 mL medium and 1.5 g of carrier was inoculated with 20 mL of previously prepared yeast cells suspension. After 12 h of inoculation time, O.D. at 600 nm was determined. The medium was removed by filtration (Whatman nr 1, Maidstone, UK) and the biocatalyst (carrier + immobilized cells) was collected. The biocatalyst was then washed with 400 mL of water and filtered. After filtration the biocatalyst was palced in an Erlenmeyer flask with 100 mL of medium and stirred strongly (600 rpm). Samples of O.D. are taken until stabilization – Method C. After stabilization, the liquid was removed and the carrier washed. Finally, the carrier was dried (40 °C) and weighted to calculate carrier losses.

III.4 Results and Discussion

III.4.1 General considerations

In this section the results from the performed tests (**Table III-4**) are presented and discussed. In order to achieve the main aim of carrier selection some considerations were taken into account and are the base of future discussion. These considerations include the main characteristics that a carrier particle should have to be successfully applied in a continuous primary fermentation of AFB. Both SG and Cc are cellulose-based, cheap, and available in large scale. The need to pre-treated SG particles is considered to be a drawback inherent to this carrier.

Chemical modification of cellulose-based fibres has been developed to increase initial yeast cells adhesion to the carriers. In our work we used the method proposed by Antrim and Harris (1991) . Initially the minimum concentration of DEC solution that increases cell immobilization was determined (**Table III-4**) in non-treated Cc carrier particles.

After this, Cc pre-treatments were performed (see sections 0 and III.4.5). The main objective of using these two pre-treatments was to increase both the cellulose content and porosity (cavities) to achieve a more efficient initial yeast cells adsorption. The pre-treatment A is a modification of SG's pre-treatment. Initially the hemicellulose and startch attached to Cc particles was removed with HCl followed by a delignification with NaOH. The conditions applied to SG could not be used in Cc because they were too aggressive and destroyed all Cc particles. On the other hand, the pre-treatment B is based in auto-hydrolysis and delignification (NaOH) methods to hydrolyzed hemicelluloses (Ruiz et al., 2011). Usually the conditions used in auto-hydrolysis and delignification methods are more aggressive (higher temperatures) than the conditions used in this work. The auto-

hydrolysis main aim is to produce a substrate to be used in both saccharification processes and cellulase production (Ruiz et al., 2011). In our case, we wanted only to use it for yeast cells immobilization so the objective was to do a less extensive and less costly pre-treatment to increase the immobilization capacity without reducing significantly the shape and mechanical resistance of Cc particles. Therefore less aggressive conditions than those normally applied in auto-hydrolysis methods were chosen.

Finally, in the adhesion tests, the method used to measure cell adhesion was the reduction of O.D. (at 600 nm) of free cells in distilled water during time – Method A (**Figure III-1** and **Eq. III-1**). This method is based on the assumption that all cells that are not free are adsorbed on the carrier. This is supported by the short time of this kind of tests (maximum of 30 min), which avoids the influences of cellular growth and death rates. The method proposed by Brányik et al (2004) – Method B – was not used in this case because the error present in Cc and SG particles due to carrier losses (around 10%) was too big considering the low amount of yeast cells that are initially attached (Brányik et al., 2004). For the same reason, when immobilization tests with yeast cells growing were made the method used was a mechanical method initially proposed by Brányik et al (2001) – Method C.

III.4.2 Corncob composition

Before immobilization tests, Cc chemical characterization was performed. The composition of Cc particles is given in **Table III-5**.

The results are given as the content of glucan (corresponding to cellulose), xylan and acetyl groups (both corresponding to hemicelluloses), and soluble lignin and Klason lignin (corresponding to total lignin). These data is in good agreement with other results reported earlier (Garrote et al., 2002).

Table III-5. Chemical composition of the Cc particles

Compounds	Corn Cobs (%)
Cellulose	31.8 ± 0.8
Glucan	31.8 ± 0.8
Hemicelluloses	33.6 ± 1.1
Xylan	29.4 ± 0.2
Acetyl Group	3.1 ± 0.4
Total Lignin	27.9 ± 0.4
Soluble Lignin	11.3 ± 0.2
Klason Lignin	16.6 ± 0.4
Total weight	92.2 ± 0.9

III.4.3 Selection of best DEC concentration

The derivatization method proposed by Antrim and Harris (1999) was used in order to increase the Cc and SG adsorption capacities by increasing their ion exchange capacity (IEC). In **Figure III-2A** the values of IEC obtained for the three different shapes of Cc and SG at different concentrations of the derivatization agent (DEC) are shown.

Figure III-2A shows that, generally, the derivatization increased slightly the IEC of Cc particles. It also shows that there is a size effect of the Cc particles on IEC, being this effect higher for smaller particles (Cc3 and SG). This result was expected in these particles due to their higher superficial area. The highest IEC was obtained for SG particles. To obtain a more effective derivatization, i.e., to achieve a good IEC by derivatization of cellulose-based carriers, the cellulose must be available. In the case of Cc, cellulose represents ca 30% of its composition (**Table III-5**) while in pre-treated SG it represents 90% (wt./wt.) (Brányik et al., 2004). Being so, is not strange that for SG the increase of IEC was more effective than for Cc. For concentrations above 50% of DEC solutions, the IEC in Cc did not increase as much as expected. This might be due to the cellulose amount in Cc, which is limited. So the higher DEC concentration has no effect on the degree of derivatization of Cc particles.

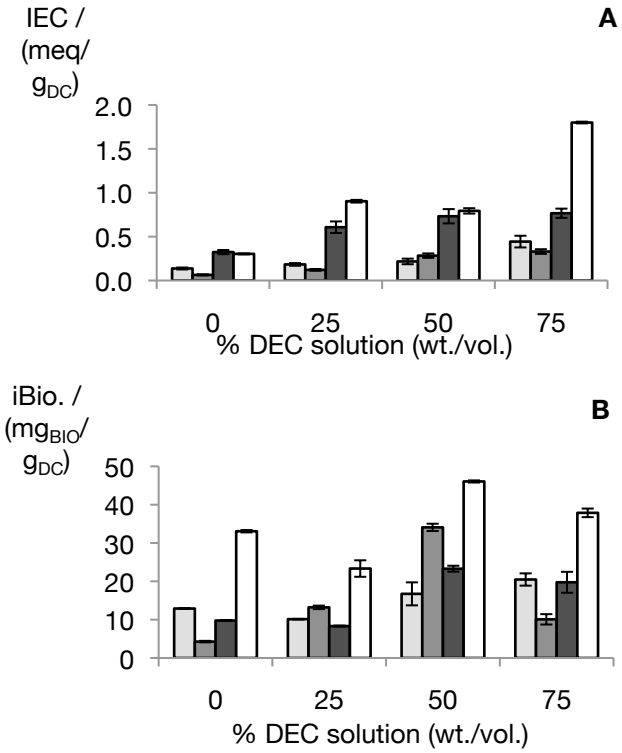

Figure III-2. A: Ion exchange capacities (IEC) of different carrier particles at different concentrations of DEC solution. B: Influence of derivatization on the immobilized biomass (iBio) for different carriers. Legend: ■ - Cc1; ■ - Cc2; ■ - Cc3; □ - SG.

Brányik et al. (2001) used SG as immobilization carrier for fermentation in bubble columns and obtained values of IEC between 0.45 and 0.8 meq/g_{DC}. Cc1 and Cc2 particles showed lower IEC when compared with SG, which is an indication that these particles have lower adsorption capacity than SG and Cc3. Up to 50% (wt./vol.) of DEC solution the values of IEC for Cc3 (IEC: 50% DEC=0.73 meq/g_{DC}) and SG (IEC: 50% DEC=0.79 meq/g_{DC}) are similar to those reported in literature. For SG the maximum IEC (1.8 meq/g_{DC}) was obtained when 75% (wt./vol.) were used. In order to analyze cellulose-based carriers with similar IEC and sizes, and based in the results presented in **Figure III-2A**, the concentration of 50% (wt./vol.) of DEC solution was selected as the best compromise.

In **Figure III-2B** it is possible to verify that for Cc2, Cc3 and SG the derivatization increased the carriers' load capacity for concentration of DEC solutions above 50% (wt./vol.). On the other hand for Cc1 particles

there was no real difference of immobilization for the non–derivatized and derivatized carrier. The low values of yeast cells adhesion ($iBio_{MAX}$=20 mg_{BIO}/g_{DC}) in these particles can be also explained by their size. They are bigger and the area in contact with the cell suspension is lower thefore less immobilization is expected to occur.

The values of immobilization, taking in account the technique used in this work, are considered good. It must be pointed out that this method is used only for adsorption of yeast cells and does not allow the complete formation of yeast biofilm due to the absence of cell growth.

The results obtained when the adsorption time is evaluated also help sustaining this statement. The adsorption time is the time that is needed to achieve the equilibrium between cells adsorption/desorption in each assay. The time of adsorption is determined when the results of O.D. are stabilized, i.e., when the values of O.D. of free cells are less than 10% of the O.D. final value (see **Figure III-1**). The adsorption time is a qualitative data, which can be used to evaluate the time of adsorption in a real fermentation. **Table III-6** presents the adsorption times for each assay.

In general, the adsortion time increases with the increased concentration of DEC solution due to high load capacity of derivatized particles, which need more time to achieve the equilibrium between adsorption and desorption.

Table III-6. Immobilization time (min) for different types of carrier.

% (wt./vol.) DEC solution	Immobilization time (min)			
	SG	Cc1	Cc2	Cc3
0	10	15	15	15
25	20	20	20	15
50	25	30	10	20
75	25	20	15	25

From all these results (**Figure III-2** and **Table III-6**) it is possible to determine that 50% (wt./vol.) of DEC solution is the best concentration to perform Cc and SG derivatization according to the proposed method.

This concentration is selected because we can achieve good IEC and biomass adsorption load without increasing too much the adsorption time.

III.4.4 The effect of Cc pre-treatment in carrier adsortion capacity

Having in mind that better results were obtained with SG in the previous section, and considering that derivatization had more effect on this carrier due to the higher cellulose concentration, two different pre-treatments were tested on Cc particles (with and without derivatization using a DEC solution of 50% (wt./vol.)). The results of IEC and adsorbed biomass are presented in **Figure III-3** and **Figure III-4**, respectively.

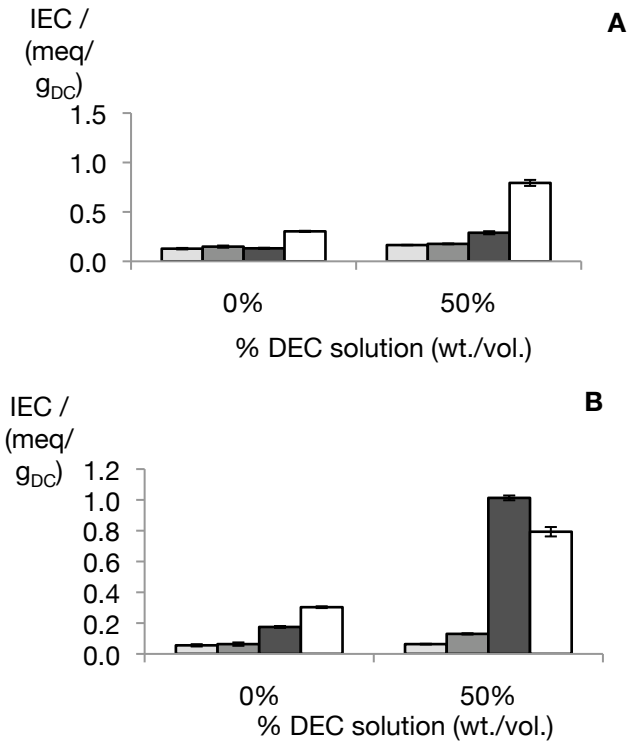

Figure III-3. Ion Exchange Capacity for: A – Cc pre-treatment A; B – Cc pre-treatment B. Legend: ■ - Cc1; ■ - Cc2; ■ - Cc3; □ - SG.

Figure III-3 indicates that IEC increased only for the pre-treatment B in Cc3 particles. This suggests that the pre-treatment did not increase

significantly the cellulose ratio in Cc particles, as expected. Consequently the value of IEC did not increase.

Figure III-4 clearly shows that the cell adsorption was higher for Cc pre-treated with HCl and NaOH. Nevertheless the results were similar to the ones obtained for Cc particles without any pre-treatment (**Figure III-2**). Pre-treatment of carrier particles at industrial scale is only justified if the impact on adsorption (and consequently on immobilization) is high. The results suggested that a pre-treatment in Cc particles is not justified, because no real improvement of the adsorption properties of the carrier was observed.

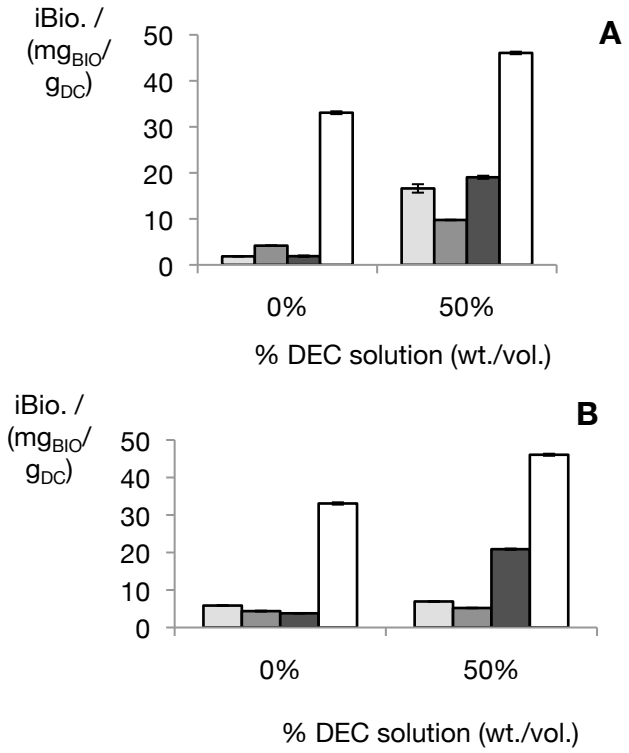

Figure III-4.Yeas cells adsorption for: A – Cc pre-treatment A; B – Cc pre-treatment B. Legend: ■ - Cc1; ■ - Cc2; ■ - Cc3; □ - SG.

III.4.5 Effect of yeast cell growth on Cc immobilization capacity

The previous tests indicate that DEC solution can play an important role on adsorption capacity of cellulose-based carriers. However it does not provide futher information on how it can really increase

immobilization. Cell immobilization involves initial adsorption and biofilm formation in the carrier. It is known that yeast cells, when immobilized, suffer changes in physiology and their growth rate can be affected when compared with free cells' growth (Junter et al, 2002). In order to confirm this, immobilization tests during yeast cells growth were performed. In **Figure III-5** the results of yeast immobilization during yeast growth are presented for the situations indicated in **Table III-4**. As explained before, the method used in this situation was a bit different due to the significant particles' degradation caused by NaOH – Method C.

In **Figure III-5** the results suggest that no immobilization occurs in carrier particles SG and Cc3. For other Cc particles there are cells attached, and yeast cell immobilization onto SG is described either in bubble columns or air-lift reactors (Brányik et al., 2001; Brányik et al., 2002b). The explanation for low immobilization relies on the method used. In terms of size, Cc3 and SG are similar. So it is expected they have similar behaviour under similar immobilization conditions. The lack of immobilized cells is due to the tension forces present during yeast cells growth. The high liquid velocity and turbulence increases shear forces in the liquid-phase and this influences biofilm formation. Thus the immobilization is reduced and similar adsorption results are obtained. Several works relating these two factors have been reported and the relation between high shear stress forces and biofilm formation indicates the adverse effect of shear on immobilized biomass (van Loosdrecht et al., 2002). As particles Cc1 and Cc2 are bigger, it is possibly that they have a higher number of bigger cavities for cells to colonize and in these regions the shear stress effect is reduced. Thus the yeast biofilm has better conditions to growth and form a biofilm.

Analysing only these two last Cc particles (Cc1 and Cc2), from **Figure III-5**. it can be concluded that pre-treatment A showed to be slightly better for yeast immobilization and biofilm formation. It has been described that acid/base pre-treatments are quite effective in reducing the hemicellulose and lignin from lignocellulosic compounds.

This will allow more cellulose to be present either for enzymatic degradation of cellulose (Zhang and Lynd, 2004) or cell immobilization. The pre-treatment A is based on typically acid/base pre-treatments. Considering that in pre-treatment B the conditions used are less aggressive than usual (Ruiz et al., 2011), it is expected that after applying the pre-treatment A to Cc, more cellulose is available. Therefore a higher immobilization is expected for this pre-treatemnt, which is confirmed by the results in **Figure III-5**. In both pre-treatments the immobilization results in derivatized particles (Cc1 and Cc2) were higher. However from **Figure III-5** only for Cc1 the derivatization was shown to have an influence on yeast immobilization being more than the double for both pre-treatments (A and B).

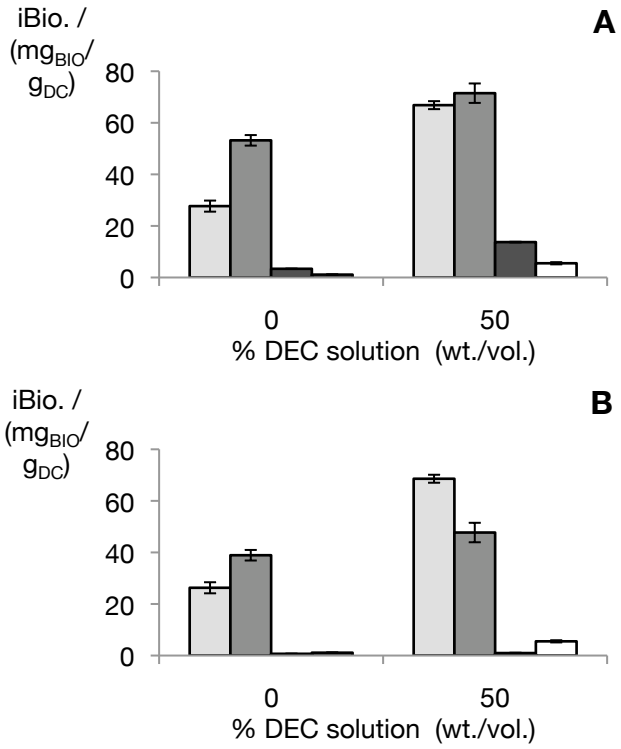

Figure III-5. Immobilized biomass (iBio) expressed in amount of biomass per gram of dry Carrier (mg_{BIO}/g_{DC}) versus DEC solution concentration for: A – Cc pre-treatment A; B – Cc pre-treatment B. Legend: ■ - Cc1; ■ - Cc2; ■ - Cc3; □ - SG.

The derivatization process is laborious and costly if applied at industrial scale. These results indicate that derivatized Cc particles did not increase significantly biofilm growth, as expected. Similar results

were obtained by Brányik et al (2001) using DEAE modified SG in bubble columns. The results suggest that the initial adhesion improvement obtained previously in the derivatized carriers, has no real impact on biofilm formation.

The results obtained for Cc and SG particles derivatized with DEC solution as well as the results obtained by Brányik and co-workers (2001), indicate that derivatization of cellulose-based carriers with these compounds (DEAE and DEC) does not have a positive impact in yeast cells immobilization.

III.5 Conclusions

In this chapter the capacity of two cellulose-based carriers (Cc and SG) for cell immobilization was evaluated and the influence of several factors was studied.

It was concluded that non pre-treated Cc particles and SG derivatized by the proposed method have better adsorption properties; the concentration of 50% (wt./vol.) in DEC was the best compromise between IEC, adsorption time and cell adsorption. Among all tested particles the smaller (SG and Cc3) were considered to be the best. The pre-treatment methods used in Cc particles did not increase the adsorption properties of Cc.

It was proved that size effect could play a key role in immobilization where bigger Cc particles showed better results for immobilization. However the particle size should depend on reactor type and configuration. It is suggested that bigger Cc particles can be used in packed bed-like reactors, while Cc3 and SG particles can be used in gas lift-like reactors, mainly due to minimum fluidization of gas necessary to obtain a homogeneous solid flow inside this reactor.

The main conclusion is that the derivatized carriers showed better adsorption properties, but that did not mean better final cell immobilization (biofilm formation) properties. Being so, Cc particles and

SG should be applied in continuous fermentation without any additional treatment, as they already have a good cell immobilization capacity.

III.6 References

Al-Adhami, A. J. H., Bryjak, J., Greb-markiewicz, B., and Peczyn, W. (**2002**). Immobilization of wood-rotting fungi laccases on modifed cellulose and acrylic carriers. *Process Biochemistry*, 37, 1387-1394.

Antrim, R. L., and Harris, D. W. (**1991**). Treatment of cellulosic ion exchange composites in hot aqueous medium to increase adsortion of macromolecules. US Patent nr.º 5001063.

Bezbradica, D., Obradovic, B., Leskosek-Cukalovic, I., Bugarski, B., and Nedovic, V. (**2007**). Immobilization of yeast cells in PVA particles for beer fermentation. Process Biochemistry, 42(9), 1348-1351.

Brányik, T., Vicente, A. A., Machado Cruz, J. M., and Teixeira, J. A. (**2001**). Spent grains–a new support for brewing yeast immobilisation. *Biotechnology Letters*, 23(13), 1073–1078.

Brányik, Tomás, Vicente, A. A., Machado Cruz, J. M., and Teixeira, J. A. (**2002a**). Continuous primary beer fermentation with brewing yeast immobilized on spent grains. *Journal of the Institute of Brewing*, 108(4), 410-415.

Brányik, Tomás, Vicente, A. A., Oliveira, R., and Teixeira, J. A. (**2004a**). Physicochemical surface properties of brewing yeast influencing their immobilization onto spent grains in a continuous reactor. *Biotechnology and bioengineering*, 88(1), 84-93.

Brányik, Tomás, Vicente, A. A., Machado Cruz, J. M., and Teixeira, J. A. (**2004b**). Continuous primary fermentation of beer with yeast immobilized on spent grains - The effect of operational conditions. *Journal of The American Society of Brewing Chemists*, 62(1), 29-34.

Brányik, Tomás, Vicente, A. A., Dostálek, P., and Teixeira, J. A. (**2005**). Continuous beer fermentation using immobilized yeast cell bioreactor systems. *Biotechnology progress*, 21(3), 653-663.

Dömény, Z., Smogrovicová, D., Gemeiner, P., Sturdík, E., Pátková, J., and Malovíková, A. (**1998**). Continuous secondary fermentation using immobilized yeast. *Biotechnology Letters*, 20(11), 1041–1045.

D'Souza, S. F., and Melo, J. S. (**2001**). Immobilization of bakers yeast on jute fabric through adhesion using polyethylenimine: application in an annular column reactor for the inversion of sucrose. *Process Biochemistry*, 36, 677-681.

D'Souza, S. F., Melo, J. S., Deshpande, A., and Nadkarni, G. B. (**1986**). Immobilization of yeast cells by adhesion to glass surface using Plyethylenimine. *Biotechnology Letters*, 8(9), 643-648.

FAO, F. and A. O. of the U. N. (**2008**). FAOSTAT statistics database. Retrieved July 8th, 2008, from: http://faostat.fao.org/site/567/DesktopDefault.aspx?PageID=567

Fujii, N., Sakurai, A., Onjoh, K., and Sakakibara, M. (**1999**). Influence of surface characteristics of cellulose carriers on ethanol production by immobilized yeast cells. *Process Biochemistry*, 34(2), 147–152.

Gama, F. M., Aires-Barros, M. R., and Cabral, J. (**2003**). Engenharia Enzimatica (in portuguese) (p. 272). Lidel Edições Técnicas, Lisboa.

Junter, G. A., Coquet, L., Vilain, S., and Jouenne, T. (**2002**). Immobilized-cell physiology: current data and the potentialities of proteomics. *Enzyme and Microbial Technology*, 31(3), 201–212.

Junter, G.-A., and Jouenne, T. (**2004**). Immobilized viable microbial cells: from the process to the proteome em leader or the cart before the horse. *Biotechnology Advances*, 22(8), 633-658.

Kang, S., and Choi, H. (**2005**). Effect of surface hydrophobicity on the adhesion of S. cerevisiae onto modified surfaces by poly(styrene-ran-sulfonic acid) random copolymers. *Colloids and surfaces. B, Biointerfaces*, 46(2), 70-77.

Kobayashi, O., Hayashi, N., Kuroki, R., and Sone, H. (**1998**). Region of FLO1 Proteins Responsible for Sugar Recognition. *Journal of Bacteriology*, 180(24), 6503-6510.

Kourkoutas, Y., Bekatorou, A., Banat, I. M., Marchant, R., and Koutinas, A. A. (**2004**). Immobilization technologies and support materials suitable in alcohol beverages production: a review. *Food Microbiology*, 21(4), 377–397.

Melo, J. S., and D'Souza, S. F. (**1999**). Simultaneous filtration and immobilization of cells from a flowing suspension using a bioreactor containing polyethylenimine coated cotton threads: Application in the continuous inversion of concentrated sucrose syrups. *World Journal of Microbiology and Biotechnology*, 15, 17-21.

Mussatto, S., Dragone, G., and Roberto, I. (**2006**). Brewers' spent grain: generation, characteristics and potential applications. *Journal of Cereal Science*, 43(1), 1–14.

Rocha, G.J.M. (2000). PhD. Thesis, São Carlos/Universidade de São Paulo, Brazil

Ruiz, H., Ruzene, D. S., Silva, D. P., da Silva, F. F. M., Vicente, A. A, and Teixeira, J. A. (**2011**). Development and characterization of an environmentally friendly process sequence (autohydrolysis and organosolv) for wheat straw delignification. *Applied biochemistry and biotechnology*, 164(5), 629-641.

Ruzene, D. S., Silva, D. P., Vicente, A. a, Teixeira, J. a, de Amorim, M. T. P., and Gonçalves, A. R. (**2009**). Cellulosic films obtained from the treatment of sugarcane bagasse fibers with N-methylmorpholine-N-oxide (NMMO). *Applied biochemistry and biotechnology*, 154(1-3), 38-47.

Sato, T., and Tosa, T. (**1999**). Enzymes, Immobilization methods. In M. C. Flickinger and S. W. Drew (Eds.), *Encyclopedia of Bioprocess Technology: Fermentation, Biocatalysis and Bioseparation* (1st ed., pp. 1062-1064). New York: John Wiley and Sons, Inc.

Torre, P., Aliakbarian, B., Rivas, B., Dominguez, J. M., and Converti, A. (**2008**). Release of ferulic acid from corn cobs by alkaline hydrolysis. *Biochemical Engineering Journal*, 40(3), 500-506.

Verbelen, P. J., De Schutter, D. P., Delvaux, F., Verstrepen, K. J., and Delvaux, F. R. (**2006**). Immobilized yeast cell systems for continuous fermentation applications. *Biotechnology letters*, 28(19), 1515–1525.

Virkajarvi, I., and Linko, M. (**1999**). Immobilization: A revolution in traditional brewing. *Naturwissenschaften*, 86(3), 112–122.

Willaert, R., and Nedovic, V. (**2006**). Review Primary beer fermentation by immobilized yeast – a review on flavour formation and control strategies. *Jounal of Chemical Technology and Biotechnology*, 81, 1353-1367.

Yoshioka, T., and Shimamutra, M. (**1986**). Studies of Plystyrene-based ion-exchange fiber. V. Immobilization of microorgnism cells by adsorption on a novel fiber-form anion exchanger. *Bull. Chem. Soc. Jpn*, 59, 77-81.

Zhang, Y. H. P., and Lynd, L. R. (**2004**). Toward an aggregated understanding of enzymatic hydrolysis of cellulose: noncomplexed cellulase systems. *Biotechnology and bioengineering*, 88(7), 797-824.

IV. Chapter IV – Effect of Spent Grains on Flow Regime Transition in a Bubble Column

IV.1 Objectives

The aim of this work is to contribute to the study of the effect of SG on the flow regime transition in a bubble column. SG are solids with unique characteristics -flat, cellulose-based, completely wettable, low size and low-density particles (Brányik et al., 2001) and there is an absence of studies on the influence of this type of particles in three-phase bubble columns. This was the driving force to perform this work. Considering the previous importance of SG for continuous AFB production in an iGLR the study of the influence of the solids-phase in bubble columns regime flow transition will allow: (1) mimic the riser conditions; (2) understand the physical mechanism by which SG may, or may not influence the iGLR hydrodynamics.

Other objectives arise as the determination of specific SG properties and the development of a calibration method to determine gas hold-up in three-phase iGLR.

IV.2 Introduction

Over the last decades hydrodynamics of gas-liquid-solid (*g-l-s*) systems has been intensively study due to their applications in several industrial fields such as petrochemical, chemical, biochemical and biotechnology processes. The study of the hydrodynamics on three-phase systems presents a challenge to several research communities, which are dealing with bubble columns, airlift reactors, flotation columns, bubbly flow and fluidized beds. Most of the recent work dealing with bubble columns (BC) is focused on the stability of its flow regime (Mena et al., 2005a; Ruzicka, et al.,2001a, 2003; Zahradnik et al., 1997)

IV.2.1 Bubble columns: flow regime transition

In BC two main flow regimes occur: the homogeneous regime and the heterogeneous regime, that may be identified by varying gas input (Ruzicka et al., 2001a; Zahradnik et al., 1997). The homogeneous regime (HoR) is characterized by a uniform bubble rise through the column. Bubbles usually have similar size, are spherical, small and rise almost vertical. There is any large-scale liquid circulation and other phenomena as coalescence and break-up are negligible (Ruzicka, et al., 2001a). In contrast, the heterogeneous regime (HeR) is characterized by a large bubble size distribution. Macro-scale liquid circulation, coalescence and a parabolic/non-uniform radial profile of hold-up with a maximum at centre are typical on this regime (Mena et al., 2005a). The transition starts when the HoR loses its stability and gradual process occurs where there are an increasing number of coherent structures (circulations) with increasing size and intensity (Mena et al., 2005a; Ruzicka et al., 2001a; Zahradnik et al., 1997).

Due to their characteristics, HoR and HeR have a different hydrodynamic behaviour. This results in different mass, heat, and momentum transfer properties. Consequently, it is important to clarify how operating parameters (reactor geometry, gas and liquid flow rates, properties of the contacting phases) act on flow regime properties and transition (Zahradnik et al., 1997).

Parameters such as superficial gas velocity, column diameter, liquid and gas phase properties and distributor geometry act simultaneously on regime transition (Shaikh and Al-Dahhan, 2007). The selection of the correct distributor is required to study regime transition, being perforated or porous plates the most commonly applied at laboratory and industrial scale (Zahradnik et al., 1997). Zahradnik et al. (1997) demonstrated that perforated plates with holes inferior to 1 mm and porous plates are adequate to characterize regime transition. Vijayan et al (2007) studied the influence of sparger geometry in the regime transition, evaluating the influence of the ratio between area of sparger

and area of column cross section. They found that if this ratio is increased the critical and global values of gas hold-up also increase (Vijayan et al., 2007).

Generally, regime evolution is observed by the increasing of gas flow rate input and by determined the correspondent gas hold-up. There are several techniques to determine local or global gas hold-up such as: bed expansion (Mena et al., 2005a; Ruzicka et al., 2001a, 2003; Zahradnik et al., 1997), pressure drop, dynamic gas disengagement (Schumpe and Grund, 1986; Yang et al., 2010), conductivity (Warsito et al., 1997) and optical fibers (Cartellier, 1990). The analysis of the gas hold-up versus superficial gas velocity (**Figure IV-1**) shows that HoR appears as a convex line while HeR follows a rational function (concave line). These lines are connected by a transition zone for intermediate gas velocity values (Ruzicka et al., 2001a).

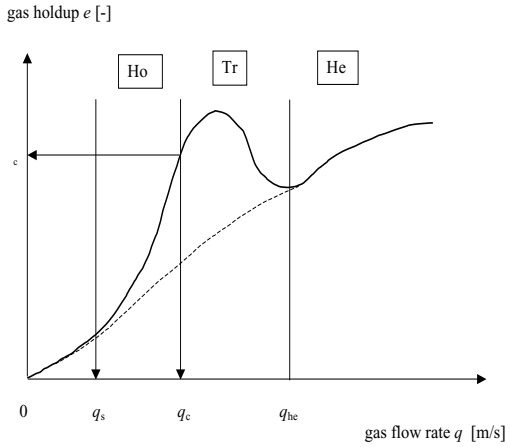

Figure IV-1. Definition of flow regime transition in BC and identification of flow regimes and critical values. Legend: Ho – Homogeneous regime; Tr – Transition regime; He – Heterogeneous regime; q_S – Beginning of Ho regime; q_C – Critical point (End of Ho regime); q_{He} – End of Transition regime. Adapted from Ruzická et al. (2003).

IV.2.1.1 Identification of the flow regime transition

Regime transition identification is possible by applying the drift-flux concept initially proposed by Wallis (1969). In this method, the drift flux, j_{GL} (the volumetric flux of either phase relative to a surface moving at the volumetric average velocity) is plotted against the gas hold-up. The change in the slope of the curve represents the transition from

homogeneous to heterogeneous flow. This concept has been used and modified by several authors for determining regime transition (Krishna, et al., 1999; Mena et al., 2005a; Ruzicka, et al., 2001a, 2001b; Vial et al., 2000) Several models for regime transition have been proposed based on: (1) bubble drag force, (2) gas phase slip velocity, (3) energy balance of the two flow, (4) bubble size, (5) coupling between phases (Gharat et Joshi, 1992; Hyndman et al., 1997; Joshi et Lali, 1984; Krishna, 1991; Riquarts, 1979; Ruzicka et al., 2001a). The model proposed by Ruzicka et al. (2001a) based on the concept of the Darwinian drift of bubbles was able to describe with good accuracy the transition between HoR and HeR in a two-phase system. However some factors that affect regime stability as column dimensions, liquid phase properties and solids presence are not explicitly involved in the proposed model and experiments have been done over the last years to validate particular aspects of the stability criteria (Mena et al., 2005a; Ruzicka et al., 2001a, 2008).

IV.2.2 Solids effect on three-phase bubble column

In three-phase BC reactor, the effect of solids on gas hold-up has been the focus of several studies (Banisi et al., 1995; Gandhi et al., 1999; Mena et al., 2005a, 2055b, 2008). These systems can be classified as liquid-gas flow with the presence of solids or as liquid–solid fluidized beds with the presence of gas bubbles. However comparison between the different studies is difficult and results are often contradictory, due to differences in column design, operating parameters (mainly liquid throughput) and solids properties. Properties of the solid particles can be quite different depending on the size, shape, density, wettability, hydrophobic and surface properties. Having this in mind, their effect in gas hold-up and flow regime transition is far from being totally explained despite several attempts. Banisi et al. (1995) reported that the presence of solids decreased gas hold-up while a dual effect was observed by other authors (Mena, et al., 2005a; Xie et al., 2003). The presence of solids on bubble columns affects the

gas-liquid mixture in several ways: bubble formation (Yoo et al., 1997), bubble rise, axial and radial profiles (Gandhi et al., 1999; Warsito et al., 1997), mixing and dispersion, mass transfer (Mena et al., 2005b), gas hold-up and flow regimes (Mena et al., 2005a).

Generally gas hold-up decreases with solids concentration. There are several possible explanations for this kind of effect such as increased coalescence (Gandhi et al., 1999; Lu et al., 1995) and reduction of bubble breakup (Gandhi et al., 1999), increased apparent viscosity, steric effect.

In what concerns the effect of apparent viscosity, some authors consider the solid and liquid phase as a “pseudo-homogeneous” phase, this requiring the need to define an apparent viscosity due to solid presence in liquid (Freitas et al., 1999; Lu et al., 1995). In a similar way to what has been reported for two-phase flows where a higher viscosity decreases gas hold-up, while at low viscosities the opposite occurs (Eissa and Schugerl, 1975; Ruzicka et al., 2003), an identical behaviour might be expected for the effect of solids concentration on gas-hold-up. Nevertheless, recent studies in regime transition studying the effect of liquid viscosity reported that even at low viscosity values the global hold-up decreases (Yang et al., 2010). In general, an increase of viscosity is related with a decrease on gas hold-up. When solids are present, some authors consider the solid and liquid phase as a “pseudo-homogeneous” phase. This leads to the need of defining an apparent viscosity due to the solid presence in the liquid that would affect liquid phase properties as density and viscosity (Freitas et al., 1999; Lu et al., 1995). As far as we are aware some relations to determined viscosity are reported in literature being the most common the ones by Oliver et al. (1961) (cited by Lu et al. (1995)); Thomas (1965) (cited by Yoo et al. 1997); Barnea and Mizrahi (1973) (cited by Gandhi et al., (1999)) and Metzner (1985) (cited by Yoo et al., (1997)).

The change in viscosity promoted by solids in the liquid-phase reveals that possible relations/interactions between solids and viscosity are likely to occur on their effect on flow regime destabilization of *g-l-s*

systems. Mena et al. (2005a) noticed that only for a high solid content the viscosity had an important contribution for this; however, this cannot be generalized as the solid effect on the apparent viscosity of the mixture depends on the properties of the solids applied. It seems that the BC design and size also play an important role when all these aspects are considered (Ruzicka, et al., 2001b,; Ruzicka et al., 2003; Yang et al., 2010).

IV.2.2.1 Solids dual effect on regime transition

The dual effect that has been reported in the recent years lead to a discussion of what is the real effect of solids in BC. It seems that size, concentration and wettability play an important role on this effect. Accordingly to Banisi et al. (1995) fine particles in small amount (suppressing coalescence) and large particles in high amount (promoting breakup) tend to increase hold-up, while moderate concentrations and sizes seem to decrease gas hold-up. Concerning the influence of the wetability, its real effect on gas hold-up remains unclear. Jamialahmadi and Muller-Steinhagen (1991) report that wettable particles increased hold-up while non-wettable particles have the opposite effect. However, Mena et al. (2005a), worked with alginate beads (low density and completely wettable solids) and found that a dual effect is present - for low solid content (< 3.0 %) solids enhanced the HoR regime stabilization and global hold-up increased while for higher solids content (> 3.0 %) the opposite effect was observed (Banisi et al., 1995; Jamialahmadi and Muller-Steinhagen, 1991; Mena, et al., 2005a).

From a critical point of view the actual knowledge of the flow regime transition in three-phase system remains scarce. The main reason is related not only with the correct data interpretation in terms of physical mechanism but also with the difficulty of relating all results reported in literature

IV.3 Material and Methods

IV.3.1 Apparatus and measurements

Measurements were performed in a cylindrical Plexiglas bubble column with internal diameter of 0.142 m. The distributor was a ceramic porous plate with 0.09 m of diameter and an approximate porosity of 38% (vol.). It ensures the three regimes: homogeneous, transition and heterogeneous. Compressed filtered air was the gas-phase (T=25 ºC, P=1.01 bar) and water the liquid-phase (T=20 ºC). The clear liquid height was H_{L0}=1.09 m for all experiments (no liquid throughput). The dependence of the gas hold-up (ε) on the gas flow rate (Q_G) was measured three times and then averaged. The gas superficial velocity varied in the range U_G=0 m/s (0 dm^3/s) to U_G=0.027 m/s (0.43 dm^3/s), covering the homogeneous and part of the transition regime. The gas flow was measured with a Mass Flow Controller (Alicat Scientific, Inc., Tucson – AZ, USA) and variations in gas superficial velocity close to the transition point were within 2 mm/s (0.033 dm^3/s).

IV.3.2 Solid-phase characterization: spent grains

SG, almost flat particles, with equivalent diameter d_{EQ}<2.1 mm were the solid phase. The size distribution of the particles was determined by sieving into fractions using a portable sieve shaker (Model Analysette, Fritsch, Germany).

IV.3.2.1 Preparation of spent grains

Spent Grains were prepared accordingly section III.3.4.1 without the acid hydrolysis step (Brányik et al., 2004).

IV.3.2.2 Water absorption index (WAI) determination

WAI was determined accordingly Mussato et al (2009). Mainly a sample of 2.5 g of spent grains (dry base) was suspended in 30 mL of distilled water in a 50 mL centrifuged tube. The slurry was stirred for one minute at room temperature and then centrifuge at 3000 *g* and 25 ºC for 10 min. The supernatant was discarded and WAI was calculated from weight remaining gel and express as $g_{WET\ SG}/g_{DRY\ SG}$.

IV.3.2.3 Specific weight of wet spent grains (wSG)

SG are a cellulose-base material an consequently is able to absorb water. Thus specific weight determination became difficult. Being so wSG specific weight was determined by volume increased method. A large amount of dry SG (d_{SG}) – 15 g – was suspended in 30 mL of distilled water and centrifuged (3000 *g* and 25 ºC for 10 min). The supernatant was discarded and the remaining w_{SG} were added to 500 mL of distilled water. Volume of w_{SG} was determined by water volume increase and specific weight (V_{wSG}/W_{wSG}) determined. The results were performed in triplicate.

IV.3.3 Gas hold-up

Gas hold-up was measured using two techniques described below.

IV.3.3.1 Bed expansion

In each experimental run, the gas flow was set, the bed height was recorded after the time required to reach a steady value was achieved (never less than five minutes). Each of the eight runs was repeated three times and the voidage values were averaged. Gas hold-up was determined according to (Deckwer, 1992; Mena et al., 2005a; Ruzicka et al.,200a, 2003, 2008; Yang et al., 2010):

$$\varepsilon_G = \frac{H_{GL} + H_L}{H_L} \qquad \textbf{Eq. IV-1}$$

IV.3.3.2 Water columns differential pressure

The gas hold-up was determined by measuring static pressure difference between two heights in the BC. Our interest in using this technique is related with future tests to be performed in a iGLR. Moreover, it is reported that pressure difference per se is not enough when three phase systems are applied (Boyer et al., 2002) and an additional technique should be applied to determine solids hold-up. Differential pressure was measured by the difference in water columns. For each set of experiments, pressure differences (H_1-H_2) were measured at least three times during 5 min (gassing time bigger than 5 min). The mean value was then used to determine gas hold-up by the following equation (Freitas and Teixeira, 1998a, 1998b):

$$\varepsilon_G = \frac{H_1 - H_2}{d_{12}} - \frac{\rho_L - \rho_S}{\rho_L} \times \varepsilon_S \qquad \textbf{Eq. IV-2}$$

IV.3.4 Solids hold-up

Solids hold-up and distribution were determined by using the method developed by Freitas et al. (1997). Briefly, a sampler adapted to retain spent grains with 60 mL of volume is used for collecting solids. The solids sample is collected between the two points where the ε_G is measured. The solids were filtrated and dried at 105 ºC for 12 h. The solids volume was determined (considering their WAI and specific weigth) and solids hold-up (ε_S) calculated accordingly (Freitas et al., 1997):

$$\varepsilon_S = V_S \Big/ V_{spl} \qquad \textbf{Eq. IV-3}$$

IV.3.5 Measurements errors

The relative error for bed expansion method is considered to be less than 5%. On the homogeneous and in the beginning of transition regime the layer is uniform and the interface is easy to locate with a 1 mm precision (precision of scale – millimetre paper). This resolution was considered adequate due to the height of the column used (1090 mm). However, when transition starts to occur and waves appear the determination of the height of the BC is difficult (H_{G+L}). To minimize this effect, the obtained value corresponds to the mean of the values measured during several oscillations. At the end of transition and in the beginning of heterogeneous regime oscillations were at maximum 30 mm around the mean value. Having in mind the increase in height column for these superficial gas velocities, it was possible to have an experimental error not exceeding 5%.

The resolution obtained on the water column method was the same as for bed expansion, for the highest flow rates. However, for the low gas flow rates, the error is larger (up to 10%), considering the measured differences of the height in water columns (10 to 120 mm). The measurement error associated with solids hold-up determination is considered to be no more than 10 % (Freitas and Teixeira, 1998). Overall, the combined error for the determination of gas hold-up using is at its maximum 15%.

IV.3.6 Evaluation of critical gas hold-up and critical gas velocity

Considering the primary data obtained (ε vs U_G), the critical point could be determined as the inflexion point of the data graph. However, its direct determination in the graph is difficult and inaccurate. Consequently, the data were re-plotted according to the drift-flux model and the inflexion point determined from the deviation of the data from the theoretical line of the uniform regime. This is a standard procedure.

The theoretical line $j=j(\varepsilon_G)$ is defined as:

$$j_{theo} = \varepsilon_G \times (1-\varepsilon_G) \times u \qquad \textbf{Eq. IV-4}$$

Where u is the mean slip speed in case of no liquid flux through the column. The concept of Darwinian drift was used to determine the bubble mean slip speed (Ruzicka et al., 2001a). Thus:

$$u_{theo} = u_0 \times \left(1 - \frac{a \times \varepsilon_G}{1-\varepsilon_G}\right) \qquad \textbf{Eq. IV-5}$$

Where u_0 – is the bubble terminal speed, and a – the bubble drift coefficient. For each data line $\varepsilon_{Gexp}(Q_{EXP})$, they are obtained by linearization of Eq. V-5, using the basic relation:

$$\varepsilon_{G\exp} = \frac{Q_{\exp}}{U_{\exp}} \qquad \textbf{Eq. IV-6}$$

The experimental drift-flux is obtained from **Eq. IV-4** together with **Eq. IV-6**:

$$j_{\exp} = (1-\varepsilon_G) \times Q_{\exp} \qquad \textbf{Eq. IV-7}$$

The transition begins where **Eq. IV-7** separates from **Eq. IV-4** : it is the critical point $[U_C, \varepsilon_C]$, the instability threshold. The values of U_C and ε_C are the quantitative measures of the homogeneous regime stability. The evaluation procedure is an iterative process. The homogeneous data range is initially assessed, then is used for the linearization, till the correlation coefficient of the linearization is sufficiently close to unity.

The regime transition was also found using the slip-speed concept, where, at the critical point, the slip speed data u_{exp}, departs from the u_{theo} obtained from the model line.

The first criteria of the drift flux model is based on the coupling of phases, i e., on the mass conservation of the phases. The slip speed concept is based on the fact that, in HoR, the bubble speed decreases with the increase of hindrance caused by the increase of bubble concentration.

The obtained results are the average of these two methods. Since these two methods are equivalent, only different co-ordinates are used, the results should be similar. This was the test of correctness (Mena et al., 2005a; Ruzicka et al., 2008).

In the literature, the stability criteria normally used on *g-l-s* systems are scarce and several principles have been applied. Initially, they have been based on correlations obtained from experimental data but they lack in terms of universal application due to their specificity (Krishna, 1991; Reilly et al., 1994; Wilkinson et al., 1992). Theoretical criteria based on theoretical concepts are more accurate and may be applied a priori (Ruzicka and Thomas, 2003; Shnip et al., 1992) or a posterior as the slip speed concept and the drift-flux model (used in this work).

IV.4 Results and Discussion

In this chapter it was evaluated the influence of solids in BC regime flow transition. The solids used were SG and possible physical mechanisms that influence the regime flow transition in BC is discussed bellow.

IV.4.1 Spent grains characterization

The solid particles (SG) used in this chapter are a little different from the ones used in the previous chapters (III and VIII). The main reason is the lack of the acid pre-treatment step (III.3.4.1). Considering the need of high amount of SG (about 5 kg of d_{SG}) to work in the BC described, the low yield (2 kg_{dSG}/100kg_{BGS}), the reagent and energy costs, and the time necessary to obtain such amount it was decided to remove the acid step from the SG preparation. Moreover during the SG characterization no relevant differences were found both in WAI and density between base-treated and acid/base-treated SG.

SG after pre-treatment are mainly cellulose (Brányik et al., 2001). They are completely wettable particles and increase size when in contact with water. In order to determine their density is important to distinguish between density of d_{SG} and w_{SG}. Initially it was tried to determine the density of d_{SG}. However either using the proposed method (section IV.3.2.3) or other methods proposed in literature (picnometer method) it was impossible to determined with accuracy the dSG density. This was mainly due to their unique characteristics of wettability and size change. Having this in mind it was only determined the specific density of wSG particles. This was important not only because density of particles is crucial when hydrodynamic studies are performed but also because the real effect on reactor hydrodynamic will be due to the "wet" particles in aqueous solutions. In order to determine the density of w_{SG} particles it is also necessary to determine the WAI. On **Table IV-1** the values of w_{SG} properties (density and WAI) determined are present.

Table IV-1. Spent grains properties in wet basis at T=25 ºC and P=1 atm

Property	Average	Stdev	Qv
WAI / (g_{WET}/g_{DRY})	8.121	0.112	1.37%
$\rho_{WET\ SG}$ / (g/mL)	1.037	0.010	0.97%
ρ_{WATER} / (g/mL)	0.998	0.000	0:02%

Mussato et al. (2009b) obtain a WAI for SG of 9.03 being the difference explained either by the different pre-treatment used (base-treat only) or by different barley variety used in this work. The high WAI is a measure of the ability to adsorb water, which is very important aspect for immobilization of microorganisms. This ability allow that water is always present for cells to growth and developed (Mussatto et al., 2009b). Besides this high water adsorption, which proves their wettability capacity, SG have hydrophobic character (Brányik et al., 2004) and high critical humidity point, which indicates that normally low amounts of water are bounded to the particles (Mussatto et al., 2009b). This ambiguous capacity of SG are ideal for microorganisms growth and immobilization because manage to keep high water content and at the same time create a hydrophobic environmental that decreases the ability of immobilized yeast (more hydrophobic) to be release in the bulk (Brányik et al., 2004).

IV.4.2 Bed expansion versus water columns differential pressure for gas hold-up determination

For the system considered, the determination of gas hold-up using both techniques showed similar results. The measuring of gas hold-up by water columns combined with the modified method for solid hold-up determination used by Freitas et. al (1997) appears to be a suitable method to determined gas hold-up in three-phase systems where SG are present. In fact and considering the solid distribution in the entire BC the difference between the experimental and theoretical values of solid load determined by this technique was 2.97%; 3.32%; 3.98% and 6.94% for 4%; 8%; 12%; 20% ($wt._{WET\ BASIS}$ /vol.) respectively. The

obtained errors are in the same range of the ones obtained by other authors (Freitas and Teixeira, 1998a, 1998b; Freitas et al., 1997). Having in mind that these values have been calculated with the experimental values for gas hold-up, it is clear that the applied technique may be applied with a good accuracy.

Moreover, the results presented in **Figure IV-2** that show the experimental errors for the two techniques confirm this conclusion. In **Figure IV-2A**, the deviations for all range of solids loads used are shown while in **Figure IV-2B** only the first three solids loads are considered (4% 8% and 12% (wt.$_{WET\ BASIS}$ /vol.)).

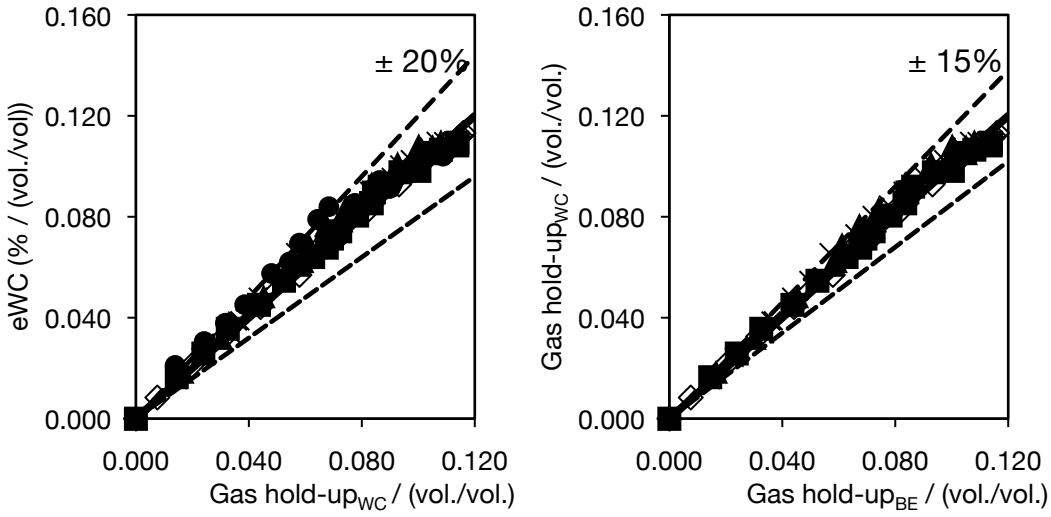

Figure IV-2. Comparison between gas hold-up obtained by Water Columns (Gas hold-up$_{WC}$) and Bed expansion (Gas hold-up$_{BE}$): A – Solids load up to 20% (wt.$_{WET\ BASIS}$/vol.); B – Solids load up to 20% (wt.$_{WET\ BASIS}$/vol.). Legend: ♦ – water; ■ - 4% (wt.$_{WET\ BASIS}$/vol.); ▲ - 8% (wt.$_{WET\ BASIS}$/vol.); + - 12% (wt.$_{WET\ BASIS}$/vol.); • - 20% (wt.$_{WET\ BASIS}$/vol.).

The maximum and mean deviations between the results obtained with the two different techniques are, respectively, 26% and 7%, with most of the measured values with errors in the range ±8% an acceptable result having in mind the applied techniques. Nevertheless the highest errors occur at the lowest gas flow rates and high solids content. In fact, for the maximum solids content and due to the non-homogeneity of solids in the column, especially at low gas flows, the combined method for solids and gas hold-up determination is not suitable. It

seems that, for these type of solids, only solids load values below 12% (wt.$_{WET\ BASIS}$/vol.) are accurate enough to perform a correct evaluation of the data in terms of regime transition. Thus, for 20% (wt.$_{WET\ BASIS}$/vol.) solids load the results were not used for the determination of regime transition. Anyway no regime transition was observed at this solids load. For higher gas flow rates the agreement between the data was always below 4%. Therefore both techniques were considered for the determination of critical values (ε_C and U_C) for regime transition.

IV.4.3 Gas-hold up vs gas-flow: solids influence

In the graph of the **Figure IV-3** are plotted the curve $\varepsilon(q)$ obtained for each concentration of solids (0 – 20% (wt.$_{WET\ BASIS}$ /vol.)).

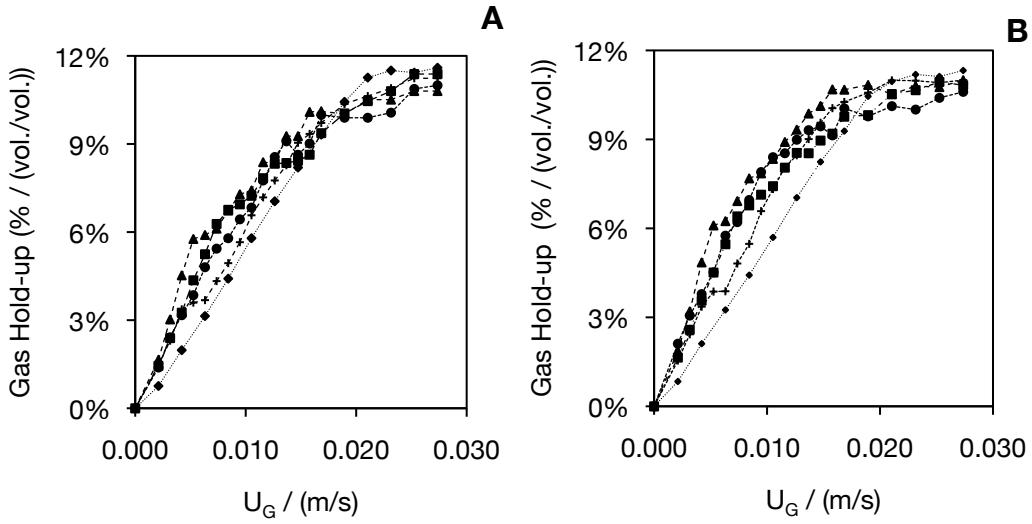

Figure IV-3. Primary data obtained from different gas hold-up methods: A – Bed Expansion; B – water Columns. Legend: ♦ – water; ■ - 4% (wt.$_{WET\ BASIS}$/vol.); ▲ - 8% (wt.$_{WET\ BASIS}$/vol.); + - 12% (wt.$_{WET\ BASIS}$/vol.); • - 20% (wt.$_{WET\ BASIS}$/vol.).

Figure IV-3 shows that, in this column, regime transition occurs at lower gas flows than the ones obtained by other authors in BC (Mena et al., 2005a; Ruzicka et al., 2001a, 2001b). However the values of gas hold-up are in the same range. There are two possible explanations for this: bubble column size and the effect of the distributor.

It is reported that column size (diameter and height) influences the global hold-up. Also, sparger influence over the column axis can go up to four times the column diameter (Gandhi et al., 1999; Lu et al., 1995). For the same gas flow, Ruzická et al. (2001b) observed that gas hold-up values are usually lower when BC diameter increases and/or column height increases. Thus the critical values (ε_C vs. U_C) for regime transition also diminish (Ruzicka et al., 2001b). Generally, gas spargers in BC have a diameter that occupies all cross-section of the BC. As in our case the sparger corresponds to 2/3 of the bubble diameter, this characteristic is responsible for a higher height until gas flow stabilizes and for local liquid circulation near the sparger. This means that the height of the column necessary for the gas to achieve a flat profile is higher as there is a region at the bottom of the column where liquid circulation occurs (less visible at low flows), which difficult a rapid stabilization of the gas profiles as typically occurs in HoR. The liquid circulation is a consequence of the higher amount of bubbles in the center of the column immediately above the distributor, resulting in "local" lower hold-up values. The influence of sparger geometry on gas hold-up values has also been studied by Vijayan et al. (2007). As the gas hold-up values obtained in this work are in the same range values as those reported by these authors when similar H/D and $A_{sparger}/A_C$ ratios are considered, our experimental values may be considered to be within the expected range (Vijayan et al., 2007).

The selection of this distributor is related with our interest on the study of the three-phase hydrodynamics in an internal airlift reactor, as in these systems the distributor cross section is of the same order of magnitude of the airlift riser cross section and always smaller than the total column cross section. The applied distributor allowed to reach the objective of solids fluidization at low gas flow rates (except for the maximum solids concentration).

Even if this system would behave differently from those reported in literature, which is not the case, it would still possible to conclude on the effect of the solid phase on flow regime transition, as experiences

were done for all cases in the same BC. In addition, the presence of both regime flow (HoR and HeR) in air-water systems was clearly identified.

From **Figure IV-3**, it is also possible to observe, at low gas flows, that the presence of the solid phase causes an increase in gas hold-up. This may be attributed to a stabilization effect of the bubbles at low gas flows, being the opposite effect observed as gas flow is increased. This "stabilization" effect causes an increase in gas residence time and consequently hold-up is higher. This is also related with a decrease of the height that the gas needs to achieve the flat profile, typical for HoR.

The effects associated with the use of a sparger not occupying the entire cross section of the column may also contribute to the observed increase in gas hold-up. As due to their sedimentation properties an increase in solids concentration near the distributor occurs (specially at low gas flow and high solids load), a higher interaction between bubbles and particles occurs. There is also the steric effect (presence of solids) of spent grains as well as its surface properties that can have an important effect on the interactions between solids and bubbles. This effect reduces bubble rise velocity leading to a slight increase on hold-up (Lu et al., 1995; Mena et al., 2005a). In fact, when solids were present, a larger amount of smaller bubbles near the wall was observed in comparison with air-water systems as observed in next figure.

Figure IV-4. Exemple of small bubbles near the BC wall.

Spent grains wettability is another factor that may contribute to the obtained results. Also, it has been reported that the influence of the physical properties of solids is higher when solids have a small size compared with bubble size, as is the case of SG (Mena et al., 2005a). A higher drag force on the bubble surface (gas-liquid interface) is created by the presence of small size solids with a consequent reduction on bubble rise velocity and gas hold-up increase (Mena et al., 2005a). The combination of the above-mentioned effects contributes for the observed increase in gas hold-up at lower gas flows when solids are present. This is in agreement with Jamialahmadi and Muller-Steinhagen (1991) that concluded that wettable particles increased hold-up by suppressing coalescence while non-wettable particles had the opposite effect. It may also be noted that the resistance promoted by solids sedimentation characteristics was evident when maximum solid concentration was tested (20% (wt.$_{WET\ BASIS}$/vol.)), as no fluidization of solid particles was observed at the lowest gas flow rates.

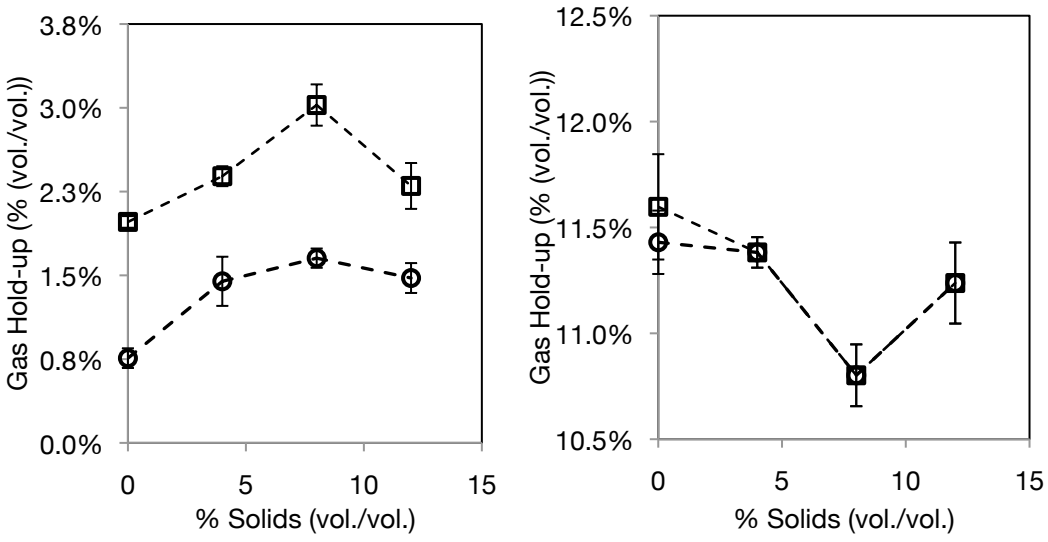

Figure IV-5. A - Solids influence at low gas flow rates in gas hold-up (Bed Expansion). Legend: O – q = 0,2 cm/s; □ - 0,4 cm/s; B – Solids influence at high gas flow rates in gas hold-up (Bed Expansion). Legend: O – q = 2,5 cm/s; □ - 2,7 cm/s

On **Figure IV-5A**, it is possible to verify that when solids are present, at low gas flows, global gas hold-up tends to increase with a maximum

around 8% (vol./vol.) of solids. In HoR, this result is a consequence of particle-bubble interactions that result in bubble break-up and dispersion, reduced bubble rise velocity and consequent increase in hold-up.

On the other hand, **Figure IV-5B** shows that in HeR at high flows the opposite effect is present revealing a dual effect of the particles. At these values of gas flow (HeR) liquid circulation is higher and more pronounced, the effect of particle-bubble interaction being lower. Bubble-bubble interactions increased and coalescence occurred. At this stage, coalescence does not seem to be significantly affected by the presence of the solid phase. However, with the obtained data, it is impossible to identify/evaluate the importance of the physical mechanisms related with solid properties (wettability, size, density). At high gas flows, larger bubbles were visually observed revealing coalescence phenomena at these stages. The absence of 20% ($wt._{WET\ BASIS}$/vol.) solids data is related with the fact that HoR was not achieved under this solids load condition (see **Figure IV-6**).

IV.4.4 Gas-hold up vs gas-flow: drift-flux

In **Figure IV-6** are plotted the Drift-flux results for the data obtained by the Bed Expansion method. This method allows for an accurate determination of the critical point (point at which HoR stability disappears). The critical point, which corresponds to the inflexion points on **Figure IV-3**, is now clearly identified on **Figure IV-6** (open symbols) for the different experimental conditions. As previously said, this point corresponds to the beginning of separation of the plots of the experimental and calculated data.

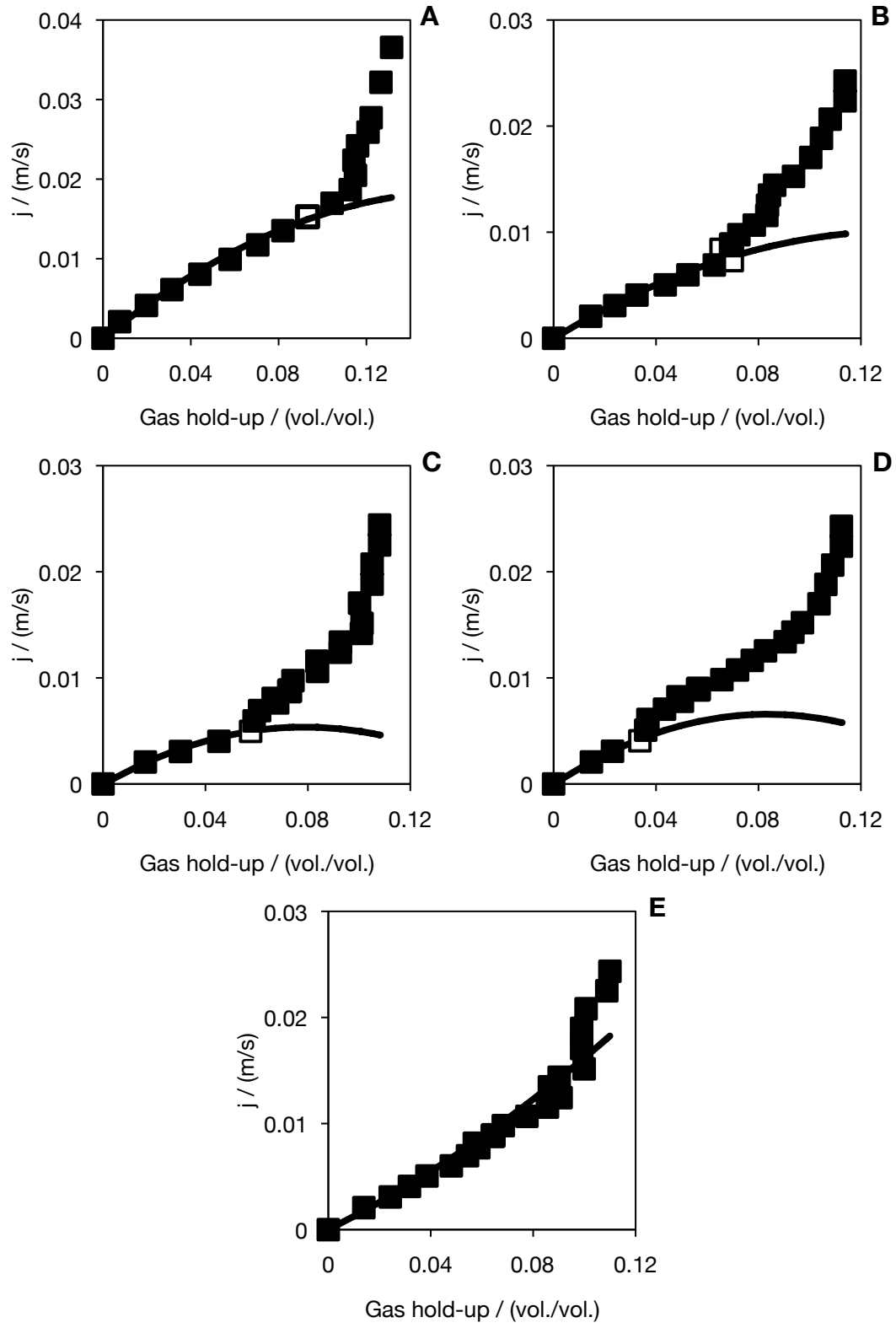

Figure IV-6. Drift-flux plot: Drift-flux – j (m/s) *vs.* Gas hold-up (vol./vol.). Legend: — (smooth line): j_t by **Eq. IV-4**; ▪ (Data points): j_{EXP} by **Eq. IV-7**; □ (Blank Data): Critical point. A, B, C, D, E: Different solid loads (0, 4, 8,12 % ($wt._{WET\ BASIS}$ /vol.))

From the results plotted in **Figure IV-6**, a decrease of critical gas hold-up and critical gas flow with solids load is clearly observed. Critical gas hold-up decrease presents a linear behaviour, while critical gas flow has an exponential trend. This suggests that above 12% (wt.$_{WET\ BASIS}$/vol.) of SG loading the critical gas flow is similar to the minimum gas fluidization flow for this system. In fact, as said before, when the highest solids load was applied, the value for minimum fluidization gas velocity was only 20% inferior to the critical gas flow for 12% (wt.$_{WET\ BASIS}$/vol.) loading. This indicates that, under the tested solids load, 12% (wt.$_{WET\ BASIS}$/vol.) solids load was the minimum concentration where HoR could be established and only for a small range of gas velocities (0.2 cm/s < U_G < 0.5 cm/s). Concerning the critical gas hold-up, the following correlation can be found to describe its dependence on solids load (**Eq.IV-8**):

$$\varepsilon_C = 0.10 - 0.56 \times \delta_S \quad R^2 = 0.94; R_{xy} = 0.97 \qquad \textbf{Eq. IV-8}$$

This equation indicates the way spent grains influence regime transition on the studied bubble column. **Eq.IV-8** intercepts y-axis at a value lower than the ones found in the literature (Mena et al., 2005a), this being related with the above addressed specific issues of this BC. When comparing the slope of **Eq. IV-8** with the one reported by Mena et al. (2005a) for alginate beads as the solid phase, the obtained value with SG is two times larger. This allows concluding that SG have a more pronounced effect on regime transition than alginate beads. This is not unexpected as the properties of both solids are different, mainly size, shape and wettability.

Presented results indicate that a reduction in HoR regime stability is observed when solids are present (**Figure IV-6** and **Figure IV-7**). It was visually verified that when gas flow was increased big bubbles start to appear, especially in the column centre, due to coalescence. In fact, at maximum solids load where no HoR was established, bubble coalescence was observed even at the lowest flows. At the highest flow, slug regime was present, a typical situation for BCs with diameters inferior to 20 cm (Deckwer, 1992). This result contradicts the

one obtained by Jamialahmadi and Muller-Steinhagen (1991) that observed that wettable particles increase gas hold-up by suppressing coalescence. In fact this occurs at low gas flows (**Figure IV-5A**), but not at higher ones (**Figure IV-5B**). As above said, this dual effect of SG is attributed to the BC design. The increase in gas hold-up by the action of SG means that more bubbles are present and interactions between bubbles are higher. This increased rate of collisions promotes coalescence. With the gas hold-up increase in the HoR by the presence of the solid phase, non-uniformities are formed in the gas phase and the stability of HoR is reduced. Thus the HeR is achieved earlier and the critical values (ε_C vs. U_C) are lower when solids are present.

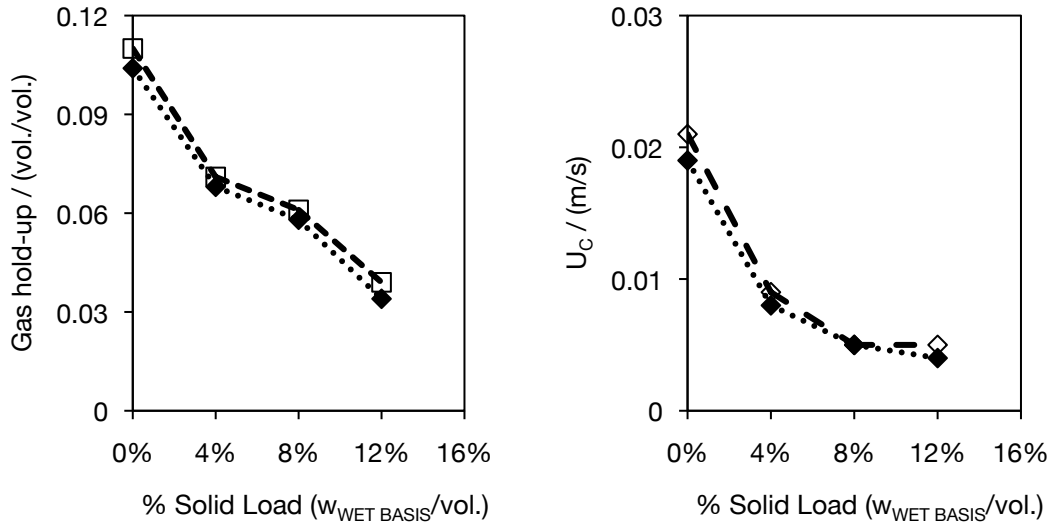

Figure IV-7. Evaluation of critical gas hold-up and critical gas flow with solid load. Legend: ◆ - Bed Expansion; □ - Water Columns

It is also possible to observe that either bed expansion and water columns techniques show similar results (**Figure IV-7**). This indicates or confirms that, for solids loads inferior to 12% (wt.$_{WET\ BASIS}$ /vol.), the combination of solid hold-up method and water columns appear to be a suitable technique to evaluate gas hold-up in different reactors configurations.

It was suggested that solids effects can be similar to what occurs in a low viscosity liquid on bubble columns (Mena et al., 2005). In our

case, critical values (ε_C *vs.* U_C) decrease with solids load, which is in agreement with published results on viscosity effect on flow regime transition (Yang et al., 2010). Ruzická et al., (2003) reported a dual effect of liquid viscosity when low viscosity (< 2,1 mPa.s) and high viscosity liquids are present. Meanwhile, recent studies published by Yang et al. (2010) identified that at low viscosity liquids there is a fast decrease of critical values (gas hold-up and gas flow) followed by a small decrease. The critical viscosity where this change occurs was around 3 mPa.s. The behaviour of critical gas flow vs. viscosity was (Yang et al., 2010):

$$q_{C1} = -0.019\ln(\mu_L) + 0.025; q_{C2} = -0.018\ln(\mu_L) + 0.056 \text{ for } \mu_L < 2.8\ mPa \cdot s \quad \textbf{Eq. IV-9}$$

These authors considered that the first value for the critical gas flow - q_{C1} – corresponds to the end of the homogeneous regime when the first big bubbles are formed and the second one - q_{C2} – is obtained when full heterogeneous regime is established (Yang et al., 2010). Accordingly, they suggest that the values obtained for critical values of transition correspond to the value when homogeneous regimes loses stability (q_{C1}).

Oliver et al. (1961) cited by Lu et al. (1995) suggested the determination of a pseudo-homogeneous viscosity for a solid-liquid mixture according to the following equation:

$$\mu_{S-L} = \mu_L\left[f(\delta_S)\right]^{-1} \qquad \textbf{Eq. IV-10}$$

Where,

$$f(\delta_S) = \frac{\left(1 - 0.75 \times \delta_S^{1/3}\right)\left(1 - 2.15 \times \delta_S\right)}{\left(1 - \delta_S\right)^2} \qquad \textbf{Eq. IV-11}$$

The application of this equation to our experimental data was based on the fact that the solid phase used – alginate beads - by Lu et al. (1995) had similar properties – density and size - to the solids used in this work. In our case, the following empirical curve relating critical gas flow with the pseudo-homogeneous viscosity (1 mPa·s<μ_{S-L}<1.7 mPa·s) was obtained:

$$q_{C1} = -0.032\ln(\mu_L) + 0.02 \left(R^2 = 0.98\right) \qquad \textbf{Eq. IV-12}$$

This relation was obtained for solids load 0%, 4%, 8% and 12% (wt.$_{\text{WET BASIS}}$ /vol.) as only in these situations transition regime was observed. The obtained values are in the same range as those of **Eq. IV-9** (Yang et al., 2010).

These results demonstrate that the influence of SG load in the critical value corresponding to the end of HoR (q_C) follows the same pattern of low viscosity liquids. It seems that, depending on the column size (diameter and height), type of distributor and type of solids, the dual effect of solids and viscosity suggested by some authors (Mena et al., 2005a; Ruzicka, et al., 2001) may or may not occur (Yang et al., 2010) as in this case. It is important to notice that **Eq. IV-12** is limited to this particular system (air-water-SG), being similar evaluations possible and desirable for other gas-liquid-solid systems in order to have a better understanding of its hydrodynamics

Although the presented information aims at contributing to the effect of a solid phase on the hydrodynamics of *g-l-s* systems, further work is required to clarify how solids influence regime transition and the magnitude of this influence. Obtained results allowed to confirm that that solid influence is related with the low viscosity of the "pseudo-homogeneous" liquid phase formed and that other parameters such as steric effect, wettability, BC design and distributor geometry play also an important role in flow regime transition.

IV.5 Conclusions

The effect of SG particles on homogeneous regime stability and regime transition in a three-phase BC was investigated experimentally. The stability was expressed by the critical values of gas holdup and gas flow rate. The experiments showed that the solids promoted stabilization on HoR for low gas flow rate. Moreover, it was demonstrated that spent grains decrease the critical values where the HoR prevails. This influence was demonstrated to have similar effect to the one found for low viscosity liquids on regime transition. In addition, it was possible to conclude on the importance of the steric effect of solids as well as their specific properties (wettability) on regime transition.

Despite this, the mechanisms by which solids affect the regime transition is far from being understood. Furthermore the influence of column size and type of solids makes difficult a real assessment when all results available in literature are compared

IV.6 References

Banisi, S., Finch, J. A., Laplante, A. R. and Weber, M. E. (**1995**). Effect of solid particles on gas holdup in flotation columns - I. measurement. *Chemical Engineering Science*, 50(14), 2329–2334.

Brányik, T., Vicente, A. A., Machado Cruz, J. M. and Teixeira, J. A. (**2001**). Spent grains – a new support for brewing yeast immobilisation. *Biotechnology Letters*, 23(13), 1073–1078.

Brányik, T., Vicente, A. A., Oliveira, R. and Teixeira, J. A. (**2004**). Physicochemical surface properties of brewing yeast influencing their immobilization onto spent grains in a continuous reactor. *Biotechnology and bioengineering*, 88(1), 84-93.

Cartellier, A. (**1990**). Optical probes for local void fraction measurements: Characterization of performance. Review of Scientific Instruments, 61(2), 874-886.

Deckwer, W. D. (**1992**). *Bubble Column Reactors*. (Wiley, Ed.). Chichester.

Eissa, S. H. and Schugerl, K. (**1975**). Holdup and backmixing investigation in co- and counter-current bubble columns. *Chemical Engineering Science*, 30, 1251-1256.

Freitas, C., Vicente, A. A., Mota, M. and Teixeira, J. A. (**1997**). A new sampling device for measuring solids hold-up in a three-phase system. *Biotechnology Techniques*, 11(7), 489-492.

Freitas, C. and Teixeira, J. A. (**1998a**). Solid-phase distribution in an airlift reactor with an enlarged degassing zone. *Biotechnology Techniques*, 12(3), 219-224.

Freitas, C. and Teixeira, J. A. (**1998b**). Hydrodynamic studies in an airlift reactor with an enlarged degassing zone. *Bioprocess and Biosystems Engineering*, 18(4), 267–279.

Freitas, Carla, Fialová, M., Zahradnik, J., and Teixeira, J. A. (**1999**). Hydrodynamic model for three-phase internal-and external-loop airlift reactors. *Chemical Engineering Science*, 54, 5253-5258.

Gandhi, B., Prakash, A. and Bergougnou, M. A. (**1999**). Hydrodynamic behavior of slurry bubble column at high solids concentrations. *Powder Technology*, 103(2), 80–94.

Gharat, S. D. and Joshi, J. B. (**1992**). Transport phenomena in bubble column reactors I: flow pattern. *The Chemical Engineering Journal*, 48, 141-151.

Hyndman, C. L., Larachf, F. and Guy, C. (**1997**). Understanding gas-phase hydrodynamics in bubble columns : a convective model based on kinetic theory. *Chemical Engineering Science*, 52(1), 63-77.

Jamialahmadi, M. and Muller-Steinhagen, H. (**1991**). Effect of solid particles on gas hold-up in bubble columns. *Canadian Journal of Chemical Engineering*, 69, 390-393.

Joshi, J.B. and Lali, A. M. (**1984**). Velocity-hold up relationship in multiphase contactors—A unifed approach. *Frontier in chemical reaction engineering*. New Delhi: Wiley.

Krishna, R. (**1991**). A Model For Gas Holdup In Bubble Columns Incorporating The Influence Of Gas Density On Flow Regime Transitions, 46, 2491-2496.

Krishna, R., Ellenberger, J. and Maretto, C. (**1999**). Flow regime transition in bubble columns. *International Communications Heat Mass Transfer*, 26(4), 467-475.

Lu, W-J., Hwang, S-J. and Chang, C-M. (**1995**). Liquid velocity and gas holdup in three-phase internal loop airlift reactors with low-density particles. *Chemical Engineering Science*, 50(8), 1301–1310.

Mena, P. C., Ruzicka, M. C., Rocha, F. A., Teixeira, J. A. and Drahos, J. (**2005a**). Effect of solids on homogeneous–heterogeneous flow regime transition in bubble columns. *Chemical Engineering Science*, 60(22), 6013-6026.

Mena, P. C., Pons, M. N., Teixeira, J. A. and Rocha, F. A. (**2005b**). Effect of Solids on Gas-Liquid Mass Transfer and Bubble Characteristics in Three-Phase Systems. *7th World Congress of Chemical Engineering*.

Mena, P. C., Rocha, F. A., Teixeira, J. A., Sechet, P., and Cartellier, A. (**2008**). Measurement of gas phase characteristics using a monofibre optical probe in a three-phase flow. *Chemical Engineering Science*, 63(16), 4100-4115.

Mussatto, S. I., Aguilar, C. N., Rodrigues, L. R. and Teixeira, J. a. (**2009a**). Colonization of Aspergillus japonicus on synthetic materials and application to the production of fructooligosaccharides. *Carbohydrate research*, 344(6), 795-800.

Mussatto, S. I., Aguilar, C. N., Rodrigues, L. R. and Teixeira, J. A. (**2009b**). Fructooligosaccharides and B-fructofuranosidase production by Aspergillus japonicus immobilized on lignocellulosic materials. *Journal of Molecular Catalysis B: Enzymatic*, 59, 76-81.

Reilly, I. G., Scott, D. S., de Bruijn, T. J. W. and MacIntyre, D. (**1994**). The role of gas phase momentum in determining gas holdup and hydrodynamic flow regimes in bubble column. *Canadian Journal of Chemical Engineering*, 72, 3-12.

Riquarts, H. P. (**1979**). Model representation of homogeneous and heterogeneous two-phase flow in fluidized beds and bubble columns. *German Chemical Engineering*, (2), 268–274.

Ruzicka, M. C., Zahradnik, J., Drahoš, J., and Thomas, N. H. (**2001a**). Homogeneous-heterogeneous regime transition in bubble columns. Chemical Engineering Science, 56(15), 4609–4626

Ruzicka, M. C., Drahoš, J., Fialová, M. and Thomas, N. H. (**2001b**). Effect of bubble column dimensions on flow regime transition. *Chemical Engineering Science*, 56, 6117-6124.

Ruzicka, M. C. and Thomas, N. H. (**2003a**). Buoyancy-driven instability of bubbly layers: analogy with thermal convection. *International Journal of Multiphase Flow*, 29, 249-270.

Ruzicka, M. C., Drahoš, J., Mena, P. C. and Teixeira, J. A. (**2003b**). Effect of viscosity on homogeneous–heterogeneous flow regime transition in bubble columns. *Chemical Engineering Journal*, 96(1-3), 15–22.

Ruzicka, M. C., Vecer, M. M., Orvalho, S. and Drahos, J. (**2008**). Effect of surfactant on homogeneous regime stability in bubble column. *Chemical Engineering Science*, 63(4), 951-967.

Schumpe, A. and Grund, G. (**1986**). The Gas Disengagement Technique for Studying Gas Holdup Structure in Bubble Columns. *The Canadian Journal of Chemical Engineering*, 64, 891-896.

Shaikh, A. and Al-Dahhan, M. H. (**2007**). A Review on Flow Regime Transition in Bubble Columns. *International Journal of Chemical Reactor Engineering*, 5, R1.

Shnip, A. I., Kolhatkar, R. V., Swamy, D. and Joshi, J. B. (**1992**). Criteria for the transition from the homogeneous to the heterogeneous regime in two-dimensional bubble column reactors. *International Journal of Multiphase Flow*, 18, 705-726.

Vial, C., Camarasa, E., Poncin, S., Wild, G., Midoux, N. and Bouillard, J. (**2000**). Study of hydrodynamic behaviour in bubble columns and external loop airlift reactors through analysis of pressure fluctuations. *Chemical Engineering Science*, 55, 2957-2973.

Vijayan, M., Schlaberg, H. I. and Wang, M. (**2007**). Effects of sparger geometry on the mechanism of flow pattern transition in a bubble column. *Chemical Engineering Journal*, 130, 171-178.

Wallis, G. B. (**1969**). One-dimensional Two-phase Flow. New York: McGraw-Hill.

Warsito, Ohkawa, M., Maezawa, A. and Uchida, S. (**1997**). Flow structure and phase distributions in a slurry bubble column. *Chemical Engineering Science*, 52(21-22), 3941-3947.

Wilkinson, P. M., Spek, A. P. and van Dierendonk, L. L. (**1992**). Design parameters estimation for scale-up of high-pressure bubble columns. *A.I.Ch.E. Journal*, 38, 544-554.

Xie, T., Ghiaasiaan, S. M., Karrila, S. and Mcdonough, T. (**2003**). Flow regimes and gas holdup in paper pulp – water – gas three-phase slurry flow. *Chemical Engineering Science*, 58, 1417 - 1430.

Yang, J. H., Yang, J-I., Kim, H-J., Chun, D. H., Lee, H-T. and Jung, H. (**2010**). Two regime transitions to pseudo-homogeneous and heterogeneous bubble flow for various liquid viscosities. *Chemical Engineering and Processing: Process Intensification*, 49, 1044-1050.

Yoo, D. H., Tsuge, H., Terasaka, K. and Mizutani, K. (**1997**). Behavior of bubble formation in suspended solution for an elevated pressure system. *Chemical Engineering Science*, 52(21-22), 3701–3707.

Zahradnik, J., Fialova, M., Ružička, M., Drahoš, J., Kaštánek, F. and Thomas, N. H. (**1997**). Duality of the gas-liquid flow regimes in bubble column reactors. *Chemical Engineering Science*, 52(21-22), 3811–3826.

V. Chapter V – Global Hydrodynamic Properties of Three-phase iGLR

V.1 Objectives

The main objective of this chapter was to determine the influence of SG loading on hydrodynamic parameters (solids and gas hold-ups, liquid velocity, circulation/mixing times) for three different configurations of an iGLR with enlarged top degassing zone. The main goal was to determine the best iGLR design that confers suitable hydrodynamic conditions for a fermentation of AFB in continuous mode.

V.2 Introduction

Gas-lift reactor hydrodynamics have been studied over the past years due to their ability to be used in several chemical and biotechnology processes. The importance of studying the gas-lift reactor hydrodynamics on biotechnology processes has been already referred especially in fermentation processes, where solid phase with similar density to fermentation broths is present (Freitas and Teixeira, 1998; Klein et al., 2003).

In this thesis (Chapter III and VIII) two solids have been studied for continuous AFB production in an iGLR. The results presented in Chapter VIII (section VIII.3.1) indicate that bottom-fermenting strains using SG as carrier are suitable for the continuous production of AFB in an iGLR. In Chapter IV the influence of SG as solid-phase on the regime flow transition in BC, as well as the possible involved physical mechanisms are studied. The previous results (Chapter IV) showed that the properties of SG are very important, because they reduce the time where the HoR is present.

The behaviour of SG in the iGLR hydrodynamics is still unknown. Moreover, it is also important to well define some aspects of the iGLR riser configuration: a crucial design parameter for this type of reactors (Klein et al., 2003). In order to establish the limits where the biotechnology processes for AFB using SG in an iGLR can operate, it is important to understand how these cellulose-based particles can affect three-phase iGLR hydrodynamics.

V.2.1 Gas-lift reactor design and configurations

The gas-lift reactor is a modified bubble column and three general configurations are considered: internal, split or external (**Figure V-1**).

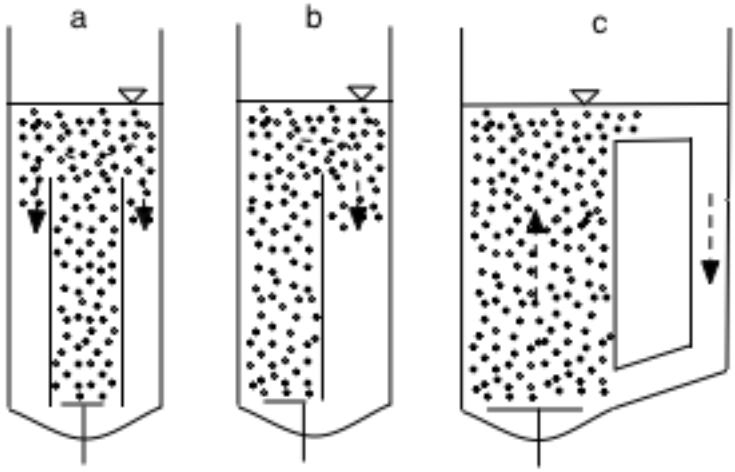

Figure V-1. Different configurations used in GLR. Legend: a) Internal-loop GLR (iGLR); b) Split GLR; c) External-loop GLR.

Among the GLR types, different specific configurations are present: (1) the position of the gas distributor; (2) presence or absence of an enlarged top section. These specifications depend mainly on their final application (Freitas and Teixeira, 1998; Van Benthum et al., 2000).

The *g-l* separation in an iGLR takes place at the top part of the reactor. In terms of iGLR terminology, the presence of a separator is considered when: $D_{SEP}>D_C$ (Chisti, 1989; Klein et al., 2003). The presence of an enlarged top section is usually applied to easier the gas release. In addition it allows the sedimentation of particles that may be present in the liquid medium that are expected to be kept indefinitely inside the iGLR (for example when continuous mode of operation is applied). This is achieved because the cross-sectional area increase reduces the downwards liquid (and solids) velocity into the downcomer and thus a better gas disengagement and solids sedimentation occurrs (Dolgos et al., 2001). Due to these reasons, the iGLR used in previous experiments was equipped with a degassing section in the top part (**Figure V-3**). In **Figure V-3** it is possible to observe the presence of a

double-barrier in the reactor outlet. This double-barrier helps in the reduction of the biocatalyst losses when we are operating the iGLR at continuous mode. The outer barrier is opened at bottom and top and the inner barrier is opened only at the top. Thus, it is the inner barrier that defines the reactor contents level. This arrangement obliges liquid phase to a specific movement: initially the liquid phase goes down to pass the first barrier and then upwards to leave the reactor. The first barrier avoids not only the presence of gas-phase during the liquid-solid separation but also reduces the liquid fluctuations near the inner barrier. When the liquid is going upwards in the space between the two barriers, it is then easier to complete the separation of bigger particles (carrier, yeast flocs, etc), which the operator wants to maintain inside the reactor. In our case, we want to keep the biocatalyst (SG + yeast cells) inside the iGLR during a long-term fermentation and this configuration with the enlarged top section plus the double-barrier in outlet, plays an important role to avoid big losses of biocatalyst.

The majority of published papers about the influence of reactor configuration on its hydrodynamics studies the effect of: ratio between downcomer and riser areas (A_d/A_r), riser length (H_r), gas sparger design and location, liquid height and the presence/absence of an enlarge top degassing section (Klein et al., 2003; Lu et al., 1995; Olivieri et al., 2007). Klein et al. (2003) indicated that using the same enlarged top degassing zone, simply by changing the riser length different iGLR configurations can be achieved. It is suggested that if the riser top end matches the opening of top section, it is only considered one separator. The separation of gas and solid phases from the liquid then takes place only in the enlarged top degassing section. On the other hand, if the riser top end is below the top section opening then it is called a dual separator (**Table V-1** and **Figure V-3**). This dual separator consists of two parts: the lower part acting as a bubble separator and a top part (enlarged zone) acting as a particle separator (Klein, et al., 2003).

The types of spargers commonly used in biotechnology processes are the perforated plate and in a lesser degree the porous plates. Different spargers originate different bubbles sizes, which can have a significant effect on reactor hydrodynamics. Generally sintered plates with porosity “1” and perforated plates with 0.5 mm orifices and 0.2% of free plate area ratio are ideal to obtain both flow regimes (HoR and HeR) (Zahradnik et al., 1997). In an iGLR it is believed that sparger location has a higher effect on bubbles distribution and on the reactor's hydrodynamics (Chisti, 1989) than its type (porous or perforated plate). For sintered plates with porosity “1” and perforated plates with 0.5 mm orifices and 0.2% this is valid since the bubbles formed are similar in size and shape.

The three-phase iGLR hydrodynamic behaviour involves the study of several parameters as: gas and solid hold-up, mixing time, circulation time and liquid velocity in riser and downcomer (Freitas and Teixeira, 1998a; Klein et al., 2003; Korpijarvi et al., 1999; Lu et al., 1995; Merchuk et al., 1998; Olivieri et al., 2007).

The interaction between all these parameters with the operation parameters (gas flow, solid content, liquid and solids properties) will determine the best iGLR configuration to be used on each process. A compromise between reactor configuration, operation parameters and hydrodynamic properties is essential to establish the best conditions to achieve better fermentation performances.

V.2.2 Gas-phase global properties and methods

In iGLR the gas-phase is injected in the riser (draft tube) promoting the mixing and liquid circulation inside the reactor (**Figure V-1.a**). It is known that solids influence the behaviour of gas-liquid (*g-l*) mixture. This influence can be either in gas-phase and/or in liquid-phase. In order to understand the real solid influence, it is important to understand and characterize liquid and gas phases either in the *g-l* and in gas-liquid-solid (*g-l-s*) systems.

The influence of solids in the gas-phase is characterized by: (1) changing bubbles properties such as: shape, rise and formation velocity (Fan et al., 1999; Yang et al., 2007; Yoo et al., 1997); (2) altered radial and axial gas-phase (hold-up) profiles (Gandhi et al., 1999; Warsito et al., 1997); (3) influence mixing and dispersion (Matsumoto et al., 1989); (4) modified gas hold-up (Banisi et al., 1995a, 1995b; Gandhi et al., 1999; Jamialahmadi et Muller-Steinhagen, 1991) and flow regimes profile (Mena et al., 2005; Warsito et al., 1997; Xie et al., 2003).

Generally, in iGLR the presence of solids decreases the gas hold-up in the riser. This decrease is bigger at gas superficial velocities higher than 0.2 m/s. Depending on the iGLR configuration the gas-phase may or not be present in the downcomer. Generally bubbles enter in the downcomer when gas superficial velocities are between 0.1 m/s and 0.3 m/s (Freitas et al., 1998a; Klein et al. 2003a). At these conditions, liquid velocity in downcomer is such that it drags bubbles to this part of the reactor. The solids also influence the presence of gas-phase in the downcomer of iGLR, especially when in the presence of a dual separator. Freitas et al (1998a) and Klein et al (2003a) results indicated that the presence of solids (up to 20% (vol./vol.)) on the same iGLR configuration (A_d/A_r=3.67; dual separator top section) increases the downcomer gas hold-up at lower gas superficial velocities (0.1 m/s to 0.2 m/s). There is a dual effect of solids in dowcomer's gas hold-up: at low gas superficial velocities (up to 0.3 m/s) solids increase gas hold-up in downcomer, at higher velocities (>0.4 m/s) solids presence decreases the downcomer gas hold-up (Freitas and Teixeira, 1998a; Klein et al., 2003a). A possible explanation for this dual effect lies in the combined effect of coalescence and the bubble slip velocity. In downcomer, bubble slip velocity has a direct influence on gas hold-up. If bubbles slip velocity is smaller than the downcomer's liquid linear velocity, bubbles are entrained by the liquid. The space occupied by the solids reduces the space for bubbles to flow and the hindrance cause by it decreases their slip velocity. Moreover at low gas superficial velocities, the coalescence phenomena is reduced, thus bubbles are small and with low slip velocity. Bubbles with these

characteristics are easily arrested to downcomer increasing the gas hold-up in this section. On the other hand, at high gas superficial velocities the interactions between bubbles increase due to their amount and less space available (occupied by solids), which promotes coalescence. At this point the coalescence impact is higher than the hindrance caused by solids presence. Consequently the bubbles are bigger with high slip velocity and then fewer bubbles are entrained to the downcomer reducing the gas hold-up in this part of the iGLR. It is important to refer that this is used to explain the downcomer's gas hold-up difference between the *g-l-s* and *g-l* systems. Moreover, this may not be as simple as it seems, because in GLRs there are a lot of different mechanisms that may influence gas hold-up in downcomer and the impact of each one of them is not yet clear (Chisti, 1998).

The mechanism by which solids influence the global gas hold-up has been studied and some attempts have been made to explain it (Banisi et al, 1995a, 1995b; Mena et al., 2005). The solids influence has been identified mainly for BC. The solid physical mechanism influence in GLR should be identical to BC, especially in riser where three-phases are always present. Theoretically and due to the differences between these reactors (liquid flow, design, mixing profile), the intensity of each mechanism might be different.

To determine global gas hold-up in the riser and downcomer generally non-invasive techniques are used. In iGLR design the pressure drop between two points in the riser/downcomer, and the Dynamic Gas Disengagement techniques are commonly applied (Boyer et al., 2002; Deckwer, 1992). Pressure drop between two points allows to measure the liquid or gas hold-up and can be obtained by differential pressure sensors (Boyer et al., 2002; Freitas et al., 2000; Klein, et al., 2003) or by a inverted manometer tube (Chisti, 1989; Merchuk et al., 1998) used in this work **Figure V-2**.

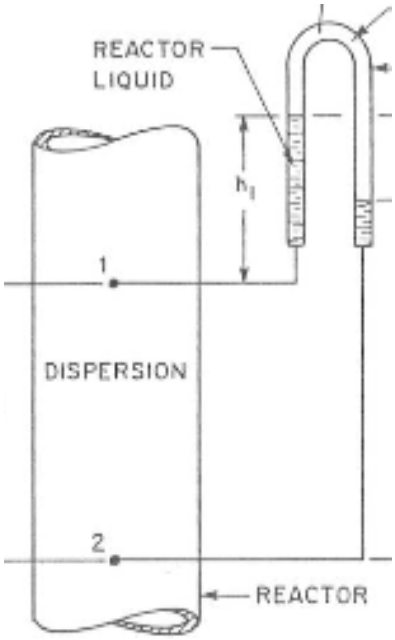

Figure V-2. Inverted tube manometer arrangement. (Adapted from Chisti, 1989)

In two phase-flow, the gas hold-up is determined according to:

$$\varepsilon_G = \frac{\rho_L}{\rho_L - \rho_G} \times \frac{d_h}{d_{12}} \qquad \textbf{Eq. V-1}$$

Where d_h is the distance between liquid columns (**Figure V-2**) and d_{12} is the distance between the measuring points (1 and 2 in **Figure V-2**).

Is important to note that in *g-l-s* systems the pressure drop per se is not enough to measure all phases hold-up and an additional technique must be used. Generally, it is preferred to use a different technique to measure the solid-phase hold-up (Boyer et al., 2002; Freitas and Teixeira, 1998a, 1998b; Klein, et al., 2003).

V.2.3 Solid-phase global properties and methods

In iGLR not only solid influence on gas hold-up is important, but also solid distribution throughout the reactor. Freitas and Texeira (1998b) found that for low-density particles (alginate beds) in an iGLR there is an axial and radial solids distribution at low gas flows (Freitas and Teixeira, 1998b). Using the same solids, Klein et al (2003a, 2003b)

found that solid distribution are also affected by riser configuration where uniform solid distribution is achieved at lower ratio between downcomer and riser (Klein et al., 2003a). The work of Klein et al. (2003a) showed that for a small solid load gas velocity does not have a big influence on solid distribution and these are mainly located in the bottom part of both riser and downcomer for different internal draft configurations (Klein et al., 2003a). Therefore, it is expected to have similar solids distribution for our reactor configuration, due to similar properties between SG and alginate beds. Moreover, in a fermentation using SG as carrier for biomass immobilization the solid concentrations used are normally up to 12% ($wt._{WET\ BASIS}$/vol.) (Klein et al., 2003a; Brányik et al., 2002). From Klein et al. (2003) work it is not clear if riser length has any influence on solids distribution for higher ratios between riser and downcomer cross-section (A_d/A_r=3.67), normally found in iGLR for continuous AFB primary fermentation (Lehnert et al. 2008, 2009) and the same used in Chapter VIII.

Several methods can be used to measure solids hold-up and distribution. These methods can be either (1) non-invasive using a tracer (Boyer et al., 2002) or pressure drop (Klein et al., 2003a; Rodríguez et al., 1999); and/or (2) invasive using samplers (Freitas and al., 1999). Tracer methods are normally applied in fluidization columns. The solid tracer is a particle that should have the same shape size and density of study particles. There are different kinds of tracers: coloured, magnetic and fluorescent (Boyer et al., 2002). Wenge at al (1999) cited by Klein et al (2003a) initially proposed the pressure drop method. This method starts by the measurement of hydrostatic pressure in the *g-l-s* dispersion followed by interruption of gas flow (complete gas disengagement). Then a second measurement in the resulting two-phase (solid–liquid) dispersion is performed. The measurement period has to be short enough to avoid significant sedimentation of the solid particles. Klein et al. (2003a) used this method for alginate beads and the measuring time was around 250 s (Klein et al., 2003a, 2003b). However the SG's sedimentation is very fast and formed a compact layer in less than a minute, which is very hard to remove without

physical interference. Moreover, this method lacks information about solids distribution, which is also a very important parameter in iGLR. Sampler devices as the developed by Freitas et al. (1997) can be very useful for solids hold-up determination and allow also to study the solids distribution in the iGLR with relative errors less than 10% (Freitas and Teixeira, 1997, 1998b).

V.2.4 Liquid-phase global properties and methods

It is also important to take into account the liquid-phase properties in three-phase systems, mainly the changes that occur in this phase. These may or may not be caused by the presence of solids. Usually, circulation and mixing times are important parameters to study the mixing and dispersion of the iGLR. Associated to this, liquid velocities in downcomer and riser are normally determined. Liquid velocity is a crucial parameter that is applied in several models for describing the iGLR hydrodynamics (Chisti, 1989; Freitas et al., 1999; Garcia-Calvo et al., 1999; Lu et al., 1995) and also used when scale-up is performed (Chisti, 1989; Freitas et al., 1999; Lu et al., 1995; Rodríguez et al., 1999).

To measure the parameters listed above, tracer techniques are applied. Different kinds of tracers can be used: thermal (Garcia-Calvo et al., 1999), acid (Freitas and Teixeira, 1998a; Lu et al., 1995; Merchuk et al., 1998; Chisti, 1989) and magnetic (Bla et al., 2004; Klein et al., 2004; Van Benthum et al., 2000) tracers. Acid tracers are used mainly to determine the downcomer liquid linear velocity. In summary, two pH electrodes (same response time) are placed in downcomer and a pulse of sulphuric acid (4 M to 8 M) is injected at the top of the downcomer. The liquid linear velocity is then calculated from the equation:

$$v_{Lr} = \frac{d_{electrodes}}{\Delta t_{probes}} \qquad \textbf{Eq. V-2}$$

Then by a mass balance (**Eq. V-3**), it is possible to determine the downcomer liquid linear velocity and also the riser and downcomer

liquid superficial velocities – **Eq. V-4** (Chisti, 1989; Freitas and Teixeira, 1998a):

$$v_{Lr} = v_{Ld} \times \frac{A_d}{A_r} \times \frac{1-\varepsilon_{Gd}-\varepsilon_{Sd}}{1-\varepsilon_{Gr}-\varepsilon_{Sr}} \qquad \textbf{Eq. V-3}$$

$$U_{Li} = v_{Li} \times (1-\varepsilon_{Gi}-\varepsilon_{Si}) \qquad \textbf{Eq. V-4}$$

Knowing the length of riser and downcomer, it is then possible to determine the circulation time by (Chisti, 1989):

$$t_c = \frac{L_r}{U_{Lr}} + \frac{L_d}{U_{Ld}} \qquad \textbf{Eq. V-5}$$

Circulation time is also related with mixing time, which is defined as the time (t_M) necessary to obtain a required degree of mixing (α_M):

$$\alpha_M = \frac{C-C_0}{C_\infty - C_0} \qquad \textbf{Eq. V-6}$$

Several methods are used to measure the mixing time. These are similar to the methods used to measure liquid linear velocity: (1) conductimetric; (2) thermal; (3) acid; (4) radioactive; and (5) colorimetric. Mixing time indicates the mixing quality of the reactor and depends on iGLR configuration and design (Fonseca and Teixeira, 2007). Generally, in iGLR, mixing time decreases rapidly at lower gas flows (0.01 m/s to 0.3 m/s), after that there is a stabilization and only a big increase of gas flow can reduce significantly the mixing time (Freitas and Teixeira, 1998a; Klein et al., 2003; Merchuk et al., 1998). Similar behaviour can be found in circulation time (t_C). Considering that circulation and mixing times are very important parameters on the characterization of the mixing performance of a iGLR, the methods used should have enough time resolution to capture the liquid fluctuations between the two points where the measurement takes place.

V.3 Material and Methods

V.3.1 Gas-lift reactor: dimensions and characteristics

The experiments were done in a Perspex® iGLR with a top enlarged degassing zone (**Figure V-3**). The iGLR has total volume of 60 L and the relevant dimensions are indicated. Measurements were done for three different riser tubes described in **Table V-1**. The risers were located 2.3 cm above the distributor.

Table V-1. Riser configurations used in this work.

Riser Label	D_{ri} / cm	H_r / cm	D_{ci} / cm	A_{ri}/A_d
Riser A	6.2	120	14.2	3.97
Riser B	6.2	140	14.2	3.97
Riser C	8.7	120	14.2	1.79

Legend: D_{ri} – Riser internal diameter; H_r – height of riser; D_{ci} – Column internal diameter; A_{ri}/A_d – Ratio between internal riser area and downcomer area.

The gas entered the airlift through the 10 cm diameter porous plate sparger. The diameter of the ‘‘active’’ zone of the sparger, through which the gas flow was passing, was around 8 cm. Air (20 º – 25 ºC) and tap water (18 ºC – 22 ºC) were used as the gas and liquid phase. The net water flow through the airlift was zero.

Table V-2. Resume of all conditions used in this work

U_{AIR}/ (cm/s)	$Q_{G(A/B)}$ / (L/min)	$Q_{G(C)}$ / (L/min)	% Solids ($wt._{WET\ BASIS}$/Vol.)
1	1.9	3.6	0; 4; 8; 12; 20
2.5	4.5	8.9	0; 4; 8; 12; 20
5	9.1	17.8	0; 4; 8; 12; 20
7.5	13.6	26.8	0; 4; 8; 12; 20

Four gas superficial velocities in the riser ranging from 1 to 7.5 cm/s were studied and five solid loads were tested (**Table V-2**). The air flow was controlled by a 100 SLPM mass flow controller (Alicat Scientifics, Tucson, USA).

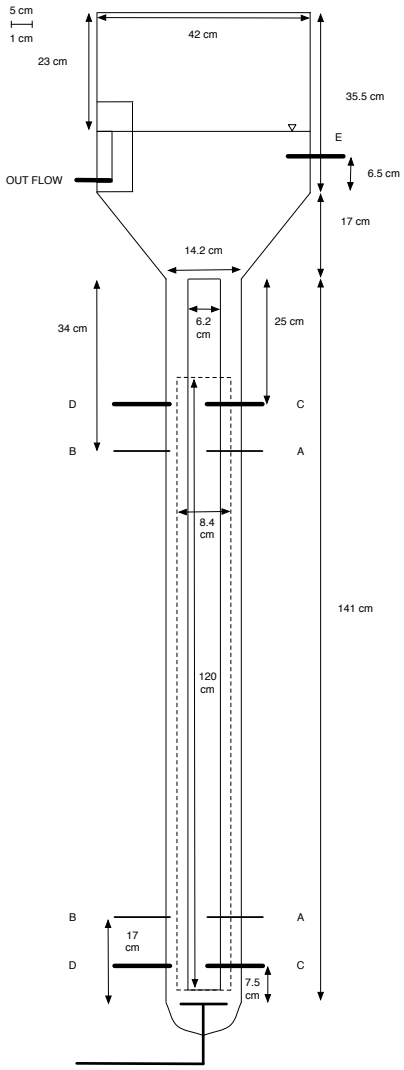

Figure V-3. Internal Gas-lift reactor design used in this chapter. Legend: A - Riser Hold-up measuring points; B - Downcomer Hold-up measuring points; C - Riser pH probes; D - Downcomer pH probes; E - Conductivity probe point

V.3.2 Solids distribution and hold-up

The same solids used in previous chapter (section IV.3.2.1) were used in the present chapter. Solids hold-up and distribution were determined by using the method developed by Freitas *et al* (1997) as described in section IV.3.4. The sampler was introduced into the reactor in several points: A,B,C,D,E (**Figure V-4**). Then solids volume was determined and solids hold-up calculated accordingly **Eq. IV-3**:

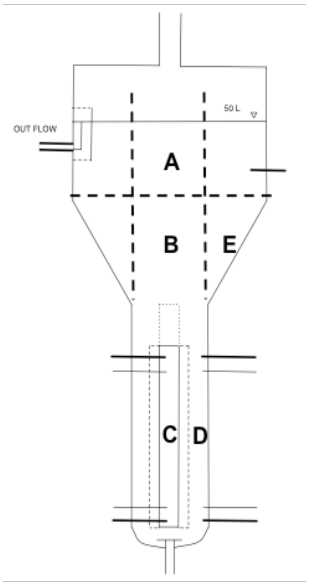

Figure V-4. Solids sampling locations for solid distribution determination.

V.3.3 Gas hold-up

Gas hold-up was determined using Freitas and Teixeira (1998a) procedure by measuring pressure difference between Top and Bottom of both riser and downcomer (d=1.09 m). Differential pressure was measured by water columns weight difference. For each set of experiments, pressure differences (d_{hi}) in riser and downcomer were measured at least three times during no less than 5 minutes. The mean value was then used to determined gas hold-up (riser/dowcomer) using the **Eq. IV-2**. Each measurement was done in triplicate (Chisti, 1989; Freitas and Teixeira, 1998a)

V.3.4 Mixing time determination

Mixing time was determined as the time for variation of NaCl concentration (50 mL of 300 g/L NaCl solution were injected at bottom of reactor (E point in **Figure V-3**)), to be within 5% of final value (Freitas and Teixeira, 1998a). Each experiment was repeated three times.

V.3.5 Circulation time determination

Circulation time was determined by injecting 10 mL of H_2SO_4 solution (4.5 M). The pH evaluation in riser and downcomer was recorded by 4 pH meters: two Methrom model 620 probes in the riser and two model 691 probes in the downcomer (Methrom,Herisau ,Switzerland) connected to a PC with a NI data acquisition board (National Instruments, Austin, Texas, USA) and recorded to files using Labview (National Instruments, Austin, Texas, USA). By averaging consecutive peaks in each pH response curve, circulation time was determined according to **Eq. V-5** (Chisti, 1989; Freitas and Teixeira, 1998a).

V.3.6 Liquid velocity determination

The liquid velocity in riser and downcomer was determined from the curves obtained on two pH meters (d_{12}=1.09 m) located in riser/downcomer. By knowing the time the tracer takes to travel from one electrode to the other, the liquid velocity was determined using the **Eq. V-2**. In order to avoid measuring errors due to acid dissociation only the initial peaks in pH response curves were used. Each experimental assay was repeated in triplicate (Chisti, 1989; Freitas and Teixeira, 1998a).

V.4 Results and Discussion

In this chapter the main hydrodynamic parameters for three different risers configuration in an iGLR with an enlarged top section were studied. The main objective was to choose one of these configurations for continuous primary AFB fermentation. Klein et al (2003b) determined that for *g-l* and *g-l-s* systems the main hydrodynamic parameters (gas hold-up, liquid velocity, solids hold-up and circulation time) do not suffer relevant changes when the reactor is operating in batch or in continuous mode (Klein et al., 2003b). The main reason was the maximum dilution rate used in biotechnology processes. Normally it is bellow 0.6 h^{-1} (in AFB production bellow 0.4 h^{-1}), so the liquid flow rate that passes throughout the GLR bioreactor is less than 1% of the liquid flow rate inside the iGLR. Therefore the tests were made using the same solids as in previous chapter and in batch system. Tap water instead of synthetic mineral medium (SMM) or real wort was used in the hydrodynamic studies. The main work was to determine the best reactor configuration for complete mixing and distribution of SG in the iGLR. The use of SMM or real wort would increase the risk of contamination between the different experiments, which would undoubtedly alter the liquid medium composition and influence the final results. Fresh tap water from municipal water company was used. Every two/three days, before testing new conditions the experiments in *g-l* systems were repeated in order to control if some relevant changes in water (liquid-phase) could be found, however no relevant variations were detected.

V.4.1 Solid particles distribution

As referred the solids distribution along the iGLR is really important, especially when fermentation processes are involved, because it will reduce the probability of having dead zones in the iGLR, which may lead to inappropriate fermentation performances. On the figures below (**Figure V-5**, **Figure V-6**, and **Figure V-7**) the values of solid hold-up for all configurations at different gas flow and solids load are displayed.

The average solid loads obtained among the five sections used are presented in **Table V-3**. The error between the measured values and the expected values is on average 7% with a maximum and minimum error of 14% and 0% respectively. The values are in agreement with Freitas and Teixeira (1998b) who used the same method and obtained around 10% error between experimental and expected value of solid load (Freitas and Teixeira, 1998b). **Table V-3** also indicates the variation coefficient, which may be used as an indicator of solids distribution inside the iGLR. Statistically the variation coefficient (VC) indicates the reproducibility of the experimental points. This coefficient was obtained from the solids hold-up measurements in the different iGLR areas (A,B,C,D,E in **Figure V-4**). In our case it can be used to obtain a qualitative evaluation of SG's particles distribution inside the iGLR. In terms of value if VC is near 100%, it means that the solids hold-up in different reactor positions are similar, thus a good solids distribution is obtained. The main drawback of using this criterion for evaluation of solids distribution is that at lower solid loads the method suffers the maximum variations, thus the VC criteria can only be used to compare the same solid load conditions.

V.4.1.1 Riser A

Results obtained for Riser A presented in **Figure V-5** and **Table V-3** indicated, as referred in the literature, that for this configuration there is an axial and radial distribution of solids, which is more pronounced at the two lower gas superficial velocities (1 cm/s and 2.5 cm/s) (Freitas and Teixeira, 1998b; Klein et al., 2003a, 2033b). More solid particles are present in the bottom part of the reactor (sections B, C and D in **Figure V-4**), while it is the opposite in the top part (sections A and E in **Figure V-4**). Dolgos et al (2001) define three main regimes that may occur in this (riser A in a working volume of 50 L) iGLR configuration: (A) liquid flows directly to the downcomer (particle residence time from 5 s to 10 s); (B) liquid prevails in the eddies between the top of the riser and the beginning of the enlarged top section (residence time 10 s to

20 s) and (C) the liquid that flows to the top enlarged section (residence time above 30 s).

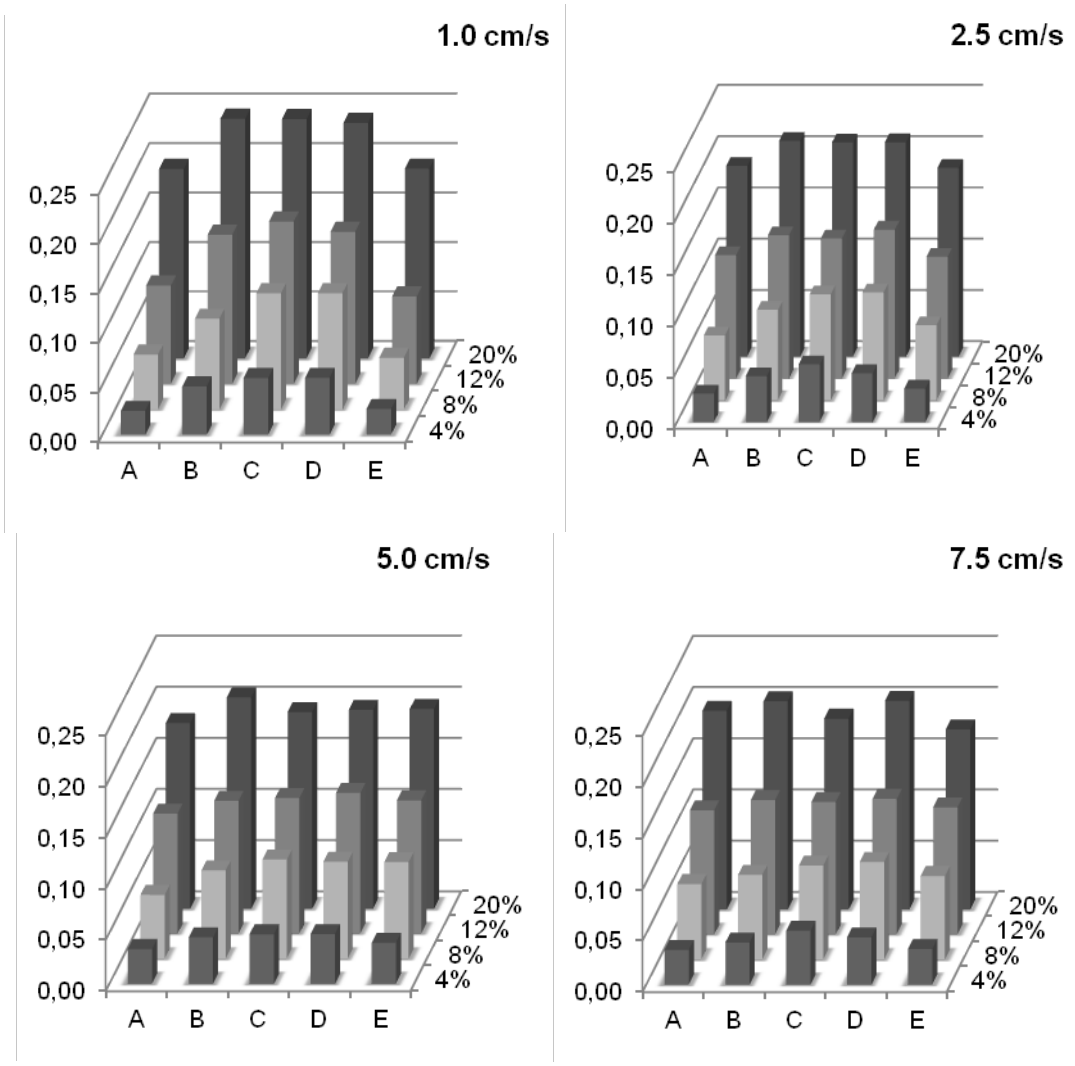

Figure V-5. Solids hold-up at different GLR positions (A,B,C,D,E) for riser A configuration at different gas superficial velocity (1 cm/s; 2.5 cm/s; 5 cm/s and 7.5 cm/s) in riser.

They found that the flow pattern A and B occurs more often than the flow pattern C at U_{Gr}=4.6 cm/s. Therefore at low gas flow rates the liquid flows mainly in the riser and the downcomer, which may explain the solids distribution obtained for the lower gas flow rates. The solids distribution in our case is influenced not only by the liquid exchange between the bottom and the top part of the reactor, but also by the settling properties of the particles used. These two phenomena are opposite. The liquid exchange acts to equalize the solid particle

concentrations, while the settling particles act to increase the particle concentration in the bottom part of the iGLR. When a low riser length is set (riser A) there is a dual separator, which has an effect on the reactor flow field of the top part. At low gas superficial velocities the liquid exchange is weaker and regime A and B are favoured (Dolgos et al., 2001), which together with the particles settling tendency leads to a poorer solids distribution in our iGLR. As the riser tube is shorter, the entrance in the top enlarged zone is further away and intermediated by a turbulent region (under the top of the riser tube). Liquid circulation eddies are presented in this region, which accordingly to Dolgos et al (2001) induces a typical liquid behaviour: most of the liquid that reach this region is entrained in the eddies and after a short circulation in this zone goes back to the downcomer, without reaching the top enlarged section. Therefore at lower gas superficial velocities the liquid circulation follows the patterns A and B, considering that SG particles moved in the same way as the liquid flows and their settling properties make more likely the existence of axial and radial solids distribution. Moreover, the axial solid distribution results are in accordance with the obtained by Klein et al (2003a) that used alginate beads and similar reactor design (except sparger configuration).

V.4.1.2 Riser B

In **Figure V-6** it is indicated that no axial and radial distributions are present, with the exception of lowest gas flow and high solid loads where a lower solid content in the conical part (section E) may be detected. In addition, the results presented in **Table V-3** for this riser indicate that the maximum variation coefficient (15%) is obtained at minimum gas superficial velocity (1 cm/s) and minimum solid load (4% ($wt._{WET\ BASIS}$/vol.)). Comparing between riser B and A it seems that increasing riser length has a significant effect on improving solid distribution inside the rector. Riser B was able to increase the solids homogeneity even at low gas flow rates.

Table V-3. Average of the experimental values of solids hold-up and error* in iGLR sections.

Riser	% Solids$_{TEO}$ (vol./vol.)	U_G / (cm/s)	% Solids$_{EXP}$ (vol./vol.) AVG	STDEV	VC	Error*
A	4 %	1	4%	0.017	38.80%	7%
		2.5	4%	0.012	27.69%	4%
		5	4%	0.006	14.41%	8%
		7.5	4%	0.008	18.91%	4%
	8 %	1	9%	0.032	36.84%	8%
		2.5	9%	0.018	21.19%	8%
		5	9%	0.014	16.47%	9%
		7.5	8%	0.009	10.14%	6%
	12 %	1	13%	0.035	26.44%	9%
		2.5	13%	0.012	9.04%	10%
		5	13%	0.008	5.79%	8%
		7.5	13%	0.005	3.78%	6%
	20 %	1	22%	0.027	12.17%	11%
		2.5	20%	0.013	6.69%	0%
		5	19%	0.009	4.59%	3%
		7.5	19%	0.012	6.14%	4%
B	4 %	1	4%	0.007	15.65%	5%
		2.5	4%	0.006	13.87%	9%
		5	4%	0.005	11.56%	8%
		7.5	4%	0.005	11.17%	10%
	8 %	1	9%	0.008	8.83%	9%
		2.5	9%	0.003	3.87%	9%
		5	9%	0.004	4.22%	12%
		7.5	9%	0.003	3.49%	12%
	12 %	1	13%	0.011	8.50%	10%
		2.5	13%	0.008	6.22%	7%
		5	13%	0.010	7.59%	6%
		7.5	13%	0.007	5.63%	5%
	20 %	1	21%	0.017	8.27%	6%
		2.5	20%	0.007	3.33%	2%
		5	20%	0.009	4.52%	1%
		7.5	20%	0.006	2.95%	1%
C	4 %	1	4%	0.012	27.79%	12%
		2.5	5%	0.007	15.77%	13%
		5	4%	0.005	11.12%	11%
		7.5	4%	0.005	12.07%	11%
	8 %	1	9%	0.014	15.27%	14%
		2.5	9%	0.015	16.17%	13%
		5	9%	0.009	10.38%	10%
		7.5	9%	0.005	5.61%	7%
	12 %	1	12%	0.023	20.28%	4%
		2.5	11%	0.019	17.10%	7%
		5	11%	0.009	8.34%	9%
		7.5	11%	0.004	4.08%	9%
	20 %	1	20%	0.049	24.87%	1%
		2.5	19%	0.028	14.46%	4%
		5	19%	0.013	7.12%	6%
		7.5	19%	0.013	7.05%	5%

*Error is the difference between the expected (theoretical value) and the measured value (experimental value). Legend: AVG – Average; STDEV – Standard derivation; VC – Variance coeficienc

Klein et al (2003a) found that riser diameter influence was crucial for better solids distribution than riser length, especially at high gas flows (Klein et al., 2003a). In our case, if all riser configurations are compared, the riser length proves to have better influence on solids distribution than the diameter increase. The possible explanation lies in the amount of liquid (consequently SG) exchanged between the top and bottom part of the iGLR. In this case, the liquid exchange counteracts the settling tendency of the SG particles and homogenizes the solid distribution At this configuration the liquid flow patterns described by Dolgos et al. (2001) are not present because the liquid leaving the riser directly enters in the enlarged top section. This provides a better liquid exchange in the axial direction and better solids mixing. It is expected to have a sharper velocity profile at the lower boundary of the iGLR top part with upward liquid flux in the iGLR center and downward flux near the iGLR exterior walls. If the riser is shorter (riser A), then the liquid leaving the riser would need to pass the bubble separator section (turbulent region) with its flow circulations eddies before entering the airlift top section. This would result in a flatter velocity profile and thus weaker liquid exchange. Moreover, at this configuration (riser B), as this turbulent region is suppressed, the influence of solids particles settling is lower because the mixing between the upward and downward liquid is reduced. The above mentioned reasons allow a better liquid exchange throughout the axial direction resulting in a more homogeneous solid particle distribution between the bottom and the top part of the airlift (**Figure V-6**).

Nevertheless, this homogeneity can have an adverse effect, when continuous systems are used, because the probability of carrier (SG) particle to wash-out is higher. That is why in the top enlarged section there is a double-barrier at the outlet (see section V.2.1), with the objective to decrease the solids loses when the iGLR operates in continuous mode (**Figure V-3**)

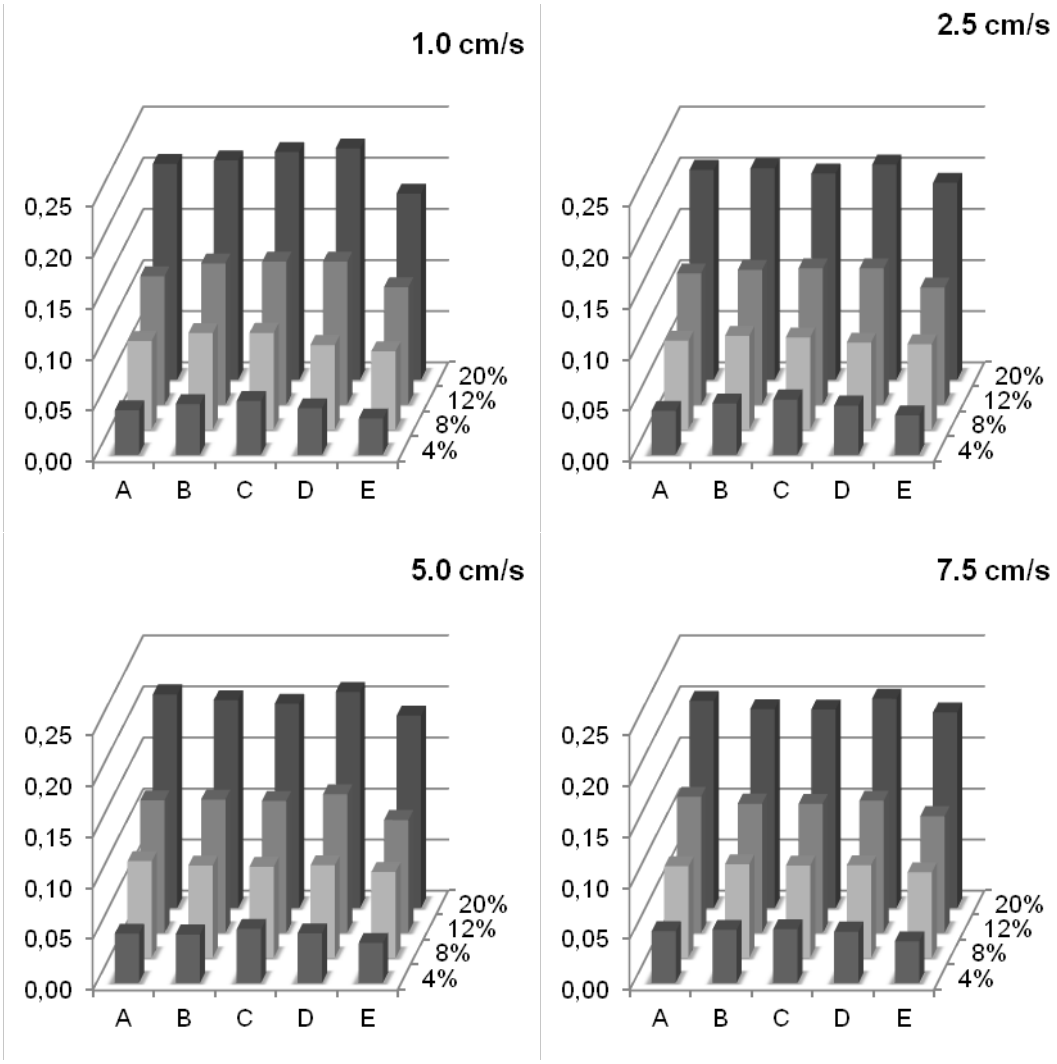

Figure V-6. Solids hold-up at different GLR positions (A,B,C,D,E) for riser B configuration at different gas superficial velocity (1 cm/s; 2.5 cm/s; 5 cm/s and 7.5 cm/s) in riser.

V.4.1.1 Riser C

In riser C (**Figure V-7**) as on riser A (**Figure V-5**), it is also present an axial and radial solids distribution at lower gas superficial velocities. By comparison with riser A at these conditions, in riser C the axial distribution is more pronouced with the highest solid concentration in the riser and downcomer sections (C and D respectively). This can be explained by the decrease of the ratio A_r/A_d (**Table V-3**), meaning that the downcomer cross-section is also smaller and the liquid velocity in that section is higher (**Figure V-11**). This will increase the mixing and the circulation eddies in the turbulence region, which favours the flow

patterns A and B, previously explained. Being so, the solids are preferably moved to the downcomer instead of going up to the top section and then they circulate mainly in the iGLR bottom part. These results suggested that an increase in riser diameter causes an increase in the solids non-homogeneities and the radial and axial distribution was more pronounced. Considering that Klein et al. (2003) obtained better solids distribution at higher A_r/A_d the possible explanation for this lies in the different properties of the solids used, alginate beads and SG, used in Klein et al (2003) work and in this work, respectively.

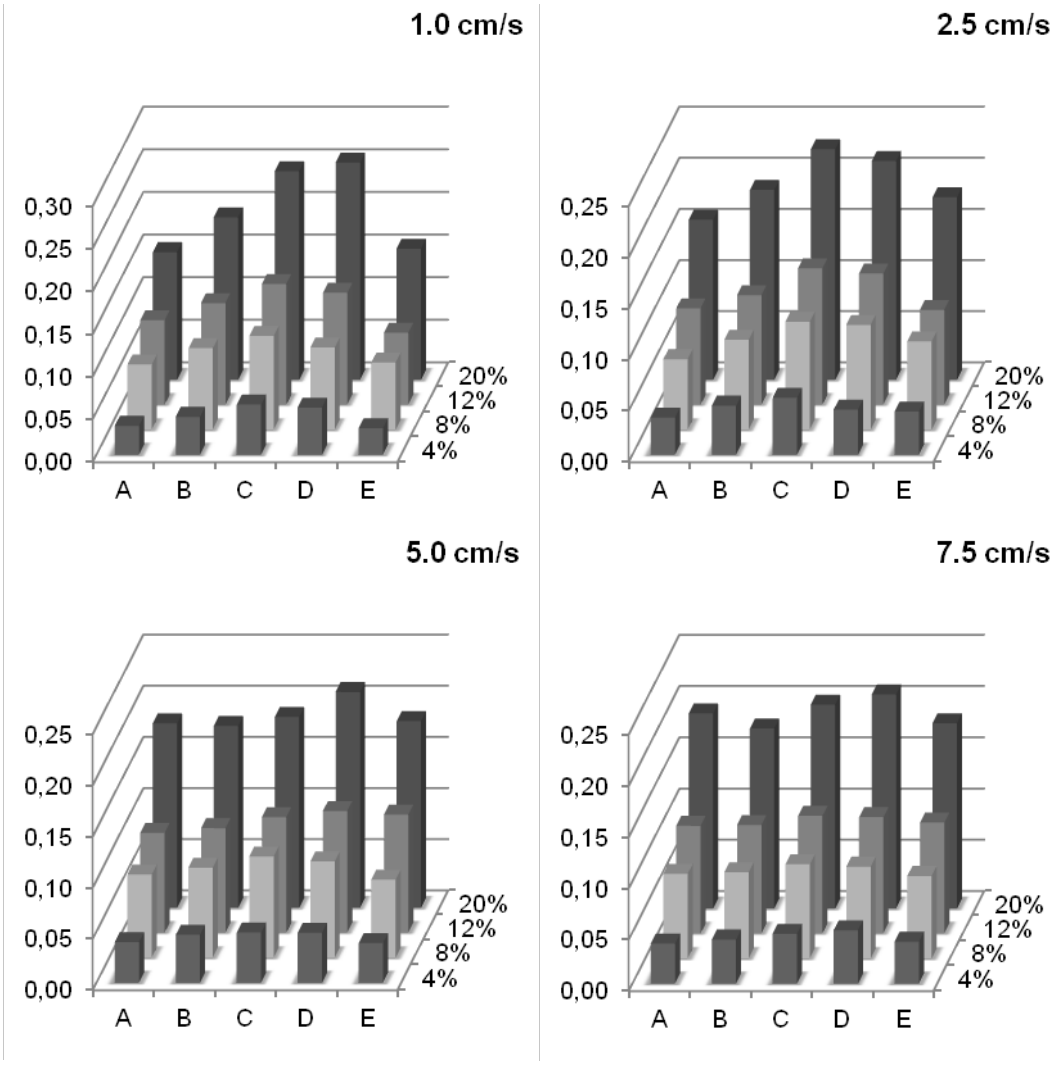

Figure V-7. Solids hold-up at different GLR positions (A,B,C,D,E) for riser C configuration at different gas superficial velocity (1 cm/s; 2.5 cm/s; 5 cm/s and 7.5 cm/s) in riser.

Theresults presented in **Table V-3** showed that for the same solid load the highest variation coefficients are always for the shortest risers (A and C). Comparing all configurations used (Riser A, B and C), it can be observed that the effect of riser length has more impact on solids distribution than the effect of riser diameter. These results suggest that riser B is better suited to achieve better homogeneity of SG distribution along all iGLR sections.

V.4.2 Gas hold-up

In **Figure V-8** it can be observed that in the iGLR the riser gas hold-up increases with gas superficial velocity. Generally there is a decrease of global gas hold-up when solids are present (**Figure V-8**). The bigger influence was detected for riser A at U_{Gr}=7.5 cm/s.

The low differences found can be explained by two factors: (1) the method accuracy, which has been proved to have an associated error between 15% and 20% (section IV.4.2); and (2) the properties (density) of SG that are very similar to water and does not influence significantly the liquid-phase properties.

The gas hold-up in riser decreases both with internal riser diameter decrease (Riser C to Riser A) and with the increase of riser length (Riser A and Riser B).

The increase of diameter increases riser cross-section area and consequently several phenomena can occur. The gas hold-up in riser when the bubble circulation regime is not present is related with liquid linear velocity by:

$$\varepsilon_{Gr} = \frac{U_{Gr}}{v_{Lr} + U_{slip}} \qquad \textbf{Eq. V-7}$$

When the bubble circulation regime is present (valid for $\varepsilon_{Gd} \geq 0.08$):

$$\varepsilon_{Gr} = \frac{U_{Gr0} + \varepsilon_{Gd}\left(v_{Ld} - U_{slip}\right) \times A_d / A_r}{v_{Lr} + U_{slip}} \qquad \textbf{Eq. V-8}$$

Where $v_{L/dr}$+/-U_{slip} *is* the total gas velocity in the riser and in the downcomer. For the same gas superficial velocities, gas hold-up depends on v_{Lr} and U_{slip}.

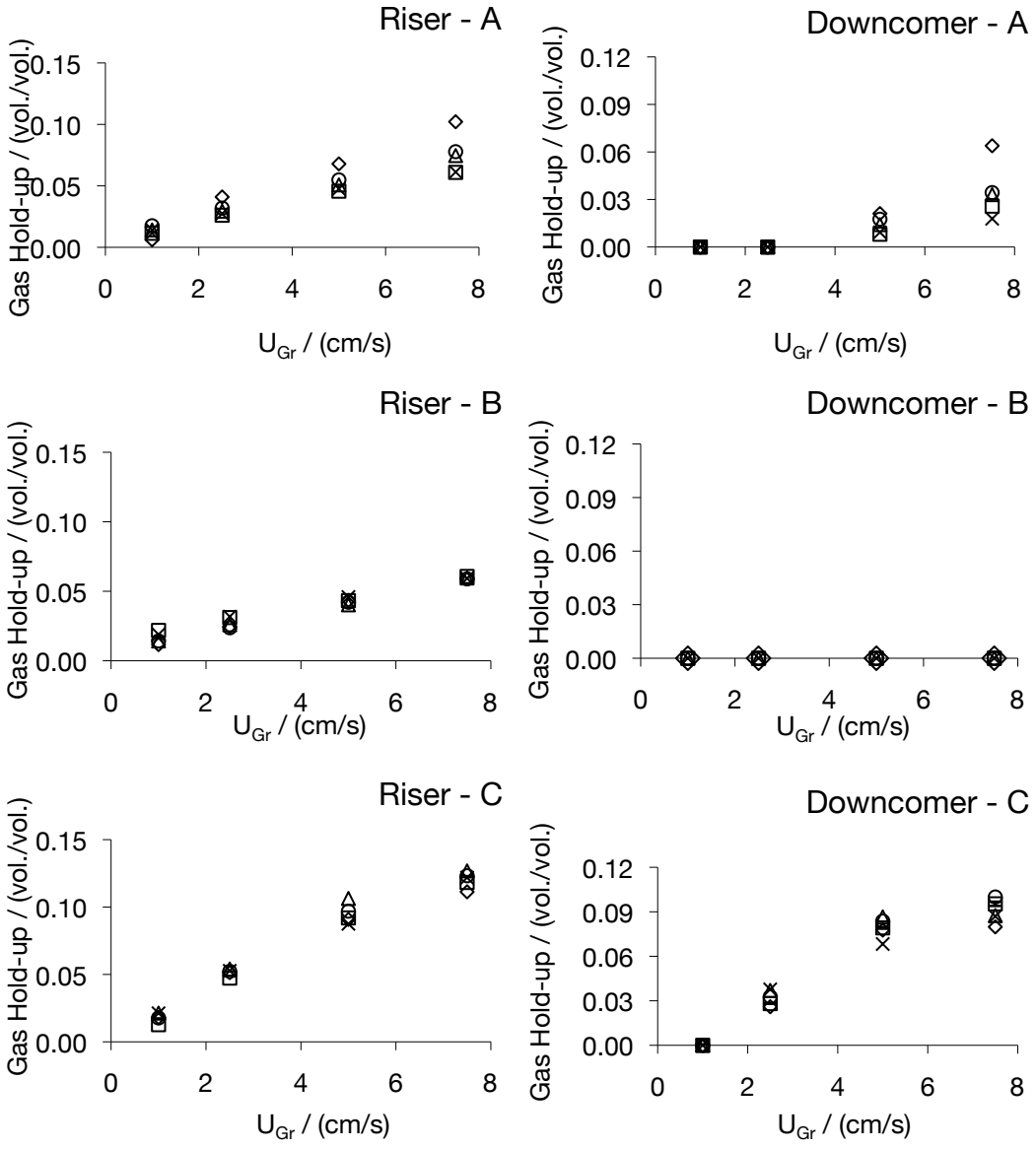

Figure V-8. Gas hold-up (vol./vol.) vs. Gas superficial velocity in riser (U_{Gr} / (cm/s)) for different risers configurations. Legend: ◇ - 0% (wt.$_{WET\ BASIS}$/vol.); □ - 4% (wt.$_{WET\ BASIS}$/vol.); △ - 8% (wt.$_{WET\ BASIS}$/vol.); ○ - 12% (wt.$_{WET\ BASIS}$/vol.); × – 20% (wt.$_{WET\ BASIS}$/vol.).

Considering that $v_{Lr} > U_{slip}$. changes in U_{slip} in the riser would have a reduced effect in riser's gas hold-up. The higher gas hold-up detected in riser C (compared with riser A) when no bubble regime circulation is present (U_{Gr}<5 cm/s) is mainly due to v_{Lr} decrease. From **Figure V-11**,

the v_{Lr} decrease is around 10% less in riser C (v_{Lr}=0.9 m/s at U_{Gr}=7.5 cm/s for 20% (wt.$_{WET\ BASIS}$/vol) of SG) than in the other risers (Riser B: v_{Lr}=1.0 m/s at U_{Gr}=7.5 cm/s for 20% (wt.$_{WET\ BASIS}$/vol) of SG). Considering the v_{Lr} decrease observed in riser C (**Figure V-11**) and by the **Eq. V-7** the maximum ε_{Gr} increase was expected to be 10%. Generally for U_{Gr}=7.5 cm/s the gas hold-up in riser C is around 20% more than in riser A which can be explained by the bubble circulation regime present in riser C and which can be explained by **Eq. V-7**. Applying **Eq. V-8** to the bubble circulation regime present in riser C when U_{Gr}=7.5 cm/s, it is possible to observe that, using the experimental values of $v_{Lr/d}$ (**Figure V-11**) and ε_{Gd} (**Figure V-8**), the U_{slip} obtained are very low. This is in accordance with visual indications that showed the presence of small bubbles (low U_{slip}) in the downcomer section.

In **Figure V-8** it is shown that gas hold-up decreases with the increase of riser length (Riser A to B), the exception occurring at high solids load (20% (wt.$_{WET\ BASIS}$/vol.)), where the gas hold-up for riser A (0.062) and riser B (0.059) are similar (**Figure V-8**). As it was shown previously, the gas hold-up in riser can be explained by factors such as the liquid linear velocity and the driving force. In this case (riser A compared with riser B) the interplay between these two phenomena may also be used to explain the observed results. Generally, the gas hold-up in riser A is higher than in riser B because when bubbles enter in the downcomer they reduce the liquid linear velocity in the downcomer (v_{Ld}). This reduction occurs because the driving force (ε_{Gr} -ε_{Gd}) is reduced (**Figure V-9**) when bubbles are entrained in the downcomer (U_{Gr}=5 cm/s and U_{Gr}=7.5 cm/s). Thus, by the mass conservation law the liquid linear velocity in the riser (v_{Lr}) is also reduced. From **Eq. V-7** the reduction of liquid linear velocity in the riser (riser A) increases the gas hold-up (considering U_{Gr} and U_{slip} constant), which can explain the higher gas hold-ups found in the *g-l* system (**Figure V-8**) for riser A. However, regarding the **Figure V-11** the riser linear velocity at U_{Gr}=7.5 cm/s is 1.02 cm/s and 0.9 cm/s respectively for riser A and B.

This contradicts **Eq. V-7** which by the values from **Figure V-11** should present higher gas hold-ups for riser B and not A as observed (**Figure V-8**). This discrepancy (mainly for the *g-l* system) can be due to several factors that interact among them and should be taken in account. Among them are: the changes in U_{slip}, liquid flow patterns (due to the presence/absence of a turbulent region above the riser top's end) and coalescence phenomena intensity at different riser configurations.

When higher solid load is present at U_{Gr}≥5 cm/s, the gas hold-up in riser A and riser B are similar. This can happen due to bubble coalescence, which can be enhanced by the SG particles. Coalescence will increase bubble size and thus the bubble slip velocity, which will decrease the downcomer gas hold-up. If due to solids presence the gas hold-up in downcomer decreases, the driving force $(\varepsilon_{Gr} - \varepsilon_{Gd})$ increases. By analysing **Figure V-8** and **Figure V-9** (at U_{Gr}=7.5 cm/s), it can be observed the decrease of gas hold-up in downcomer for all solid load (**Figure V-8**) and the consequent driving force increase (**Figure V-9**). Consequently the riser liquid velocity is higher and the gas hold-up in riser will decrease.

It can be argued that the decrease of gas hold-up in the riser will decrease the driving force. Consequently the previous explanation (for *g-l-s* system) is not valid. However, from **Figure V-9** for riser A, the driving force remains constant for all solid loads at U_{Gr}=7.5 cm/s. In the presence of solids, the gas hold-up is not only influenced by the riser configuration (liquid flow patterns, U_{slip}, coalescence) but also by the solid-phase influence in the gas-phase. The *g-l-s* is a complex system where the solids influence may alter the gas-phase properties, which may or not have influence on the flow pattern of the reactor. This influence of solids in the iGLR flow patterns has different intensities at different iGLR configurations.

.

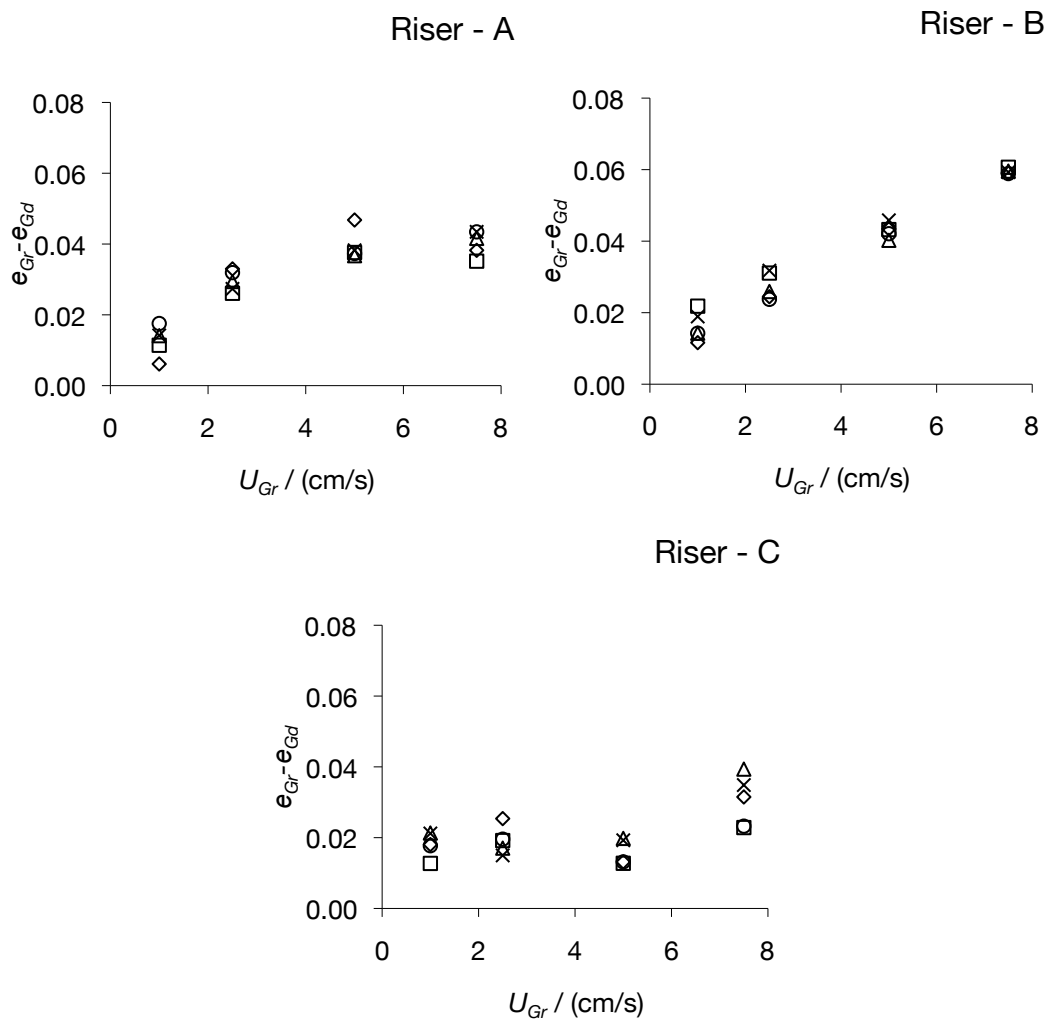

Figure V-9. Driving force (ε_{GR}-ε_{Gd}) vs. Gas superficial velocity (U_{Gr}) for different risers configurations. Legend: ◇ - 0% (wt.$_{WET\ BASIS}$/vol.); □ - 4% (wt.$_{WET\ BASIS}$/vol.); △ - 8% (wt.$_{WET\ BASIS}$/vol.); ○ - 12% (wt.$_{WET\ BASIS}$/vol.); × – 20% (wt.$_{WET\ BASIS}$/vol.).

The increase of riser length in this reactor configuration suppresses the bubble separator (lower part of dual separator) present in the other two configurations. This reactor part is small (about 20 cm in length) and creates resistance to bubble rising (turbulence region), and might lead to more bubbles being dragged to the downcomer.

For the same gas superficial velocities in the riser A, the gas hold-up values obtained with SG particles, are in the same range of the results obtained by Freitas and Teixeira (1998a) with alginate beads (and same riser configuration). In their work the riser gas hold-up decreases

slightly when solids are applied at low gas flow superficial velocities, similar results are obtained in our case(Freitas and Teixeira, 1998a). Moreover the results presented in **Figure V-8** indicate that for riser B the influence of SG was even less than in other configurations.

The downcomer results show that, only at low riser's length, bubbles are going inside the downcomer being this more significant at lower A_{ri}/A_d relation (riser C) as described in literature (Chisti, 1989; Klein et al., 2003). On **Figure V-8** it can be observed that downcomer gas hold-up in riser C is similar at high gas superficial velocities (U_{Gr}=5 cm/s and U_{Gr}=7.5 cm/s). The main reason is that at U_{Gr}=7.5 cm/s complete bubble circulation occurred, even in the presence of SG particles.

If A_{ri}/A_d ratio is low, also is the downcomer cross-section area, and consequently the liquid velocity (>0.25 m/s) that goes into the downcomer is higher, which drags more bubbles (U_{slip}<0.25 m/s) to this part of the reactor. However this does not happen when riser length is increased due to the suppressing of the intermediate part between riser and top section, which improves the degasification of the gas and reduces the probability of bubbles to go inside the downcomer. Similar results were obtained by Klein et al (2003) where almost no bubbles were present in downcomer when the riser ends matched the beginning of top section (Klein et al., 2003).

Previous studies indicated that in *g-l* systems bubbles enter in the downcomer for gas superficial velocities between 10 cm/s (Freitas and Teixeira, 1998a) and 15 cm/s. In our case gas hold-up in downcomer starts to increase at 2.5 cm/s and 5 cm/s for riser C and A, respectively. The main reason for this discrepancy is the type of distributor used. In our work it was used a porous plate, which forms smaller bubbles than the distributer used by the other authors.

From the values present in **Figure V-8** it was determined the relation between riser and downcomer gas hold-up. This relation is linear and the results from the parameters estimation are present in **Table V-4**.

The values of coefficients a_G and b_G are presented in **Table V-4** and result from the linear relation of riser and downcomer gas hold-up to different solid load and riser configuration. As in riser B no gas was present in the downcomer this relation was not possible to obtain, but the values from other two risers indicate that the values found for a_G ($\varepsilon_{Gd}/\varepsilon_{Gr}$) in *g-l-s* systems are similar to the ones found in literature and show a similar behaviour: a decrease with solid load (Freitas and Teixeira, 1998a). On the other hand, the a_G values obtained for g-*l* system (0.92 and 0.93) are slightly higher than the ones presented in literature: 0.80 (Lu et al., 1995); 0.88 (Freitas and Teixeira, 1998a) and 0.89 (Bla et al., 2004). The differences can be explained by the different reactor design and distributor used. In our case the formed bubbles are smaller, thus more prone to entrain into the downcomer, which increases the downcomer gas hold-up in this section and consequently the ratio ($\varepsilon_{Gd}/\varepsilon_{Gr}$).

Table V-4. Parameters obtained for the linear relation between downcomer's and riser's gas hold-up ($e_{Gd}=a_G{}^{10}e_{Gr}+b_G$)

% Solids	Riser A			Riser B			Riser C		
(wt.$_{WET\ BASIS}$/vol.)	a_G	b_G	R^2	a_G	b_G	R^2	a_G	b_G	R^2
0	0.92	-0.03	0.95	---	---	---	0.93	-0.02	0.96
4	0.72	-0.02	0.92	---	---	---	0.94	-0.01	0.99
8	0.73	-0.02	0.99	---	---	---	0.74	0.00	0.93
12	0.75	-0.02	0.99	---	---	---	0.61	-0.02	1*
20	0.52	-0.01	0.99	---	---	---	0.54	-0.02	1*

*Correlation based only in two experimental points

V.4.3 Mixing and circulation time

Mixing time is described as the time necessary for achieving homogeneity inside the reactor. Generally in iGLR the mixing time is related with the gas flow superficial velocity by the equation:

$$t_M = a \times u_{Gr}^b \qquad \textbf{Eq. V-9}$$

It is related with the circulation time, which is the time necessary for a single element to complete a loop in an iGLR. The correlation for mixing time was used to approximate the experimental data obtained

(**Figure V-10**) and the values from the corresponding parameters are presented in **Table V-5**.

In iGLR the mixing time decreases rapidly at low gas superficial velocities and stabilizes at higher velocities. From **Figure V-10**, it is possible to observe a similar trend in all reactor configurations. It is verified that Riser B configuration showed the lower values of mixing time (t_M) indicating a good mixing profile when compared with other two configurations. This is probably due to the absence of the bubble separator section, which leads to a fast axial mixing throughout all iGLR. The axial mixing is promoted by the liquid circulation intensity between riser and downcomer (Molina et al., 1999).

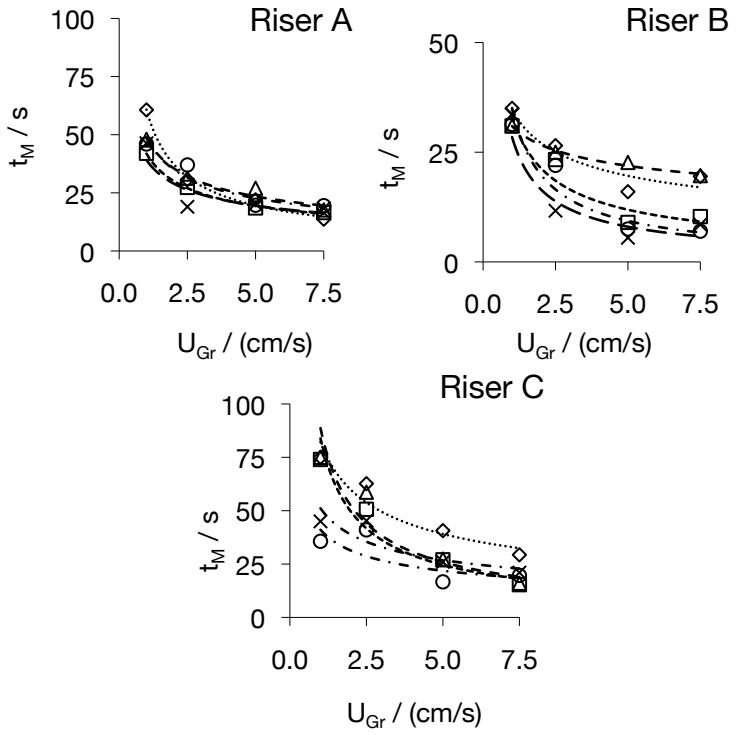

Figure V-10. Mixing time vs. Gas superficial velocity (U /(cm/s)) at different solid load. Legend: ◇ - 0% (wt.$_{WET\ BASIS}$/vol.); □ - 4% (wt.$_{WET\ BASIS}$/vol.); △ - 8% (wt.$_{WET\ BASIS}$/vol.); ○ - 12% (wt.$_{WET\ BASIS}$/vol.); × – 20% (wt.$_{WET\ BASIS}$/vol.).

As in configuration B no gas is present in the downcomer, the driving force is higher especially at high gas flows (**Figure V-9**), leading to a good mixing profile. Moreover in **Table V-5** the values of "a" are smaller

for this reactor configuration indicating the good mixing profile of it. Bello (1981) cited by Molina et al (1999) proposed a relation between the dimensionless mixing time ($\theta=t_M/t_C$) and the ratio A_d/A_{ri} to be independent from gas velocity:

$$\theta = \frac{t_M}{t_C} = \alpha \times \left(\frac{A_d}{A_r} \right)^{0.5} \qquad \textbf{Eq. V-10}$$

Where, accordingly to Bello (1981), α varies between 5.2 and 3.5 for external and internal GLRs, respectively. In our case the α values obtained for *g-l* system in riser A are similar to the values reported in literature (Bello, 1981; Molina et al., 1999).

Table V-5. Parameters for equation $t_M=a \cdot u_{Gr}^{\ b}$

Configuration	%Solids (wt. $_{WET\ BASIS}$/vol.)	a	b	R^2	t_M/t_C	α
A	0	60.78	-0.7	0.98	2.5	3.57
	4	41.87	-0.48	0.99	2.3	3.31
	8	67.3	-0.62	0.96	2.8	3.96
	12	48.76	-0.48	0.91	2.6	3.75
	20	39.13	-0.43	0.74	2.1	3.06
B	0	34.64	-0.35	0.82	1.6	2.28
	4	33.24	-0.64	0.86	1.1	1.56
	8	30.94	-0.22	0.98	1.7	2.46
	12	35.06	-0.82	0.92	1.7	2.38
	20	28.45	-0.79	0.81	2.0	2.85
C	0	82.13	-0.46	0.92	5.8	8.00
	4	83.84	-0.76	0.94	4.2	5.79
	8	88.65	-0.76	0.9	4.6	6.36
	12	41.05	-0.39	0.62	3.2	4.45
	20	51.11	-0.4	0.81	4.3	5.96

In case of riser B the low dimensionless mixing time is due to the good mixing profiles thus low α values are obtained. In opposition, the riser C configuration has α values similar to external GLR, which indicates that this configuration might work as two separated reactors. The high mixing times obtained in riser C can be a result of several factors and how they interact together. These factors are the riser diameter, the presence of a dual top section separator and conductivity

probe position (**Figure V-3**). From the point of view of the liquid phase, the increase of riser diameter leads to lower liquid velocity in the riser (**Figure V-11**). Therefore the amount of liquid that leaves riser C carries less energy, and does not reach the top enlarged section as easily as in riser A or B. Therefore, in this configuration (riser C), the liquid exchange between the riser and the downcomer may be reduced which leads to lower mixing times. In addition, the position of the conductivity probe, used to read the mixing time, is located at enlarged top section. On the other hand, the increase in the liquid linear velocity in the downcomer leads to an increase of gas hold-up in the downcomer. As presented in **Figure V-9** in riser C the driving force (ε_r -ε_d) is small when compared with riser A/B mainly due to the presence of gas in the downcomer. In theory the low driving force will reduce the mixing time. It is then important to understand better which effect is stronger in the mixing profile of iGLR. The interplay between liquid velocity, driving force, bubble slip velocity is complex and sensitive. In **Figure V-10C** it can be also verified that at high solid content the mixing time is small. A possible explanation is the occurrence of coalescence that changes the circulation profile of the reactor being more liquid transported to the top degassing section, promoting a better mixing.

The dimensionless mixing time indicates how much bigger is the number of loops necessary for a complete mixing. As predicted, better results were obtained for riser B being the only configuration that needs at most 2 loops for a complete mixing. In general, it is possible to observe (**Figure V-10**) that SG particles decrease the mixing. The exception is at 8% (wt.$_{\text{WET BASIS}}$/vol.) in riser B where the mixing was higher than the remaining solids loads used (**Figure V-10**). This may be due to coalescence promoted by SG which leads to bigger bubbles that drag more liquid to the top section improving the axial mixing. The relative velocity between gas- and liquid-phases promotes the axial mixing, thus if bigger bubbles are present, axial mixing is increased, which reduces the mixing time.

V.4.4 Liquid velocity

As the linear liquid velocity can influence mixing, mass transfer and solids suspension properties, it is very important to study this parameter in reactors hydrodynamics, especially for design and scale-up purposes (Bla et al., 2004; Freitas, 2002). The results presented in **Figure V-11** are in the same range of linear liquid velocites found in literature (Bla et al., 2004; Freitas, 2002) and, as expected indicate that liquid velocity increases with gas flow. No relevant influence of solids is observed, with the exception of some decrease found when 20% ($wt._{WET\ BASIS}$ /vol.) of SG particles were added. Even in the literature consulted, the effect of solids in linear liquid velocity remains unclear, as it can increase the liquid velocity (Freitas and Teixeira, 1998a) or decrease (Freitas and Teixeira, 1998a; Lu et al., 1995; Merchuk et al., 1998). The main reasons for this are the different GLR configurations and conditions (type of solids) used.

The results for the different risers are in accordance with the ones obtained by Klein et al (2003) and suggest that the diameter increase (riser A to C) has more influence on liquid velocity than the riser length increase (riser A to B). When the diameter is increased the gas hold-up also increases (**Figure V-8**) but for riser C the gas hold-up at U_{Gr}=7.5 cm/s is similar to the gas hold-up at U_{Gr}=5 cm/s, which might be due to bubble circulation present at the highest gas superficial velocity (7.5 cm/s). The bubble circulation regime occurs either in the presence or absence of SG particles. In this regime, the higher bubbles flow in axial position from the bottom to the top, while the smaller bubbles (with lower slip velocity) enter in the downcomer. Due to the higher downcomer liquid velocity, which results from the small downcomer cross-section area, these small bubbles are dragged to the bottom part of the iGLR and enter again in the riser.

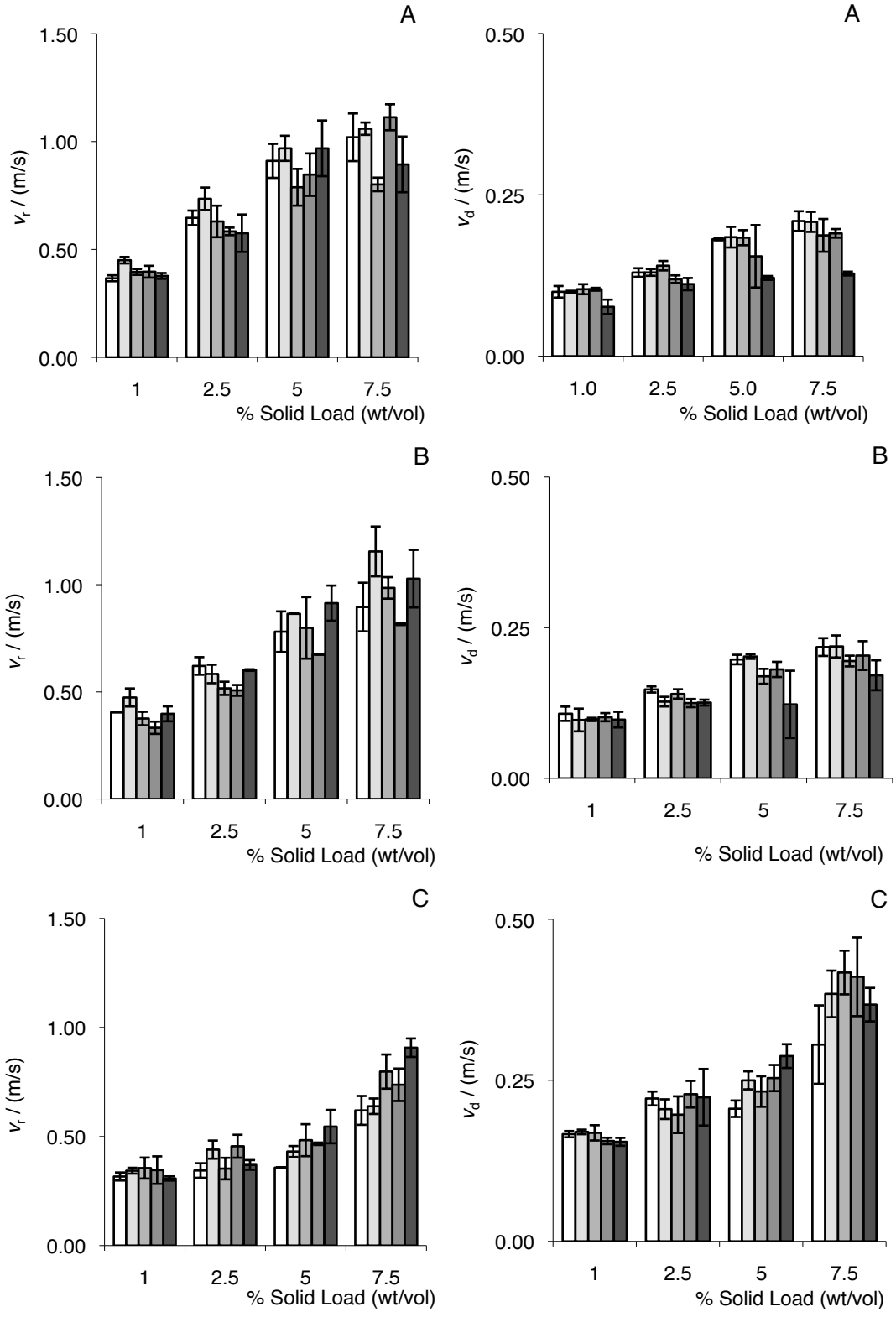

Figure V-11. Liquid velocity (m/s) in riser and downcomer vs. Solid load (% (wt.$_{\text{WET BASIS}}$/vol.)) for different risers configurations. Legend: □ - 0% (wt.$_{\text{WET BASIS}}$/vol.); ■ - 4% (wt.$_{\text{WET BASIS}}$/vol.); ■ - 8% (wt.$_{\text{WET BASIS}}$/vol.); ■ - 12% (wt.$_{\text{WET BASIS}}$/vol.); ■ – 20% (wt.$_{\text{WET BASIS}}$/vol.).

With the exception of riser C, **Figure V-11** indicates that solids influence affects more the liquid velocity in the downcomer than in the riser, especially at high gas flows. The main reason is the absence of high amounts of bubbles in the downcomers A and B. There is only contact between the liquid- and solid-phase and the influence of solids in liquid velocity is higher, particularly when high amounts of SG are present.

A final note has to be made concerning the conditions tested. In most of the hydrodynamic studies found in literature, the used gas superficial velocities are the same and higher magnitude than the ones in this work. However, in continuous AFB production the superficial gas velocity is normally 0.5 cm/s (Lehnert et al., 2008) and can go up to 3 cm/s (Brányik et al., 2004) with an acceptable amount of immobilized biomass. Being so, the presented hydrodynamic experiments were performed both in the hydrodynamic and fermentation range. The methods used, mainly for gas hold-up determination, due to the observed errors (15% to 20%), did not showed enough accuracy at gas superficial velocity lower than 1 cm/s (see section V.3.1), therefore no results were tested at this gas flow. However, it is believed that the final conclusions of this chapter about the best riser configuration would not be affected. Moreover in the next chapter local hydrodynamic studies, with more refined techniques will be performed at superficial gas velocities between 0.5 cm/s and 1 cm/s.

V.5 Conclusions

The main objective of this chapter was to understand the effect of SG in three different configurations of iGLR with and enlarged top section. The obtained results of solids distribution, gas hold-up, liquid linear velocity circulation and mixing time were used to select between the configurations tested the most suitable to perform a continuous primary AFB fermentation.

Before the final conclusion, it is important to have in mind the ideal conditions for continuous AFB fermentation: (1) good solid particles distribution, (2) minimum gas flow rate to fluidize all solid particles, (3) anaerobic conditions, (4) low gas hold-up in riser to avoid high stripping loses of flavour compounds, (5) absence of bubbles in downcomer because normally CO2 is used and it is known to have adverse effect on yeast cell metabolism, (6) good mixing properties, i e., if mixing time is smaller the influence of liquid flow will be even smaller.

A close look to the results showed the riser B is the most suitable configuration tested to perform the continuous fermentation of AFB. Comparing only the lower gas superficial velocity (1 cm/s) riser B was the one where it was found: better homogenization of SG particles; lower gas hold-ups in riser and absence of gas hold-up in downcomer; lower mixing and circulation times, as well as minimum t_M/t_C.

Therefore riser B was considered as the configuration that includes all the characteristics to perform a continuous AFB primary fermentation.

In order to have a better understanding of the real hydrodynamics in this reactor configuration local measurements were made in a 6 L GLR. This is discussed in Chapter VII.

V.6 References

Banisi, S., Finch, J. A., Laplante, A. R. and Weber, M. E. (**1995a**). Effect of solid particles on gas holdup in flotation columns-I. measurement. *Chemical Engineering Science*, 50(14), 2329–2334.

Banisi, S., Finch, J. A., Weber, M. E. and Laplante, A. R. (*1995b*). Effect of solid particles on gas holdup in flotation columns-II. Investigation of mechanisms of gas holdup reduction in presence of solids. *Chemical Engineering Science*, 50(14), 2335-2342.

Bello, R. A. (**1981**). A characterization study of airlift contactors for application to fermentations. PhD thesis. University of Waterloo, Ontario, Canada.

Bla, M., Ki, M. and Marko, J. (**2004**). Scale influence on the hydrodynamics of an internal loop airlift reactor. *Chemical Engineering and Processing*, 43(12), 1519-1527.

Boyer, C., Duquenne, A.-M. and Wild, G. (**2002**). Measuring techniques in gas-liquid and gas-liquid-solid reactors. *Chemical Engineering Science*, 57, 3185-3185.

Brányik, T., Vicente, A. A., Machado Cruz, J. M., and Teixeira, J. A. (**2002**). Continuous primary beer fermentation with brewing yeast immobilized on spent grains. Journal Of The Institute Of Brewing, 108(4), 410-415.

Chisti, M. Y. (**1989**). *Airlift Bioreactors* (1st ed.). Essex: Elsevier Science Publishers LTD.

Clift, R., Grace, J. R. and Weber, M. E. (**1978**). *Bubbles, drops, and particles* (Vol. 380). Academic press New York.

Deckwer, W. D. (**1992**). *Bubble Column Reactors*. (Wiley, Ed.). Chichester.

Dolgos, O., Klein, J., Vicente, A. A. and Teixeira, J. A. (**2001**). Behaviour of dual gas-liquid separator in an internal-loop airlift reactor – effect of top clearance. *28th Conference SSCHE* (pp. 21 - 25). Tatrankés Matliare.

Fan, L-S., Yang, G. Q., Lee, D. J., Tsuchiya, K. and Luo, X. (**1999**). Some aspects of high-pressure phenomena of bubbles in liquids and liquid–solid suspensions. *Chemical Engineering Science*, 54(21), 4681–4709.

Fonseca, M. M. and Teixeira, J. A. (**2007**). *Reactores Biológicos* (in Portuguese). L. Lidel-edições técnicas, 482.

Freitas, C., Vicente, A. A., Mota, M. and Teixeira, J. A. (**1997**). A new sampling device for measuring solids hold-up in a three-phase system. *Biotechnology Techniques*, 11(7), 489-492.

Freitas, C. and Teixeira, J. A. (**1998a**). Hydrodynamic studies in an airlift reactor with an enlarged degassing zone. *Bioprocess and Biosystems Engineering*, 18(4), 267–279. Springer.

Freitas, C. and Teixeira, J. A. (**1998b**). Solid-phase distribution in an airlift reactor with an enlarged degassing zone. *Biotechnology Techniques*, 12(3), 219-224.

Freitas, C., Fialová, M., Zahradnik, J. and Teixeira, J. A. (**1999**). Hydrodynamic model for three-phase internal-and external-loop airlift reactors. *Chemical Engineering Science*, 54, 5253-5258.

Freitas, C., Fialová, M., Zahradnik, J. and Teixeira, J. A. (**2000**). Hydrodynamics of a three-phase external-loop airlift bioreactor. *Chemical Engineering Science*, 55(21), 4961–4972.

Freitas, Carla. (**2002**). Bioreactores Multifásicos - Caracterização Hidrodinámica e de Transferência de Massa (in Portuguese). PhD thesis, University of Minho.

Gandhi, B., Prakash, A. and Bergougnou, M. A. (**1999**). Hydrodynamic behavior of slurry bubble column at high solids concentrations. *Powder Technology*, 103(2), 80–94.

Jamialahmadi, M. and Muller-Steinhagen, H. (**1991**). Effect of solid particles on gas hold-up in bubble columns. *Canadian Journal of Chemical Engineering*, 69, 390-393.

Klein, J., Vicente, A. A. and Teixeira, J. A. (**2003a**). Hydrodynamic considerations on optimal design of a three-phase airlift bioreactor with high solids loading. *Journal of Chemical Technology and Biotechnology*, 78, 935-944.

Klein, J., Vicente, A. A. and Teixeira, J. A. (**2003b**). Hydrodynamics of a Three-phase Airlift Reactor with an Enlarged Separator – Application to High Cell Density Systems. *The Canadian Journal of Chemical Engineering*, 81, 1-11.

Klein, J., Vicente, A. A. and Teixeira, J. A. (**2004**). Study of hydrodynamics and mixing in an airlift reactor with an enlarged separator using magnetic. *3rd International Symposium on Two-Phase Flow Modelling and Experiemntation* (Vol. 5, pp. 22-24). Pisa.

Korpijarvi, J., Oinas, P. and Reunanen, J. (**1999**). Hydrodynamics and mass transfer in an airlift reactor. *Chemical Engineering Science*, 54(13-14), 2255–2262.

Lehnert, R., Kurec, M., Brányik, T. and Teixeira, J. A. (**2008**). Effect of Oxygen Supply on Flavour Formation During Continuous Alcohol-free Beer Production: A Model Study. *Journal of American Society of Brewing Chemist*, 66(4), 233-238.

Lehnert, R., Novák, P., Macieira, F., Kurec, M., Teixeira, J. A. and Brányik, T. (**2009**). Optimisation of Lab-Scale Continuous Alcohol-Free Beer Production. *Czech Journal of Food Science*, 27(4), 267-275.

Lu, W-J., Hwang, S-J. and Chang, C-M. (**1995**). Liquid velocity and gas holdup in three-phase internal loop airlift reactors with low-density particles. *Chemical Engineering Science*, 50(8), 1301–1310. Elsevier.

Matsumoto, T., Hidaka, N. and Morooka, S. (**1989**). Axial distribution of solid holdup in bubble column for gas–liquid–solid system. *A.I.Ch.E. Journal*, 31, 1701-1709.

Mena, P. C., Ruzicka, M. C., Rocha, F. A., Teixeira, J. A. and Drahos, J. (**2005**). Effect of solids on homogeneous–heterogeneous flow regime transition in bubble columns. *Chemical Engineering Science*, 60(22), 6013-6026. doi:10.1016/j.ces.2005.04.020

Merchuk, J., Contreras, A., Garcia, F. and Molina, E. (**1998**). Studies of mixing in a concentric tube airlift bioreactor with different spargers. *Chemical Engineering Science*, 53(4), 709-719.

Molina, E., Contreras, A. and Chisti, Y. (**1999**). Gas holdup, liquid circulation and mixing behaviour of viscous newtonian media in a split-cylinder airlift bioreactor. *Trans*

Olivieri, G., Marzocchella, a, Vanommen, J. and Salatino, P. (**2007**). Local and global hydrodynamics in a two-phase internal loop airlift. Chemical Engineering Science, 62(24), 7068-7077.

Rodríguez, A., Garcia-Calvo, E., Prados, A. and Klein, J. (**1999**). A fluid dynamic model for three-phase airlift reactors. Chemical Engineering Science, 54, 2359-2370.

Van Benthum, W., Van der Lans, R., Van Loosdrecht, M. and Heijnen, J. (**2000**). The biofilm airlift suspension extension reactor-II: Three-phase hydrodynamics. Chemical Engineering Science, 55(3), 699–711.

Warsito, Ohkawa, M., Maezawa, A. and Uchida, S. (**1997**). Flow structure and phase distributions in a slurry bubble column. Chemical Engineering Science, 52(21-22), 3941-3947.

Xie, T., Ghiaasiaan, S. M., Karrila, S. and Mcdonough, T. (**2003**). Flow regimes and gas holdup in paper pulp – water – gas three-phase slurry flow. Chemical Engineering Science, 58, 1417 - 1430.

Yang, G. Q., Du, B. and Fan, L-S. (**2007**). Bubble formation and dynamics in gas–liquid–solid fluidization—A review. Chemical Engineering Science, 62, 2 - 27.

Yoo, D. H., Tsuge, H., Terasaka, K. and Mizutani, K. (**1997**). Behavior of bubble formation in suspended solution for an elevated pressure system. Chemical Engineering Science, 52(21-22), 3701–3707

Zahradnik, J., Fialova, M., Ružička, M., Drahoš, J., Kaštánek, F. and Thomas, N. H. (**1997**). Duality of the gas-liquid flow regimes in bubble column reactors. Chemical Engineering Science, 52(21-22), 3811–3826.

VI. Chapter VI – CFD Simulation of Gas Hold-up and Liquid Interstitial Velocity in Two-phase iGLR

VI.1 Objectives

The main objective of this chapter was to perform computing fluid dynamic (CFD) simulations for the two-phase iGLR in order to explain and complement the practical results obtained in the previous chapter. The main goal was to test the ability of our CFD simulation setup to capture global characteristics of the flow (mean liquid interstitial velocity and gas hold-up both in riser and downcomer sections) in our iGLR with an enlarged degassing zone. Besides this it was also important to capture the three experimentally observed bubble circulation regimes and so verify if the simulation setup could be later used to obtain the global characteristic for: (1) modified geometries; (2) different fluids. The comparison was done for the three different riser tubes used before (A, B, C see **Table VI-1**) but only for *g-l* system (air-water). To apply the CFD simulations it was used the commercial code Fluent 6.3 using algebraic slip mixture multiphase model. Simulations results using different model (full Euler–Euler) in different code (CFX 12.1) are also presented in the paper. The secondary goal was to test the sensitivity of the simulations to the different bubble slip velocity, and to the different turbulence closure models (variants of $\kappa-\varepsilon$, $\kappa-\omega$). This was done using the mixture model in Fluent 6.3 code.

VI.2 Introduction

The knowledge of the iGLR hydrodynamics is needed for the reactor's design. Basic global quantities such as gas hold-up and liquid velocities in the riser and in the downcomer, total interfacial area among others need to be known. The hydrodynamic and other relevant parameters such as the airlift geometry are interrelated and their relationship can be quite complex because they, directly or indirectly, influence each other and sometimes in complex interactions (Chisti, 1998). As an example: the driving force for the liquid circulation is the difference between the riser and the downcomer's gas hold-ups. This is balanced by friction losses in the riser, downcomer and in several parts of GLR geometry. The friction losses in the case of iGLR also occur and

are influenced by bottom and top clearances parts, while in external GLR these losses are in connecting pipes (Freitas et al., 1999). However, the resulting liquid circulation affects the riser and downcomer gas hold-up and thus the driving force. The gas hold-up depends also on bubble slip velocity, which depends on the bubble size. Bubble size is influenced by: the gas distributor, coalescence properties of the involved fluids and turbulence. Turbulence is influenced by liquid circulation. The relevant hydrodynamic parameters need to be either obtained experimentally or predicted by models of various types. A lot of experimental data and correlations have been published on global quantities (hold-up, liquid velocities) for iGLR. A large number of correlations for these parameters are compiled (Chisti, 1989, 1998; Freitas et al., 1999; Garcia-Calvo et al., 1999; Lu et al., 1995). Nevertheless the majority of the correlations presented in the literature are restricted in their validity to the same reactor size, type and *g-l* system used (Young et al., 1991). Normally, these correlations are system specific, being of little use in design or scale-up. The usual requirement is for estimation of expected performance in larger or geometrically different reactors or fluids (Chisti, 1998). Some authors employed models based on mechanical energy balance in the airlift reactor (Chisti, 1989; Heijnen et al., 1997; Verlaan et al., 1986), but the information about friction losses (friction coefficients) must be provided as an input parameter. More recent experimental measurements of airlift global hydrodynamic characteristics (riser and downcomer hold-up and velocities) can be found for iGLR (Merchuk et al., 1998; van Baten et al., 2003) and external gas-lift reactor (Freitas et al., 1999; Vial et al., 2002).

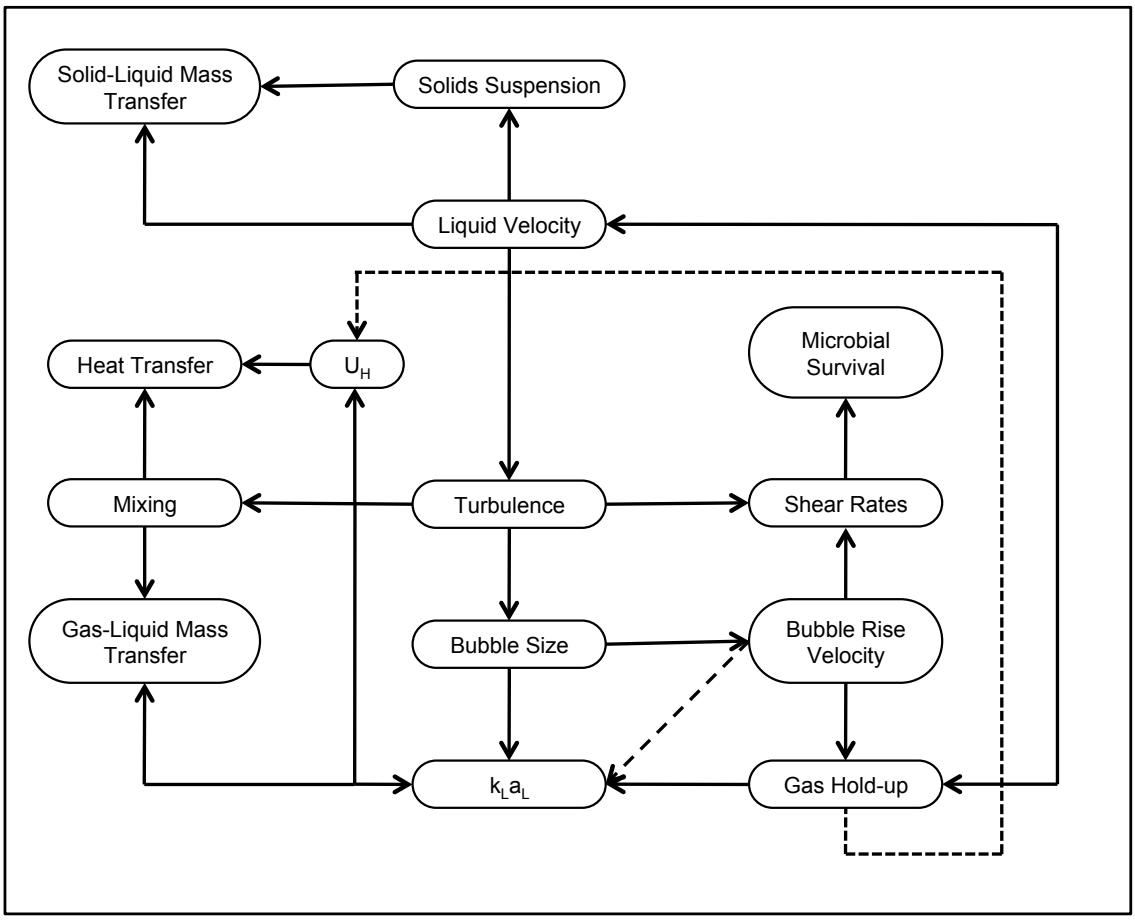

Figure VI-1. Relationships between hydrodynamic parameters and other bioreactor performance indices. Legend: U_H – Overall Heat Transfer coefficient (W/(m^2 °C)); k_La_L – Overall volumetric mass transfer coefficient (s^{-1}). Adapted from Chisti, 1989.

Luo and Al-Dahhan (2008, 2010) measured local liquid velocity profiles, turbulent quantities using the computer-automated radioactive particle tracking (CARPT) technique and local gas hold-up profiles using computed tomography in an iGLR. They observed significant effect of top and bottom clearances on the flow. They also observed that the bubbles are prone to concentrate in the riser center in radial direction and the change from bubbly to churn-turbulent flow at superficial gas velocity of 2 cm/s. Apart from experiments, empirical correlations or theoretical models such as the models based on mechanical energy balance, CFD simulations are a tool, which can be used to study gas-lift reactor hydrodynamics.

There are two main groups of multiphase flow models usable for simulations on bubble collumn and gas-lift reactors scale. In Euler–Euler models all phases are treated as interpenetrating continua, while in Euler–Lagrange models the motion of individual particles is tracked through the continuous fluid. The Euler–Lagrange models, which track the motion of every single particle (approximated as a mass point with closure equation for the interphase forces), can be used for smaller scale problems with low gas hold-up. Only Euler–Euler models (mixture model and ‘‘full’’ Euler–Euler model) were used in the presented work, thus only Euler–Euler models are considered in the following chapter.

VI.2.1 CFD simulations in iGLR: advantages and limitations

The main advantage of CFD simulations if compared to experiments is that no experimental apparatus has to be built; therefore equipment dimensions and working fluids can be easily changed in simulations. However, the quality of the CFD simulation predictions, greatly depends on how well or how badly are employed the CFD models, sub-models and closure equations that describe flow phenomena occurring in the reactor. Since the *g-l* flows are very complex with flow phenomena occurring on a wide range of space and time scales, modeling of *g-l* flows is still an open subject and far from being complete. Moreover it is still necessary to validate simulation results against experiments. The Euler–Euler models need closures for all relevant interphase force (drag, lift, added mass, etc.), for the turbulence (due to single phase flow and due to bubbles) as well as models for bubble coalescence and break-up, because the bubble size is present in most of the closure equations.

Sokolichin et al. (2004) discussed the relevance of individual interphase forces for the simulation and also turbulence modelling issues. They observed a weak dependency of simulation results (in partially aerated rectangular bubble column) on the employed value of the bubble slip velocity. They explained this weak dependence by the

fact that the bubble total velocity was the sum of the bubble slip velocity and the liquid velocity, which can be relatively high, so the change in the bubble slip velocity had lower impact on the calculated gas hold-up (Sokolichin et al., 2004). It could be expected from the same reason that the similar behaviour (weak dependence of gas holdup on the bubble slip velocity) could be found in airlift simulations, if bubbles are present only in the riser and the downcomer hold-up is zero, may be the dependence could be even weaker due to the more ordered flow in the airlift if compared to the bubble column. However, if the gas hold-up in the downcomer is positive, then the effect of the bubble slip velocity could be much stronger due to counter current flow of both phases in this gas-lift reactor section. It is then not surprising that some authors did simulations of gas-lift reactor and obtained a good agreement with experiments even when inappropriate closure for drag force was used (e.g. Schiller–Naumann correlation for rigid sphere drag used for 5 mm equivalent diameter air bubble in water) in cases with zero downcomer gas hold-up.

There are a number of papers dedicated to the Euler–Euler CFD simulations of airlift reactors. External-loop airlift simulation comparisons of radial profiles of gas hold-up and liquid velocity can be found (Cao et al., 2007; Roy et al., 2006; Vial et al., 2002). The comparison of average gas hold-up and liquid velocities with experiments for iGLR and for zero downcomer gas hold-up can be found, (Huang et al., 2008; Mudde and van den Akker, 2001; Van Baten et al., 2003). Huang et al. (2008) also reported weak dependence of the simulation results on the bubble velocity prescribed on the top boundary condition. Simulations for cases with nonzero downcomer hold-up were done (Huang et al., 2010; Jia et al., 2007; Oey et al., 2001; Talvy et al., 2007). Talvy et al. (2007) compared vertical and horizontal profiles of gas holdup in riser and downcomer, and horizontal liquid velocity profiles in downcomer with experiments in a rectangular airlift. Also Jia et al. (2007) compared simulated and experimental horizontal profiles of gas hold-up and liquid velocities in a rectangular airlift and found a good agreement.

VI.3 Material and Methods

VI.3.1 Experimental setup

The experiments were done in the same iGLR with a top enlarged degassing zone used in previous chapter (**Figure V-3** and **Table V-1** and **Table V-2** in Chapter V section V.3.1) but only data using air-water was considered for CFD simulations.

In **Figure VI-3** and **Table VI-1** are displayed the reactor dimensions and grid cells used in this work

Table VI-1. Riser configurations used in this work.

	Riser A		Riser B		Riser C	
	(mm)	nr of grid cells	(mm)	nr of grid cells	(mm)	nr of grid cells
D1	100	12	100	12	100	12
D2	62	12	62	12	87	12
D3	70	14	70	14	92	14
D4	142	28	142	28	142	28
D5	420	28	420	28	420	28
H1	23	5	23	5	23	5
H2	1200	60	1400	70	1200	60
H3	200	16	0	0	200	20
H4	170	14	170	14	170	12
H5	120	6	120	6	120	6

Legend: D1 – Distributor diameter; D2 – Riser internal diameter; D3 - Riser external diameter; D4 – Column internal diameter; D5 – Top degassing zone internal diamter; H1 – Distance between distributor and beginning of riser; H2 – Riser length; H3 – Distance between riser end and beginning of top part; H4 – Height of conical section from top part; H5 – Height of cylindrical section of top part.

The liquid interstitial velocity in the riser and in the downcomer was measured as described in section V.3.6. The gas hold-up in the riser and downcomer was estimated using U-tube manometers (section V.3.3) without the solids consideration (ε_{Si}=0 in **Eq. IV-2**). The agreement of this estimate with the real gas holdup in the apparatus may be affected by a pressure drop due to flow with a maximum error of ±15% (section IV.4.2).

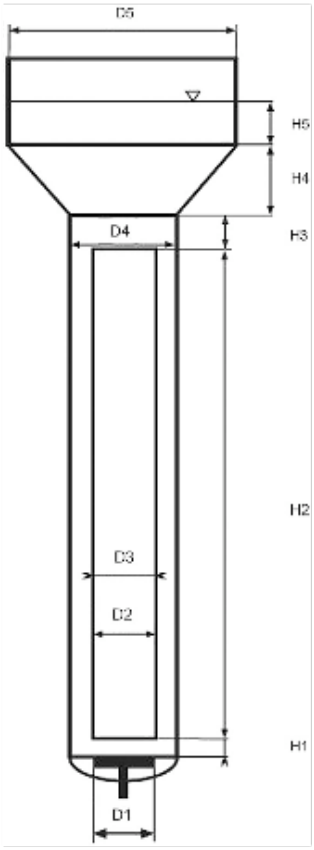

Figure VI-2. Internal Gas-lift Reactor geometry (not at scale). Legend: D1 – Distributor diameter; D2 – Riser internal diameter; D3 - Riser external diameter; D4 – Column internal diameter; D5 – Top degassing zone internal diameter; H1 – Distance between distributor and beginning of riser; H2 – Riser length; H3 – Distance between riser end and beginning of top part; H4 – Height of conical section from top part; H5 – Height of cylindrical section of top part.

VI.3.2 Simulation setup

The main part of the simulations was done in CFD code Fluent 6.3 using the algebric slip mixture model. A part of the fluent simulations was later recalculated in the CFX 12.1 code using the full Euler–Euler model and their results are also presented, although for the riser C configuration CFX simulations were not finished due to convergence problems and the results are not shown.

The airlift geometry is shown in **Figure VI-2** The gas distributor in the simulation domain geometry had the same diameter as the riser. The computational grid was the same for both simulations (Fluent and CFX) and contained 48 100 (Riser A), 44 700 (Riser B) and 49 100 (Riser C)

grid cells. The computational grid (at the airlift cross-section) is shown in **Figure VI-3** and number of grid cells per each airlift dimension can be found in **Table VI-1** The grid was sufficient to obtain grid independent results (see Section VI.4.1 for the grid independence test result). The time step in all simulations was 0.005 s.

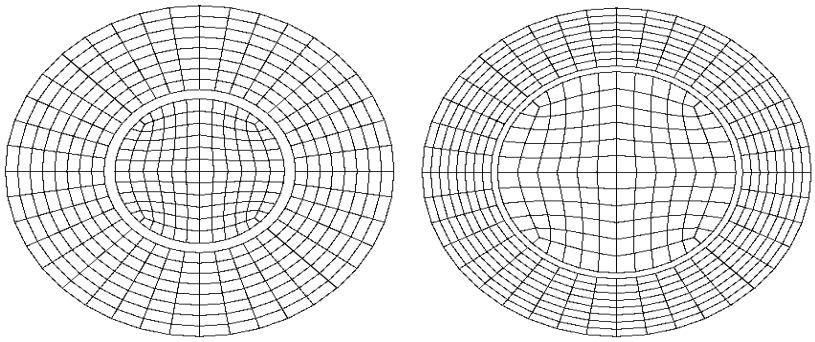

Figure VI-3. Computational grid for the iGLR cross-section at Risers A, B (left) and C (right).

VI.3.2.1 Fluent simulations

The mixture model used in Fluent 6.3 code assumes that two or more phases are interpenetrating. It can solve cases where two (or more) phases move at different velocities and it assumes local equilibrium over short spatial length scales, i.e. dispersed phases move at their terminal velocities. This model is simpler than full Euler-Euler multiphase model. The mixture model solves the continuity and the momentum equation for a mixture with averaged properties (density, velocity and viscosity), an algebraic equation for the dispersed phase(s) slip velocity and a volume fraction equation for the secondary phase(s). The mixture model should require less computational resources than the Euler-Euler model, since it solves fewer equations. However, it can be sometimes more difficult to converge with more iterations required to be done, thus diminishing the mentioned advantage over the Euler-Euler model. Model equations, boundary conditions and other solver parameters are explained below. The mixture model solves the continuity and momentum equation for the mixture, the algebraic equation for dispersed phase slip velocity and volume fraction equation

for the secondary phase (Manninen et al., 1996). The continuity equation is

$$\partial \rho_m / \partial t + \nabla \times (\rho_m \mathbf{v_m}) = 0 \qquad \textbf{Eq. VI–1}$$

Where:

$$\mathbf{v_m} = \left({}^{1}\!/\!_{\rho_m} \right) \sum_{k=1}^{n} \alpha_k \rho_k \mathbf{v_k} \qquad \textbf{Eq. VI–2}$$

Is the mass averaged velocity, and

$$\rho_m = \sum_{k=1}^{n} \alpha_k \rho_k \qquad \textbf{Eq. VI 3}$$

Is the mixture density. The sums are over all (n) phases (k). The momentum equation in the mixture model can be obtained by summing momentum equations of all phases in the Euler-Euler model. The momentum equation is:

$$\partial(\rho_m \mathbf{v_m})/\partial t + \nabla.(\rho_m \mathbf{v_m} \mathbf{v_m}) = -\nabla p + \nabla\left[\mu_\infty (\nabla \mathbf{v_m} + \nabla^T \mathbf{v_m})\right] + \rho_m g + ... \\ ... + \nabla.\left(\sum_{k=1}^{n} \alpha_k \rho_k \mathbf{v_{dr,k}} \mathbf{v_{dr,k}} \right) \qquad \textbf{Eq. VI–4}$$

Where *n* is the number of phases (two in our case: air, water), and

$$\mu_\infty = \sum_{k=1}^{n} \alpha_k \mu_k + \mu_t \qquad \textbf{Eq. VI–5}$$

Is the mixture effective viscosity, μt is the turbulent viscosity and μk is the molecular viscosity of phase k, and

$$\mathbf{v_{dr,k}} = \mathbf{v_k} - \mathbf{v_m} = \mathbf{v_{kc}} - \left({}^{1}\!/\!_{\rho_m} \right) . \sum_{i=1}^{k} \alpha_i \rho_i \mathbf{v_{ic}} \qquad \textbf{Eq. VI–6}$$

Is the drift velocity of phase k, where

$$\mathbf{v_{kc}} = \mathbf{v_k} - \mathbf{v_c} \qquad \textbf{Eq. VI–7}$$

Is the slip velocity being the "c" subscript for the continuous phase. The slip velocity is calculated from the following algebraic equation:

$$\mathbf{v_{kc}} = \tau_k (\rho_k - \rho_c) \mathbf{a} / f \rho_k - (\eta_t / \sigma_t) \left({}^{\nabla \alpha_k}\!/\!_{\alpha_k} - {}^{\nabla \alpha_c}\!/\!_{\alpha_c} \right) \qquad \textbf{Eq. VI–8}$$

The first term on the right hand side of **Eq. VI–8** is due to a drag force, where

$$\tau_k = \frac{\rho_k d_k^2}{18\mu_c} \qquad \textbf{Eq. VI–9}$$

Is k-phase particle relaxation time, and *f* is a drag function:

$$f = C_D \times \mathrm{Re}/24 \qquad \textbf{Eq. VI–10}$$

Being Re expressed by:

$$\mathrm{Re} = \frac{d_k |\mathbf{v_{kc}}| \rho_c}{\mu_c} \qquad \textbf{Eq. VI–11}$$

The acceleration (**a**):

$$\mathbf{a} = \mathbf{g} - (\mathbf{v_m}.\nabla)\mathbf{v_m} - \partial \mathbf{v_m} / \partial t \qquad \textbf{Eq. VI–12}$$

And C_D is drag coefficient. The drag coefficient (C_D) was calculated from Tomiayama's correlation (Tomiyama et al., 2002) for a single bubble:

$$C_D = \max\left[\min\left\{24/\mathrm{Re}\left(1+0.15\mathrm{Re}^{0.687}\right), 72/\mathrm{Re}\right\}, (8/3)\, E_\sigma / E_0 + 4\right] \qquad \textbf{Eq.VI–13}$$

Where,

$$E_\sigma = \frac{\Delta\rho g d^2}{\sigma} \qquad \textbf{Eq. VI–14}$$

This means that the drag coefficient is C_D=1.215 for single 5 mm bubble, with a slip velocity ~0.23 m/s. In order to test the effect of bubble slip velocity on simulation results Schiller-Naumann's closure was also employed:

$$C_D = 24/\mathrm{Re}(1+0.15\mathrm{Re}^{0.687}) \text{ for } \mathrm{Re} < 1000 \text{ and } \mathrm{C_D} = 0.44 \text{ for } \mathrm{Re} > 1000 \qquad \textbf{Eq. VI–15}$$

Eq. VI–13 was used in all simulations unless said otherwise. At this point is important to notice a possible bug either in Fluent 6.3 and Fluent12 mixture models. If a first order time discretization scheme is used then the slip velocity is calculated correctly. If a second order scheme is used then it is calculated incorrectly (1st order ~0.23 m/s, 2nd order ~0.47 m/s). This was tested for both user defined closure and

closures that are already present in the solver. The second term in **Eq. VI–8** appears due to a dispersion of secondary phase by turbulence, where σ_t is a turbulent Prandtl number and η_t is a turbulent diffusivity:

$$\eta_k = \frac{C_\mu k2}{\varepsilon_k}\left(\gamma_\gamma /(1+\gamma_\gamma)(1+C_\mu\zeta_\gamma^2)^{-1/2}\right) \qquad \textbf{Eq. VI–16}$$

Where:

$$\zeta_\gamma = \left|\mathbf{v_{kc}}\right|/(2/3k)^{1/2} \qquad \textbf{Eq. VI–17}$$

$$C_\mu = 1.8 - 1.35\cos^2\theta \qquad \textbf{Eq. VI–18}$$

$$\theta = \mathbf{v_{kc}}\mathbf{v_k}/\left(\left|\mathbf{v_{kc}}\right|\left|\mathbf{v_k}\right|\right) \qquad \textbf{Eq. VI–19}$$

C_μ was considered to be equal to 0.09. The γ_γ is a time ratio between the time scale of the energetic turbulent eddies affected by the crossing-trajectories effect and the particle relaxation time

$$\gamma_\gamma = 0.165(k/\varepsilon)^{\left(1+C_\mu\zeta_\gamma^2\right)/\tau_k} \qquad \textbf{Eq. VI–20}$$

The value of σ_t was set to 0.01. The default value was 0.75. The lower value, which was used in Fluent simulations, enhances a turbulent dispersion. The lower value was chosen, because for Riser B bubbles flowing into the riser did not disperse fast enough across the whole riser cross section as it was visually observed in experiments. The mixture composition is updated by solving the transport equation for the dispersed phases (only one dispersed phase in our case)

$$\partial(\alpha_k\rho_k)/\partial t + \nabla.(\alpha_k\rho_k\mathbf{v_m}) = -\nabla.(\alpha_k\rho_k\mathbf{v_{dr,k}}) \qquad \textbf{Eq. VI–21}$$

The standard κ–ε model was used to model turbulence. This model belongs to a group of Reynolds averaged Navier-Stokes equation models. The instantaneous velocity in the momentum equation is divided into the average and fluctuating part

$$\mathbf{u} = \mathbf{v_m} + \mathbf{v}' \qquad \textbf{Eq. VI–22}$$

Then the momentum equation is ensemble averaged and the resulting term

$$-\nabla.(\rho\mathbf{v}'\mathbf{v}') \qquad \textbf{Eq. VI–23}$$

Is modeled as

$$\nabla\left[\mu_t\left(\nabla \mathbf{v_m} + \nabla \mathbf{v_m^T}\right)\right] \qquad \textbf{Eq. VI–24}$$

Where μ_t is turbulence viscosity, which again requires a closure equation. The closure is:

$$\mu_t = \rho_m C_\mu k^2/\varepsilon \qquad \textbf{Eq. VI–25}$$

The turbulent kinetic energy, *k*, and turbulent dissipation rate, ε, are obtained by solving their transport equations:

$$\partial(\rho_m k)/\partial t + \nabla.(\rho_m \mathbf{v_m} k) = \nabla\left[\mu_{t,m}/\sigma_k \times (\nabla k)\right] + G_{k,m} + \rho_m \varepsilon \qquad \textbf{Eq. VI–26}$$

$$\partial(\rho_m \varepsilon)/\partial t + \nabla.(\rho_m \mathbf{v_m} \varepsilon) = \nabla\left[\mu_{t,m}/\sigma_k \times (\nabla \varepsilon)\right] + \varepsilon/k(C_{1\varepsilon} G_{k,m} - C_{2\varepsilon}\rho_\infty \varepsilon) \qquad \textbf{Eq. VI–27}$$

Thus unlike the molecular viscosity, the turbulent viscosity is not a constant, but it depends on a local flow field. The term $G_{k,m}$ is a turbulence production due to mean velocity shear.

$$G_{k,m} = \mu_t\left[\nabla \mathbf{v_m} + (\nabla \mathbf{v_m})^T\right] : \nabla \mathbf{v_m} \qquad \textbf{Eq. VI–28}$$

The turbulent model constants were C_μ = 0.09, σ_k = 1, σ_ε = 1.3, $C_{1\varepsilon}$ = 1.44, $C_{2\varepsilon}$ = 1.92. These are empirically determined constants found to work well for a wide range of wall-bounded and free shear flows (Fluent Inc., 2006). The boundary conditions were no-slip condition on all airlift walls. Standard wall function was used to model a velocity profile in the walls vicinity and to provide inner "boundary" condition for Reynolds averaged velocity field. Zero liquid velocity and 0.25 m/s gas vertical velocity was prescribed at the inlet for all phases. Gas volume fraction was then set to a constant value to obtain the desired gas flow rate into the airlift. Zero liquid velocity was set at the outlet boundary and no gradients were considered either for gas velocity and gas volume fraction. Initial condition was zero liquid velocity and gas volume fraction, initial turbulence kinetic energy was κ=0.001 m^2/s^2, and dissipation rate ε=0.0001 m^2/s^3. The time interval of 30 s was then simulated to let the flow reach a steady or pseudo-steady state. Then another 120 s or more of a flow time was simulated to obtain time-averaged quantities for evaluation.

The segregated pressure-based solver in Fluent was used to solve the model equations, node based gradient option was used to evaluate variables' gradients. Pressure-Implicit with Splitting of Operators (PISO) scheme was used as a pressure-velocity coupling algorithm, PRESTO! (PREssure STaggering Option) scheme was used for pressure discretization and the QUICK scheme for velocity (Fluent Inc., 2006), gas volume fraction, turbulence kinetic energy and dissipation rate. A first order implicit scheme was employed for the time discretization.

VI.3.2.2 CFX simulation

Euler-Euler two-fluid model was used in our simulations done in CFX 12.1. In opposition with the mixture model, this model solves continuity and momentum equation for each phase. Thus for a two phase flow there are two continuity and two momentum equations, one set for continuous phase (*c*) and one for dispersed phase (*d*). The two momentum equations are coupled via pressure (pressure field is shared by both phases), and via interphase force terms, which accounts for various forces (drag, lift, added mass, turbulent dispersion force and others) and cancel each other out when momentum equations of individual phases are added together. Drag force and turbulence dispersion force were accounted for in our CFX simulations. The continuity equations of phase *c* and *d* are:

$$\partial(\alpha_c\rho_c)/\partial t + \nabla.(\partial\alpha_c\rho_c\mathbf{v_c}) = 0 \qquad \textbf{Eq. VI–29}$$

$$\partial(\alpha_d\rho_d)/\partial t + \nabla.(\partial\alpha_d\rho_d\mathbf{v}_d) = 0 \qquad \textbf{Eq. VI–30}$$

The momentum equations of phase *c* and *d* are:

$$\partial(\alpha_c\rho_c\mathbf{v_c})/\partial t + \nabla.(\partial\alpha_c\rho_c\mathbf{v_c}) = -\alpha_c\nabla p + \nabla\left[\alpha_c\mu_{c,eff}\left(\nabla\mathbf{v_c} + \nabla\mathbf{v_c}^T\right)\right] + \alpha_c\rho_c\mathbf{g} + \mathbf{M_{cd}}$$

Eq. VI–31

$$\partial(\alpha_d\rho_d\mathbf{v_d})/\partial t + \nabla.(\partial\alpha_d\rho_d\mathbf{v_d}) = -\alpha_d\nabla p + \nabla\left[\alpha_d\mu_{d,eff}\left(\nabla\mathbf{v_d} + \nabla\mathbf{v_d}^T\right)\right] + \alpha_d\rho_d\mathbf{g} + \mathbf{M_{dc}}$$

Eq. VI–32

Where:

$$\mathbf{M_{cd}} = -\mathbf{M_{dc}} \qquad \textbf{Eq. VI–33}$$

Is a force acting on the phase *c* due to phase *d* (drag, lift, ...), and $\mu_{c,eff}$ and $\mu_{d,eff}$ are effective viscosities consisting of a molecular and a turbulent viscosity:

$$\mu_{c,eff} = \mu_c + \mu_{tc} \text{and } \mu_{d,eff} = \mu_d + \mu_{td} \qquad \textbf{Eq. VI–34}$$

Only drag and turbulence dispersion force were considered in our simulations:

$$\mathbf{M_{cd}} = \mathbf{M_{cd,D}} + \mathbf{M_{cd,TD}} \qquad \textbf{Eq. VI–35}$$

$$\mathbf{M_{cd,D}} = \mathrm{K_{cd}}(\mathbf{v_d} - \mathbf{v}_c) = (3/4)(C_D/d)\alpha_d \rho_d |\mathbf{v_d} - \mathbf{v}_c|(\mathbf{v_d} - \mathbf{v}_c) \qquad \textbf{Eq. VI–36}$$

Where *d* is dispersed phase particle (bubble) equivalent diameter. Drag coefficient was set to C_D = 1.215 resulting in a bubble slip velocity ~0.23 m/s (~5 mm bubble in water).

$$\mathbf{M_{cd,TD}} = C_{TD} K_{cd} v_{tc}/\sigma_{tc} \times \left(\nabla\alpha_d/\alpha_d - \nabla\alpha_c/\alpha_c\right) \qquad \textbf{Eq. VI–37}$$

Where C_{TD}=1, K_{cd} is momentum transfer coefficient for drag force, ν_{tc} is turbulent kinematic viscosity of the continuous phase, σ_{tc}=0.9. Two equations κ–ε model were used to model turbulence and to obtain a closure for turbulent viscosity in the continuous phase:

$$\mu_{tc} = C_\mu \rho_c k_c^2/\varepsilon_c \qquad \textbf{Eq. VI–38}$$

$$\partial(\alpha_c\rho_c k_c)/\partial t + \nabla.(\alpha_c\rho_c\mathbf{v_c}k_c) = \nabla\left[\alpha_c(\mu_c + \mu_{tc}/\sigma_k)(\nabla k_c)\right] + \alpha_c G_c - \alpha_c\rho_c\varepsilon_c \qquad \textbf{Eq. VI–39}$$

$$\partial(\alpha_c\rho_c\varepsilon_c)/\partial t + \nabla.(\alpha_c\rho_c\mathbf{v_c}\varepsilon_c) = \nabla\left[\alpha_c(\mu_c + \mu_{tc}/\sigma_k)(\nabla\varepsilon_c)\right] + \alpha_c\varepsilon_c/k_c(C_{1\varepsilon}G_c - C_{2\varepsilon}\rho_c\varepsilon_c) \qquad \textbf{Eq. VI–40}$$

Where

$$G_c = \mu_{tc}\left[\nabla\mathbf{v_c} + (\nabla\mathbf{v_c})^{\mathrm{T}}\right] : \nabla\mathbf{v_c} \qquad \textbf{Eq. VI–41}$$

The turbulent model constants were C_μ=0.09, σ_k=1, σ_ε=1.3, $C_{1\varepsilon}$=1.44, $C_{2\varepsilon}$=1.92. Turbulence viscosity in the dispersed phase was calculated as:

$$\mu_{td} = (\rho_d/\rho_c)\mu_{tc}/\sigma \qquad \textbf{Eq. VI–42}$$

Where σ=1. The boundary conditions were no-slip condition for liquid and free-slip condition for gas phase on walls. Zero velocity for liquid and 0.25 m/s for gas phase were used. The volume fraction of gas

phase was set to obtain the desired value of gas flow rate. The "degassing" condition was used at the outlet – liquid velocity is set to zero, while the gas phase is allowed to escape.

VI.4 Results and Discussion

The results section is divided in two parts. Auxiliary simulation results are presented in section VI.4.1. This section consists of grid independence test result, brief comparison of few simulations with different turbulence models for a selected iGLR riser configuration, and finally a comparison of two different closures for the drag force. The main results and their comparison with experimentally measured data (liquid interfacial velocity and gas hold-up in the riser and downcomer) are presented in section VI.4.2.

The results for both simulation setups (Fluent, CFX) are presented. In experiments, there were higher liquid velocities in the downcomer for the larger diameter riser (Riser C), due to the lower downcomer cross-section area, which lead the bubbles (gas-phase) to entrain into this section. If Riser A (shorter draft tube) and B (longer draft tube) are compared, then for the longer tube the gas separation was better resulting in no gas in the downcomer, while for the shorter draft tube (case A) bubbles were entrained into the downcomer for the highest gas flow rate. These results are in agreement with the results obtained in the former chapter (see section V.4.2).

VI.4.1 Auxiliary simulation results

The grid independence test was done for the iGLR with riser B for an airflow rate of 3.6 L/min (U_G=1 cm/s see **Table V-2** in section V-3.1). One simulation (Fluent) was run on a refined "fine" grid with 8x more grid cells than in the standard "coarse" grid case (357600 *vs* 44700 cells). The difference in the liquid interstitial velocity and gas hold-up in

the riser was within 1%. Therefore it could be verified that the standard grid was enough to obtain grid independent results.

Four additional turbulence models in addition to standard κ–ε model were tested (in Fluent) at same conditions (riser B, 3.6 L/min), prior to the main simulation campaign. These four models were RNG κ–ε model, RNG κ–ε model with swirl modification for turbulence viscosity, realizable κ–ε model and standard (not SST) κ–ω model. For additional details about these models (simulations were run with default solver settings) a complete description is present in Fluent's 6.3 User Guide (Fluent Inc., 2006). Using the mentioned turbulence models instead of standard κ–ε model had only a minor impact on results of the simulations. The largest difference between standard κ–ε model results and the other model results was 1.4% for interstitial liquid velocity and 4.9% for gas hold-up in riser on "coarse grid" and 1.7% and 4.9% on the fine grid respectively. Standard κ–ε model was then kept for all subsequent simulations.

Different closures for drag coefficient were tested on Risers A and B to test the effect of changing the bubble slip velocity on simulation results. Tomiyama et al. (2002) closure for drag (**Eq. VI-13**) for a single bubble (5mm equivalent diameter) and Schiller-Naumann closure (**Eq. VI-15**) for 5mm bubble were compared for case A, and Tomiyama closure for 3mm and 5mm bubble were compared for case B. Simulations were done for five gas flow rates in range 1.9 – 13.6 L/min (1.0 – 7.5 cm/s) for both risers configurations (A and B).

Riser A comparison between the drag closures is shown in **Figure VI-4**. We are aware that the Schiller-Naumann closure is valid only for rigid spheres, which is certainly not the case of 5mm air bubble in water. However, the aim of this comparison was only to examine an influence of changing a slip velocity of bubbles on simulation results. The Tomiyama closures resulted in bubble slip velocities (riser volume average) in range 22.2 to 22.9 cm/s depending on the gas flow rate (was lower for higher gas flow rates). The Schiller-Naumann slip

velocity was around 70% higher, from 37.6 to 38.6 cm/s. Nevertheless, this difference in slip velocities did not cause very significant changes in simulation outputs. The relative difference between the gas hold-up in riser was from 11.2 to 15.8% and was decreasing with increasing gas flow rate (maximum absolute hold-up difference between the two closures was 0.8%).

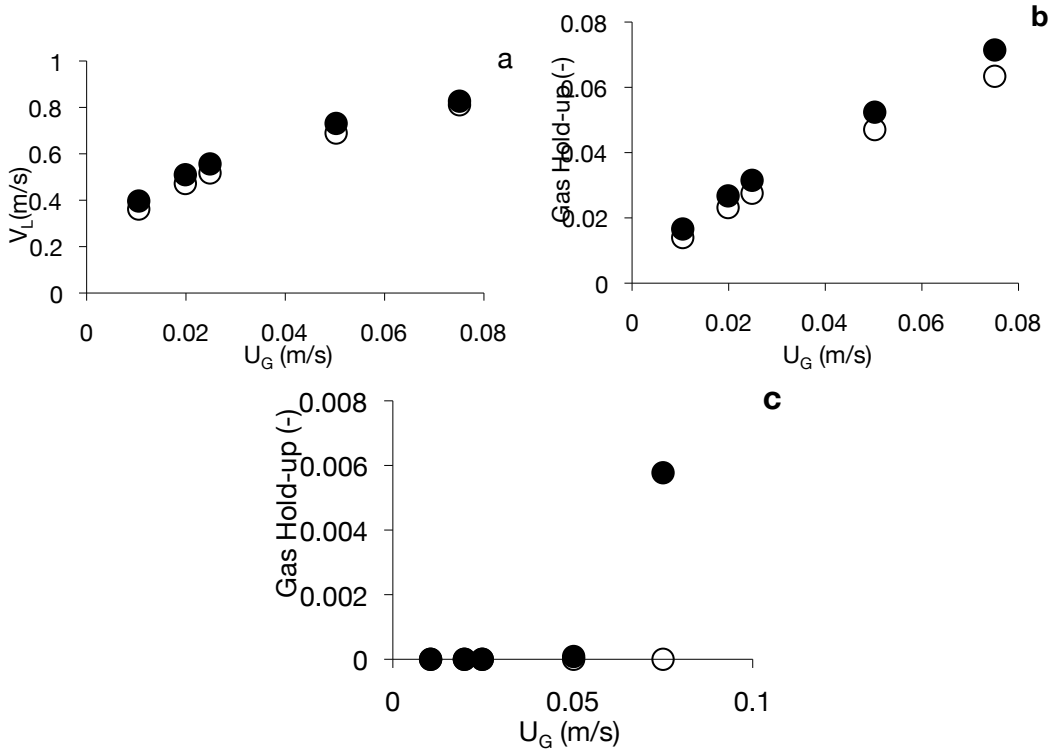

Figure VI-4. Riser A simulation results (section VI. 4.1). Comparison of two drag closures for 5mm bubbles. (a) Riser liquid interstitial velocity V_L (m/s), (b) riser gas holdup α, and (c) downcomer gas holdup α vs. riser gas superficial velocity U_G (m/s). Legend: ● - Tomiyama (**Eq. VI-13**); ○ - Schiller-Naumann (**Eq. VI-15**).

The reason for this is the co-current flow of liquid and gas phases in the riser. The gas holdup in the riser is given by

$$\alpha_{Gr} = \frac{U_G}{v_G} \qquad \textbf{Eq. VI–43}$$

Where U_G is gas superficial velocity given by airflow rate into the airlift and V_G is gas interstitial velocity in the riser, which is

$$V_G = V_L + V_{Slip} \qquad \textbf{Eq. VI–44}$$

As referred in the literature the effect of changing the bubble slip velocity V_{slip} on the holdup in the airlift riser is then smaller then it would be in a case of bubbles rising through a stagnant liquid (V_L=0 cm/s), because the liquid velocity V_L in the riser is relatively high if compared to bubble slip velocity V_{slip} (Sokolichin et al., 2004). The situation would be different in the downcomer, where the phases flow counter-currently and the slip velocity value could have a deep impact on the downcomer and consequently on the whole airlift hydrodynamics. There was effectively zero gas holdup in the downcomer for all gas flow rates where riser A was used, except for the highest one with Tomiyama drag correlation, when the gas just started to be entrained into the downcomer, and the downcomer holdup was ~8% of the riser holdup. The difference between liquid interstitial velocities for the two drag coefficient correlations was from 1.6 to 8.5% and was decreasing with increasing of the gas flow rate with a sharper drop of this difference for the highest gas flow rate, where the driving force for liquid circulation was decreased by the small amount of gas entrained into the downcomer (Tomiayama correlation case).

For Riser B configuration, the comparison between simulations assuming 3mm and 5mm diameter bubbles is shown in **Figure VI-5**. Tomiyama drag correlation was used for both.

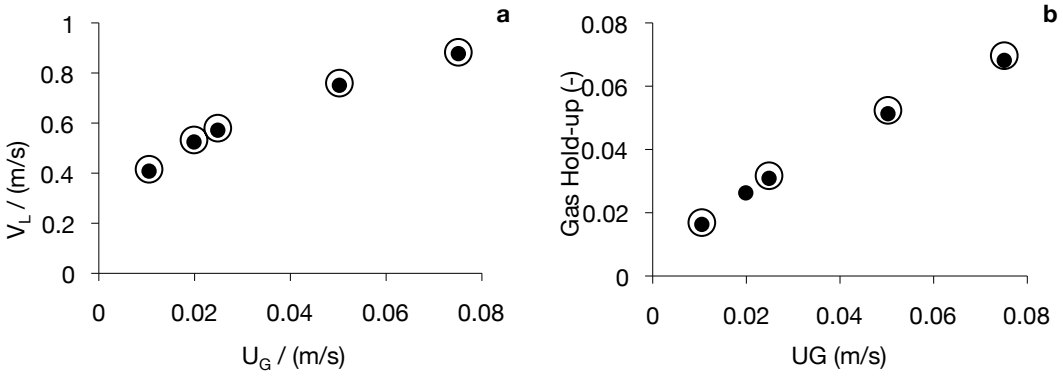

Figure VI-5. Case B simulation results (section VII.4.1). Tomiyama drag closure (**Eq. VI-13**) results for 3 mm (○) and 5mm bubble (●). Legend: (a) - Riser liquid interstitial velocity V_L (m/s), (b) - riser gas holdup vs. riser gas superficial velocity U_G (m/s).

The resulting volume averaged bubble slip velocities in the riser were from 19.4 to 20.0 cm/s (3 mm bubble) and from 22.3 to 23.0 cm/s (5 mm bubble). There was only a very small difference between 3 mm and 5 mm bubble simulations, being reasons for this the same previously described. The relative difference between gas hold-up in the riser was from 2.2% to 3.5%, and from 0.6% to 1.8% for the riser liquid interstitial velocity. Once more this difference was decreasing with increasing of gas flow rate and no gas was present in the downcomer at all gas flow rates.

It could be stated that if the gas phase is present only in the riser and not in the downcomer, then the impact of a bubble slip velocity change is not so significant due to co current flow of both phases. However, if the gas phase is rising through a stagnant liquid or even if the phases are flowing counter currently (downcomer), then, of course, this impact can be much more significant.

VI.4.2 Comparison with experiments

Simulation results for the three airlift configurations (A, B and C) and their comparison with experimentally measured data are presented in this section. Both Fluent and CFX simulation results are shown for risers A and B, simulations for riser C were done only in Fluent. Gas flow rates in the simulations were from 1.9 to 13.6 L/min (1.05 – 7.51 cm/s gas superficial velocity based on riser cross section) for risers A and B, and from 1.9 to 26.8 L/min (0.53 – 7.51 cm/s) for riser C.

VI.4.2.1 Case A

Liquid interstitial velocities and gas hold-up in the riser and in the downcomer obtained from simulations (Fluent and CFX) and from experiments as a function of gas flow rate are shown in **Figure VI-6**. Gas holdup fields for different gas flow rates can be seen in **Figure VI-7**. A very good agreement was obtained for liquid interstitial velocity.

The relative difference between simulations (Fluent) and experiments was from 0.7 to 4.4% and it was increasing with gas flow rate.

The Fluent and CFX simulations also agreed very well with each other with CFX predicting slightly lower values. The situation was worse in the case of gas hold-up.

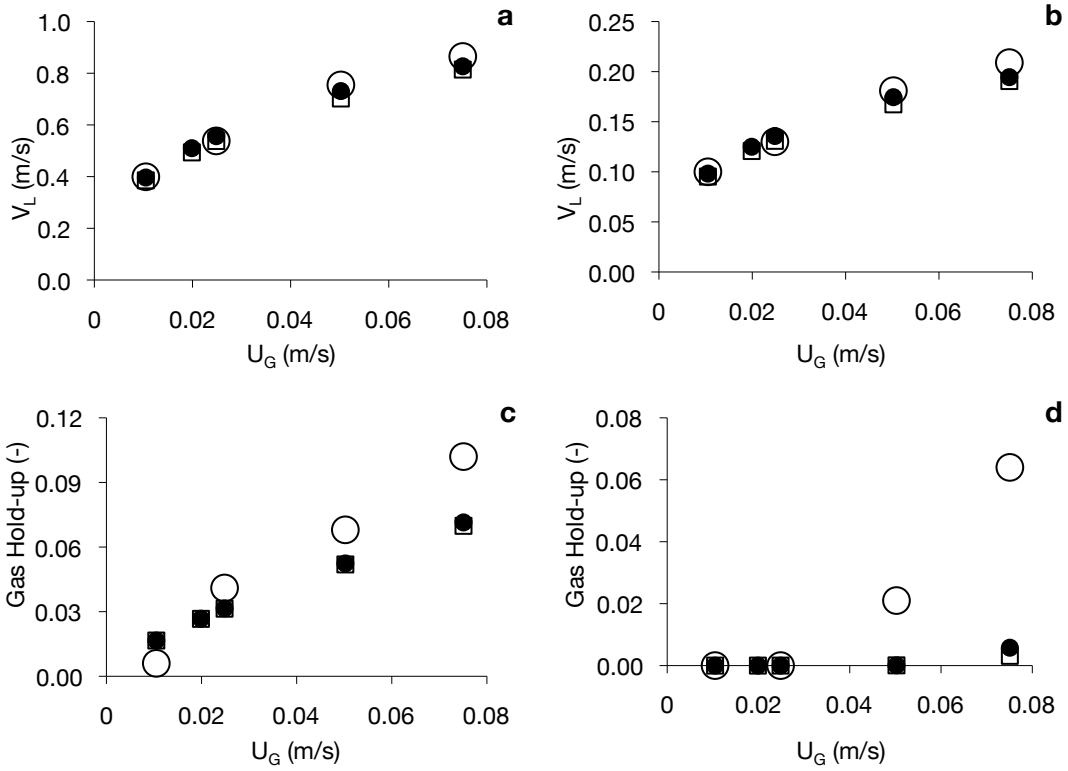

Figure VI-6. Riser A simulations vs. experiments (Section VII-4.2): Fluent simulations (●), CFX simulations (□), experiments (○). (a) Riser liquid interstitial velocity V_L (m/s), (b) downcomer liquid interstitial velocity V_L, (c) riser gas holdup (α), and (d) downcomer gas holdup α vs. riser gas superficial velocity U_G (m/s).

Simulations strongly underpredicted both gas hold-up in the riser (30% relative difference at the highest gas flow rate used) and in the downcomer, at the moment when bubbles were starting to be entrained into the downcomer. The gas hold-up from simulations in the downcomer for the highest gas flow rate was less than 1/10 of the experimentally obtained value. If a gas interstitial velocity is estimated from $V_G=U_G/\alpha_G$, where U_G is the gas superficial velocity given by gas flow rate and α_G is the experimentally measured gas holdup, then for

the highest gas flow rate the V_G would be ~74 cm/s. This V_G value is actually lower than the measured and simulated liquid velocity (V_{Lexp}= 86.5 cm/s at maximum gas flow rate: in **Figure VI-6**) and, considering the **Eq. VI-44** would result in a negative bubble slip velocity, which is of course not possible.

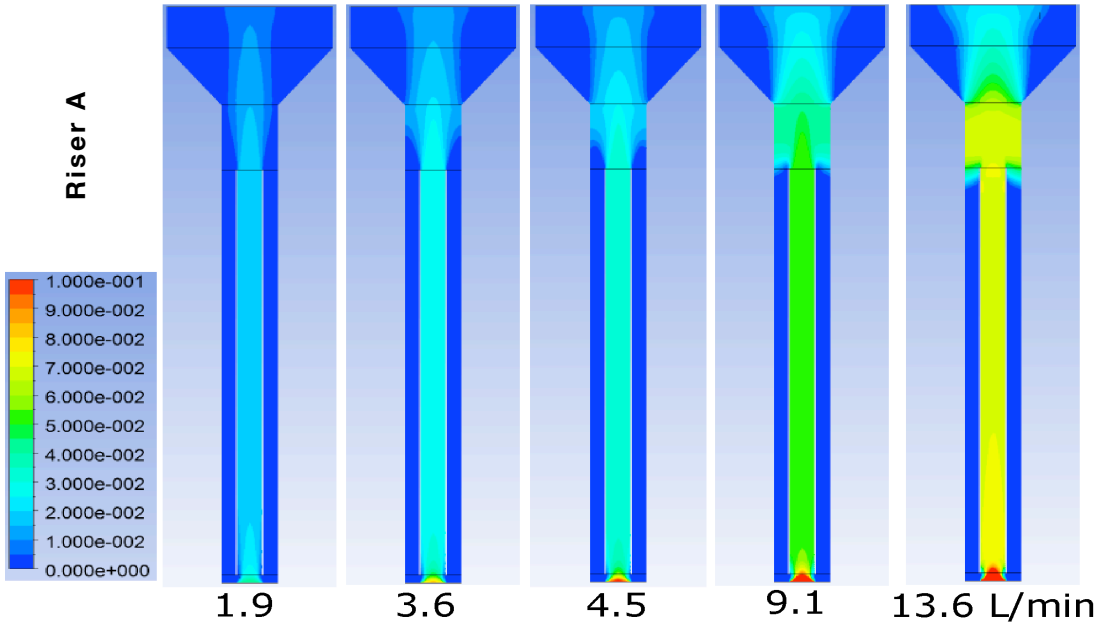

Figure VI-7. Riser A simulations: Gas holdup fields for gas flow rates 1.9, 3.6, 4.5, 9.1 and 13.6 L/min (riser gas superficial velocity ~ 1.0, 2.0, 2.5, 5.0, 7.5 cm/s).

The reason of the discrepancy between simulation and experiment is then probably either due to the experimental method used to obtain estimates of gas hold-up in the downcomer or due to imperfect model considerations (bubble shape, rise velocity, etc). A pressure drop due to liquid flow can negatively influence hold-up measured with U-tube manometers. Nevertheless, it was visually observed gas bubbles in the downcomer at higher gas superficial velocities in riser A configuration. Being so the discrepancy obtained for downcomer gas hold-up can be influenced either by the measuring method and by simulation considerations.

VI.4.2.2 Case B

Simulations (Fluent and CFX) and experiments of riser B are compared in **Figure VI-8**. Gas holdup fields for different gas flow rates can be seen in **Figure VI-9**.

A good agreement was obtained for liquid interstitial velocity. The relative difference between simulations (Fluent) and experiments varied from 4.6 to 8.3%. As for the case A, the Fluent and CFX simulations gave very similar results with CFX predicting slightly lower values of liquid interstitial velocity. The simulated and experimentally measured gas hold-up agreement in the riser was poor. The relative difference in the riser hold-up for the lowest gas flow rate was 40.4% and continually decreased to 15.5% for the highest gas flow rate.

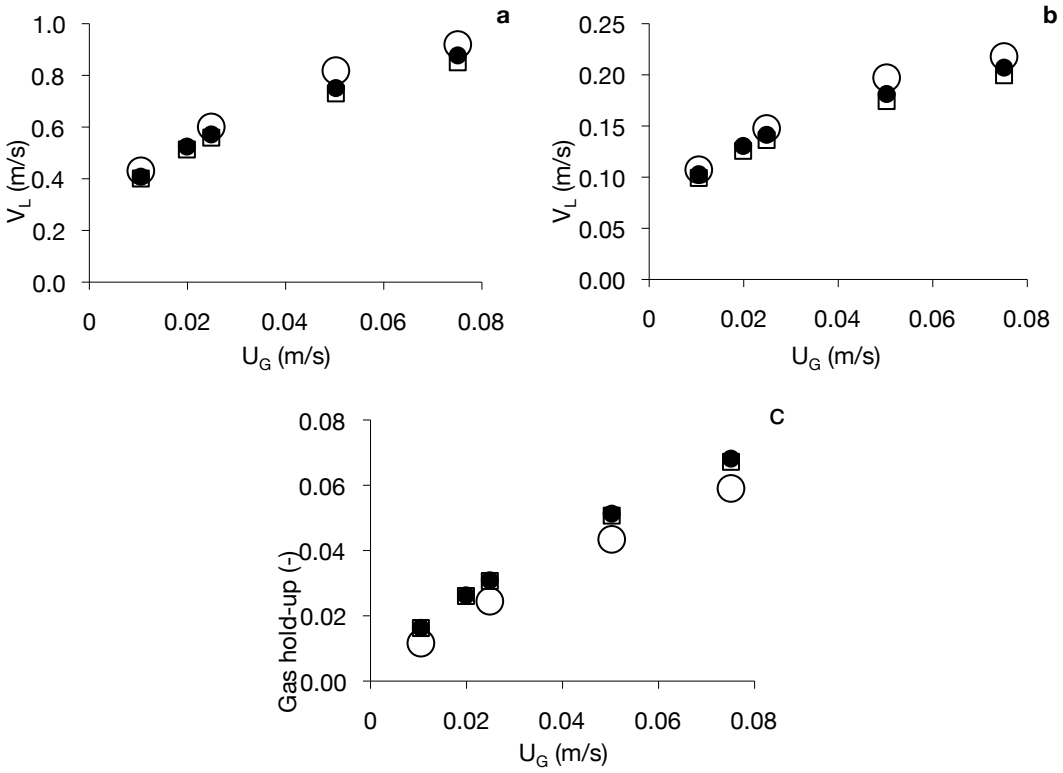

Figure VI-8. Riser B simulations vs. experiments. Legend: ● - Fluent simulations (black marks), □- CFX simulations (stars), ○ - experiments (white marks). (a) Riser liquid interstitial velocity V_L, (b) downcomer liquid interstitial velocity V_L(m/s), and (c) riser gas holdup α vs. riser gas superficial velocity U_G(m/s).

The gas hold-up was overpredicted by simulations in this situation (riser B) contrary to the previous riser configuration (A). If riser B simulations are compared with riser A simulations (Riser B has 20 cm longer draft tube), then it can be noticed that the predicted liquid interstitial velocities are very similar, with riser B velocities 2.7% – 2.9% higher if compared to riser A except for the highest gas flow rate, where the Riser B velocity is 6.1% higher, because of starting bubble penetration into the downcomer in riser A. Experimentally measured riser liquid interstitial velocities for riser B were 6.3-11.6% higher then in riser A depending on the gas flow rate. If the same comparison is done for gas hold-up (Riser A vs. Riser B) then for simulations the relative difference is again low (Riser B riser holdup 1.7-4.6 relative % lower). However, the experimentally measured hold-up in Riser B was 24.7% - 33.2% relative lower than in riser A (except for the lowest gas flow rate). The difference between riser A and Riser B in experiments was much higher than in simulations.

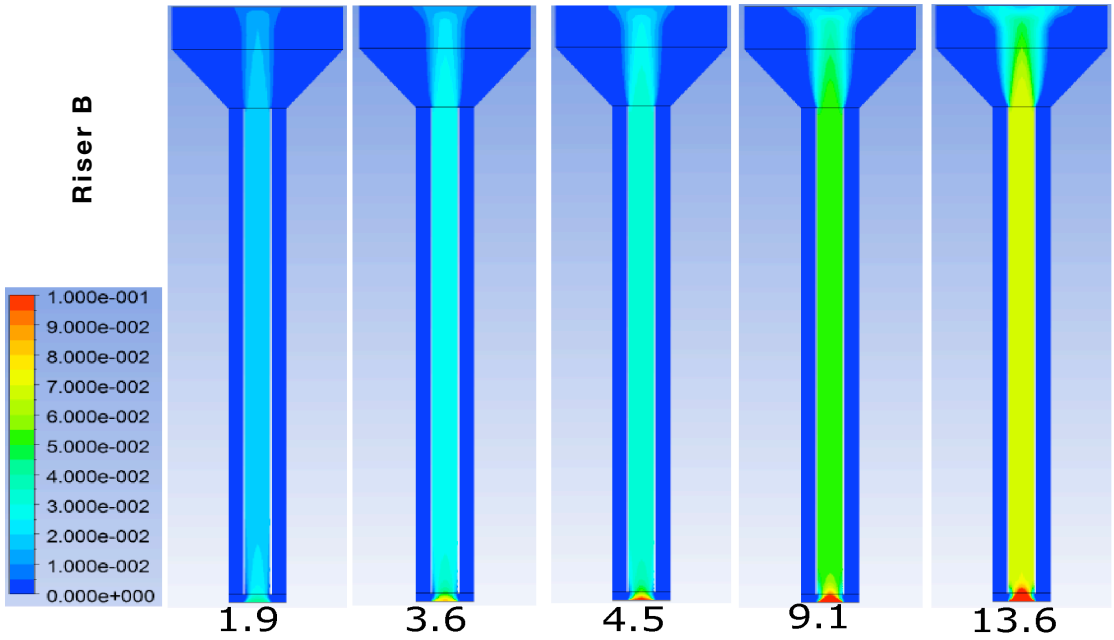

Figure VI-9. Riser B simulations: Gas holdup fields for gas flow rates 1.9, 3.6, 4.5, 9.1 and 13.6 l/min (riser gas superficial velocity ~ 1.0, 2.0, 2.5, 5.0, 7.5 cm/s)

This suggest that the reason for bigger discrepancy between experimental and simulation data in Riser B is probably a consequence of the experimental method used to estimate gas holdups (U-tube manometers).

VI.4.2.3 Case C

In the Riser C three different regimes were experimentally observed with the change of gas flow rate. At first, for the lowest gas flow rate, there were no gas bubbles inside the downcomer. Then for higher rates the bubbles started to be entrained into the downcomer, but the bubble front did not reach the downcomer bottom yet. And finally, for the highest gas flow rate, the front reached the airlift bottom and bubbles started to circulate with a corresponding change of interstitial liquid velocity and gas holdup vs. gas flow rate curve trends.

The results are shown in **Figure VI-10** (gas hold-ups and liquid interstitial velocities) and in **Figure VI-11** (simulated gas hold-up fields).The main question was if the simulations were able to capture this behaviour. The answer was that they could, but only partially. There was an initially good agreement in liquid interstitial velocities. The difference between the simulation and the experiment for the lowest experimentally measured gas flow rate was <3.5 % and it was continually increasing with gas flow rate. It was 8.5 % for the second highest flow rate, which is still ok, but for the highest flow rate, where there was a steeper rise of the experimentally measured liquid velocity due to the regime change, the experiment/simulation difference was 46%.

Gas hold-up in the riser and in the downcomer and also the point at which bubbles start to enter the downcomer was captured very well. However, the agreement for the highest gas flow rate was rather bad. The bubble front did not reach the airlift bottom in the simulations and there appeared no bubble circulation regime even for the maximal gas flow rate.

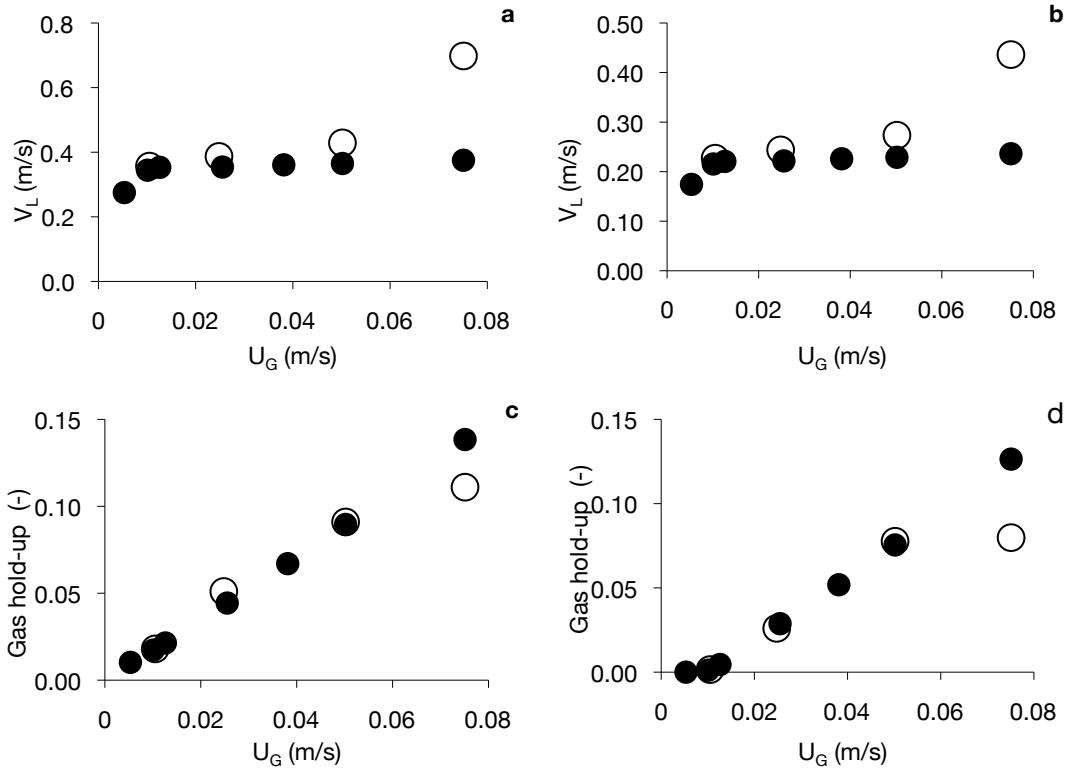

Figure VI-10. Riser C simulations vs. experiments Legend: ● - Fluent simulations (black marks), □- CFX simulations (stars), ○ - experiments (white marks). (a) Riser liquid interstitial velocity V_L(m/s), (b) downcomer liquid interstitial velocity V_L(m/s), (c) riser gas holdup α, and (d) downcomer gas holdup α vs. riser gas superficial velocity U_G (m/s).

The liquid interstitial velocity did not change much with an increase in gas flow rate in the simulations, except for the lower rates (only 6.2% increase from gas flow rate 4.5 L/min to 26.8 L/min). The liquid superficial velocity in simulations (and thus a total circulating liquid flow rate), was even decreasing with gas flow rate. The reason was that the driving force for the liquid circulation, the difference between average hold-up in the riser and in the downcomer, was slowly decreasing with gas flow rate from a certain point (Q_G=4.5 L/min, U_G=1.26 cm/s), while the gas hold-up in the riser and the downcomer were rising linearly. The absolute difference between them (riser/downcomer) was 1.7 % at Q_G = 4.5 L/min (U_G=1.26 cm/s) and 1.2% at 26.8 L/min (U_G=7.51 cm/s). The liquid superficial velocity in the riser dropped from 34.6 cm/s to 32.3 cm/s in this gas flow rate range in simulations.

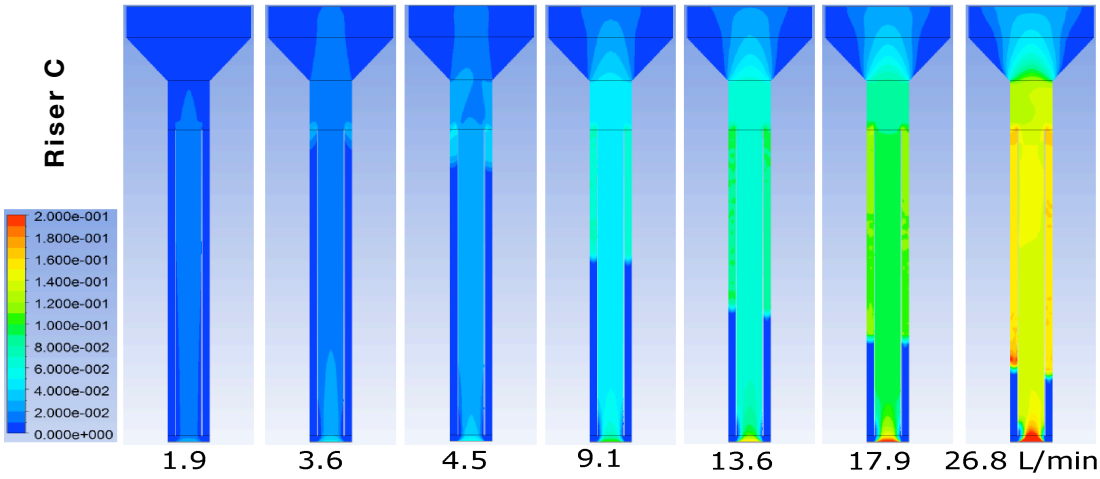

Figure VI-11. Riser C simulations: Instantaneous gas holdup fields for gas flow rates 1.9, 3.6, 4.5, 9.1, 13.6, 17.9 and 26.8 l/min (riser gas superficial velocity ~ 0.5, 1.0, 1.3, 2.6, 3.8, 5.0, 7.5 cm/s).

For riser C simulations, there was a very good agreement with experiments for low gas flow rates. The deviation from experiments then started to increase slowly with gas flow rate and then it rose suddenly for the highest gas flow rate with the onset of a bubble circulation regime, which was not captured. As it was pointed out earlier, flow in a downcomer (counter-current flow) is influenced by a bubble slip velocity much more than a flow in a riser (co-current). Demands on the accuracy of drag force closure are then quite high if bubbles are present in the downcomer. Drag coefficient and bubble slip velocity for given fluids depend on bubble size, shape, local gas holdup and other factors (presence of surfactants). To obtain a correct bubble slip velocity (a) a reliable closure equation for it is needed and (b) correct inputs into this closure are required. Our closure was **Eq. VI-8**. A bubble size can be either prescribed directly or it can be a result from a bubble coalescence/break-up model solution. Solving governing equations of the flow provides the local gas hold-up. In our simulations the bubble size was prescribed directly (5 mm for all flow rates, all bubbles assumed to have a same size). The weak point of our simulations and the cause of disagreement between simulations and experiments can be any of the above-mentioned issues, probably the specification of bubble size and/or the slip velocity adjustment on the

local gas holdup. Although measurements of bubble size were done with a high-speed camera, they could be done only for very low gas flow rates not relevant for our study. The bubbly layer soon became opaque as the holdup increased.

The use of local techniques (eg. optical probes) to measure the bubbles properties (velocity, size) is now very important and it seems the next step in this process. Local axial measurements will also allow studying the occurrence of coalescence and break-up as well as measuring its intensity, which can be computed latter using similar CFD's setups. This information seems crucial in order to get closer the simulations and the experimental values. Finally this can be complemented by measurements and simulation using SG as solid phase in a *g-l-s* system.

VI.5 Conclusions

The primary goal of this work was to make a comparison between simulations and experiments to see how well the simulations are able to predict liquid interstitial velocity and gas hold-up both in the riser and in the downcomer for a *g-l* system. Three different airlift riser tubes for a range of gas flow rates were tested. It was shown that there was a good agreement regarding the liquid interstitial velocities in the riser and the downcomer with errors mostly well below 10% with an exception of higher gas flow rates (and especially the highest one) in larger diameter riser (Riser C). The agreement of the gas hold-up (riser and downcomer) between simulations and experiments was poorer. The simulations over-predicted the riser gas holdup in riser A and under-predicted it in riser B. However, as it was discussed, it could be an error in experimental measurements rather than a simulation error. The agreement of the gas hold-up (riser and downcomer) for Riser C was good, except for the highest gas flow rate, where a flow regime had already changed to a bubble circulation regime, which was not captured by simulations. A more accurate modelling of the drag

force/bubble slip velocity would be needed to obtain better agreement with experiments in the cases, when there is a gas phase present in the downcomer. The simulation setup is considered to be good enough to model cases with no gas phase being entrained into the downcomer.

The secondary goal was to test an effect of various models and parameters on simulation results. This included comparison between two commercial codes with two different models, mixture model (Fluent) and Euler-Euler model (CFX), testing different drag force closures and turbulence models (variants of $\kappa-\varepsilon$, $\kappa-\omega$). The Fluent simulations with mixture model and CFX simulations with Euler-Euler model gave the same results with only minor differences between them. The testing of drag closures suggested that an accurate modelling of drag force/bubble slip velocity is required, if there are bubbles present in a downcomer due to counter-current flow of gas- and liquid-phase. Not so much accuracy is needed for a riser flow modelling, because the co-current flow of gas- and liquid-phase and the relatively high liquid velocity if compared to the bubble slip velocity. Three versions of a $\kappa-\varepsilon$ turbulence model and a $\kappa-\omega$ model gave very similar results.

VI.6 References

Cao, C., Dong, S. and Guo, Q. (**2007**). Experimental and numerical simulation for gas– liquid phases flow structure in an external-loop airlift reactor. *Industrial and Engineering Chemistry Research*, 46, 7317–7327.

Chisti, M. Y. (**1989**). Airlift Bioreactors (1st ed.). Essex: Elsevier Science Pub. LTD.

Chisti, Y. (**1998**). Pneumatically agitated bioreactors in industrial and enviromental bioprocessing: Hydrodynamics, hydraulics and transport phenomena. *Applied Mechanic Reviews*, 51(1), 33-112.

Fluent Inc. (**2006**). Fluent 6.3 User ' s Guide. Lebanon, NH: Fluent Inc.

Freitas, C., Fialová, M., Zahradnik, J. and Teixeira, J. A. (**1999**). Hydrodynamic model for three-phase internal-and external-loop airlift reactors. *Chemical Engineering Science*, 54, 5253-5258.

Garcia-Calvo,E., Rodríguez,A., Prados,A. and Klein,J. (**1999**). A fluid dynamic model for three-phase airlift reactors. Chemical Engineering Science, 54, 2359-2370.

Heijnen, J., Hols, J., van Der Lans, R. M. van Leeuwen, H. M., Mulder, A., and Weltevrede, R. (**1997**). A simple hydrodynamic model for the liquid circulation velocity in a full-scale two- and three-phase internal airlift reactor operating in the gas recirculation regime. *Chemical Engineering Science*, 52(15), 2527-2540.

Huang, Q., Yang, C., Yu, G. and Mao, Z. S. (**2008**). Sensitivity study on modeling an internal airlift loop reactor using a steady 2D two-fluid model. *Chemical Engineering and Technology*, 31, 1790–1798.

Huang, Q., Yang, C., Yu, G. and Mao, Z. S. (**2010**). CFD simulation of hydrodynamics and mass transfer in an internal airlift loop reactor using a steady two-fluid model. *Chemical Engineering Science*, 65, 5527-5536.

Jia, X., Wen, J., Wei, F. and Yuan, Q. (**2007**). Local hydrodynamics modeling of gas–liquid–solid three-phase airlift loop reactor. *Industrial and Engineering Chemistry Research*, 46, 5210-5220.

Lu, W-J., Hwang, S-J. and Chang, C-M. (**1995**). Liquid velocity and gas holdup in three-phase internal loop airlift reactors with low-density particles. *Chemical Engineering Science*, 50(8), 1301–1310.

Manninen,M., Taivassalo,V. and Kallio,S. (**1996**). On the mixture model for multiphase flow. (p. 288).

Merchuk, J., Contreras, A., Garcia, F. and Molina, E. (**1998**). Studies of mixing in a concentric tube airlift bioreactor with different spargers. *Chemical Engineering Science*, 53(4), 709-719.

Mudde, R. F. and van den Akker, H. E. A. (**2001**). 2D and 3D simulations of an internal airlift loop reactor on the basis of a two-fluid model. *Chemical Engineering Science*, 56, 6351-6358.

Oey, R. S., Mudde, R. F., Portela, L. M. and van den Akker, H. E. A. (**2001**). Simulation of a slurry airlift using a two-fluid model. *Chemical Engineering Science*, 56, 673-681.

Roy, S., Dhotre, M. T. and Joshi, J. B. (**2006**). CFD Simulation of Flow and Axial Dispersion in External Loop Airlift Reactor. *Chemical Engineering Research and Design*, 84, 677-690.

Sokolichin,A., Eigenberger,G. and Lapin,A. (**2004**). Simulation of buoyancy driven bubbly flow: established simplifications and open questions. *AIChE Journal*, 50(1), 24–45.

Talvy, S., Cockx, A. and Line, A. (**2007**). Modeling hydrodynamics of gas–liquid airlift reactor. *AIChE Journal*, 53, 335–353.

Tomiyama,A., Tamai,H., Zun,I. and Hosokawa,S. (**2002**). Transverse migration of single bubbles in simple shear flows. *Chemical Engineering Science*, 57, 1849-1858.

Van Baten, J. M., Ellenberger, J. and Krishna, R. (**2003**). Hydrodynamics of internal air-lift reactors: experiments versus CFD simulations. *Chemical Engineering and Processing*, 42(10), 733–742.

Verlaan, P., Tramper, J., VanT Reit, K. and Luyben, K. C. H. A. M. (**1986**). A hydrodynamic model for an airlift-loop bioreactor with external loop. *Chemical Engineering Journal*, 33, B43-B53.

Vial, C., Poncin, S., Wild, G. and Midoux, N. (**2002**). Experimental and theoretical analysis of the hydrodynamics in the riser of an external loop airlift reactor. *Chemical Engineering Science*, 57, 4745-4762.

Young, M. A., Carbonell, R. G. and Ollis, D. F. (**1991**). Airlift bioreactors: analysis of local two-phase hydrodynamics. *AIChE Journal*, 37(3), 403-428.

van Baten, J. M., Ellenberger, J. and Krishna, R. (**2003**). Hydrodynamics of internal air-lift reactors: experiments versus CFD simulations. *Chemical Engineering and Processing*, 42, 733-742.

VII. Chapter VII – Local Hydrodynamic Properties of Three-phase iGLR

VII.1 Objectives

The main objective in this chapter was to study the local influence of SG in the GLR hydrodynamics, in order to understand better the influence of such particularly particles. In addition and due to initially technical problems other objectives lie under the main objective, such as:

- Development and calibration of a method to measure gas-phase properties using an OP,

- Evaluation of the effect of low solid concentration in iGLR local hydrodynamics at similar gas flow conditions used in continuous AFB primary fermentation,

- Study the influence of yeast cells in optical probe measurements as well as the influence of microorganisms growth on the gas-phase after star-up and immobilization stage (see chapter IV).

VII.2 Introduction

In chapter V. the global hydrodynamic parameters of three-phase iGLR were studied and discussed. The main conclusion indicated the adequate iGLR configuration for continuous AFB primary fermentation. Among the options tested, the ideal configuration should have an A_d/A_r ratio equal to 3.67 and the length of riser should go from two centimetres above sparger (should ensure bubbles diameter between 2 and 4 mm) to the beginning of conical part from enlarged top section. The influence of SG particles on gas hold-up for this configuration was not entirely clear (see section V.4.2). Therefore in this chapter it will be studied the influence on local iGLR hydrodynamics of SG particles for a similar configuration iGLR.

As referred before local measurements of gas-, solid- and liquid-phase require the use of different and refined techniques to better understand the effect of SG have in the *g-l* mixture.

VII.2.1 Measurement of local gas-phase properties

In chapter V global gas hold-up and liquid velocity for the selected riser configuration were not significantly affected by the presence of solids. However it was mentioned that it was due to the low sensibility of the methods used. Therefore it was important to study the local hydrodynamics of the three-phase iGLR using SG as solid-phase.

There are several techniques to study local flow structures (Boyer et al., 2002) and are represented in **Figure VII-1**. below.

Among these techniques, the main non-invasive are tomography (γ- or X-ray, capacitance or resistivity, ultrasound) and visualization (High Speed Camera (HSC), PIV, etc) techniques, while among invasive techniques are phase detection probes: needle, heat transfer and ultrasound probes (Boyer et al., 2002; Alain Cartellier, 1990).

Invasive techniques besides more expensive and hard to apply are often used at industrial scale. The reasons for this are: (1) the typical turbulent flow regimes found in industrial reactors; (2) opaque reactors; and (3) ability to collect data online and continuously (Boyer et al., 2002). Although, in the later years, tomography begins to be applied in some industrial process, the main drawback of this technique application in *g-l-s* systems remains the equipment cost. On the other hand, phase detection probes are cheaper and easier to apply in industrial processes. Sensors based on temperature, capacitance, optical properties and conductivity are commonly used. Frequently they are applied for two-phase flow (Olivieri et al. 2007; Jhawar and Prakash 2007) and more recently to three phase flow systems (Mena et al. 2008), usually at low solids hold-up (Boyer et al. 2002). In our work, to study the gas-phase two techniques were used: photographic method (high speed camera) and optical probe (OP). The choice for these two methods was to measure with maximum accuracy the local gas-phase properties in the *g-l-s* system present in the riser of an iGLR.

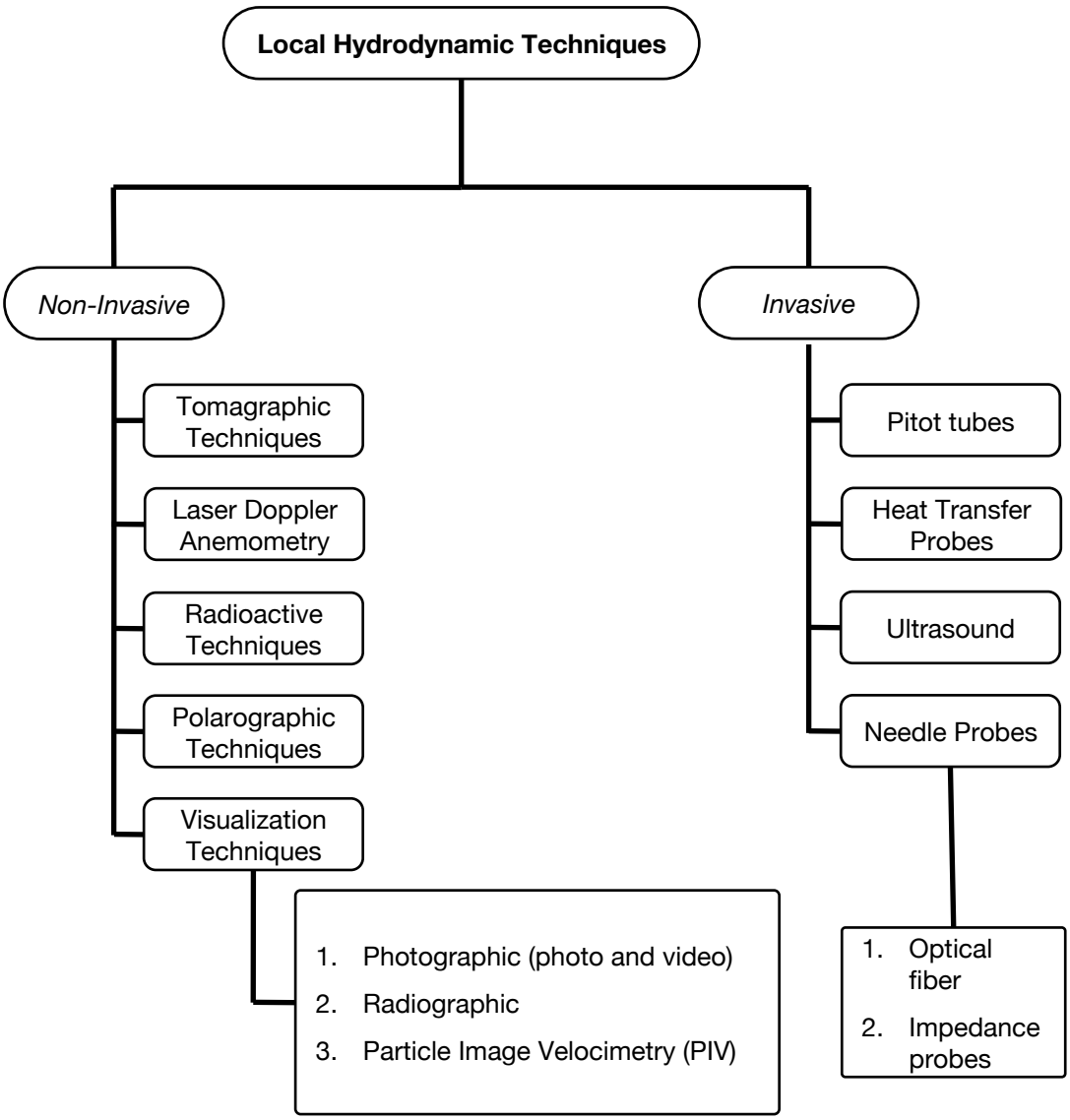

Figure VII-1. Techniques used for local hydrodynamics characterization in *g-l* and *g-l-s* systems.

VII.2.1.1 Photographic technique: high speed camera

High speed camera (HSC) is the tool for the photographic technique. This is a method used in visualization techniques mainly applied for qualitative flow analysis and quantitative bubble properties such as: shape, size, area and volume. Basically, it consists in filming the system (*g-l* or *g-l-s*) flow, which is very important because due to their small scale and fast bubble raising human eye is limited to capture all information. However some limitations are known as the inability to use this technique at high gas flows, reactor wall transparency, out of

focus, illumination and image analysis (Boyer et al., 2002; Ferreira et al., 2011). The reactor wall, as well as focus and illumination can be solved, or reduced experimentally, especially by using a backlight were light passes trough a diffusion layer before illuminating the reactor. (Mena et al, 2005a, 2005c, 2008). Nevertheless, treatment of the obtained images is not an easy task to perform. Most of the commercial systems for bubble population characterization, i e., the identification of single and overlapping bubbles are done by manual or semi-manual methods (Ferreira et al., 2011). This identification can be done by a criterium as the concavity index (CI) but it is normally used at gas superficial velocities below 3 cm/s. When bubbles are separated and classified then the commercial programs are able to determine successfully the bubbles properties as: the projected area, equivalent diameter, the Feret diameters distribution, elongation and sphericity (Ferreira et al., 2011; Mena et al., 2005c).

Recently Ferreira et al. (2011) developed an automatic method based on an online technique for sucrose crystal morphology to identify between single and a group (two or more) of bubbles. This classification is based on a series of probabilities and also allows the characterization of system complexity/turbulence (Ferreira et al., 2011).

Usually when three-phase systems are applied, the use of automatic image analysis of bubbles is very difficult, especially when the difference of grey level between solids and bubbles is not significant. HSC videos can be also used to determine particles (bubbles or solids) velocity, however even in commercial programs the treatment is done manually.

VII.2.1.2 Optical probes characteristics: the LEGI optical probe

Over the last two decades optical probes have been developed and successfully applied in BC reactor local gas-phase hydrodynamics (Dias et al., 2000; Hamad and He, 2010; Hong et al., 2004; Poupot and Cartellier, 1999; Shen et al., 2008). They operation is relatively simple and consequently their utilization have been increased. They allow

measuring not only gas-phase concentrations (hold-up) but also bubble velocities, size distributions, mean interfacial area, mean Sauter diameter and are also able to identify flow regimes. However, this is only possible if some flow structures or bubble shape assumptions are taken in account (Cartellier, 1992; Mena et al., 2008).

Double (or multi) tip probes are also applied in order to measure parameters such as bubble velocities, diameter and interfacial area (Boyer et al., 2002; Chaumat et al., 2005; Dias et al., 2000). The major drawback on this is the reduction of spatial resolution. In addition, when double tip probes are applied on *g-l-s* systems, there is a higher probability to promote an increase of solids near the tip, which can lead to inaccurate measures.

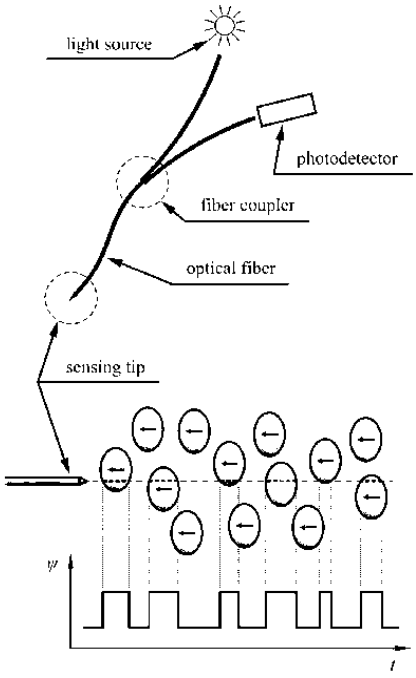

Figure VII-2. Optical fiber typical operation method and indicator function obtained during bubble piercing. From Vejrazka et al. (2010).

Cartellier (1990) developed a single tip probe, which allows a refined description of the flow. This probe is able to measure void fraction and bubble velocity (Cartellier, 1990). Due to their small size the spatial resolution is very high, which also allows the description of microstructuration. However some complex interactions (tip-bubble

interaction) must be taken in account on this system, particularly when bubble velocity is measured (Cartellier and Rivière, 2001).

Optical probe principle is very simple (**Figure VII-2**). The light is generated in a LED or Laser diode (600 to 800 mm) and passes trough a fiber connected to a coupler. This device connects the probe and receives its response signal that is transmitted to an optical/electric convertor. The optical signal is then convert into electrical signal (Olivier 1999).

The electrical signal is fragmented in order to extract all characteristic points (fragments) and carried out a sampling ordering based on its amplitude.

In **Figure VII-3** are presented the most important points to be detected from the signal when a bubble is pierced by the fiber. The electrical signal treatment method, called Treatment for Gaseous Velocity (TVG), was proposed by Cartellier (1992), and can be divided in four stages:

1. Detection of typical amplitudes (V_L and V_G);
2. Detection of the characteristic points A and B;
3. Detection of the characteristics points C and D;
4. Exploitation of the reduced data.

Initially the knowledge of three amplitudes is important: liquid (V_L), gas (V_G) and noise (V_B) voltage levels, which represent the surrounding phase around the probe tip. VG is not easy to define mainly due to difference between V_G in a dry probe and V_G of a bubble. V_B, the electric noise, is considered similar both in liquid- or gas-phase. These parameters can be manually introduced or computed. The V_B can easily be determined from a scope reading while the V_L and V_G determination implies the assurance of two criteria: (1) V_G-V_L>1 and (2) V_L/V_B>3. To avoid possible fluctuations a safety coefficient (SC) is taken in account and for computation purposes V_B is define as $V_{BC}=S_C x V_B/2$, where S_C is usually lower than 2. Then, signal fragmentation is done by isolating all time intervals from raw signal from which voltage exceeds V_L+V_{BC}.

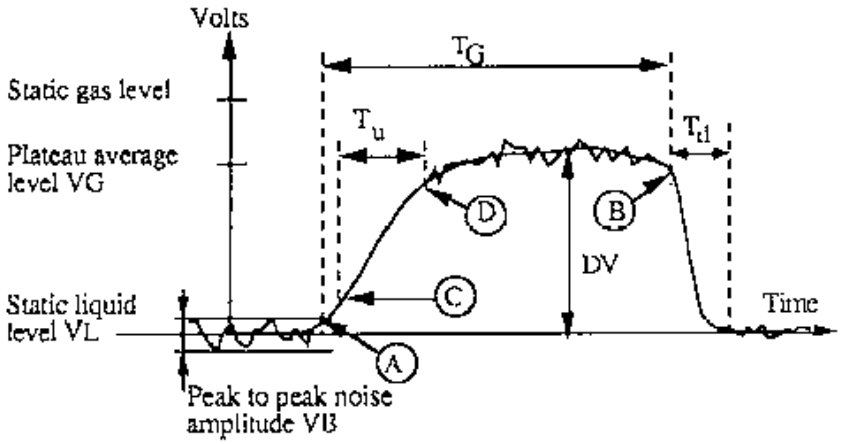

Figure VII-3.Bubble detection and determination of "bubble caracteristic points". Legend: A – Beginning of Bubble; B – End of Bubbles; C – Begin rising; D – End of Rising. (in Cartellier, 1992)

For each interval, A and B are determined, the used criteria for A and B being the very beginning of the ascending and the very beginning of the descending ramp, respectively. To reduce errors that may occur, criteria parameters are introduced to ensure the correct determination of A and B. Determination of C and D points depends on a correct bubble piercing and several criteria are used to ensure that only bubbles signal with the well define plateau are used. For every interval, the difference in amplitude (D_V) between liquid and gas is computed.

Then, using the levels 10% and 90% of D_V, points C and D are obtained by interpolation between the closest points corresponding to such levels. The TGV software determines the times series of t_A, t_B, t_C and t_D. The latter two are zero if the previous referred criteria are not achieved. Gas residence time (T_G) is given by t_B-t_A while rising time (T_U) is calculated by t_D-t_C. If T_U values are less than the sampling rate they are eliminated. Using T_G and T_U is possible to determined local gas phase and bubble properties according the following equations:

Gas hold-up

$$\alpha_G = \frac{\sum T_G}{t_{acq}} \qquad \textbf{Eq. VII–1}$$

Bubble Velocity:

$$v_B = A \times T_M^B \qquad \textbf{Eq. VII–2}$$

Bubble Chord:

$$ch_B = v_B \times T_G \qquad \textbf{Eq. VII–3}$$

The analysis of all measurements in a T_G-T_U or ch_B-$|V_0|$ plane can be useful to distinguish several bubble populations and get information about the flow regime.

Some errors have been reported for local characteristic measurements using optical probes and are related mainly with the piercing between optical fiber and bubble as exemplified in **Figure VII-4** (Cartellier 1992, 1998; Cartellier and Barrau, 1998). The most usual are effects of: (1) blinding; (2) drifting and (3) crawling. In addition, avoiding errors in T_U and v_B measurement as well as in probe cleanliness is essential to achieve an accurate measurement.

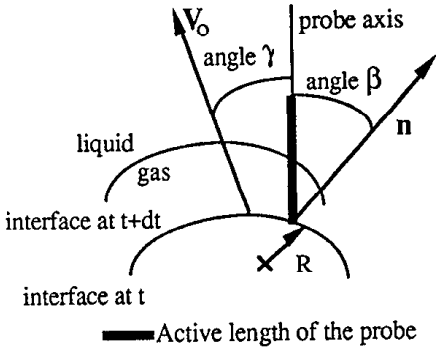

Figure VII-4. Bubble interface/probe interaction parameters. In Cartellier, 1992.

The “blinding” effect occurs when small chords are not detected due to imperfect tip dewetting. The “drifting” effect happens when the bubble trajectory changes leading to a small chord detecting or even to no detection at all. Finally the “crawling” effect is due to bubble deformation and desaceleration of the bubble when is pierced by the tip. Blinding and drifting lead to an underestimation of gas hold-up,

while the crawling leads to an overestimation as the bubble "stays" more time pierced by tip.

Errors related with piercing are very important because rising time (T_U) depend on β (angle between the probe and the normal to interface) and γ (angle between the probe and the bubble velocity vector) (Cartellier and Barrau, 1998). It was shown that for β values inferior to 10° T_U is weakly sensible however when β increases the rising time T_U starts to be impossible to determine ($T_U * v_B \neq cte = L$). Thus, it is difficult to arrange some correlation between all these parameters especially, in real situations, where it is difficult to predict β. In order to have low values of β, and be able to determine velocity from T_U, the probe needs to be almost in perpendicular position compared to the flow direction (Cartellier and Barrau, 1998; Mena et al., 2008).

Vejrazka et al (2010) found that gas hold-up measurement errors are due to the intrusive property of probes. They studied the interaction between an optical probe and a bubble where both optical probe displacement and bubble deformation were found to be the causes for the measurement errors displayed, especially when chords distribution is calculated (Vejrazka et al., 2010). However it is believed that the ability to evaluate gas hold-up is not so roughly affected by these causes.

When optical probes are applied in *g-l-s* systems the solids should not: (1) have such rigidity so that they could break the optical fiber when interaction occurs; (2) contaminate the optical fiber. Optical fiber contamination depends mainly from the solids properties and size. In general solid properties are such that have no influence in optical probe signal, but there are exceptions. For example it was found by Mena et al (2008) that alginate beds, a semi-rigid solid, let some residues after tip-solid interaction and wrong signals in probe voltage were reported as it can be observed in **Figure VII-5** (Mena et al., 2008).

On the other hand small particles may form an agglomerate around the optical fiber avoiding the interaction between tip and bubbles. This

agglomeration of small particles depends on their properties (hydrophobicity; surface charge; etc) leading to the formation of a solids cluster around the tip.

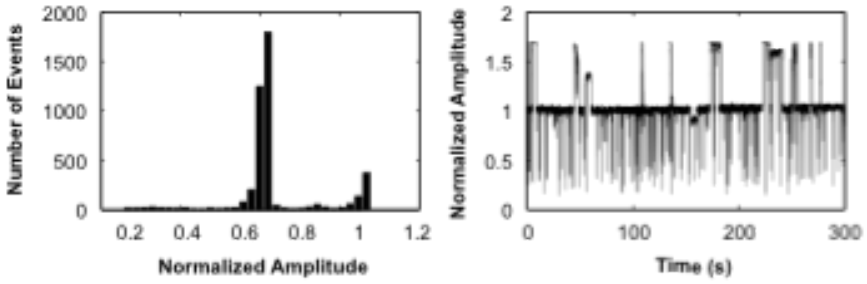

Figure VII-5. Signal amplitude distribution (Left Graph) and time series amplitude (Right Graph) obtained by Mena et al (2008) for *g-l-s* system using alginate beads. Adapted from Mena et al. (2008).

Solid-tip interaction may induce inadequate signals due to contamination of the optical fiber. Mena et al (2008) found that alginate beds contamination induces a significant signal increasing (voltage peak) affecting the signal processing (**Figure VII-5**). Having in mind that all methods developed in signal processing are optimized for two-phase flow, it is necessary to adapt them when three-phase systems are used. Therefore a new problem arises due to tip mechanical sensitivity and their resistance to solid particles impact. In their work other solids (glass and polystyrene) were tested in order to evaluate the effects of solids on measurement accuracy. Among all studied solid only alginate beds induces errors in optical probe response signal. Considering the complex experimental and signal analysis procedures used, the successfull application of this specific probe on three phase systems was achieved (Mena et al., 2008).

The contamination caused by cluster formation around the tip is a very different type of contamination and distinct from the one that occurred in Mena et al (2008) work. The particle agglomeration avoids bubble-tip interaction and it is not possible to accurately measure the local properties of the system.

VII.2.2 Solid-phase properties and distribution

The particles tested on this work were the cellulose-based (SG). The SG are generally hydrophobic and have a negative charge at low pH, which along with their rugosity and non-uniform surface full of cavities and holes allows them to immobilize cells very effectively. The ability of SG, when in the presence of water, to form aggregates especially in the sections of the reactor (conical part, see Section V.4.1) where the liquid velocity is lower (dead zones) can result from their hydrophobic surface. Particles and bubbles size are in the same range so the tip can pierce one or more SG particles that are flowing upwards in the riser. These pierced particles will then interact with the moving particles and agglomeration of SG is observed around the probe tip until no bubble signal is detected.

To overcome this problem it was implemented an injection system (**Figure VII-6**) that acts periodically near the probe tip. The liquid-phase is injected periodically and the turbulence that it promotes cleans the tip of all cluster formed.

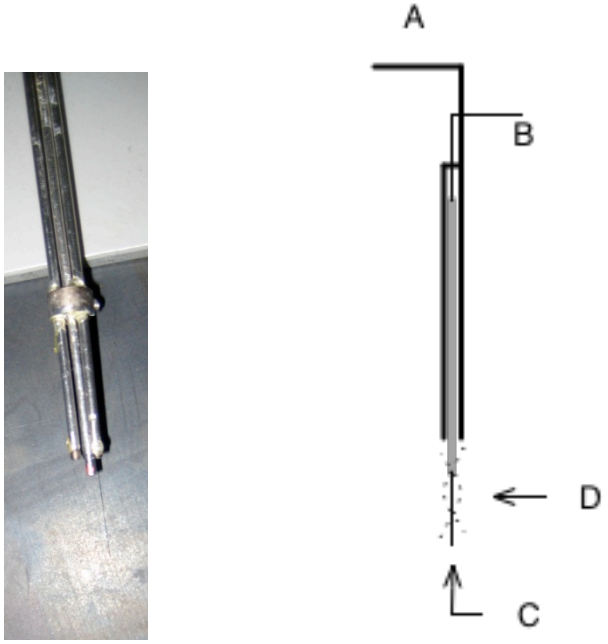

Figure VII-6. Photo of injection tip developed around the optical fiber (left). Diagram of Injection system operating (right). Legend: A liquid injection tubes; B – Optical probe output signal; C – Optical probe tip (optical fiber); D – Liquid injected arount optical fiber (dashed line)

However there are some drawbacks when injection near the probe is applied: because of the induced perturbations, parts of the signal, corresponding to the times when injection is done, must be removed from the optical probe raw signal in order to achieve an accurate signal evaluation. In practical terms, the injection system was not able to be used at more than 6.1 % solids (wt $_{WET\ BASIS}$./vol.).

As verified in Chapter V, in an iGLR not only solid influence on gas hold-up is important but also solid distribution throughout the reactor. Considering the results from previous chapter, it is expected to have similar solids distribution in the iGLR tested. Being so and to easier future evaluation, the solids distribution throughout the iGLR was considered to be almost homogeneous (see section V.4.1.2).

VII.2.3 Liquid-phase

It is also important to take into account the liquid-phase properties in three-phase systems. The solids may induce changes in the liquid-phase properties, which will affect the *g-l* mixture. Usually circulation and mixing times are important parameters to study the mixing, dispersion and tension field properties of the GLRs. Associated to this, liquid velocities in downcomer and riser are normally determined, these velocities being important parameters to use in several models that describe the GL reactor hydrodynamics.

Tracer techniques used in the previous chapter do not allow us to know the local flow characteristics in the downcomer. For this, fine techniques may be used (**Figure VII-1**.) as, for example, LDA – Laser Doppler Anemometry (non invasive); PIV – Particle Image Velocimetry (non-invasive); Heat probes (invasive). In this work, considering the liquid velocity and the influence of SG, PIV was used.

VII.2.3.1 Particle image velocimetry

Particle image velocimetry (PIV) is a technique that has been successfully used to determine velocity fields in single-phase flow at low gas hold-up values. A laser sheet is used to illuminate a defined part of the fluid that contains seeding particles (density similar to the fluid). A HSC is synchronized with the laser beam and two or more pictures are taken in short time intervals (Δt). Then these images are treated (filtered and "cleaned" of noise) and the distance between the two seeding particles is calculated. Knowing the time interval between the pictures, it is then possible to determine the instantaneous velocity field of the liquid. By processing the instantaneous velocity, the average velocity in different zones of the reactor can be obtained. The main problem of using PIV is to identify the seeding particles between the frames. Usually to discriminate well the different phases fluorescent seeding particles are used for the liquid and the filtered signal is analysed (Boyer et al., 2002; Unadkat et al., 2009). PIV technique is a refined technique generally used to obtain instantaneous liquid velocity and fluid properties. In our case, we used it to determine the type of flow in the dowcomer where only liquid and solid-phase were present. In gas-lift reactors the liquid-phase velocity and circulation depends on the gas flow rate according to:

$$v_{Li} = a \times U_{Gr}^{b} \text{ for } i = r \text{ or } d \qquad \textbf{Eq. VII–4}$$

Where a depends on the fluid properties while U_{Gr} is determined by the flow regime and both by the reactor geometry (Onken and Weiland, 1983). Liquid velocity influences circulation and mixing time in this kind of reactors, as showed in a previous chapter, depends on geometry properties as the ratios: A_d/A_r and H_r/H_C, the presence or absence of a top section as well as its configuration (Fonseca et Teixeira, 2007). Klein et al (2003) working with a similar gas-lift reactor found that liquid flow through the reactor (to dilution rates up to 0.6 h-1) has no relevant influence in the main hydrodynamic parameters (section VI.3) (Klein et al., 2003). So, all measurements were done in batch system.

VII.2.4 Hydrodynamic model: local hydrodynamics

For this work a hydrodynamic model was developed based on the hydrodynamic models present in literature (Chisti 1989; Lu et al. 1995; Freitas et al. 1999). This allows having a better understanding of the influence of the solid phase on system hydrodynamics. Some assumptions were made:

- reactor contains four sections: Bottom (b), Riser (r), Downcomer (d) and Top (t).

- a pseudo-homogeneous phase (H) was considered.

- solids distribution is homogeneous which leads to the fact that the properties of the pseudo-homogeneous phase are constant in all parts of the reactor.

- no gas is present in downcomer.

From the "drift-flux" model developed by Zuber et Findlay (1965) the relation between gas linear velocity and superficial velocity of gas and liquid, as well as bubble terminal velocity can be written as:

$$v_G = C \times (U_G + U_L) + U_{bt} \qquad \textbf{Eq. VII–5}$$

Where C is the distribution parameter and indicates the flux pattern. When C=1 it means that the flux distribution is flat. C is related to gas distribution and not velocity profile. In the air-lift reactor riser:

$$v_{Gr} = C \times (U_{Gr} + U_{Lr}) + U_{bt} \qquad \textbf{Eq. VII–6}$$

The relation between liner and superficial velocity with gas hold-up can be defined as:

$$\alpha_{Gr} = \frac{U_{Gr}}{v_{Gr}} \qquad \textbf{Eq. VII–7}$$

Combining **Eq. VII–6** and **Eq. VII–7** one gets:

$$\alpha_{Gr} = \frac{U_{Gr}}{C \times (U_{Gr} + U_{Lr}) + U_{bt}} \qquad \textbf{Eq. VII–8}$$

Eq. VII–8 will be used to obtain, by fitting to experimental data, the parameters: C and U_{bt}. The determination of liquid velocity in riser is done considering that the pressure difference between donwcomer and riser (P_d) is equal to the total friction loss ($-\Delta P_T$)(Lu et al., 1995):

$$P_d = \left[\left(\rho_H \alpha_{Hd} \times \rho_G \alpha_{Gd}\right) - \left(\rho_L \alpha_{Lr} + \rho_G \alpha_{Gr}\right)\right] \times g \times H \qquad \textbf{Eq. VII–9}$$

Knowing that $\rho_H >> \rho_G$ and considering that $\alpha_{Hr}=1-\alpha_{Gr}$ and $\alpha_{Hd}=1$, $\alpha_{Gd}=0$, the P_d equation can be re-written:

$$P_d = \rho_H \times \alpha_{Gr} \times g \times H \qquad \textbf{Eq. VII–10}$$

The total friction loss in each reactor section is given by the equation:

$$-\Delta P_T = \sum \left(-\Delta P_f\right)_i \qquad \textbf{Eq. VII–11}$$

Where $(-\Delta P_f)_i$ is the pressure drop in section "*i*" (i=riser, downcomer, top, bottom) and is determined by:

$$\left(-\Delta P_f\right)_i = 1/2 \times \rho_H \times k_{fi} \times v_{Li}^2 \qquad \textbf{Eq. VII–12}$$

For Riser and Downcomer k_{fi} is determined accordingly:

$$k_{fr} = 4 \times f_r \times H_r / d_r \text{ and } k_{fr} = 4 \times f_d \times H_d / (d_c - d_{r,ext}) \qquad \textbf{Eq. VII–13}$$

Where f_i (for *i*=*r* or *d*) is determined by the Blasius equation:

$$f_i = 0.0791 \mathrm{Re}^{-0.25} \qquad \textbf{Eq. VII–14}$$

And

$$\mathrm{Re}_{Hi} = \frac{\rho_{Hi} \times v_{Li} \times d_i}{\mu_{Hi}} \qquad \textbf{Eq. VII–15}$$

Using correction factor proposed (a) by Garcia-Calvo and Letón (Freitas 2002) and considering ρ_{Hi} and μ_{Hi} constant throughout all reactor, the k_{fi} equation can be re-written:

$$k_{fi} = \frac{4 \times \phi \times 0.0791 \times H_i \times \mu_{Hi}^{0.25}}{\rho_{Hi}^{0.25} \times d_i^{0.25} \times v_{Li}^{0.25}} \qquad \textbf{Eq. VII–16}$$

As ϕ, ρ_{Hi} and μ_{Hi} depend on solid concentration a parameter β was considered (Freitas et al. 1999):

$$\beta = \phi \times 4 \times 0.0791 \times \mu^{0.25} \times \rho^{-0.25} \qquad \textbf{Eq. VII–17}$$

As $k_{ftop} << k_{fbottom}$ only the pressure drop in the bottom will be considered and determined accordingly (Chisti 1989):

$$k_{fbb} = 11.4 \times \left(\frac{A_d}{A_{lb}}\right)^{0.79} \quad 0.2 < \frac{A_d}{A_{lb}} < 1.8 \qquad \textbf{Eq. VII–18}$$

Thus at steady-state considering the relation:

$$P_d = -\Delta P_T \qquad \textbf{Eq. VII–19}$$

Combining **Eq. VII–10**, **Eq. VII–11**, **Eq. VII–12** and **Eq. VII–13** considering:

$$v_{Li} = \frac{U_{Li}}{1 - \alpha_{Gi} - \alpha_{Si}} \qquad \textbf{Eq. VII–20}$$

And

$$A_i \times U_{Li} = A_r \times U_{Lr} \qquad \textbf{Eq. VII–21}$$

The final equation for liquid superficial velocity is

$$2 \times g \times H_{r,d} \times (\alpha_{Gr} - \alpha_{Gd}) = \left(\frac{A_r}{A_d}\right)^2 \times \frac{k_{fbb}}{\left(1 - \alpha_{Gd} - \alpha_{Sd}\right)^2} U_{Lr}^2 + \ldots$$
$$\ldots + \left[\frac{D_r^{-1.25}}{(1 - \alpha_{Gr} - \alpha_{Sr})^{1.75}} + \left(\frac{A_r}{A_d}\right)^{1.75} \times \frac{(D_c - D_r)^{-1.25}}{(1 - \alpha_{Gd} - \alpha_{Sd})^{1.75}}\right] \times H_{r,d} \times \beta \times U_{Lr}^{1.75}$$

Eq. VII–22

These equations are solved according to the following diagram (**Figure VII-7**).

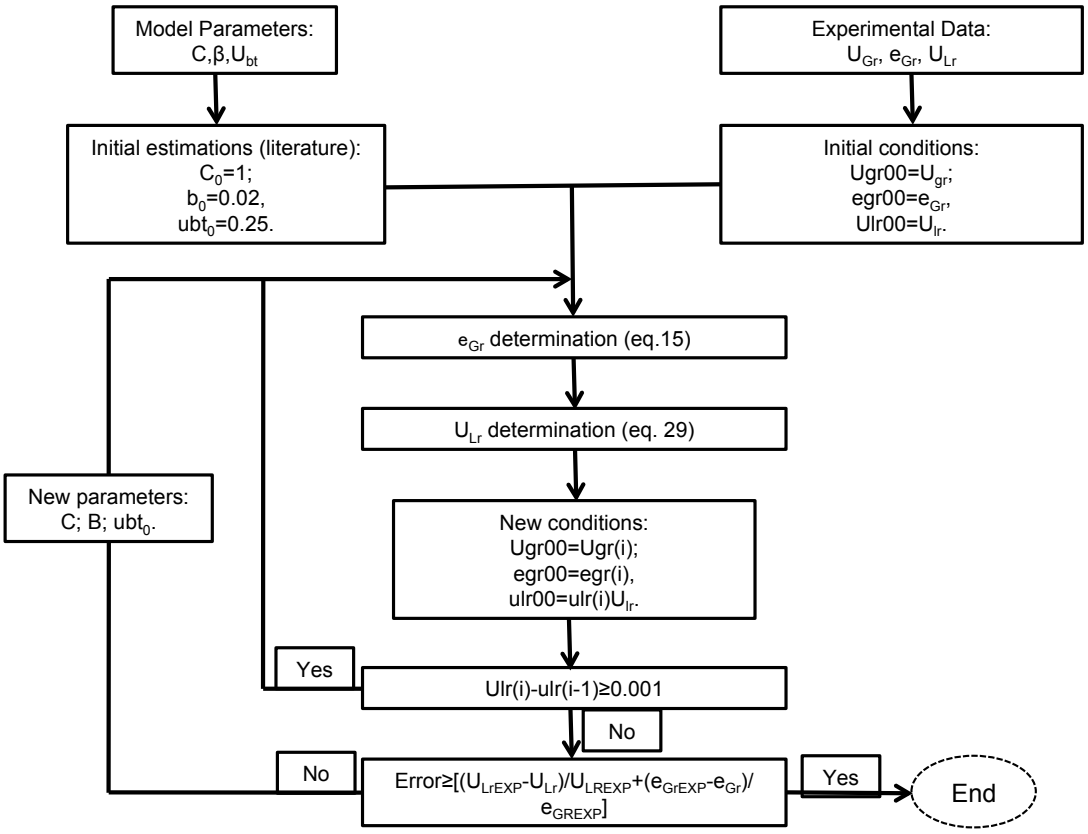

Figure VII-7.Flow diagram for MATLAB program used in this model. Starting from initial model parameters and experimental data, new parameters are calculated in order to achieved values of U_{Gr}, e_{Gr} and U_{Lr} that are similar (±5%) to the experimental data.

VII.3 Material and Methods

VII.3.1 Experimental apparatus for gas hold-up measurements

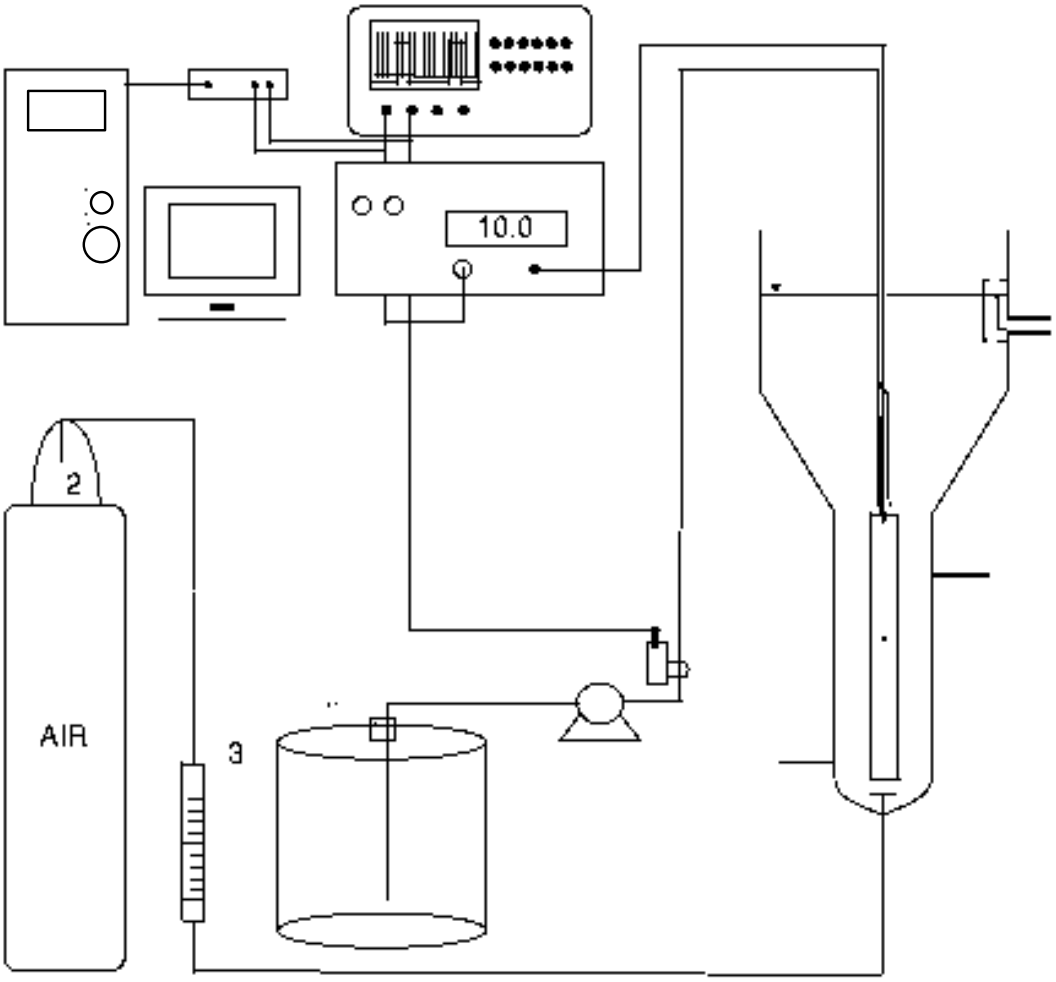

Figure VII-8. Experimental setup for gas hold-up experiments. Legend: 1. Air-Lift Reactor; 2. Optical Probe; 3. Electro valve; 4. Light source+ Photo detector; 5. Oscilloscope; 6. Acquisition Board

The iGLR used in this work is of the concentric draught tube type with an enlarged top section for degassing and a total working volume of 6 L (**Figure VII-8**). The dimensions of the reactor are as follows: total height= 96 cm; downcomer's length= 66 cm and inside diameter= 7 cm; draught tube length= 64 cm, diameter=3 cm, and thickness= 0.5 cm; and cylindrical part's length= 19.5 cm and diameter= 19 cm. The angle

between the conical sector and the main body was 51°. Gas was injected through a distributor (1-cm diameter) with five needles, each of 0.2 mm in diameter, and placed 1.7 cm below the annulus of the riser. The outflow of the reactor was placed behind a sedimentation barrier, thus minimizing carrier losses. The water level in the reactor was always kept constant at the same height. Temperature and pressure were ambient (21 °C and 1 atm). The desired gas flow was adjusted with a rotameter (MR3000 series Flowmeter, Key Inst., Trevose, USA) operating at 1 atm and 21 °C.

The cyclic injection (Injection time(s)/Total cycle time(s)=0.5/2.5) was performed by using one electro-valve (Sirai, Milan, Italy) controlled by PC equipped with LABVIEW (National Instruments, Austin, Texas, USA). The signal acquisition of the electro-valve and optical probe were recorded using an acquisition board NI BNC-2110 (National Instruments, Austin, Texas, USA) and LABVIEW program, which saves the signal in a binary file per assay. Then each file was treated using MATLAB 6.1 (MathWorks, Natick, MA, USA) developed to read the binary files obtained. The same program was used to determinate all characteristic points from optical probe signal (t_A, t_B, t_C and t_D), as well as to calculate all gas phase properties determined from **Eq. VII–1, VII-2** and **VII-3**. The sampling rate was 10kHz and the duration of each assay was 800 s. Each experimental condition was repeated 5 times in order to have enough measured bubbles (at least 1000) that assure statistical evaluation.

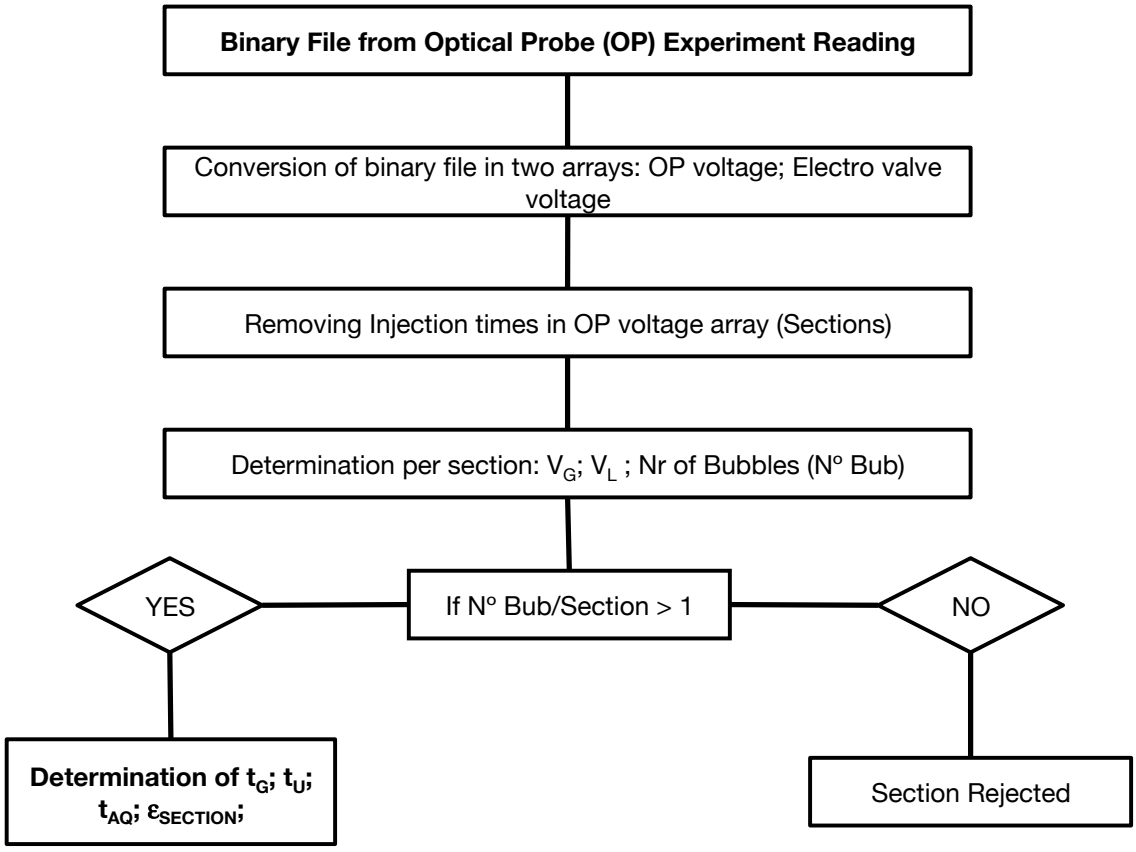

Figure VII-9. MATLAB program layout (see Appendix I).

VII.3.2 New signal processing and validation

In the raw data treatment the influence of the injection is removed and only the data where no injections are performed is analysed to determined gas-phase properties: gas hold-up, bubble chord and velocity. For validation of the new system, tests were performed only in *g-l* system in order to evaluate if the modification (injection system plus new method) made has a real influence in the measurement.

The obtained signal is composed by two curves: one where the signal recorded by the OP is present and other which corresponds to the signal of the injections (**Figure VII-10**).

At each injection there is a perturbation in the probe and in the flow leading to measurement errors due to: (1) probe movement; (2) increased bubble residence time (higher t_G); (3) bubble deflection (detection of a bubble that normally was not detected and vice-versa).

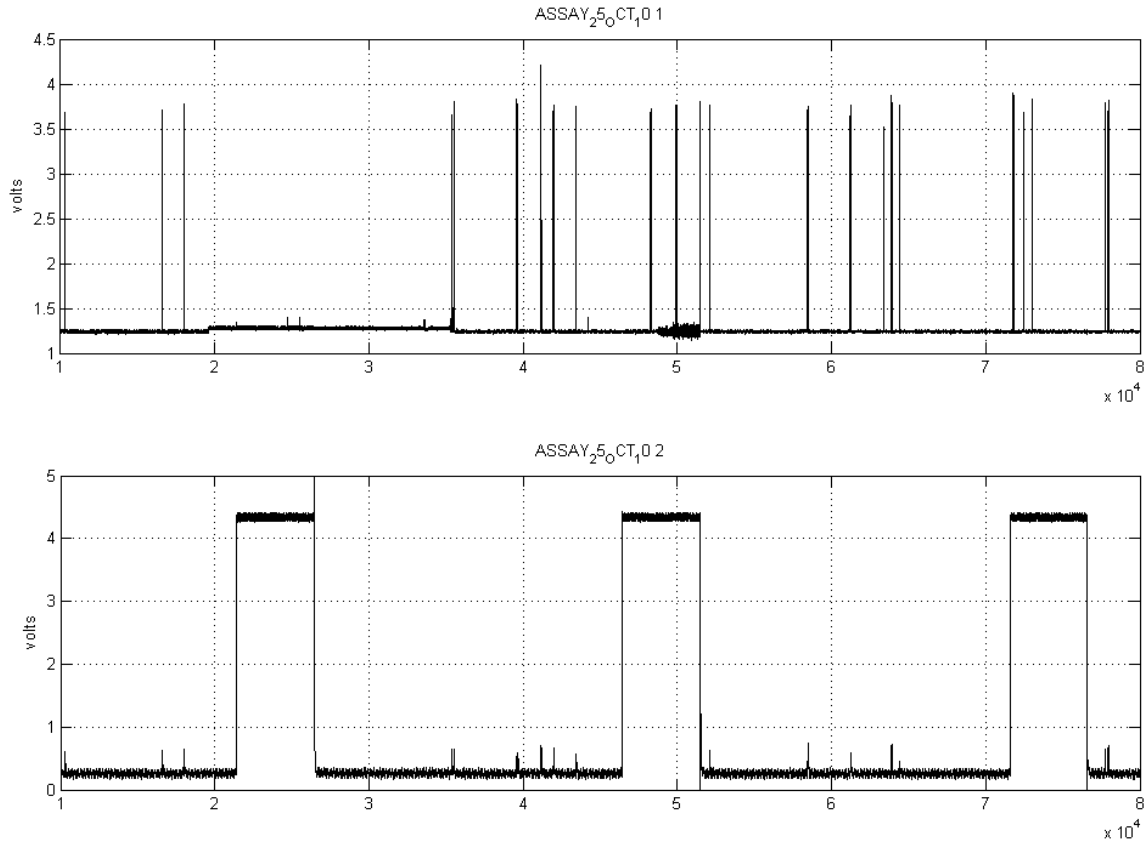

Figure VII-10. Raw signal obtain for riser radial central position at Q_{GAS}=400mL/min. Top graph shows optical probe signal. Bottom Graph shows electovalve signal. (The total time where corresponds to 7 seconds)

In order to avoid these errors the signal is then cut before and after the injection and only the rest of the signal is used for gas hold-up determination. The cut signal is then analysed and the gas hold-up calculated. So the cutting time (percentage of injection time) becomes one of the critical parameters for hold-up determination. Different cutting zones around the injection were performed and gas hold-up determined for each zone. The validation experiments were performed in air-water mixture using the injection system and without the injection system. Then the results were compared between the new system and the obtained using the algorithm developed by Alain Cartellier (1992) – TGV. The results from the new developed system were performed at different cutting percentages before and after the injection time (different cutting zones). The cutting zones (**Figure VII-11**) include not

only the time when the injection was performed but also fractions of time before and after the referred injection. Considering that the injection influence is bigger after it occurs than before, the zones evaluated were: ADD1 - up to 50% less time before the beginning of injection; ADD2 - up to 100% more after the injection time. This means that, per each injection period (2.5 s), the minimum time removed was 0.5 s corresponding only to the injection and the maximum time was 1.25 s corresponding to a cutting of 50% before and 100% after the injection (included) as explained in **Figure VII-11**.

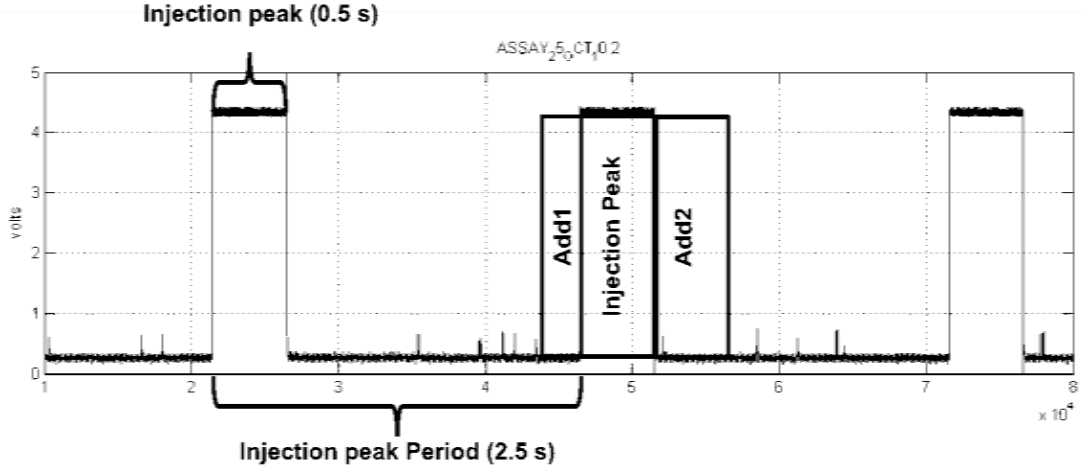

Figure VII-11. Graphical explanation of cutting zones. Legend: Add1 area removed before injection (from 0% to 50% of Injection peak time). Add2 area removed after injection (from 0% to 100% of Injection peak time)

The error between gas hold-up measure using the TGV program and using the new method was calculated using the equation:

$$\%Error = \frac{abs(x_{TGV} - x_{INJ})}{x_{TGV}} \times 100 \qquad \textbf{Eq. VII–23}$$

Where x represents the gas-phase properties: hold-up (α_B); bubble velocity (v_B) or bubble chord length (ch_B).

VII.3.3 Experimental conditions

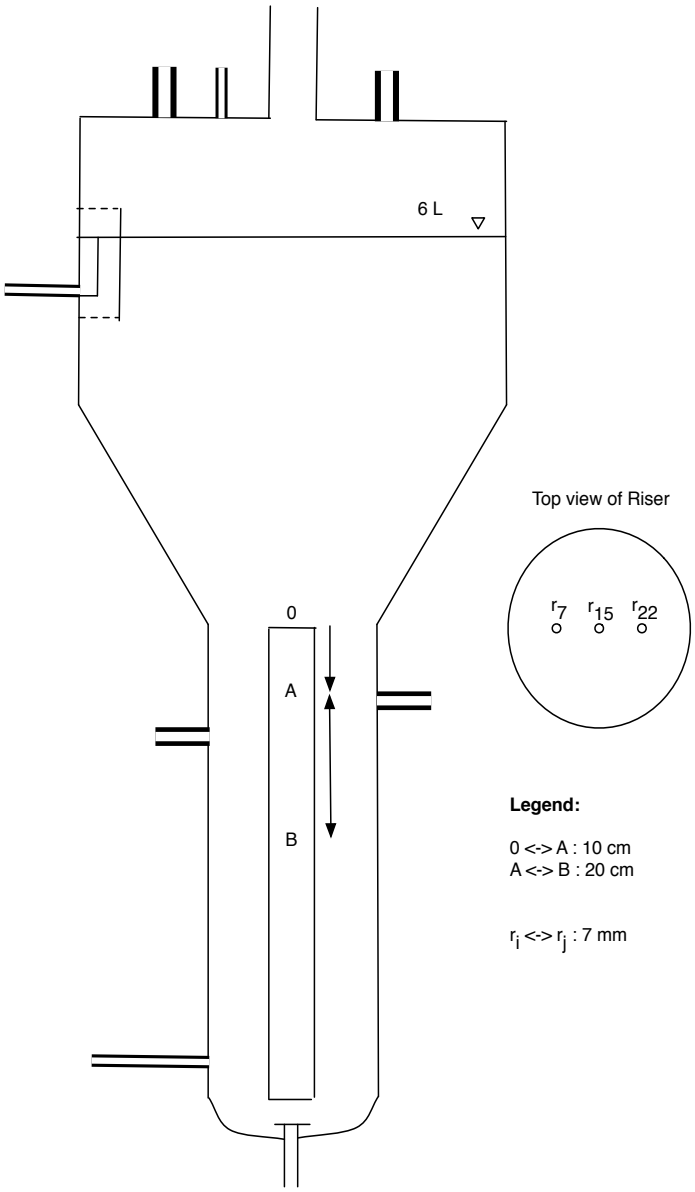

Figure VII-12.Optical probe measurement location in the GL reactor

The optical probe was located at two heights from the top of the riser: h_A=10 cm and h_B=30 cm and measurements were performed varying the radial position. The radial positions were, respectively, r=0, ±7 mm. r=0 corresponds to the column axis. The few positions studied in the radial positions were because of (1) the lower spatial resolution due to injection system used, and (2) the time/storage space that was necessary to obtained enough data for each studied position.

VII.3.4 Solids properties

Spent grains were pre-treated according to the acid/base method proposed by Brányik et al. (2001). Spent grains after pre-treatment are almost flat particles, with equivalent diameter d_{EQ}<2.1 mm and density ρ=1037 $kg_{WET\ BASIS}/m^3$. The size distribution of the particles was determined by sieving into fractions using a portable sieve shaker (Model Analysette, Fritsch, Germany). With the obtained data, the equivalent diameter was calculated. The solids are completely wettable with a water adsorption index (WAI) of 8,12 g_{WET}/g_{DRY} and sedimentation velocity is about (0.83 ± 0.16) cm/s. The following five solid loadings were used 0% (water), 2%, 4%, 6% ($wt._{WET\ BASIS}$/vol.).

VII.3.5 High speed camera measurements and image analysis

To analyse the specific behaviour and influence of the SG in *g-l* mixture a HSC, recording at 1000 frames per second, was used. This allows visual evaluation and confirmation of the information obtained by the optical probe using the new method. However this was only achieved at low solid concentration (up to 2% ($wt._{WET\ BASIS}$/vol.)) because at higher values no information from images was possible to be obtained. HSC videos were recorded using FlowView ™ program and the bubble properties (mean chord and minimum and maximum Feret diameters) analysis was performed manually. Image sizes obtained have a 1280x1024 resolution and the manual measurement error was below 5%. In order to confirm the quality of the manual analysis process, some experiments were also analysed using the statistical tool proposed by Ferreira *et al.* (2011). This tool was successfully applied in the automatic identification of single bubbles and bubble groups with a minimum agreement of 90% (Ferreira et al., 2011).

VII.3.6 Statistical method

The statistical analysis of the gas-phase properties (hold-up, velocity, chord size) was carried out using single-factor analysis of variance (ANOVA), while multiple comparison tests were used to determine the statistical significance with a 95% confidence level. For the data analysis, MATLAB software was used.

VII.3.7 PIV measurements

PIV measurements were made to determine the liquid velocity field in the downcomer. The PIV-LIF system was a LaVision DAVIS with a Twins Ultra Yag 2x30 mJ Laser (wave peak 532 nm). The camera (ProX2M) with a minimum interframe of 110 ns was used to recorde PIV-LIF images. The laser was passed through a lens, which shaped the resulting beam into a light sheet. The delay between two pictures was 120 μs. The field of view was 232 mm×150 mm and included the dowcomer center. Consequently, 150 double image pairs were obtained in each assay, and were considered to be sufficient to obtain statistics results. Each assay was performed in triplicate

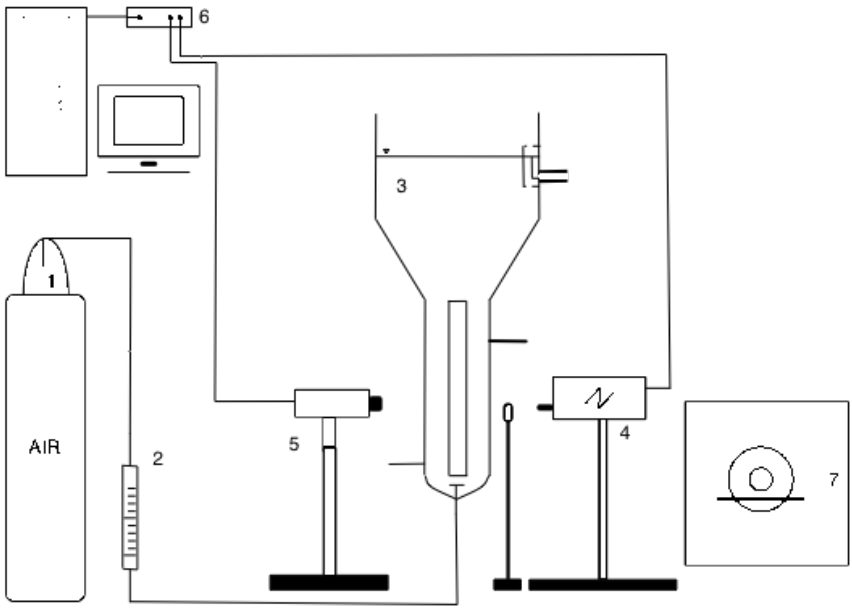

Figure VII-13. Experimental setup for PIV measurements. Legend: 1. Air Source; 2. Rotameter; 3. Air-Lift Reactor; 4. Laser + Laser sheet maker; 5.

Recording camera; 6. Acquisition and Synchronized System; 7. Laser sheet measurement viewed from above

VII.3.8 Microorganism and medium

The microorganism used during the experimental work was a brewing yeast strain (*Saccharomyces cerevisiae*) supplied by the company UNICER (Bebidas de Portugal, S.A., S. Mamede de Infesta).

The yeast was cultivated in a synthetic model medium (SMM) with same composition as presented in Chapter VIII.2. Barrels with 50 L of SMM were sterilized by autoclaving at 120 ºC, 100 kPa for 60 min.

VII.3.9 Free biomass determination

A sample of 10 mL was removed from the reactor outflow and it was centrifuged (Hettich, Universal 320R) for 5 min at 5000 rpm and 4 ºC. The supernatant was removed and the sediment was diluted (1:5 ratio) with isotonic solution (0.9% (wt./vol.) NaCl). The optical density of the solution was measured with a spectrophotometer (WPA - Biowave II) at 600 nm wavelength. Each sample determination was done in triplicate. The results of biomass concentration were calculated using a calibration curve that related $g_{BIOMASS}$/L vs. O.D. (600nm).

VII.3.10 Immobilized biomass determination

A sample containing approximately 1 g of dry biocatalyst (carrier + immobilized cells) was taken from the reactor. The bulk liquid was removed with a syringe and the carrier was washed with distilled water in order to remove the free cells captured between the carrier particles and dried at 80 °C. Then the dry sample was weighed and divided in three Erlenmeyer flasks (previous weighted) with 50 mL of 3% (w/v) NaOH solution and was shaken at 150 rpm for 24 h. During this time the immobilized cells were completely removed from the carrier. The released cells were washed with distillate water and dried at 80 ºC. The

amount of immobilized yeast biomass was determined from the weight difference before and after the treatment with NaOH solution. Corrections of the biomass weight were carried out admitting 6% of losses.

VII.3.11 Cell viability – flow cytometry

The flow cytometry measurements were taken using a Accuri C6 flow cytometer (Accuri, Michigan, USA). The FCM analyzer contains a solid state 488 nm (FL1-H) and a 640 nm (FL2-H) diode laser and is also equipped with an auto sampler unit. The cell viability was determined by staining yeast cells with Propidium iodide (PI). For that, 1 mL of yeast cells suspension was mixed with 10 μL of PI in a dark room for 10 min. Then 10 μL of yeast suspension was analysed by flow cytometry. Cell suspension was diluted in order to achieve a concentration that corresponds to a minimum of 150 events (or cells)/μL detected in FL1-H channel. The dead cells stained in red by PI were detected in FL2-H channel and considered non viable. A calibration curve that related number of Total cells/mL vs. O.D. (600 nm) was determined.

VII.4 Results and Discussion

VII.4.1 Calibration of new system

Before measuring the gas phase properties in *g-l-s* systems it was necessary to know the range of cutting zones where the new method is valid, i e., where the error between the new and TGV methods is lower. An initial observation indicated that the new system generally over estimates the gas-phase properties for 250 mL/min, while for 400 mL/min the results are underestimated. The relative error between the two methods is presented in **Figure VII-14**. It is shown that either Bubble Velocity or Chord Size are not very affected by the different cutting zones. However, the same does not happen for gas hold-up. It is important to have in account that among the gas-phase characteristics determined using the OP, only the gas hold-up is dependent on the acquisition time (**Eq. VII–1**). So it is understandable why different cutting zones ratios affect the final acquisition time, and therefore influence the gas hold-up. Thus the best (less error) cutting zones obtained were: for 250 mL/min – Add1<37.5% and Add2<37.5%, and for 400 mL/min – 25%<Add1<50% and 50%<Add2<100%. Inside these values the error for 250 mL/min was always below 10% and for 400 mL/min below 5%. The error for bubble velocity was 10% and 20% for 250 mL/min and 400 mL/min repectively, while for bubble chord was 15% and 20%. The biggest error in bubble properties (velocity and chord) is mainly related with low frequency acquisition used – 10 kHz, when compared with the used in the TGV method – 50 kHz (Cartellier, 1998). The low frequency of signal used was necessary to avoid huge binary files that were not possible to be treated by available methods.

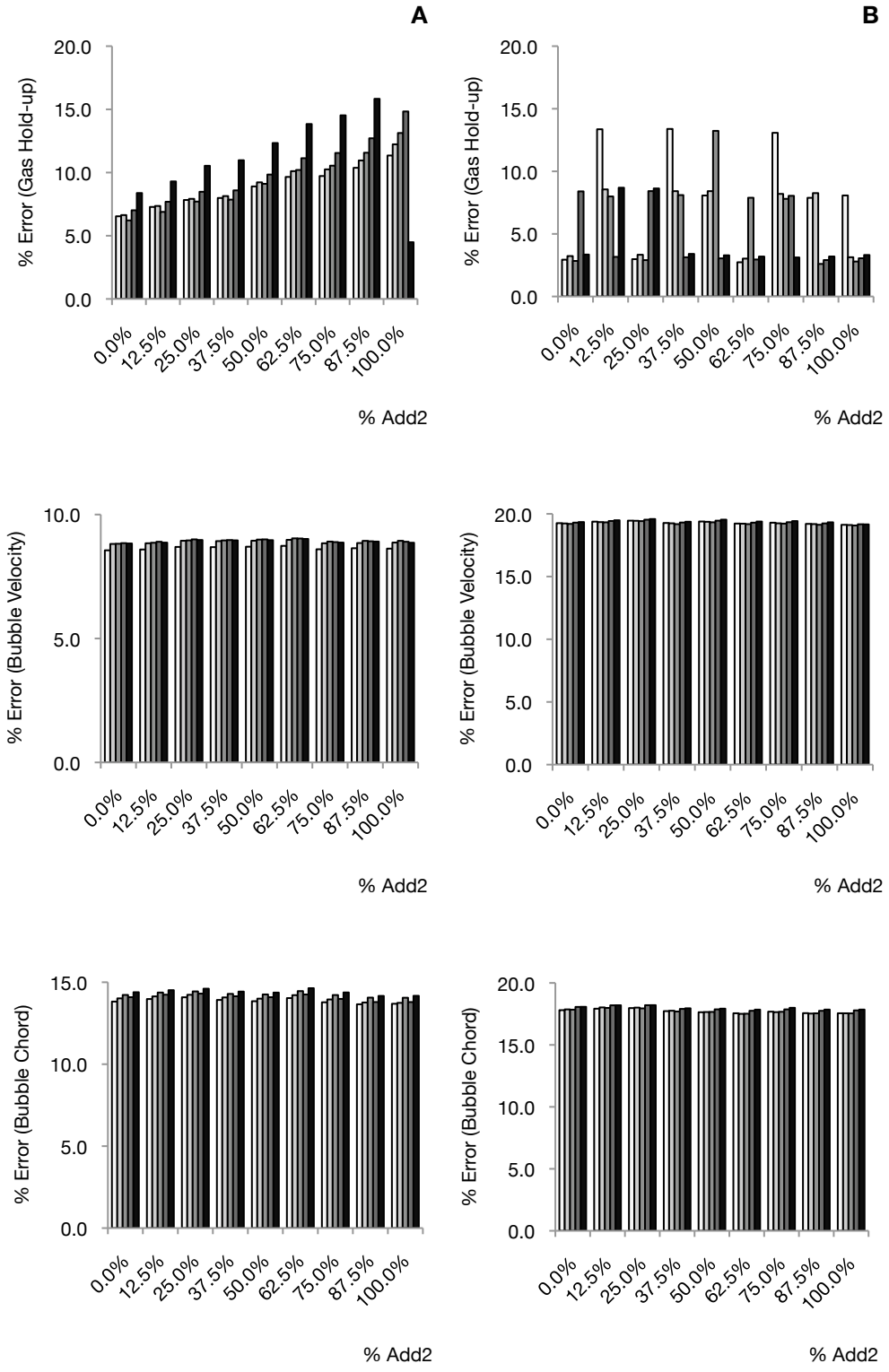

Figure VII-14. Error obtained at different Add1 and Add 2 for different gas-phase characteristics: Gas hold-up, Bubble Velocity and Bubble Chord. Legend: A – Q_{AIR}= 250 mL/min; B – Q_{AIR}= 400 mL/min; □ - 0.0% Add1; ■ - 12.5% Add1; ■ - 25.0% Add1; ■ - 12.5% Add1; ■- 50.0% Add1

VII.4.2 Gas-phase measurements

The main results obtained to determine the gas-phase properties in the riser were done using an optical probe. However and due to the implementation of the new method to use this probe for this system some bubble characteristics were also determined using a HSC in order to evaluate and validate the results. The maximum solid content that the new system was able to work was 6% SG ($wt._{WET\ BASIS}$/vol.). Above this value, the cleaning system was not able to do an efficient tip cleaning.

To check the significant differences between all measurements, the results were statistically evaluated. As indicated in section VII.3.3, data from two different axial positions in the riser (A and B in **Figure VII-12**) were analysed. For each solids concentration, two different gas flows were tested: 250 and 400 mL/min. Branyik et al (2005) found that 250 mL/min was a good compromise between mixing time, biocatalyst sedimentation, and the maximum immobilization for yeast cells (around 0.6 $g_{BIOMASS}/g_{CARRIER}$). As at lowers gas flows SG sedimentation was observed, the gas flow of 400 mL/min was also tested in order to study gas flow effect. Between the two axial studied points (A and B in **Figure VII-12**), no statistic difference was found. Being so and considering that the experiments using the HSC were made at the axial position in the middle of the riser (B in **Figure VII-12**) only the values obtained using the optical probe at this position are presented in the results.

Radial gas-phase properties was also analysed for each condition (axial positions, different gas flows and solid loads) as indicated in **Figure VII-12**. However it was verified that no significant differences in the results were detected between the radial positions studied. Then, for the gas-phase a flat regime in radial position can be considered. In addition, this was valid not only in gas hold-up measurements, but also for bubble velocity and bubble chord.

From **Figure VII-15**, it is possible to verify that gas hold-up decreases when solids are present. By the statistical analysis and for

the lowest gas flow tested (250 mL/min), the gas hold-up decrease is only significant for solids load above 4% (wt.$_{WET\ BASIS}$/vol.). On the other hand, for the highest gas flow (400 mL/min) the gas hold-up decrease when solids are added. However no significant difference on gas hold-up decreases was noted among the different solids concentrations. SG are known to generally decrease the gas hold-up at high gas velocities in BC mainly due to occurrence of coalescence (Chapter IV). Coalescence increases bubble size and velocity. In our case the chord size and velocity increased with solid load. Chord size increase is not directly related with bubble size as bubble properties (shape, shericity) can also change. From statistical analysis, it is clear that bubble chord increased, which is an indication for bubble coalescence to occur. Similar results were found when an identical optical fiber was used and tested with alginate beads (Mena et al., 2008). To access the real bubble size distribution, it is necessary to assume a specific flow structure (Mena et al., 2008). Moreover, to transform chord in actual diameter is not an easy task even at a narrow bubble chord distribution for almost spherical bubbles in homogeneous regime.

In addition the gas hold-up results at 400 mL/min (0.94 cm/s) presented in **Figure VII-15** for *g-l* and *g-l-s* systems (4% (wt.$_{WET\ BASIS}$/vol.)) and the results obtained for the lowest gas superficial velocity (1 cm/s) in Chapter V are similar (range of gas hold-up between 1% (vol./vol.) and to 2% (vol./vol.)). These results show accordance between global and local hydrodynamic methods used in this thesis. Even at different reactor scales 60 L and 6 L in Chapter V and VII respectively this similarity between the results is in accordance with the scale results obtained by Bla and co-workers (2004). They worked with three iGLR (10 L, 32 L and 200 L) and their results indicated that for gas superficial velocities below 0.15 m/s the gas hold up in riser of iGLR is not influenced by the increase of reactor scale (Bla et al., 2004).

To get a better understanding of the underlying physical mechanisms involved in the chord size and velocity increase, data were obtained using the HSC.

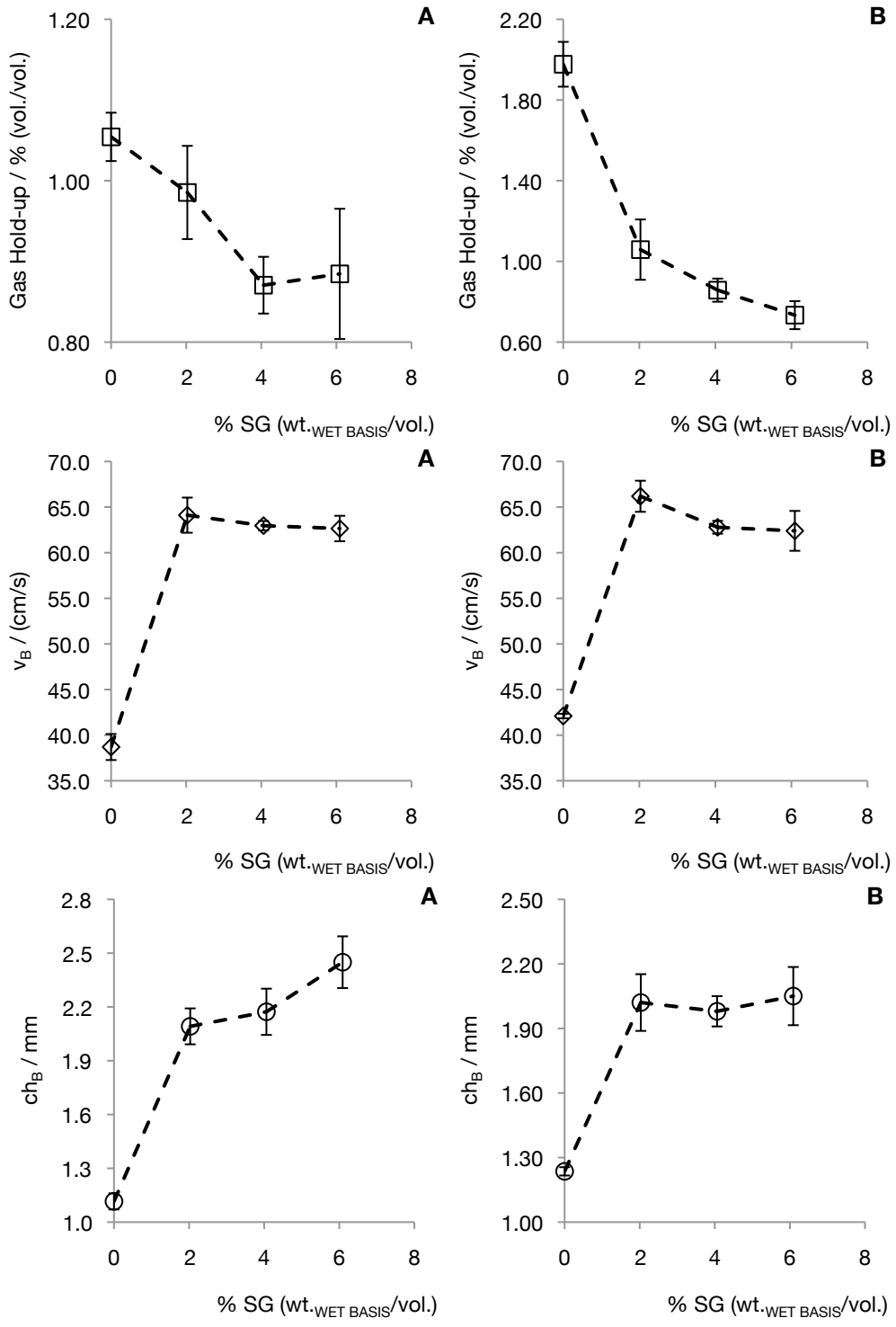

Figure VII-15. Solids influence in local gas-phase properties. Legend: A – Q_{AIR}= 250 ml/min; B – Q_{AIR}= 400 ml/min; □ - Gas Hold-up (% (vol./vol.)); ◇ - Bubble Velocity (cm/s); ○ - Bubble Chord (mm).

Visualization techniques are very useful in *g-l* and *g-l-s* systems (Boyer et al. 2002; Mena et al., 2005; Maceiras et al., 2010; Ferreira et al., 2011). The obtained information may be either qualitative or quantitative. Despite the commercial methods developed to perform automatic image analysis there is still the need for the operator to do a semi-manual bubble characterization. This is more relevant when image analysis is applied to determine bubble properties in *g-l-s* systems. When solids are present, it is possible to use automatic methods if the solids grey level is different from bubbles' grey level (Mena et al., 2005b). Otherwise these methods can loose accuracy due to solids presence. In our case the solids used limited the images obtained by HSC because the grey level of SG is similar to bubbles grey level. That made more difficult to distinguish between bubble and particle (see **Figure VII-16**). Even the manual determination of bubble properties above 2% (vol./vol.) was not possible below the reported error. The statistical tool proposed by Ferreira et al. (2011) was used, but only to analyse the *g-l* systems and *g-l-s* system images at lowest gas flow and solid content (0.8% (vol./vol.)). Being so, the results were obtained manually and then compared with the possible results obtained by the statistics tool method.

The main aim of using HSC in this work was to obtain more data that confirms and validates the results obtained from optical probe measurements. To do this, HSC images and videos were used to determined bubble velocity and bubble chord (manually). Bubble velocity was determined by manually tracking bubbles between 20 frames that correspond to a time interval of 20 milli-seconds. Bubble Chord was determined by considering a virtual optical probe piercing a bubble in a perpendicular position (see image below).

In **Table VII-1** are presented the differences between HSC results and Optical Probe for the lowest gas flow at 0 and 2% (vol./vol.) solid load.

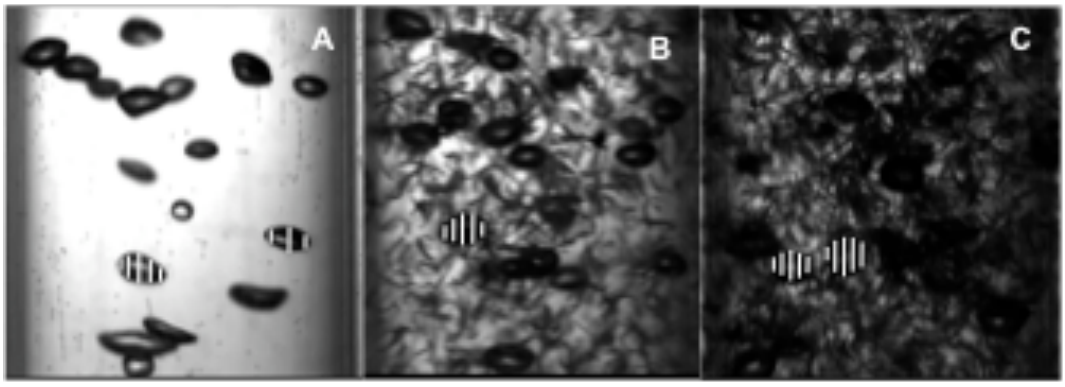

Figure VII-16. HSC Images from GL reactor's riser. White lines are the simulated theoriacally piercing of a bubble and each length was used to determined chord. Legend. A – Air-Water; B – Air-Water-SG (0.8% (wt.$_{WET\ BASIS}$/vol.)); B – Air-Water-SG (2% (wt.$_{WET\ BASIS}$ /vol.));

In **Table VII-1** it is possible to observe that the results obtained with the optical probe are in accordance with the ones obtained by the HSC. Generally, for velocity values the HSC results are higher, while for bubble chord these only occur in *g-l* (air-water). When SG particles are present the analysis of the images is more difficult (**Figure VII-16**), even using the manual methods and maintaining the same criteria. For these cases, the solids "noise" in the image affects the identification and determination of bubble boundary, i. e., the interface between gas and liquid phases. (**Figure VII-16**). This may explain the lowest bubble chord obtained by HSC results.

Table VII-1.Results evaluation by OP and HSC for Q_{AIR}=250 mL/min.

Gas-phase properties	Air-Water		Air-Water-2 % SG (wt.$_{WET\ BASIS}$/vol.)	
	HSC	OP	HSC	OP
Bubble Velocity (cm/s)	48.4±5.7	44.3±7.5	66.9±5.9	64.8±5.0
Bubble Chord (mm)	1.7±0.5	1.3±0.3	2.0±0.3	2.1±0.4

For the velocity determination using the HSC, the bubble reference point used was the bubble central point, which is easier (less error) to access even when solids are present.

The mean Sauter diameter and bubbles sphericity were determined for all tested conditions using the HSC (see Material and Methods). This

was then compared with the results obtained by the statistics tool method proposed by Ferreira et. al (2011). In **Table VII-2** the results show that the error between Manual Image Analysis (MIA) and Automatic Statistics Tool (AST) analysis is no more than 6% and 7% for D_{32} and Sphericity respectively.

Table VII-2. D_{32} (mm) and Sphericity determined by Manual Image Analysis (MIA) and using the Automatic Statistics Tool (AST). Both were obtained from the same images by the HSC.

% Solids	Q_{AIR} (mL/min)	D_{32} (mm) MIA	D_{32} (mm) AST	Sphericity MIA	Sphericity AST
0	250	3.82	3.86	0.599	0.564
	400	3.96	3.90	0.598	0.586
0.1	250	3.62	3.43	0.588	0.563
	400	3.86	NP	0.576	NP
0.25	250	3.80	NP	0.625	NP
	400	3.72	NP	0.620	NP

Legend: NP – Not possible to evaluate by the program due to bad image quality.

In **Table VII-2** it is possible to verify that for 250 mL/min the value of D_{32} (for bubble) is lower when solids are present with a minimum at 0.8% (vol./vol.), while at 400 mL/min the values decreased with solid content. However in terms of bubble sphericity there is a small decrease for 0.8% (vol./vol.) solids and for 2% (vol./vol.) an increase is noted. At this solid content the sphericity is even higher than the one observed in air-water system. This result is in accordance with the previous where an increase in chord size occurs in the presence of solids. If bubbles are considered as a flattened obletenoid, the sphericity is determined by the ratio between the minor and major axes (Mena et al., 2008). Therefore the increase in sphericity can be due to: increase of minor axe (which correspond to the chord measured with the optical probe) or the decrease of major axis. In fact the results from HSC showed an increase in minor axis accomplished by a decrease of major axis. Generally, bubble sphericity increases with gas flow and for high solids load (Mena et al., 2008). Increasing solid content or gas blows promotes bubble-bubble interaction and coalescence, which leads to bigger and rounded bubbles. In our case, sphericity increased at low solid content, which is consistent with the previous results

obtained. The obtained results suggested that our particles promote coalescence. Bubble coalescence occurs in three steps: (1) initial film formation, (2) film thinning and finally, (3) film rupture. Zon et al (2002) showed that the increase of hydrophobic particles concentration leads to a bubble population swift from small to bigger. Hydrophobic particles act in *g-l* interface reducing the energy barrier to film rupture and consequently coalescence is promoted (Zon et al., 2002). On the other hand completely wettable particles were found to increase gas hold-up (Zon et al., 2002). SG are completely wettable particles, however their surface is mainly hydrophobic (Jamialahmadi and Muller-Steinhagen, 1991). Being so, and considering the observed gas hold-up decrease, it means that hydrophobic properties of SG have more influence in bubble properties than their wettability. Thus coalescence can occur in *g-l-s* where SG are present.

For all experiments (gas flows and solids loads) by analysing **Figure VII-15** and **Figure VII-16** as well as **Table VII-1** and **Table VII-2**, it is possible to conclude that optical probes results are consistent and feasible. Nevertheless, it was necessary to certify the results, ensuring that our data obtained by the optical probe were indeed accurate. To do this, the theoretical gas flow across the riser cross-section was calculated from the bubble velocity results. In the next figure (**Figure VII-17**) it is shown that the gas flow was underestimated at 400 mL/min while for 250 mL/min it is shown the results are around the theoretical value.

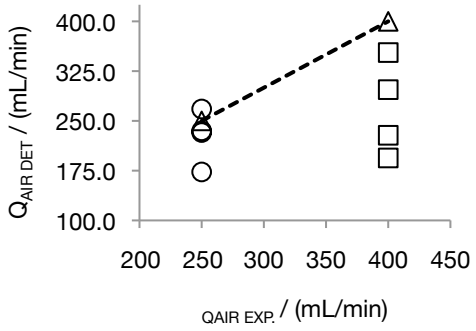

Figure VII-17. Expected gas flow (◇) vs. Experimental gas flow (○and□).

As referred before the optical probe underestimation is related with blinding and drifting effects. In the case of our iGLR it was possible to observe during the HSC measurements that some bubbles were not raising vertically and this was more frequent when solids were present. This behaviour from bubbles is defined by the liquid properties, as well as by the reactor configuration. In this particular iGLR there is a degassing top part where there is a sedimentation barrier that reduces carrier losses during a continuous fermentation. As the top part is not exactly symmetrical the liquid that goes down the downcomer is not uniformly distributed through all the cross section. It means that the liquid flow is not exactly the same in some parts of the bottom-riser connection whereas the amount of liquid that goes into the riser is higher in some zones promoting bubble spin and drifting. This has an effect in the optical probe accuracy to measure the rising time (T_U). Moreover the acquisition rate (10 kHz) used was five times inferior to the normally one used by commercial program where the TGV method (Cartellier, 1992) is applied for two-phase flow. In addition, calibration studies already indicated that at 400 mL/min the errors obtained to measure bubble velocity in two-phase flow are underestimated by 20% when comparing the new with the former TGV method. At 250 mL/min gas flow, the new system over estimated bubble velocity by 10% (Cartellier, 1992). This 10% diference is inside the optical probe error for two-phase flows (Cartellier, 1992). It is then possible to conclude that the system used was successfully applied at the lower gas flow rate used and the results can be evaluated with accuracy. The method/technique applied was hand-made; especially the injection system, and all this system can be largely improved. This improvement will allow for example a stronger injection flux and consequently a more accurate measure at higher gas flows.

VII.4.2.1 Cell influence in gas properties of two-phase flow

The driving force of this work was to understand not only the influence of SG in GL reactors hydrodynamics but also how it is

affected by a fermentation using yeast cells: *S. cerevisiae*. Being so, it was necessary to evaluate how the yeast by itself influences gas-phase properties. Studies where increasing amounts of a concentrated cell solution (0.105 g/mL) were added to air-water system were performed, results from optical probe and HSC were taken and evaluated. In **Figure VII-18** are presented the influence of cell concentration in gas-phase properties. **Figure VII-18** shows that little cell concentration has a lot of influence in the gas-phase properties. Generally it is observed an increase of gas hold-up, bubble velocity and chord size. This indicates that a minimum volume of cells was able to induce changes in the gas-phase. However, bubbles properties did not change significantly above the lower cell concentration, i. e., gas hold-up, bubble velocity/chord difference at high cell concentration is similar to the values obtained at low cell concentration.

In **Figure VII-18** it is possible to observe that an increase of gas hold-up is accomplished by an increase of bubble chord and velocity. These results are odd because if gas hold-up increases the bubble velocity was expected to decrease as well as bubble chord. Smaller bubbles rise slower thus residence time is higher, which increases the gas hold-up. One possible explanation for this phenomenon is the cell influence on the optical fiber measurement mechanism. This influence can be: (1) generic influence in all parameters (gas hold-up; bubble velocity and chord); (2) specific effect by affecting only the measurement of bubble velocity and bubble chord. In the first case, the overestimation was due to crawling effect caused by the presence of cells. Cells may act on the liquid properties influencing also the reflective index of the liquid and consequently T_G and T_M measurements are affected leading to wrong values. The second explanation takes into account the fact that T_U measurement is more sensible to errors than T_G. This is justified considering the tendency to underestimate bubble velocity for this probe (see **Figure VII-16**). In this case, cells will act on liquid-gas interface leading to wrong T_M measurements. According to Brányik et al. (2004), yeast cells hydrophobicity increases by 30% in continuous systems when the biofilm starts to be developed (Brányik,

et al. 2004). Moreover, it is known that in BC reactors, hydrophobic particles promote coalescence (Zon et al. 2002).

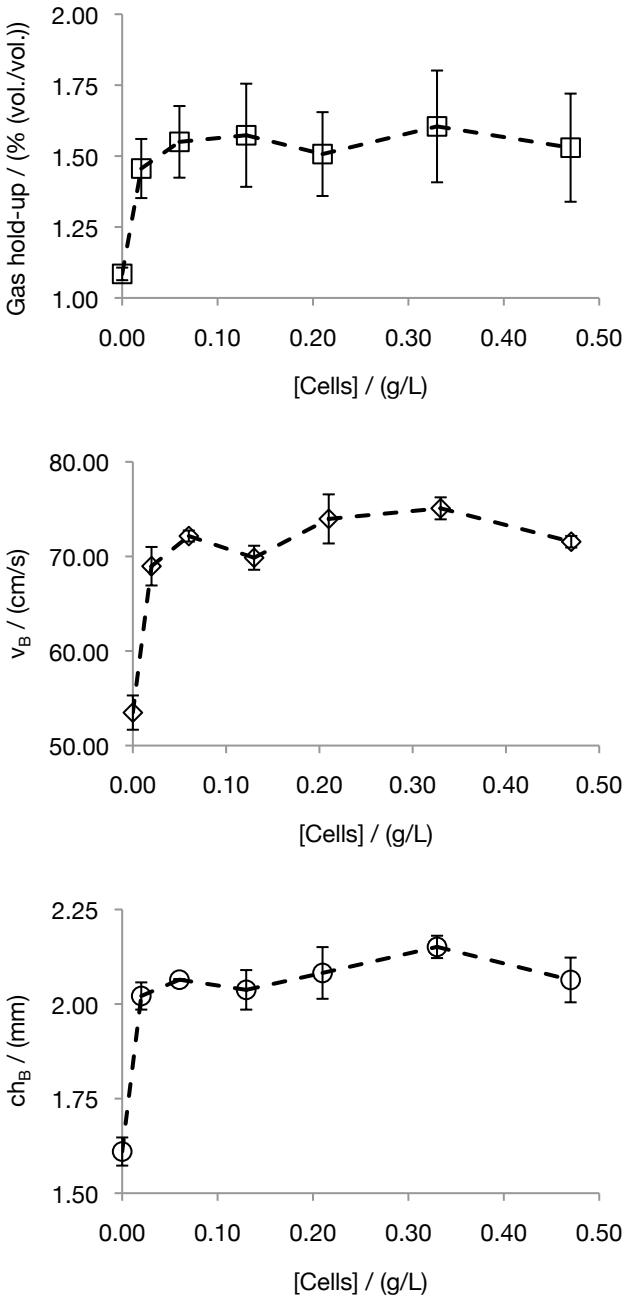

Figure VII-18. Cell concentration influence in gas-phase properties (voidage, bubble velocity and chord) on water-air system at 250 mL/min.

According to **Figure VII-18**, coalescence does not occur in our system because no gas hold-up decrease is observed. Considering this, it is more likely that cells induce some error on the bubble-tip

interaction and the signal over estimation in their presence is an important aspect to consider when optical probe is used to determine gas-phase characteristics in fermentations broth. Being so the increase of gas hold-up, bubble velocity and bubble chord when in the presence of these yeast cells was found to be: 42.74±3.31%, 36.74±4.42% and 30.26±3.57% respectively. Further studies are needed to have a better of this type of phenomena and how biomass can really affect bubble properties (shape, velocity, frequency). Further studies using HSC were made when cells were present. As when SG where used, only a small concentration of cells were tested, because the increase of cells leads to an increase of the turbidity when they are added to *g-l* systems.

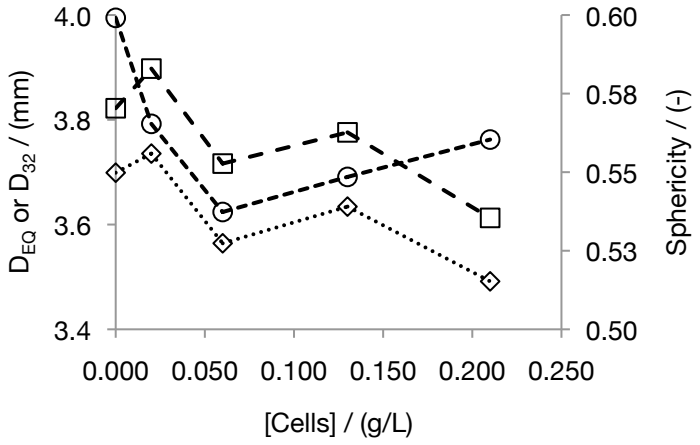

Figure VII-19. The evolution of Sauter (D_{32}), equivalent (D_{EQ}) diameter and sphericity with the yeast cells concentrations. Values obtained from the HSC images. Legend: □ - D_{EQ} (mm); ◇ - D_{32} (mm); ○ - Sphericity (-).

This turbidity was measured in terms of cell absorption and the relation between absorption and cell concentration was plotted. **Figure VII-19** shows that a small amount of cells does not have significant influence either on sphericity, equivalent or Sauter diameter. Even though a small decrease is detected, the results indicated that used yeast cells did not have a real influence on gas-phase properties. Therefore the variation obtained by the optical probe is more likely to be due to yeast cell influence in optical probe measurement mechanism.

VII.4.3 Liquid-phase measurements

The PIV technique used allows us not only to determine the average liquid velocity in the downcomer for different solid load, but also to obtain the liquid velocity profile.

In **Figure VII-20A/B** it is possible to observe that the liquid velocity profile in the downcomer is higher at central position between riser and downcomer than near the column wall (r=1.5 cm). These results were only obtained in the outer part of the downcomer, but the profile in the inner part should have similar behaviour. If we consider the dimensions of the gas-lift reactor, in two-phase flow (air-water) the theoretical flow regime is transient (Re<2300) for liquid velocities in downcomer below 8 cm/s. Adding solids, according to the equations proposed by Lu et al. (1995) for pseudo-homogeneous phase, the apparent viscosity and density will increase. For these two properties the apparent viscosity increase is higher than the apparent density increase. According to Reynolds (Re) equation (**Eq. VII-15**), if the former phenomenon occurs then the Re number will decrease and theoretically the solids added will help to stabilize the laminar flow of the pseudo-homogeneous phase in the downcomer section. Considering the laminar regime stabilizaton by SG, it is feasible to admit a transient profile of the pseudo-homogeneous phase in the downcomer. In **Figure VII-20C/D** it is shown that for both gas flows the influence of SG in the average liquid velocity in the downcomer is negligible at 400 mL/min. Nevertheless at 250 mL/min, a small decrease in liquid velocity is present. The values presented in **Figure VII-20C/D** are obtained by averaging the two central radial points (**Figure VII-20A/B**). The results in **Figure VII-20C/D** are a mere indication that solids increase stabilized the flow in downcomer, which means that the turbulence decreases. In a limit situation, if solids amount is significantly increased, no circulation would be observed because the gas flow would not be enough to fluidize all solids. This is in accordance with results obtained by other authors (Freitas, 2002).

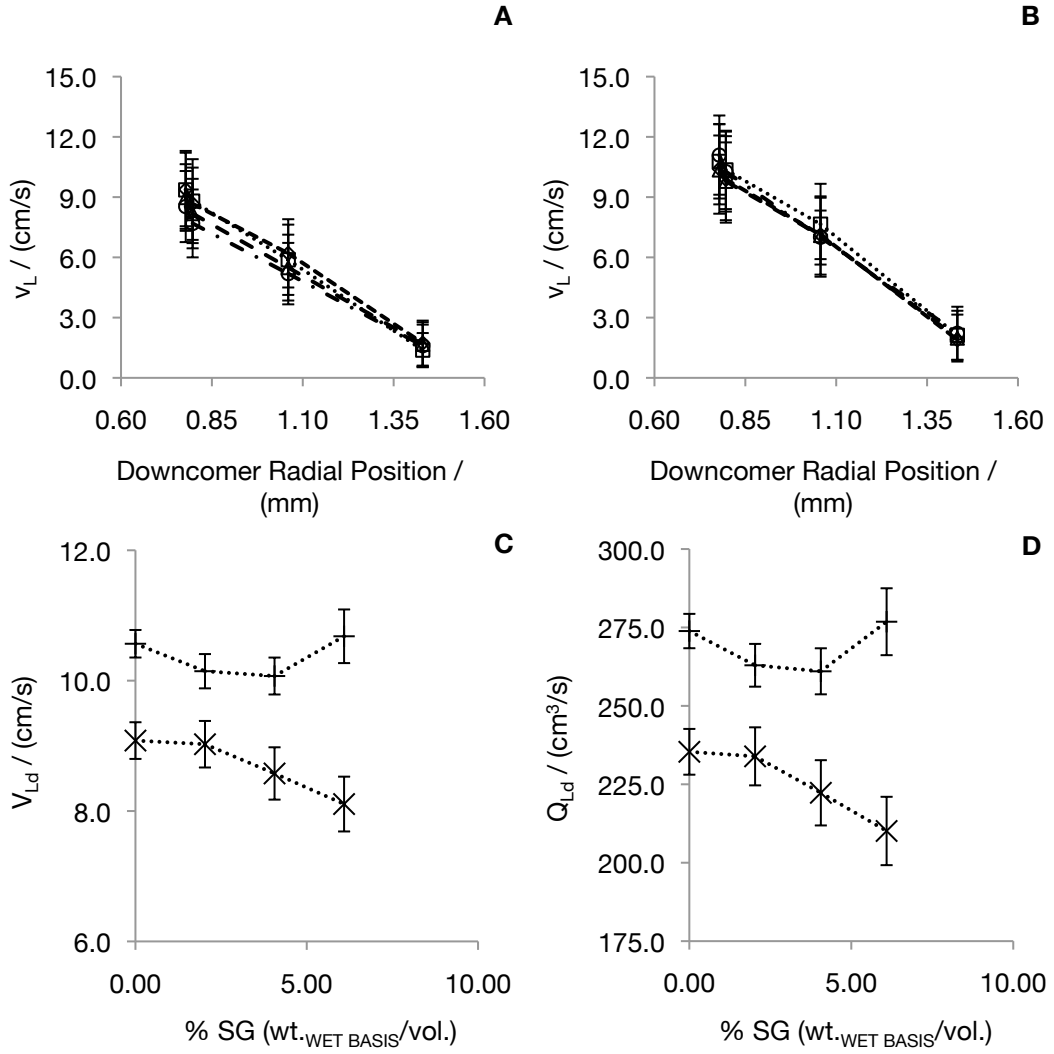

Figure VII-20. Study of liquid velocity in the downcomer. vs radial profile (A – Q_{AIR}=250 mL/min; B – Q_{AIR}=400 mL/min) and the influence of SG concentration in average liquid velocity (C) and liquid flow (D) in the downcomer. Legend: □ - 0% (wt.$_{WET\ BASIS}$/vol.) SG; ◇ - 2% (wt.$_{WET\ BASIS}$/vol.) SG; △ - 4% (wt.$_{WET\ BASIS}$/vol.) SG; ○ - 6% (wt.$_{WET\ BASIS}$/vol.) SG; × - Q_{AIR}=250 mL/min; + - Q_{AIR}=400 mL/min.

The SG concentration effect in pseudo-homogeneous phase is affected by the SG properties (density, wettability, hydrophobicity), which induces a small drag force when v_{Ld} is higher than 10 cm/s as it occurs at 400 mL/min. By the values from linear liquid velocity in downcomer, is possible to obtained the linear velocity in riser, as well as the superficial velocity using **Eq. VII-20** and **VI-21** (Freitas, 2002). In

Table VIII-3 are present these values that will be used in the modelling section.

Table VII-3. Values of riser linear and superficial velocities calculated from equations 9 and 10 for all studied situations.

Q_{gi} (mL/min)	e_{Sd} % *(wt./vol.)*	v_{Ld} / (cm/s)	e_{Gd} % *(vol./vol.)*	e_{Sd} % *(vol./vol.)*	U_{Ld} / (cm/s)	A_d/A_r
250	0.00	9.1	0.0	0.0	9.1	3.7
	0.25	9.0	0.0	2.0	8.8	3.7
	0.50	8.6	0.0	3.9	8.2	3.7
	0.75	8.1	0.0	5.9	7.6	3.7
400	0.00	10.7	0.0	0.0	10.6	3.7
	0.25	10.1	0.0	2.0	9.9	3.7
	0.50	10.1	0.0	3.9	9.7	3.7
	0.75	10.7	0.0	5.9	10.1	3.7
Q_{gi} (mL/min)	e_{Sd} % *(wt./vol.)*	A_d/A_r	U_{Lr} / (cm/s)	e_{Gr} % *(vol./vol.)*	v_{Lr} / (cm/s)	A_d/A_r
250	0.00	3.7	33.3	1.1	33.7	3.7
	0.25	3.7	32.5	1.0	33.5	3.7
	0.50	3.7	30.2	0.9	31.8	3.7
	0.75	3.7	28.0	0.9	30.0	3.7
400	0.00	3.7	38.8	2.9	39.6	3.7
	0.25	3.7	36.5	1.1	37.6	3.7
	0.50	3.7	35.6	09	37.3	3.7
	0.75	3.7	36.9	0.7	39.5	3.7

VII.4.4 Solids-phase measurements

To complete the analysis of the three-phase system, it was also important to study and analyse the solid-phase (SG) behaviour. A previous study shows that, for this riser length, the solids distribution is almost constant even at low gas flows (Chapter V). So it was considered in this work that solids hold-up and distribution is homogeneous throughout the entire iGLR.

In this case, the study was focused on the downcomer and using the images from HSC, the average solid velocity in the downcomer was manually determined. The results are presented in **Figure VII-21**.

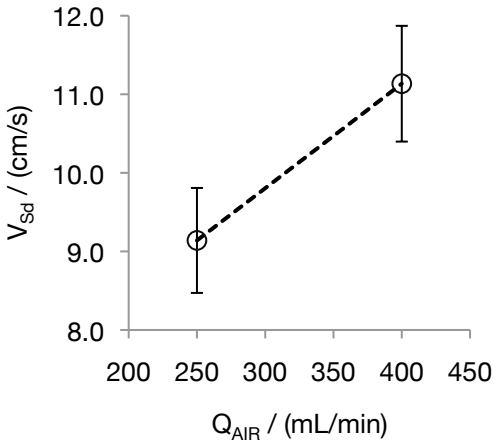

Figure VII-21. Solids Velocity (cm/s) in downcomer versus the air flow rate. The values were obtained by HSC videos and determined manually. The SG load was 2% ($wt._{WET\ BASIS}$/vol.).

As expected and as for the liquid-phase the solids velocity increased with the gas-flow increase. It is interesting to verify that this increase is similar to the increase that occurs in liquid phase, which indicates that the assumption of a pseudo-homogeneous phase can be used in order to simplify the application of hydrodynamic models in the three-phase reactor.

Having in mind all the techniques applied in this work, it was possible to determine the average velocity of liquid- and solid-phase in the iGLR's downcomer. With these values it was possible to determine by calculation the average velocity of the different phases in the riser mainly the liquid and the pseudo-homogeneous phases. In **Table VII-4** are indicated these values. The pseudo-homogeneous phase velocity was determined considering the equation:

$$v_{Hd} = v_{Ld} \times (1 - \alpha_{Sd}) + v_{Sd} \times \alpha_{Sd} \qquad \textbf{Eq. VII–24}$$

This equation (**Eq. VII–24**) means that both liquid and solid-phase have influence in the average velocity of pseudo-homogeneous flow. Looking at **Table VII-4**, it is possible to verify that the pseudo-homogeneous velocity is similar to the liquid velocity at both gas flows. This is because the amount of liquid is about 98% (vol./vol.). However it

is also interesting to note that solids velocity are 1.3% and 9.8% higher than liquid velocity in the downcomer for 250 mL/min and 400 mL/min respectively. Moreover, the pseudo-homogeneous velocities in downcomer are 0.02% and 0.2% higher than liquid velocity for the referred gas flows. This result validates the application of a pseudo-homogeneous phase to be used later in hydrodynamic models. The riser velocities of liquid and pseudo-homogeneous phases were determined according the following equations, respectively (Chisti 1989; Freitas and Teixeira, 1998):

$$v_{Lr} = v_{Ld} \times \left(\frac{A_d}{A_r} \right) \times \frac{1 - \alpha_{Gd} - \alpha_{Sd}}{1 - \alpha_{Gr} - \alpha_{Sr}} \qquad \textbf{Eq. VII–25}$$

$$v_{Hr} = v_{Hd} \times \left(\frac{A_d}{A_r} \right) \times \frac{1 - \alpha_{Gd}}{1 - \alpha_{Gr}} \qquad \textbf{Eq. VII–26}$$

Finally in **Table VII-4** are presented the values of gas velocity relative to the pseudo-homogeneous phase. This value was calculated according to the relative velocity equation between these two phases. As they flow both upwards the equation for slip velocity in riser is:

$$Us_{lip,r} = v_{Gr} + v_{Hr} \qquad \textbf{Eq. VII–27}$$

The results presented in **Table VII-4** allow us to also determine, according to **Eq. V–5** the circulation time of the gas-lift reactor, which is 9.00 s and 8.00 s for 250 mL/min and 400 mL/min respectively. Considering the previously determined mixing time of 22.6 and 12.76 s, it is possible to establish a relation between Tc and Tm for these gas flows. According to Molina et al. (1999) t_m is affected by two mechanisms. The driving force is the relative velocity between gas and liquid in the riser that promotes axial mixing, as the gas transports the liquid upwards. Also the distance in which the former mechanism occurs (twice the dispersion distance) directly affects the mixing time. The equation proposed by Molina et al. (1999) for t_m determination is:

$$t_m = 5.03 \left(\frac{U_{Gr} - U_{Lr}}{2h_D} \right)^{-0.797} \qquad \textbf{Eq. VII–28}$$

In **Table VII-4** it is possible to observe that **Eq. VII–28** is well adjusted to the data obtained at 250 mL/min, but the result is very different for the other gas flow (400 mL/min). The main reason for that is the relative velocity in the riser. As the gas flow is almost double, although the pseudo-homogeneous phase velocity does not increase too much, the gas velocity should be higher. Thus with higher gas flow it was expected to increase the relative velocity. As such did not occur, the mixing time determined by **Eq. VII-28** was overestimated when compared with the mixing time from experimental results. This result is in agreement with the previous results where the gas flow was underestimated at 400 mL/min. In fact it confirms that the lower acquisition rate did not allow a correct evaluation from optical probe of T_U values at this condition. That eventually led to an underestimation of v_B and consequently U_{Gr} and Q_G (previously reported). In addition, if we use the theoretical gas linear velocity (around 94 cm/s) based only on the gas hold-up at this condition (2%SG (vol./vol.)) and gas flow (400 mL/min) the estimated mixing time will be 12.19 s which is 4 % lower than the determined experimentally.

Table VII-4. Velocity values of different phases in different zones of GL reactor for 2%(vol./vol.) of solids.

Parameter	Gas Flow	
	250 mL/min	400 mL/min
v_{Ld} /(cm/s)*	9.0	10.1
v_{Sd} /(cm/s)**	9.1	11.1
v_{Hd} /(cm/s)#	9.0	10.2
v_{Lr} /(cm/s)#	33.4	37.6
v_{Hr} /(cm/s)#	33.4	37.7
U_{slip_r} /(cm/s)#	97.5	103.9
$t_C{}^+$ / (s)	9.00	8.0
$t_m{}^{++}$/ (s)	22.3	12.8
$t_{mTEO}{}^+$/ (s)	19.9	21.1
Error	10.7%	65.3%

* Determined by PIV
** Determined manually using HSC videos
# Calculated value using equations VII-26, VII-27, VII-28 and VII-29.
+ Calculated using Equation VI-5
++ Determined by injection tracer technique using H_2SO_4

VII.4.5 Model optimization results

The model used it was a multi-parameter model were the optimization parameters (C, U_{bt}, β) were adjusted to the experimental data. In **Figure VII-22** it is presented the relations between the results obtained from experimental data and the model. Generally the gas hold-up and superficial liquid velocity in the riser were in agreement and errors are within 20% for gas hold-up and 10% for liquid superficial velocity. These errors are considered to be acceptable and in accordance with the errors obtained by Freitas (2002). It is also important to consider the experimental errors from optical probe new method plus PIV method.

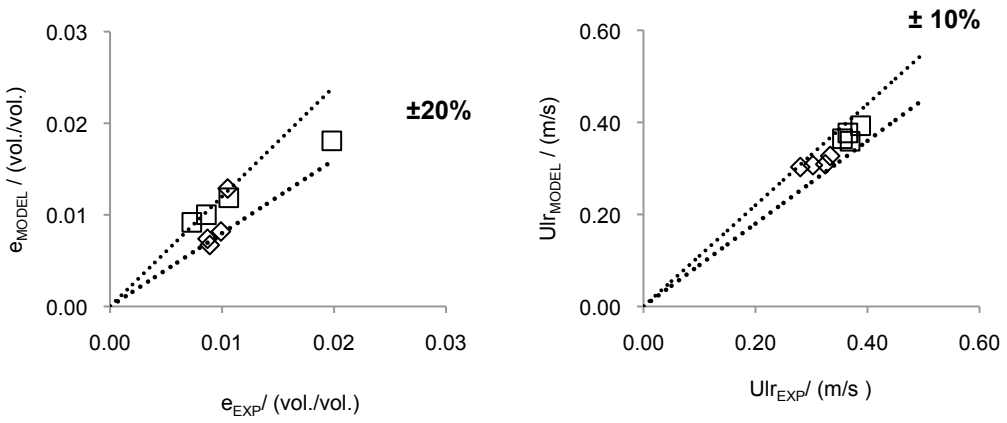

Figure VII-22. Modelization Values versus Experimental results. Legend: ◇ - 250 mL/min; □ - 400 mL/min.

In **Table VII-5** it can be found the results of model parameters after optimization for each solid condition. The distribution parameter (C) was near unity as expected (Freitas et al., 1999; Lu et al., 1995). However, this does not mean that plug flow prevails because the magnitude of C is related with the gas hold-up distribution rather than phase velocity profile (Freitas et al., 1999; Lu et al., 1995). This is can be confirmed by the optical probe results above where no significant differences were found in radial position.

Considering the β parameter and for air-water system, it is possible to determine a value of ϕ = 1.37 (**Eq. VII–16**), which is similar to the proposed value for ϕ (ϕ=2) (Garcia-Calvo and Letón) for two-phase system. However, when SG are added ϕ values decrease. This decrease can be attributed to the hydrophobic properties of SG that act in the *g-l* interface.

Table VII-5. Parameters obtained after optimization.

% Solids (vol./vol.)	C	β	U_{bt}	Error
0.00	0.897	0.014	0.160	14.65%
2.00	0.999	0.008	0.406	18.74%
3.90	1.010	0.006	0.714	23.66%
5.90	1.065	0.005	0.632	21.83%

Generally U_{bt} increases with solid load which is in agreement, and in the same range, with the results obtained by other authors (Freitas et al., 1999). U_{bt} is the bubble terminal velocity in the drift-flux model and it is assumed that bubbles do not interact or are affected by neighbouring bubbles. Moreover the normal values for U_{bt} are between 0.2 m/s and 0.45 m/s (Lu et al., 1995). The higher values obtained can be a clue that explains coalescence as bigger bubbles rise fast then their terminal velocity. Freitas et al (2002) considered that the riser small cross section area was the factor that increases bubble interaction and cause the formation of bubbles rising with higher speed in the riser centre (Lu et al., 1995). This explanation is consistent with the occurrence of coalescence in *g-l-s* system.

VII.4.6 Fermentation results

In this chapter our objective was also to do an experiment that allow us to study how the biomass (free + immobilized) can affect hydrodynamic behaviour of the bioreactor at local scale after the start-up stage. In order to do that, it was performed a fermentation that simulates the initial stage of a continuous primary AFB fermentation.

Previous studies reported that this stage can take from seven to twelve days at dilution rate of 0.2 h^{-1} and 0.15 h^{-1}, respectively (Brányik, et al. 2004). In our case, the dilution rate was between 0.05 h^{-1} and 0.09 h^{-1} and the time to achieve the stabilization of iBio was about 13 days. It is possible to observe that the temperature was higher than normally reported which, even at lower liquid flow, lead to a reduction in the time for biofilm stabilization in the carrier (**Table VII-6**). The stabilization of iBio occurred around the 8th day.

In **Table VII-6** are presented the results from the final day of fermentation. At that time, gas-phase properties were also measured in order to have a clue if yeast cells (free + immobilized) influence GL reactor hydrodynamics. At 13th day of fermentation the total amount of biomass was about 14.7 g/L being iBio only 10% of total yeast biomass present. The final SG concentration leads to a solid hold-up near 4% ($wt._{WET\ BASIS}$/vol.). The results after fermentation showed for a similar solid concentration that gas hold-up increased up to 22% (for corrected value). Bubble velocity decreased by 2% indicating that yeast cells have more influence in GL bioreactor hydrodynamic than SG. It is reported that yeast cells (free and immobilized) become more hydrophobic when exponential growth starts in the carrier. However during the fermentation ethanol is produced and, as it is a coalescence inhibitor, the increase of gas hold-up occurs. Kennard et Janekeh (1991) found that from 0 g/L to 2 g/L of ethanol in solution bubble diameter decreases significantly and consequently gas hold-up increases. For ethanol concentration above 2 g/L this effect was not noted (Kennard and Janekeh, 1991). Zahradnik et al. (1997) found that limit ethanol concentration was around 5.06 g/L in accordance with Oolman et Blanch (1986) that suggested a value of 6.48 g/L (Kennard and Janekeh, 1991). In BC reactor at the maximum value of ethanol concentration defined by Zahradnik et al. (1997) the gas hold-up may increase by 20%. AFB can contain up to 0.5% (vol./vol.) of ethanol (around 3.9 g/L). In our case ethanol at 13th day had a concentration of 6 g/L above all limit concentration defined in literature, so the 20% gas hold-up increase observed can be considered due to ethanol presence.

Moreover this fact confirms that the influence of yeast cells in optical probe measurement is real. This was out of the scope in this thesis, however further studies should be done to access the real influence of yeast cells in optical probe measurements.

Considering SG as a carrier for yeast cells in continuous fermentations seems ideal for immobilization, not only due to their high cells load capacity, but also because even if they influence the iGLR hydrodynamics this has little effect when compared by the microorganisms effect mainly if compounds which ar known to have hydrodynamic influence such as ethanol are produced.

Table VII-6. Fermentation and Gas-phase properties obtained at last day of fermentation.

Day	**Free Cells / (g/L)**	**iBio ($g_{Bio}/g_{Carrier}$)**	**$W_{CARRIER}$ / g**
13	13.1	0.3	27.7
e_S % ($wt._{WET\ BASIS}$/vol.)	**e_G / % (vol./vol.)**	**v_B / (cm/s)**	**ch_B / mm**
4	1.9±0.1 (1.1±0.1)*	97.2±26.0 (61.5±9.5)*	5.7±3.4 (3.9±1.0)*

* values corrected considering free cells influence in Optical probe measuring mechanism.

Moreover at this immobilization levels almost all SG surface is colonized by yeast cells, which have different surface properties and lower hydrophobic properties. Then the negative effect of SG is also reduced by the yeast cells that are immobilized on the carrier (Bránýik et al., 2004). Overall, more investigation seems to be necessary to really access biomass influence on gas-lift bioreactors hydrodynamics.

VII.5 Conclusions

At the end of this Chapter it was possible to study and better understand the SG effect on gas-lift bioreactor hydrodynamics, with and without active yeast cells. Considering only the *g-l-s* system composed by Air-Water-SG, it is clear that SG due to their particular surface properties decrease gas hold-up increasing bubble velocity and

bubble chord. However those results are more reliable for the lowest gas flow tested (250 mL/min) as at the highest gas flow the new injection system used (applied in the optical probe) seemed not to be enough for a correct measurement of bubble velocity. In addition the experiments made with HSC allowed us to confirm the optical probe results and together with PIV measurements, it was possible to conclude that an assumption of a pseudo-homogeneous phase can be made for this system, this being used on the model proposed. The developed model shows a good agreement with the experimental data. It seems that SG promotes coalescence and this was proved by the increase of bubble terminal velocity up to 4 % (vol./vol.) of SG. Finally it was proved that yeast cells influence OP measuring mechanism by increasing 42.74±3.31%, 36.74±4.42% and 30.26±3.57% the local gas hold-up, bubble velocity and chord size, respectively. Considering this and a correction value after fermentation, it was noted that gas hold-up generally increases by 22% in the presence of cells. As SG reduce gas hold-up, it is clear that immobilized yeast cells and ethanol production play an important role on gas-lift bioreactor hydrodynamics having a higher influence than the solid-phase (SG), at least for the SG concentration considered.

VII.6 References

Bla, M., Ki, M., and Marko, J. (**2004**). Scale influence on the hydrodynamics of an internal loop airlift reactor. *Chemical Engineering and Processing*, 43(12), 1519-1527.

Boyer, C., Duquenne, A.-M., and Wild, G. (**2002**). Measuring techniques in gas-liquid and gas-liquid-solid reactors. *Chemical Engineering Science*, 57, 3185-3185.

Brányik, T., Vicente, A., Machado Cruz, J., and Teixeira, J. (**2001**). Spent grains – a new support for brewing yeast immobilisation. *Biotechnology Letters*, 23(13), 1073–1078.

Brányik, Tomás, Vicente, A. A., Oliveira, R., and Teixeira, J. A. (**2004**). Physicochemical surface properties of brewing yeast influencing their immobilization onto spent grains in a continuous reactor. *Biotechnology and bioengineering*, 88(1), 84-93.

Cartellier, Alain. (**1990**). Optical probes for local void fraction measurements: Characterization of performance. *Review of Scientific Instruments*, 61(2), 874-886.

Cartellier, A. and Achard, J. L. (**1991**). Local phase detection probes in fluid/fluid two-phase flows. *Review of Scientific Instruments*, 62 (2), 279-303.

Cartellier, A. (**1992**). Simultaneous void fraction measurement, bubble velocity, and size estimate using a single optical probe in gas-liquid two-phase flows. *Review of Scientific Instruments*, 63(11), 5442-5453.

Cartellier, A. (**1998a**). Measurement of gas phase characteristics using new monofibre optical probes and real time signal processing. *Nuclear Engineering and Desing*, 184, 393-408.

Cartellier, A. and Barrau, E. (**1998b**). Monofiber optical probes for gas detection and gas velocity measurements: conical probes. *International Journal of Multiphase Flow*, 24(8), 1265–1294.

Cartellier, A., and Rivière, N. (**2001**). Bubble-induced agitation and microstructure in uniform bubbly flows at small to moderate particle Reynolds numbers. *Physics of Fluids*, 13, 2165-2181.

Chaumat, H., Billetduquenne, A., Augier, F., Mathieu, C. and Delmas, H. (**2005**). Application of the double optic probe technique to distorted tumbling bubbles in aqueous or organic liquid. *Chemical Engineering Science*, 60(22),

Dias, S. G., França, F. A. and Rosa, E. S. (**2000**). Statistical method to calculate local interfacial variables in two-phase bubbly flows using intrusive crossing probes. *International Journal of Multiphase Flow*, 26, 1797-1830.

Ferreira, A., Pereira, G., Teixeira, J. A. and Rocha, F. (**2011**). Statistical tool combined with image analysis to characterize hydrodynamics and mass transfer in a bubble column. *Chemical Engineering Journal*. 180 (2012) 216–
228.

Freitas, C., Fialová, M., Zahradnik, J. and Teixeira, J. A. (**1999**). Hydrodynamic model for three-phase internal-and external-loop airlift reactors. *Chemical Engineering Science*, 54, 5253-5258.

Freitas, C. (**2002**). Bioreactores Multifásicos - Caracterização Hidrodinámica e de Transferência de Massa (in Portuguese). PhD thesis, University of Minho.

Gandhi, B., Prakash, A. and Bergougnou, M. A. (**1999**). Hydrodynamic behavior of slurry bubble column at high solids concentrations. *Powder Technology*, 103(2), 80–94.

Hamad, F. A. and He, S. (**2010**). Evaluation of hot-film, dual optical and Pitot tube probes for liquid–liquid two-phase flow measurements. *Flow Measurement and Instrumentation*, 21(3), 302-311.

Hong, M., Cartellier, A. and Hopfinger, E. J. (**2004**). Characterization of phase detection optical probes for the measurement of the dispersed phase parameters in sprays. *International Journal of Multiphase Flow*, 30(6), 615-648.

Kennard, M. and Janekeh, M. (**1991**). Two- and three-phase mixing in a concentric draft tube gas-lift fermentor. *Biotechnology and bioengineering*, 38(11), 1261-70.

Lu, W-J., Hwang, S-J., and Chang, C-M. (**1995**). Liquid velocity and gas holdup in three-phase internal loop airlift reactors with low-density particles. *Chemical Engineering Science*, 50(8), 1301–1310.

Maceiras, R., Álvarez, E. and Cancela, M. A. (**2010**). Experimental interfacial area measurements in a bubble column. *Chemical Engineering Journal*, 163(3), 331-336.

Mena, P. C., Ruzicka, M. C., Rocha, F. A., Teixeira, J. A. and Drahos, J. (**2005a**). Effect of solids on homogeneous–heterogeneous flow regime transition in bubble columns. *Chemical Engineering Science*, 60(22), 6013-6026.

Mena, P. C., Pons, M. N., Teixeira, J. A., and Rocha, F. A. (**2005b**). Effect of Solids on Gas-Liquid Mass Transfer and Bubble Characteristics in Three-Phase Systems. *7th World Congress of Chemical Engineering*.

Mena, P. C., Pons, M. N., Teixeira, J. A., and Rocha, F. A. (**2005b**). Using image analysis in the study of multiphase gas absorption. *Chemical Engineering Science*, 60(18), 5144-5150.

Mena, P. C., Rocha, F. A., Teixeira, J. A., Sechet, P. and Cartellier, A. (**2008**). Measurement of gas phase characteristics using a monofibre optical probe in a three-phase flow. *Chemical Engineering Science*, 63(16), 4100-4115.

Molina, E., Contreras, A. and Chisti, Y. (**1999**). Gas holdup, liquid circulation and mixing behaviour of viscous newtonian media in a split-cylinder airlift bioreactor. *Trans IChem E*, 77(Part C), 27–32.

Olivieri, G., Marzocchella, a, Vanommen, J. and Salatino, P. (**2007**). Local and global hydrodynamics in a two-phase internal loop airlift. Chemical Engineering Science, 62(24), 7068-7077.

Olivier, J.-M.M., (**1999**). Instrumentation temps réel pour la caractérisation d'écoulements diphasiques à bulles à l'aide de sondes optiques (in French). Masters thesis. Institut National Polytechnique de Grenoble.

Onken, U. E. and Weiland, P. (**1983**). Airlift fermenters: construction behaviour and uses. *Advances in Biotechnology Procedings*, 1, 67-95.

Poupot, C. and Cartellier, A. (**1999**). Single and double optical probes in air-water two-phase flows : real time signal processing and sensor performance. *International Journal of Multiphase Flow*, 25, 229-256.

Shen, X., Mishima, K. and Nakamura, H. (**2008**). Error reduction, evaluation and correction for the intrusive optical four-sensor probe measurement in multi-dimensional two-phase flow. *International Journal of Heat and Mass Transfer*, 51(3-4), 882-895.

Unadkat, H., Rielly, C. D., Hargrave, G. K. and Nagy, Z. K. (**2009**). Application of fluorescent PIV and digital image analysis to measure turbulence properties of solid – liquid stirred suspensions. *Chemical Engineering Research and Design*, 87, 573-586.

Vejrazka, J., Vecer, M., Orvalho, S., Sechet, P., Ruzicka, M. C. and Cartellier, A. (**2010**). Measurement accuracy of a mono-fiber optical probe in a bubbly flow. *International Journal of Multiphase Flow*, 36, 533-548.

Xie, T., Ghiaasiaan, S. M., Karrila, S., and Mcdonough, T. (**2003**). Flow regimes and gas holdup in paper pulp – water – gas three-phase slurry flow. *Chemical Engineering Science*, 58, 1417 - 1430.

Zon, M. V., Hamersma, P. J., Poels, E. K., and Bliek, A. (**2002**). Coalescence of freely moving bubbles in water by the action of suspended hydrophobic particles. *Chemical Engineering Science*, 57, 4845–4853.

VIII. Chapter VIII - Continuous Primary Alcohol-free Beer Fermentation: Influence of Yeast Strain, Reactor Conditions, Carrier Type and Ageing

VIII.1 Objectives

In this chapter continuous AFB primary fermentaion is studied and the influence of several parameters is evaluated, such as:

- the effect of different yeast strains, reactor types and carriers in AFB primary fermentation performance and flavour compunds formation

- the influence of the gas-phase composition in continuous primary AFB fermentation performance and in the flavour compunds, using an iGLR and SG as a carrier.

- the influcence of yeast ageing in a continuous primary AFB using an iGLR and SG as carrier.

VIII.2 Introduction

The application of continuous primary fermentation for AFB production at industrial scale is not yet implemented (Chapter II.3.1). The reasons behind this are mainly: unbalanced flavour; engineering problems (process hygiene); contamination issues; accuracy of economic prospects; the use of limited yeast strains that only allow the continuous production of a limited type of beers; and tradition in brewing industry (Brányik et al, 2005; Willaert and Nedovic, 2006).

Among all different reactor configuration and systems using ICT already studied (see Chapter II and III) it is possible to distinguish two main types that have been more studied: packed-bed (Van Iersel et al, 1995; Virkajarvi and Pohjala, 2000) and gas-lift (Bezbradica et al, 2007; Brányik, et al, 2004) reactors. Both have advantages and disavantages in continuous AFB production. Between these two reactor types the choice depends mainly on the type of carrier and the type of immobilization method applied. Thus it is difficult to compare all systems present in literature with accuracy.

VIII.2.1Gas-lift reactor

The gas-lift is a reactor without moving parts, where the mixing and circulation are promoted by the gas-phase injected (perfectly agitated reactor). This confers to gas-lifts reactors good mass transfers and mixing properties, which associated with the low value of tension forces field make this reactor ideal for using ICT with high immobilization load capacity and consequently higher productions can be obtained (Fonseca and Teixeira, 2007). Several configurations of gas-lift reactor can be found in literature (see Chapter V) for different purposes. In a three-phase iGLR, the gas phase is injected into the riser tube through a distributor to provide the driving force for liquid circulation and energy for the solid-phase distribution (Brányik et al., 2004a).

For continuous AFB production the iGLR is usually used in main fermentation (Bezbradica et al., 2007; Brányik et al., 2004; Domény et al., 1999; Lehnert et al., 2008). The immobilization of yeast cells in the carrier may occur by adsorption onto the solid phase (carrier), during the first days of fermentation (Brányik et al, 2004b) or by previous entrapment prior to fermentation (Bezbradica et al., 2007; Decamps et al , 2004). Nevertheless, detachment of biomass under conditions of mechanical stress (Bezbradica et al., 2007; Brányik et al., 2004a), gradual disintegration and wash out of carrier (Brányik et al, 2004a, 2004b) may influence stability of immobilized biomass in a long-term fermentation. This problem is more significant if the immobilization occurs by adsorption and it is necessary to obtain a balance between mixing time, sedimentation, and the maximum load of immobilized biomass (Brányik et al, 2004b). Moreover in long-term continuous fermentations, replacing fresh carrier might be needed to maintain cell concentration and avoid/reduce cell ageing problems. It was observed that, in around one week after adding new carrier, the immobilized biomass achieved the values before addition (Brányik et al, 2004b). The main disadvantages of using a iGLR to preform main fermentation are

foaming formation and the complexity of scale-up (Pilkington et al. , 1998).

Continuous primary fermentation of AFB in an iGLR is normally divided in two stages. The initial one, also called start-up, is characterized by: air as gas-phase; higher temperature (around 12 ºC); lower dilution rate (0.05 h^{-1} to 0.15 h^{-1}); medium as liquid phase (instead of beer wort). This conditions are ideal to a rapid yeast cells growth and immobilization of these onto SG. Normally dilution rate used is below the maximum yeast growth rate (μ_{MAX}) at given temperature to allow the increase of yeast cells inside the reactor. Then the second stage, which corresponds to the primary fermentation begins. The main characteristics are: CO_2 as gas-phase; lower temperature (8 ºC); higher dilution rate (0.2 h^{-1} to 0.4 h^{-1}) and wort as medium (Brányik et al, 2002, 2004b; Lehnert et al., 2008, 2009).

Normally the gas phase present in GLR reactors varies from the first to the second stage. In the first one the main aim is to increase yeast cell growth as well as the formation of a solid yeast biofilm around carrier particles. Being so the gas-phase is air to promote yeast gowth. When the biofilm is formed around the carrier the gas-phase is gradually changed to CO_2 in order to maintained the reactor at anaerobic conditions (Brányik et al., 2004a; Lehnert et al., 2008, 2009). The gas-phase leaving the reactor can be recover and the CO_2 is then purified and re-used in the iGLR (Kourkoutas et al., 2004).

In order to maintain anaerobic conditions it is important to understand all oxygen flux present in an iGLR operating in continuous mode. Oxygen is important to synthetize esterols for membrane lipids production, that will be used during yeast growth. Lehnert et al (2008) obtained better results at minimum oxygen transfer rate (OTR) used (1 mg/(L·h)). If the wort barrel is not maintained at anaerobic conditions, some oxygen can be dissolved in the inflow medium. Moreover while the wort is added to the reactor, the barrel headspace increases which will increase slighty the dissolved oxygen in the wort. Being so the OTR also depends on the inflow that enters in the GLR when operating in

continuous mode, (OTR_{DO}). When the inflow is maintained at 8 ºC the average oxygen concentration ($C_{OD\ AVG}$) is 3 mg/L (Macieira, 2008) and the average OTR is calculated by: $OTR_{TOTAL}=OTR_{OS}+OTR_{DO}$

If the gas-phase is CO_2 the $OTR_{OS}=0$ mg/(L·h) and the $OTR_{DO}=D*C_{OD\ AVG}$ mg/(L·h), where D is the dilution rate. Considering that dilution rate normally are not above 0.3 h^{-1} (Lehnert, 2009) when AFBs are produced in continuous the final OTR will always be inferior to the ones present in the literature (Lehnert et al., 2008, 2009; Macieira, 2008). These minimum oxygen conditions are considered to be the ideal to ensure a good final product quality in terms of flavour compounds and at the same time to maintain yeast cell growth at a minimum.

VIII.2.2 Packed-bed reactor

The packed-bed reactor (PBR) or plug flow reactor, is usually used for maturation and in that case low temperatures (0 ºC to 5 ºC) are applied (Dömény et al., 1998; Van Iersel et al., 1995; Virkajarvi and Pohjala, 2000; Perpète and Collin, 1999b). These conditions lead to: (1) low yeast growth and consequently a low risk of clogging; (2) high viability over longer periods; (3) enough reduction of aldehydes and other carbonyls; (4) low ethanol formation; (5) simplicity of operation. In theory, the plug flow present in this reactor operating at ideal conditions allow to mimicked well the different stages present in batch fermentations. However in practice, it is very difficult to achieve the ideal conditions. In addition, it is reported the occurrence of channeling (deviations to ideal plug regime), mass transfer limitations, difficulties in CO_2 evacuation (gas pockets), compression of carrier materials and fouling (Brányik et al., 2005; Willaert and Nedovic, 2006; Pilkington et al. , 1998).

VIII.3 Material and Methods

VIII.3.1 Microorganisms and medium

The microorganisms used in the experiments were for initial study: a bottom fermenting brewing yeast (*Saccharomyces pastorianus*) strain *W96* (collection of Research Institute of Brewing and Malting Prague, Czech Republic); and *Saccharomyces cerevisiae* BY4743 with disruption in the *KGD2* (α-ketoglutarate dehydrogenase) gene. For studing the ageing and gas compositon efect an industrial Portuguese bottom yeast strain from UNICER, SA was used.

Table VIII-1. Wort used in this chapter (VIII) for alcohol free-beer production

Name	Type of Wort/Medium	Sugar Content$_{AVG}$ (g/L)	Manufacturer
W_A	powder wort concentrate	32.6	Research Institute of Brewing and Malting, Plc., Czech Republic
W_B	concentrated wort	39.3	UNICER SA, Portugal
SMM	Synthetic mineral medium	20	-

The powder wort concentrate (W_A) was prepared by dissolution of 1 kg in 20 L of previously sterilized water (121 °C, 60 min) in order to achieved 5 ºP wort. Then solution was heated to 100 °C during 30 min. The pH of wort was adjusted to 4.5 with the addition of lactic acid (80% wt./vol., IFC Food, Ltd., Czech Republic). For each experiment the inoculum was grown in 500 mL of wort at 8 ºC for 48 h in an orbital shaker (150 rpm). If necessary, the cells were collected by centrifugation (5000 rpm, 5 ºC, 10 min).

The concentrated wort from Unicer (W_B) was diluted in order to achieve an average concentration of 5.3 ºP. The pH was adjusted with lactic acid to 4.5 and the wort was sterilized at 100 ºC during 60 min.

The SMM composition used to study the effects of ageing in a continuous primary fermentation of AFB is presented in **Table VIII-2**.

Table VIII-2. Composition of the SMM and respective concentrations.

Compound	Concentration
KH_2PO_4	5 g/L
$MgSO_4 \cdot 7\ H_2O$	0.4 g/L
$(NH_4)_2SO_4$	2 g/L
Yeast Extract	2 g/L
Glucose	20 g/L
Antifoam	10 mL/10 L
3-methylbutanal	200 mg/L
2-methylpropanal	100 mg/L
Hexanal	100 mg/L
Furfural	100 mg/L

Barrels with 20 L of SMM were sterilized by autoclaving at 120 ºC, 100 kPa for 40 min.

VIII.3.2 Carrier preparation

For this work two types of carrier were tested: corncobs and spent grains. Each one was prepared according to the methods descibred below.

VIII.3.2.1 Corncobs

Corncobs with a diameter between 2 and 2.5 cm and total length of ca. 10 cm were cut into cylinders with a maximum height of 0.6 cm. Then each piece was cut in two pieces of the same size along the width. These half cylinder particles were used as carrier in PBR. For GLR the corncobs were disintegrated in a knife mill (Cutting Mill SM 2000, Retsch GmbH, Germany) into particles with a maximum diameter of 0.1 × cm. Then 100 g (dry base) of previously milled corncobs were further separated into two fractions (equivalent diameter: 1 mm and 0.5 mm) using a portable sieve shaker (Model Analysette, Fritsch, Germany). Smaller particles with an equivalent diameter lower than 0.5 mm were discarded due to their low sedimentation velocity and consequently easy washout from iGLR reactor.

Prior to use, all corncob particles were autoclaved (121 °C, 60 min) as a suspension (10% (wt./vol.)) in distilled water in order to remove the soluble compounds that might influence the beer flavour (Brányik et al., 2006).

VIII.3.2.2 Spent grains

Spent grains were prepared according to method present in section III.2.4.1.

VIII.3.3 Packed-bed reactor

The PBR used was made of glass and had a total working volume of 2.12 L. The dimensions of the reactor are: total height – 51 cm; diameter – 8 cm and packed bed height – 38.5 cm. Inflow was at bottom of the reactor and three samplings points were located at 3, 17.6 and 31.4 cm from the bottom of the reactor (point I,II and III in **Figure VIII-1**). The out flow is located 41 cm from bottom. The reactor was maintained at 8 °C by placing it into a controlled temperature cold room.

The PBR filled with corncob particles (210 g dry weight) had a solid voidage of 0.36. The charged PBR was autoclaved at 121 °C for 20 min. After this the PBR was washed with 10 L of sterile distilled water and finally the water was allowed to drain. Then 500 mL of previously grown inoculum was added and the remaining reactor volume was filled with fresh wort. After 24 h of batch growth, the reactor was continuously fed with wort, using a peristaltic pump (**Figure VIII-1**). The continuous system was considered to reach steady state after five residence times.

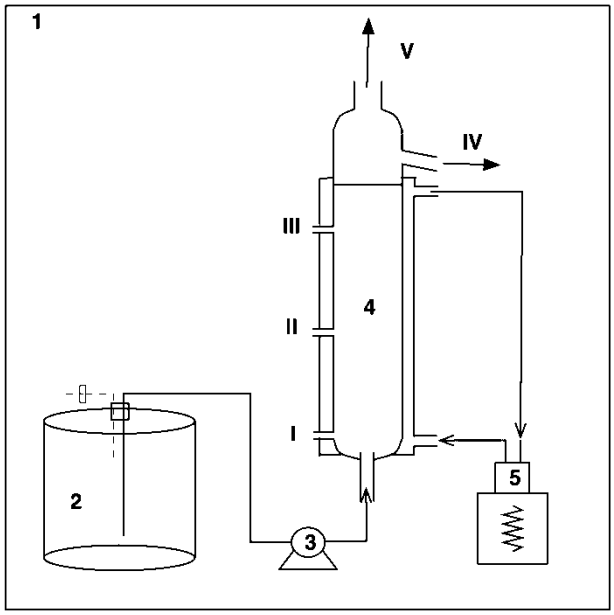

Figure VIII-1. Experimental layout of the continuous packed-bed reactor: 1 = cold room, 2 = wort barrel, 3 = peristaltic pump, 4 = PBR, 5 = cooling system; I, II and III = sampling points, IV = beer outflow, V = gas outlet.

VIII.3.4 Gas-lift reactor characteristics and startup

The gas-lift reactor layout (**Figure VIII-2**) and startup was identical for both used carriers (spent grains, corncobs) and it was described in Lehnert *et al.* (2008, 2009). The total amount of spent grains and milled corncob particles in gas-lift reactor was 40 and 55 g dry weight, respectively. Air flow (0.25 L/min) was supplied in the first 12 days of fermentation to promote yeast growth and when a fully developed yeast biofilm was formed around the carrier particles the intensity of aeration was decreased by switching to air + CO_2 mixture, while the total gas flow rate was kept constant (0.25 L/min). The switching to a fully CO_2 (0.25 L/min) gas flow was gradual to avoid cell stress. As in PBR, the continuous system was considered to reach steady state after five residence times. The iGLR used in all experiments has a working volume of 3 L (Lehnert et al., 2008, 2009) with the exception of the reactor used in the section VIII.4.5, which has 6 L (same used in section VII.4.6).

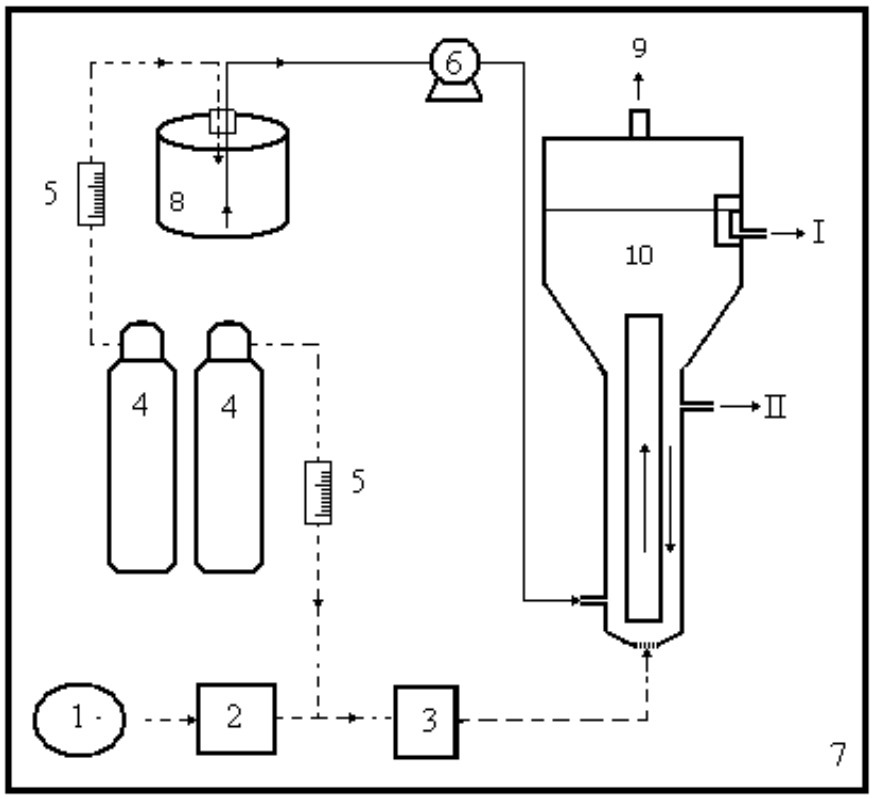

Figure VIII-2. Laboratory scale installation for primary beer fermentation: 1-air supply; 2-mass flow controller; 3-gas sterilization filter; 4-CO2 bottles; 5-rotameters; 6-peristaltic pump; 7-thermostated cold room; 8-wort barrel; 9-gas outlet; 10-gas-lift reactor; I. beer sampling; II. carrier sampling.

VIII.3.5 Batch fermentations

The batch fermentations were started by cooling the sterile wort (2 L) to 8 °C and aerating (700 mL/min) for 15 min. The final oxygen concentration in aerated wort was approximately 8 mg/L. The pitching rate with previously grown and centrifuged cells was 3×10^6 cell/mL. Initially the fermentation was performed at 8 °C for 24 hr and then the partially fermented wort was cooled to 2°C for 48 hr.

VIII.3.6 Yeast cells analysis

VIII.3.6.1 Methylene blue staining

Brewing yeast viability was determined also by methylene blue method which is applicable to all samples containing brewing yeast.

Viable cells reduce methylene blue enzymatically to a colourless compound. The yeast suspension was diluted with 1 % (wt./vol.) methylene blue solution in a test tube until a suspension with approximately 5-10 cells in a microscopic field was obtained. The counting was made using a magnification of 400 times during a maximum of 5 minutes. Cells stained dark blue were considered to be dead along with broken, shrivelled and plasmolyzed cells. Cells stained light blue should be considered alive and the yeast cells that were budded were counted as one cell if the bud is less than one half the size of the mother cell. Viability was calculated from the ratio between total and viable cells (ASBC, 1996).

VIII.3.6.2 Free biomass concentration

A sample of 10 mL was removed from the reactor outflow and it was centrifuged for 3 min at 5000 rpm. The supernatant was removed and, if necessary, the sediment was diluted (1:5 ratio) with distilled water. The optical density of the solution was measured with spectrophotometer at a wavelength of 600 nm. The results of biomass concentration were calculated using a calibration curve, biomass vs. absorbance.

VIII.3.6.3 Immobilized biomass determination

Due to difficulties with collecting biocatalyst (carrier + immobilized cells) samples from the running PBR (Bányik et al., 2006) the values of immobilized biomass on corncob particles were only determined after finishing the fermentation. Samples of biocatalysts (3 to 4 g) were collected and placed in 200 mL of 15 g/L aqueous solution of NaCl (pH=3). The suspension was then agitated at 700 rpm for 30 min. Then the cell suspension absorbance (600 nm) was read and the cell biomass was calculated by using a calibration curve.

The amount of biomass adhered to milled corncobs particles (Cc3 see chapter III.3.2) was determined in 50 mL samples taken from iGLR to a 100 mL Erlenmeyer flask. This sample contained approximately 0.5 g of dry biocatalyst. Then the bulk of the liquid phase was removed

with a syringe and the carrier was washed with 3 x 75 mL of distilled water in order to remove the free cells captured between the carrier particles. These operations were carried out very carefully avoiding shocks that would detach the immobilized cells from the surface of the carrier. After drying (40 °C for 48 h), the biocatalyst was weighted and then added into 50 mL of NaCl (15 g/L at pH=3). The attached cells were removed from the carrier by strong mixing (600 rpm) for 30 min. The amount of released biomass was determined after settling the carrier by measuring the absorbance (A_{600}) of the bulk liquid at 600 nm and was correlated to cell dry weight by a calibration curve. The whole procedure of mechanical cell removal was repeated while the bulk liquid contained a significant amount of released cells (A_{600}> 0.1) (Brányik et al., 2001). This procedure was repeated in duplicate for each sample.

The iBio in SG was determined according to the method described by Brányik et al. (2004a). Briefly a sample containing approximately 1.0 g of dry biocatalyst was taken from the reactor in a form of slurry through a sampling port (point II in **Figure VIII-2**) to a previously weight Erlenmeyer flask. The bulk liquid was removed with a syringe, and the carrier was washed with 200 mL (2 x 100 mL) of distilled water. Then the flask+biocatalyst were dried at 105 °C for 12 h and weight. After 100 mL of 3 % (wt./vol.) NaOH solution was added and shaken at 120 rpm for 24 h. During this time the attached biomass was completely removed from the carrier and this was verified with microscopy. The biomass free suspension was removed from the SG particles and the Erlenmeyer containing only SG was dried at 105 °C for 5 h. The amount of yeast biofilm was determined from the weight difference before and after the treatment with caustic. Corrections of the biomass weight for the losses of SG itself (approximately 6.3% of initial weight) during the washing procedures were carried out with blank experiments with clean carrier.

VIII.3.6.4 Microbial adhesion to solvents (MATS) analysis

The cells were harvested from yeast suspension by centrifugation at 6000 rpm, 8 ºC for 5 min, discarding the supernatant and re-suspending the cells in 150 mM NaCl solution at a concentration of about 4 x 10^7 cells/mL (optical density O.D. of 0.8 at 400 nm). A high ionic strength electrolyte was used to avoid charge interference by a masking cells' charge. At the end, the optical density of the suspension was measured ($O.D._0$) at a wavelength of 400 nm.

Then 3 mL of washed yeast suspension were vortexed for 60 seconds with 0.5 mL of the organic solvent (chloroform, hexadecane, ethyl acetate, and decane). To ensure the complete separation of the two phases the mixture was kept still for 10 min. Then 2 mL sample from the aqueous phase were removed and the O. D. was measured at 400 nm. The cells affinity for each solvent was calculated by **Eq. VIII–1**. Each assay was performed in triplicate.

$$\%affinity = 100 \times \left(1 - \frac{O.D.}{O.D_0}\right) \qquad \textbf{Eq. VIII–1}$$

VIII.3.6.5 Glycogen and neutral lipids (NL) content

Immobilized cells were harvested and kept as described below and glycogen, neutral lipids, and bud scars were analysed by flow cytometry.

The flow cytometric measurements were taken using a Partec Pas III (Partec GmbH, Münster, Germany) analyzer equipped with an argon ion laser (15 mW laser power with excitation wavelength 488 nm).

The relative content of glycogen in cells was determined using Acriflavine, which is a fluorescent dye able to covalently bind to glycogen after permeabilisation of the cell membrane by ethanol (fixation). An aliquot of 0.5 mL (OD=0.8 at 600 nm) of the sample was removed and 10 µL of Acriflavine (Sigma Aldrich, Germany) solution (1 mg/mL in PBS, stored at 4ºC) were added. Incubation occurred at room temperature in darkness for 30 min. The sample was then

analyzed by flow cytometry in FL1 channel (530 nm). The relative content of neutral lipids was detected after reaction with 20 ml of nile red solution (0.1mg/ml acetone). Reaction was carried out in dark at room temperature for 10 min. Sample was subsequently washed three times with PBS (8 g/L NaCl; 1.14 g/L Na_2PO_4; 0.2 g/L KCl; 0.8 g/L KH_2PO_4 – in distilled water) and analysed by flow cytometry in FL3 channel (630 nm).

VIII.3.6.6 Bud scars staining

An aliquot of 0.5 mL (OD=0.8 at 600 nm) of the sample was washed twice in PBS. After it was re-suspended in 0.5 mL PBS and 20 mL of Alexa Fluor 488-labelled wheat-germ agglutinin (lectin from Triticum vulgaris; Sigma-Aldrich, UK), at a concentration of 1 mg/mL. Cells were gently agitated at room temperature for 15 min in dark, harvested by centrifugation (5 000 r.p.m. for 3 min) and washed three times in PBS. The stained cell culture was re-suspended in 0.5 mL PBS and examined using flow cytometry with a 488 nm argon ion laser for fluorescence excitation. Fluorescence was detected in FL1 channel (530 nm).

VIII.3.7 Out-flow analytical methods

VIII.3.7.1 Ethanol determination

Ethanol was analyzed by HPLC (Pump LCP 4000, Column oven LCO 101, ECOM Ltd., Prague, Czech republic) using a Polymer IEX Ca form column (250x8 mm, Watrex International Inc., San Francisco, USA), and a RIDK 102 refraction index detector (Laboratorní přístroje Praha, Prague, Czech republic). Elution was performed with degassed and demineralized water at 85 °C and the flow rate was 0.7 mL/min.

VIII.3.7.2 Higher alcohols, esters and organic acids – method A

The flavour and aroma compounds (HA and ES) were measured according to the current European Brewery Convention recommended

methods (EBC, 1987). The concentration of OA was determined by a capillary zone electrophoretic analyzer (EA 101, Labeco-Villa, Ltd., Slovak Republic), with separation capillaries (PTFE, length 90 mm, diameter 0.8 mm, 150 μA) connected to analytical capillary (length 90 mm; diameter 0.3 mm; 20 μA) and a detector (conductive and UV detection at 254 nm). The analysis was carried out by a leading electrolyte (5 mM HCl + 10 mM glycylglycin + 0.05% hydroxyethylcellulose) and a finishing electrolyte (10 mM caproic acid). The concentration of reducing sugars was determined spectrophotometrically after reaction with 3,5-dinitrosalicylic acid at 530 nm.

VIII.3.7.3 Higher alcohols, esters and aldehydes – method B

These methods were used to determine the voltile compounds from the samples obtained in section VII.4.5. The quantification of the major volatile (acetaldehyde, ethyl acetate, 1-propanol, 2-methyl-1-propanol, 2-methyl-1-butanol, 3-methyl-1-butanol, 2-phenylethanol) and minor (tyrosol, isoamyl acetate, ethyl caprylate, 2-phenylethyl acetate, ethyl hexanoate, ethyl decanoate, 2-phenylethyl acetate, 5-(hdroxymethyl)furfural (HMF)) compounds were performed with the following methods.

Major volatile compounds

To 5 mL of sample, filtered previously through a 0.2 μm membrane filter (Whatman ME24), 100 μL of internal standard (4-nonanol, Merck ref. 818773, in alcoholic solution at 4.1 g/L) were added.

Major volatile constituents were analyzed directly, by injecting 1 μL of sample in the split mode on a Chrompack CP-9000 gas chromatograph equipped with a Split/Splitless injector and a flame ionization detector. A capillary column, coated with CP-Wax 57 CB (50 m × 0.25 mm i.d., 0.2 μm film thickness; Chrompack), was used. The temperatures of the injector and detector were both set to 250 ºC. The oven temperature was held at 60 ºC, for 5 min, then programmed to rise from 60 ºC to 220 ºC, at 3 ºC /min, and finally held at 10 min at

220 °C. Helium GHE5× (Praxair) at 125 kPa was used as carrier gas, and the split vent was set to 15 mL/min. Identification of volatile compounds was carried out by comparing retention indices with those of pure standard compounds. Quantification was performed with software Star – Chromatography Workstation, version 6.41 (Varian), after the determination of detector's response factor for each volatile compound.

Minor volatile compounds

Extraction of volatile compounds were determined according the method proposed by Oliveira et al. (2006). In a 10 mL culture tube (Pyrex, ref. 1636/26MP), 8 mL of beer, 3.582 µg of internal standard (4-nonanol) and a magnetic stir bar (22.2 mm×4.8 mm) were added. Extraction was done by stirring the sample with 400 µL of dichloromethane (Merck, ref. 1.06050) during 15 min, over a magnetic stirrer. After cooling at 0 °C during 10 min, the magnetic stir bar was removed and the organic phase was detached by centrifugation (RCF=5118, 5 min, 4 °C) being the extract recovered into a vial, using a Pasteur pipette. Then, the aromatic extract was dried with anhydrous sodium sulphate (Merck, ref. 1.06649) and picked up again into a new vial. Each sample was extracted in triplicate. The extreacts were analized by gas chromatographic. The analysis of volatile compounds was performed using a GC–MS system constituted by a Varian 3800 Chromatograph, with a 1079 injector, and an ion-trap mass spectrometer Varian Saturn 2000. A 1 µL injection (splitless for 30 s; split ratio of 30 mL/min) was made into a capillary column, coated with VF-Wax ms (30 m×0.15 mm i.d., 0.15 µm film thickness, Varian). Injector and transfer line temperatures were both set to 250 °C. The oven temperature was held at 60 °C, for 2 min, then programmed to rise from 60 °C to 234 °C, at 3 °C/min, and from 234 °C to 250 °C, at 10 °C/min, then held 10 min at 250 °C. The carrier gas was helium GHE5× (Praxair) at a constant flow rate of 1.3 mL/min. The detector was set to electronic impact mode (70 eV), with an acquisition range from 35 m/z to 260 m/z, and an acquisition rate of 610 ms. Identification of volatiles

was performed with Varian MS Workstation software, version 6.9.3, by comparing retention indices with those of pure standard compounds. Volatile compounds were quantified as 4-nonanol equivalents (Oliveira et al., 2006).

VIII.3.7.4 Determination of vicinal diketones

Total VDK's (2,3-butanodione (diacetyl) and 2,3-pentanodione) were measured according to the current European Brewery Convention recommended methods (EBC, 1999).

VIII.3.8 Determination of residence time distribution

Carrier prepared was added to both PBR and iGLR and the working volume of liquid phase in the reactors was calculated. Then a pulse of 2 mL of methylene blue (3.5 g/L) was injected at the inflow of both reactors and samples (1.5 mL) were collected at regular intervals (3 min) in the outflow. The amount of methylene blue in the outflow was determined by spectrophotometric measurement (600 nm) and these data were used to plot real (experimental) residence time distribution (RTD) curves.

$$\varepsilon(\theta) = 1/2\sqrt{\mathrm{Pe}/\pi} \times \exp\left(\frac{-(1-\theta)^2 \times \mathrm{Pe}}{4\theta}\right) \text{ where } \mathrm{Pe} = (uL/D); \theta = t/\tau \qquad \textbf{Eq. VIII—2}$$

$$\varepsilon(\theta_D) = 1/2\sqrt{\mathrm{Pe}/\pi} \times \exp\left(\frac{-(1-\theta_\mathrm{D})^2 \mathrm{Pe}}{4\theta_\mathrm{D}}\right) \text{ where :} \qquad \textbf{Eq. VIII—3}$$

$$\theta_\mathrm{D} = t/\tau_\mathrm{D}; \tau_D = (V_R - V_D)/Q_L$$

$$\varepsilon(\theta) = \frac{N(N\times\theta)^{n-1}}{(N-1)!}\exp(-N\theta) \qquad \textbf{Eq. VIII—4}$$

The experimental data from PBR were obtained at hydraulic residence time of 16.7 min. The axial dispersion in PBR was evaluated by adjusting the dispersion parameter (*D*/*uL*) of the model (**Eq. VIII–2**) suggested by Levenspiel (1999). In order to obtain more information about the hydrodynamic behavior in this reactor, the experimental data from PBR were also simulated with a multiparameter model (**Eq. VIII–3**)

and a CSTR in series model (**Eq. VIII–4**) suggested by same author (Levenspield, 1999).

The RTD determination in the iGLR was done at gas flow rate of 0,25 L/min, which corresponds to the normal gas flow used in this reactor for continuous fermentation of alcohol-free beer (Lehnert et al, 2008), and at a hydraulic residence time of 39.2 min. The hydrodynamic behavior inside the iGLR was determined by adjusting the RTD curve to the CSTR in series model **Eq. VIII–4** suggested by Levenspiel (1999). The experimental values on both reactors were treated by non-linear adjustment using Solver from Excel (Microsoft Corp.). Solver was applied on the minimization of the square sum of the errors between the theoretical (model) and experimental values.

VIII.3.9 Fermentations

In the Chapter VII several continuous fermentations were performed either in iGLR or in PBR. To study the influence of yeast strain, carrier type and reactor design the fermentations done are presented in **Table VIII-3**.

Table VIII-3. Conditions used for optimizing continuous primary AFB's fermentation.

Reactor	**PBR**	**GLR**	**GLR**	**PBR**	**Batch**	**Batch**	**Batch**[a]
Yeast strain	*W96*	*W96*	*W96*	*⊿KGD2*	*⊿KGD2*	*W96*	Industrial
Carrier	Cc	Cc	SG	Cc	-	-	-
Temperature (ºC)	8	8	8	8	8	8/2	NA[a]

[a] NA – Information not available

The study of gas composition in primary continuous AFB fermentaiton was performed in a iGLR using SG as carrier (IV.3.5). The same reactor system and immobilization method was used in the study of the effect of ageing in continuous primary AFB fermentation (IV.3.6).

VIII.4 Results and Discussion

VIII.4.1 General considerations

It has been stated that continuous beer fermentation could, under favourable circumstances, produce a considerable economical benefit through time savings. In spite of this expectation, most of the industrial implementation attempts stumbled on flavours defects and engineering complexness of continuously fermented beers (Brányik et al., 2008; Mensour et al., 1992; Willaert et al., 2006). Conversely to regular beer, the flavour dissimilarity of AFB is usually better accepted by the consumers. Therefore, a suitably matched yeast strain with immobilization method (carrier) and process configuration could be an attractive alternative for the industry to satisfy the AFBs worldwide growing market.

VIII.4.1.1 Measurement and modeling of mixing regimes in two different bioreactors

From the point of view of reactor design there are two fundamental and many combined approaches to design a multi-reactor continuous beer fermentation system. The fundamental systems are based on either a series of continuous stirred-tank reactors (CSTR) or plug flow-like reactors (PFR), while the combined systems use reactor vessels with both types of mixing regime. The goal of these multi-reactor systems is to mimic the sequential substrate uptake and by-product formation typical for fermentation in batch (Brányik et al., 2008; Willaert et al., 2006). Unlike for regular beers, the continuous AFBs production requires only a single reactor system. Nevertheless, the knowledge of the hydrodynamic mixing regime inside the reactor for AFB production can help avoiding the potential engineering problems, choosing the most convenient carrier material and understanding the behaviour of immobilized yeast.

Comparing the experimental and theoretical residence time distribution (RTD) curves for both reactors, a nearly perfectly mixed regime and a plug flow with significant axial dispersion can be seen for the GLR and PBR, respectively (**Figure VIII-3**).

In the case of iGLR, the best fit for experimental tracer response was achieved with a non-linear adjustment of CSTR-in-series model (**Table VIII-4**), which represents an almost ideally mixed reactor as expected. The CSTR model adjusts the number of continuous agitated tanks in series to the experimental data. In this case the adjusted parameter was nearly 1, indicating the perfectly mixed character of the studied GLR. As dispersion model is normally applied for PFR it was useless to apply it for this type of reactor. On the other hand it is commonly known that more than 10 CSTR in series mimic well the plug-flow regime, which means that this model can be applied to PBR, where a plug-flow regime is expected.

All tested models (CSTR in series, dispersion with and without dead zones) can be adjusted to plug-flow regime. The initial observations of the experimental data indicated the presence of plug flow regime in our PBR, therefore in this case all models were applied (**Figure VIII-3** and **Table VIII-4**).

For the axial dispersion model, the fitting parameter D/uL = 0 corresponds to ideal plug flow, and D/uL = ∞ to ideal mixed flow. The obtained experimental dispersion coefficient for PBR (D/uL = 0.23) suggests the presence of a significant axial dispersion (**Table VIII-4**). This high dispersion was not obtained neither by the CSTR in series or by the dispersion models. Both failed in simulating the experimental data (**Figure VIII-3**). The PBR initially did not fit into the concept of ideally mixed or plug flow-like reactors. This difference indicated the presence of dead zones inside the PBR, which caused the CSTR and dispersion models to be beyond the limits of their validity (Levenspiel, 1999).

Table VIII-4. Hydrodynamic properties of packed-bed (PBR) and gas-lift (GLR) reactors.

Experiment/ Model	Parameter	GLR	Error[a]	PBR	Error[a]
Experiment	D/uL[d]	-	-	0.23	-
CSTR[b] in series	N[c]	1.05	0.14	5.07	4.54
Dispersion	D/uL[d]	-	-	0.16	10.47
Dispersion with dead zones	V_{DZ}[e]	-	-	437.97	0.79
	D/uL[d]	-	-	0.03	

[a] Sum of the errors between the experimental curves and theoretical models as obtained from Solver application.
[b] Continuous stirred tank reactor
[c] Number of CSTR in series
[d] Dimensionless dispersion parameter (u – linear velocity, L – height of the carrier bed, D – axial dispersion coefficient)
[e] Volume of dead zones (mL)

In order to achieve a better fit to experimental data, a multi-parameter model was applied. The chosen model was a modification of the dispersion model, taking into account the presence of dead zones, and described satisfactorily the experimental data (**Figure VIII-3A**). The modified dispersion model has two main parameters: the dispersion coefficient (D/uL) and the volume of dead zones – V_{DZ} (**Table VIII-4**).

The significant volume of dead zones inside the PBR (ca 33 %) both decreases the real working volume of PBR and hinders the circulation of the liquid phase inside the reactor. The occurrence of dead zones promotes the formation of non-productive areas with mass transport limitations. In addition these limitations can influence negatively the final product quality because the mass transfer limitations might lead to autolysis of starving cells (Verbelen et al., 2006; Virkajarvi and Linko, 1999).

Considering the PBR configuration the main dead zones may be at the bottom near the inflow, because the liquid was not well dispersed. In order to decrease the volume of dead zones in PBR a porous distribution layer (glass spheres, sand, etc.) can be inserted on the bottom of the reactor, promoting a better liquid flow distribution

throughout the cross section area of the system (Richardson et al., 2002).

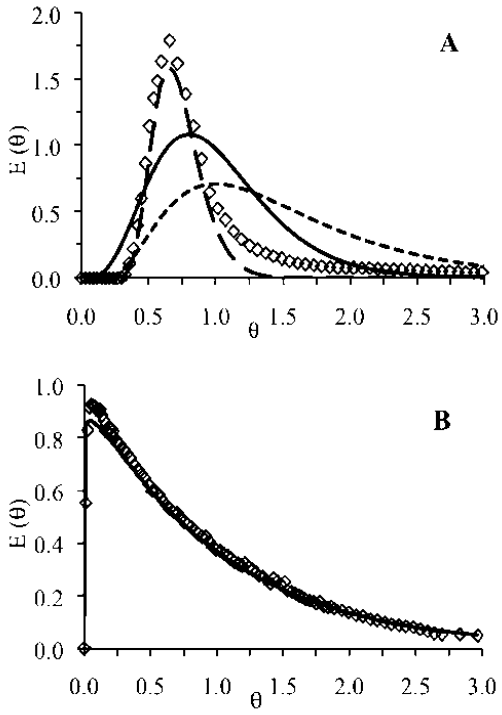

Figure VIII-3. Experimental residence time distribution (RTD) curves (◇) for PBR (A) and GLR (B) vs. mathematical simulations (models) of RTD curves: - CSTR in series model; - - - dispersion model; — — dispersion model with dead zones.

The size of carrier particles applied in PBR also influences the liquid flow distribution and consequently the utilization of bigger particles might reduce dispersion; as a result, a typical plug flow regime might be achieved if desired (Richardson et al., 2002). Generally, the granularity of the bed should reflect a compromise between the carrier and reactor size, biomass growth rate and the desired flow pattern inside the column.

VIII.4.2 Fermentations performance and flavour compounds

AFBs are often characterized by the lack of flavour compounds found in regular beers (Perpète and Collin, 1999a, 1999b). Therefore the two

strains studied in this thesis were evaluated based on total HA, ES and OA content, as well as HA/ES ratio. The comparison was made either between real or hypothetically diluted or concentrated AFBs. While dilution of more concentrated beers is nowadays a common practice, the hypothetical "concentration" of AFBs is based on a simplifying assumption that further fermentation would increase the content of each flavour active compound linearly by the same factor as that of ethanol.

VIII.4.2.1 Ethanol and higher alcohols

The final ethanol concentration at different fermentations (see...) was strongly influenced by the process conditions and the production strain.

The results obtained under comparable conditions (eg. batch fermentation) imply that the genetically manipulated ΔKGD2 strain produces less ethanol and at a considerably lower yield than the strain *W96* (**Table VIII-5**). The comparison of ethanol formation in continuous systems is less straightforward, since the trials differ in biomass content and dilution rates. However, the yield of ethanol formation by the ΔKGD2 strain in continuous systems is again significantly lower than for the strain *W96* (**Table VIII-5**).

In order to make easier the comparison of flavour active by-products (HA, ES and OA) formed in different systems two different analysis were made: (1) based on AFBs with different degree of attenuation and ethanol content and/or (2) on hypothetical products unified by the legally admitted maximum ethanol content (0.5% by volume or 3.945 g/L in the EU countries). These results are presented in **Table VIII-6** below.

The results indicate that the ΔKGD2 strain showed an increased HA formation, particularly when comparing the hypothetical potential for HA formation at unified 0.5% (vol./vol.) ethanol content (**Table VIII-6**).

Table VIII-5. Production conditions and basic parameters of real alcohol-free beers produced in continuous PBR and iGLR with SG and Cc as carriers, and in batch fermentations.

Reactor	PBR	GLR	GLR	PBR	Batch	Batch	Batch[a]
Yeast strain	**W96**	**W96**	**W96**	**ΔKGD2**	**ΔKGD2**	**W96**	**Industrial**
Carrier	**Cc**	**Cc**	**SG**	**Cc**	**-**	**-**	**-**
Temperature (ºC)	8	8	8	8	8/2	8/2	NAd
Dilution rate (hr^{-1})	0.30	0.07	0.28	0.15	-	-	-
X_{IBb} (g_{DB}/g_{DC})	0.05	0.19	1.20	0.07	-	-	-
X_{TOT}[c] (g/L)	4.8	3.8	17.5	8.1	1.08	1.26	NAd
% Ethanol (vol/vol)	0.50	0.39	1.14	0.25	0.22	0.36	≤0.50
Reducing sugars (g/L)	23.90	25.78	14.13	24.34	25.14	25.78	NAd
Yield[e] (g_E/g_{URS})	0.453	0.451	0.487	0.239	0.232	0.416	NAd

[a] Commercial AFBs produced in the Czech republic by limited fermentation using bottom fermenting yeast strains.;
[b] Immobilized biomass concentration ($g_{Dry\ Biomass}/g_{Dry\ Carrier}$).;
[c] Total biomass concentration.;
[d] Information not available.;
[e] Yield of ethanol ($g_{Ethanol}/g_{Utilized\ Reducing\ Sugars}$)

This applies both for limited batch and continuous PBR with corncobs (Cc). Simultaneously it can be seen that the real HA content in most of the AFBs produced under laboratory conditions was significantly lower than in the commercial products. The only exception is the strain *W96* immobilized in spent grains (SG) in GLR, which can be explained by the highest total biomass present (**Table VIII-5**) that, in turn, can be related with HA production (Willaert and Nedovic, 2006). The strain ΔKGD2 was able to produce amounts of HA comparable to industrial AFBs only when the hypothetical HA content corresponding to maximum allowed ethanol concentration was considered (**Table VIII-5**).

In terms of ES formation under comparable conditions (batch and PBR with Cc) the ΔKGD2 strain seems to be again superior to strain *W96*. The higher ester formation by ΔKGD2 strain is even more obvious for hypothetical AFBs with 0.5% (vol/vol) ethanol content (**Table VIII-6**). Under laboratory conditions the ES content of commercial AFBs was in

fact achieved only in the iGLR with strain *W96* and SG and theoretically it could be reached or surpassed by strain ΔKGD2 both in batch and continuous PBR with Cc (**Table VIII-6**).

The HA/ES ratio in regular beers is considered favorable in the range 3 to 4 (Kunze, 2004) but in the three analyzed commercial AFBs produced in the Czech Republic this ratio was in the range 4 to 10. Therefore all the real AFBs produced during this work are comparable to the commercial AFBs. Among them three continuously fermented products were relatively close (5.0-5.7) and one product (batch, ΔKGD2) was in the range for regular beers (**Table VIII-6**). The concentration of each individual HA and ES was below the taste thresholds found in regular beers (see **Table II-4**). On the other hand when compared with the thresholds in water, a general overproduction of isoamyl alcohol was observed both in continuous and batch systems. This fact was also verified for commercial Czech beers. This effect was not perceived in terms of the characteristic flavour on the tested samples. Some authors mentioned that the threshold of compounds in AFBs should be comparable to the threshold of the compound in water instead of comparing with the treshold in regular beers, as it is done by the majority of the studies (Perpète and Collin, 1999a). In this case, for all samples, the isoamyl alcohol has bigger concentration than the normal treshold in water and a strong banana flavour should be noted. However it was not detected even in the commercial Czech AFBs.. Therefore, and considering that regular beer thresholds are used by almost every studies (Brányik et al., 2005; Willaert and Nedovic, 2006) in the present thesis the same criteria were be used. In fact it is very important to evaluate the correct flavour componds' treshold in AFBs. The main reason is to have a correct evaluation of the influence that each compound has in the final AFB flavour. From **Table II-4** the treshold of ethanol in water is 990 mg/L while in regular beers it is 14000 mg/L. In AFB the maximum ethanol content allowed in EU countries is 3900 mg/L (**Table II-4**).

Table VIII-6. Higher alcohol (HA), Esters (ES) and Organic Acids (OA) content (mg/L) of real AFBs produced in continuous PBR and iGLR with SG and Cc as carriers, and in batch fermentations.

Reactor	**PBR**	**GLR**	**GLR**	**PBR**	**Batch**	**Batch**	**Batch[a]**
Strain	**W96**	**W96**	**W96**	**ΔKGD2**	**ΔKGD2**	**W96**	**Industrial**
Carrier	**Cc**	**Cc**	**SG**	**Cc**	**-**	**-**	**-**
Isobutanol	0.31	0.20 0.26[b]	1.15[c]	0.47 0.94b	0.69 1.57b	0.26 0.36b	0.82±0.18
1-Butanol	0.03	0.08 0.1 [b]	-	-	-	-	0.01±0.01
Amyl Alcohol	0.93	0.38 0.49 [b]	2.06 [c]	0.66 1.32 [b]	0.21 0.48 [b]	0.37 0.52 [b]	1.64±0.35
Isoamyl Alcohol	2.92	2.69 3.44 [b]	3.87 [c]	2.91 5.82 [b]	2.39 5.43 [b]	2.16 3.0 [b]	5.78±0.75
2-Phenylethanol	0.24	0.28 0.36 [b]	1.20 [c]	0.24 0.48 [b]	0.43 0.98 [b]	0.15 0.21[b]	1.73±0.82
Total HA	4.43	3.62 4.65 [b]	8.32 [c]	4.27 8.55 [b]	3.71 8.44 [b]	2.94 4.09[b]	10.3±2.14
Ethyl acetate	0.79	0.30 0.38 [b]	1.36 [c]	0.56 1.12 [b]	0.74 1.68 [b]	0.31 0.43[b]	1.56±0.55
Amyl acetate	0.04	-	0.02 [c]	0.08 0.16 [b]	0.06 0.13 [b]	-	0.01±0.02
Isoamyl acetate	0.06	-	0.12 [c]	0.11 0.22 [b]	0.11 0.25 [b]	-	0.18±0.09
Ethyl caprylate	-	0.10 0.13 [b]	0.04 [c]	-	0.20 0.45 [b]	-	0.01±0.01
2-Phenylethyl acetate	-	-	0.06 [c]	-	-	-	0.02±0.03
Total ES	0.89	0.40 0.51 [b]	1.60 [c]	0.75 1.50 [b]	1.11 2.52 [b]	0.31 0.43 [b]	1.79±0.68
HA/ES	5.0	9.2	5.2	5.7	3.35	9.5	7.1±3.2
Pyruvate	23.3	22.5 28.8 [b]	13 [c]	21.8 43.6 [b]	29.8 67.7 [b]	38.4 53.3[b]	34.5±6.4
Citrate	85.3	77.7 99.6 [b]	83.6 [c]	81 162 [b]	145 329.5 [b]	129 179.2 [b]	111.3±22.2
Malate	40.5	65 83.3 [b]	32.2 [c]	24 48 [b]	19.5 44.3 [b]	87.8 122 [b]	87.2±25.6
Lactate	66.6	46.8 60 b	44.3 [c]	214.6 429.2 [b]	276 627 [b]	57.8 80.3 [b]	156±48.4d
Succinate	8.6	12.2 15.6 [b]	9.8 [c]	71.8 143.6 [b]	124 282 [b]	45 62.4 [b]	12.4±6.7
Propionate	9.0	7.8 10 [b]	2.8 [c]	7.3 14.6 [b]	10.7 24.3 [b]	14 19.4 [b]	7.4±1.6
Total OA	233.4	232 297.3[b]	185.7[c]	420.4 841[b]	605 1375[b]	372 516.7[b]	408.9±53

[a] Three different commercial AFBs produced in the Czech republic were analyzed to obtain the average content of their flavour active compounds.; [b] Values were obtained after multiplication of the experimental higher alcohol concentration by a factor corresponding to the ratio between the maximum allowed (0.5% (vol/vol)) and experimentally determined ethanol content for the given AFB.; [c] Values were obtained after dilution of the fermented AFB to ethanol content of 0.5% (vol/vol.); [d] Acidification with lactic acid was indicated on two out of three commercial AFBs used in this work

Therefore it is essencial to determine new tresholds for the ethanol range normally found in AFBs; this was not found in the literature, and it was not the main scope of this thesis.

In order to minimize the risk of microbiological contamination, the pH of wort in barrels was adjusted to 4.5 with lactic acid prior to fermentation (see section IV.2.1). As lactate is not a fermentation by-product, it was excluded from the data shown in **Table VIII-6**. In terms of OA formation the yeast strain with disruption in the KGD2 gene behaved, both in limited batch and continuous (PBR with Cc) fermentations, as expected (Selecky et al, 2003). It showed significantly higher OA formation as compared to strain *W96* and commercial AFBs (**Table VIII-6**). The genetically manipulated strain produced amounts of OA (except malate) in concentrations comparable with those found in regular alcoholic beers (see Chapter.II.4.3); this happened both in batch and continuous operation (Briggs et al., 2004).

Besides, the formation of lactate by ΔKGD2 strain was higher than the overall content (lactate as brewing by-product plus lactate added for acidification) of this OA in commercial AFBs (**Table VIII-6**). The total OA content attained the highest values in limited batch fermentation, for both yeast strains (**Table VIII-6**). The *W96* strain showed a slightly higher formation of citrate and malate, both in batch and continuous systems, while the average OA concentration in commercial AFBs revealed a relatively low succinate content (**Table VIII-6**).

VIII.4.3 Effect of yeast strain

The AFBs produced by the two studied strains (*W96* and *ΔKGD2*) were rather different in all analyzed parameters. Their different behavior can be shown on the easily comparable examples of limited fermentation in batch mode and continuous fermentation in PBR with corncobs (Cc) as carrier. The *ΔKGD2* strain showed (in both systems) higher HA, ES and OA (**Table VIII-6**) formation, particularly when comparing the hypothetical potential for formation of volatiles at an

unified 0.5% (vol/vol) ethanol content. Understandably, the total organic acid (OA) formation by the *ΔKGD2* strain surpasses the lager yeast strains due to the OA overproduction caused by incomplete TCA cycle operation (Zawislak et al., 1999; Selecky et al., 2003). Keeping in mind that volatiles (HA, ES) and OAs are desirable for the flavour of AFBs the results show that the performance of the *ΔKGD2* strain was significantly better than that of *W96* in limited batch fermentation, while this advantage slightly diminished in continuous PBR with Cc. This slight reduction in continuous PBR proved the importance of testing in continuous systems yeast strains that have good performance in batch (Selecky et al., 2003). The importance of a careful strain selection for AFB production can be demonstrated also by comparing the products of our two studied strains with the average composition of three commercial AFBs produced by limited batch fermentation. While the strain *W96* seems to be suitable for AFB production only in continuous GLR with SG, the *ΔKGD2* strain has a potential for sufficient OA and volatile formation during both continuous (PBR with Cc) and batch AFB fermentation. The fact that different yeast strains produce volatiles and OAs in different proportions supports the promising potential of strain selection for improving the quality of industrial AFBs.

Besides the favorable fermentation performance, the *ΔKGD2* strain turned out to be unable to firmly adhere to SG. The reason for low biofilm formation by *ΔKGD2* strain on SG lies probably in different surface properties of these cells together with iGLR typical turbulent regime (especially in the riser). The practical consequence of this fact was that the use of *ΔKGD2* strain in continuous GLR with SG failed. However, the choice of a proper reactor and carrier type (PBR with Cc) showed that a well performing, but loosely adhering strain can be used in a continuous fermentation system. In PBR the yeast cells immobilization method is slight different than in iGLR. In iGLR if the adsorption is weak, the loosely attached cells may be more easily released to the fermentation bulk due to the turbulence typical of this type of reactors. In the PBR the liquid velocity is quite smaller, consequently both bulk turbulence and velocity are lower in this type of

reactor. Then, biofilm formation in the carrier is favoured (high tickness) and more yeast cells are retained inside the PBR . In addition, sedimentation of cells may be present thus allowing even higher yeast cell concentrations to be reached. This is clear if the yeast cell profile trough the reactor's length is analysed (**Figure VIII-4**).

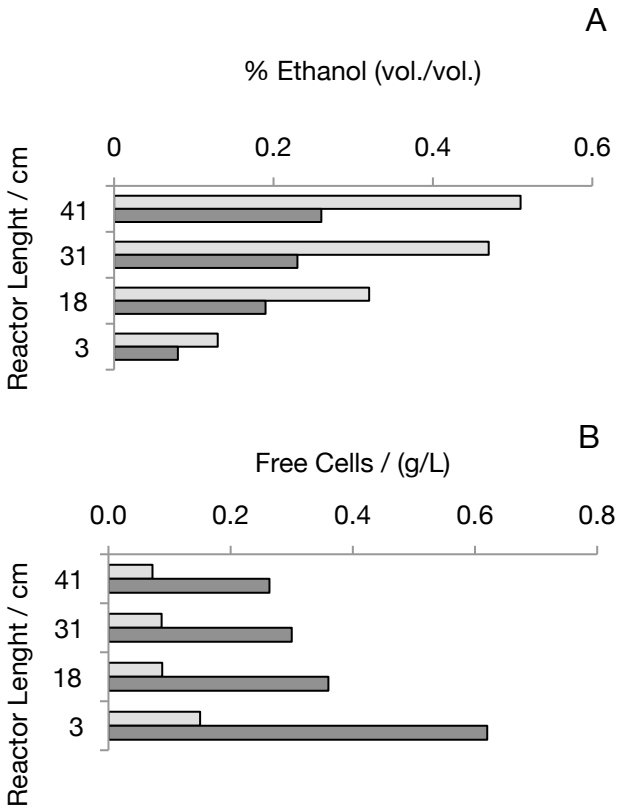

Figure VIII-4. Ethanol (A) and free cells (B) concentration troughout the PBR length (from 0 cm to 41 cm) for *S. pastorianus* strain *W96* (□) and *S. cerevisiae* BY4743 (■)

Figure VIII-4 shows that the biomass concentration is higher at the PBR bottom for both strains. The main reasons for this phenomenon are: (1) high sugar concentration in that area; (2) near fresh wort inflow with high dissolved oxygen; (3) sedimentation of yeast cells. The first two factors increase yeast growth intensity and the third one increases yeast cell in the bottom by sedimentation of cells that are detached from higher positions of the PBR. Even considering these reasons, it is very difficult to assess the real impact of each factor in the final biomass concentration at the reactor bottom.

VIII.4.4 Effect of reactor design and carrier type

The combined effect of reactor design and carrier material on formation of flavour active compounds (HA, ES, OA) can be shown by the most suitable strain: the bottom fermenting lager used (strain *W96)*, which was tested in two different continuous reactors (PBR, iGLR) with two carriers (Cc, SG), plus in limited batch fermentation.

As previously stated, the strain *W96* tends to produce lower amounts of HA and ES (**Table VIII-6**) both in continuous and batch arrangement comparing to *ΔKGD2* and industrial strains. However, in the iGLR with SG, the strain *W96* produced an AFB with HA (8.32 mg/L) and ES (1.6 mg/L), after dilution of beer to 0.5% (vol./vol.) ethanol, comparable with AFBs produced by industrial batch process. As expected, the productivity in continuous system (3.6 h residence time) is significantly higher than that in batch operation (72 h residence time).

The different composition of AFB from continuous iGLR with SG, comparing to other trials with strain *W96*, can be most probably ascribed to the significantly higher total biomass concentration with a large proportion of immobilized biomass (**Table VIII-5**). Although adhesion belongs to the most gentle and natural immobilization methods (Smogrovicová and Domény, 1999), the immobilized biomass present on SG in a form of thick yeast biofilm is certainly exposed to severe mass transfer limitations and specific microenvironment with concentration gradients of substrates and products studies (Brányik et al., 2005). The direct evaluation of immobilization effects on cell physiology is difficult, but an increased production of HA and ES has already been described in the case of cells immobilized by attachment (Shen et al., 2003). The performance of the strain *W96* in continuous iGLR with SG as a carrier was an exception, proving that even a strain that seems to be less suitable for AFB production can under favorable conditions produce an acceptable final product (**Table VIII-6**).

The hypothesis that the biofilm thickness may play an important role in by-product formation by strain *W96* can be also supported by the

experiment with the same strain in the iGLR with Cc. In this case, the biomass concentration was lower than in the continuous GLR with SG (**Table VIII-5**) and it led to a product with a similar composition as achieved by the strain *W96* in batch and PBR with Cc (**Table VIII-6**). Nevertheless in the iGLR with Cc the effect of the low dilution rate (0.07 hr^{-1}, **Table VIII-5**) has to be considered as well, because at prolonged residence time of wort in the continuous reactor a more significant stripping of volatile compounds by driving gas can be expected (Lehnert et al., 2009; Virkajarvi and Linko, 1999).

Another process parameter that significantly differs between continuous immobilized cell systems and batch fermentations and simultaneously strongly influences the production of HA, ES and OA is the oxygen supply (Lehnert et al., 2008). The total oxygen load of wort was approximately 8 and 3 mg/L for batch and continuous systems, respectively. However, the supply of oxygen not only differs on the total amount but also in its supply during the fermentation time. Batch fermentation is characterized by high initial oxygen concentration (ca. 8 mg/L) and subsequent decline while in the continuous systems oxygen is constantly supplied (0.2-0.9 mg/(L h)) into the fermentation system through wort inflow.

The content of OA was the highest for both yeast strains in limited batch fermentation (**Table VIII-6**). Therefore this difference can be most probably ascribed to the combined effect of immobilization (changes in metabolic functions induced by contact of cells with solid carrier) and reactor properties (supply of CO_2 and O_2, reactor mixing) (Shen et al., 2004). The differences in oxygen supply to continuous and batch fermentations can be important as regards OA formation since the degree of respiro-fermentative metabolism influences the activity of enzymes involved in the TCA cycle (Yamauchi et al., 1995).

VIII.4.5 Effect of gas-phase in the final product

Both purification processes of CO_2 or industrial CO_2 are expensive and its utilization at industrial scale must reduce at minimum the industrial needs. That is why it is extremely important to achieve a compromise between the minimum gas-flow and a good immobilization load capacity (Brányik et al., 2004b). In order to maintain anaerobic conditions during primary fermentation CO_2 is usually employed. Generally, in systems using iGLR for primary beer or AFB fermentation, air is initially injected to promote growth, which will increase immobilization, then the gas-phase is gradually changed to pure CO_2 (Brányik et al., 2006, 2004a; Lehnert et al., 2008, 2009).

This section discusses the effect of gradually changing the gas-phase from air to CO_2 and the use of other inert gases, which can maintain the anaerobic conditions (such as nitrogen, N_2). Dissolved CO_2 can affect yeast cells metabolism and performance by: (1) altering membrane structure influencing the compound's diffusion; (2) altering the structure of amino acids, peptides and proteins; and (3) influencing enzymes responsible for carboxilation/descarboxilation reactions. The CO_2 dissolution depends on reactor desing, presence/absence of solid particles, pH, temperature, and medium properties. High concentrations of dissolved CO_2 decrease the pH in the bulk and enter in the yeast cell cytoplasm. In order to maintain cytoplasm properties the cells spent energy to force CO_2 to leave and a decrease in HA and ES formation is reported (Shen et al., 2004). On the other hand N_2 is an inert gas at general temperatures and pressure. At 10 ºC and atmospheric pressure N_2 solubility in water is around 24 mg_{N2}/kg_{H2O}, while for CO_2 at same conditions is around 25 000 mg_{CO2}/kg_{H2O}. In addition, N_2 seems to be economically better than CO_2. Considering the availability of N_2 in atmosphere it will be cheaper for brewery industry to collect and purify N_2 instead of CO_2. Considering this and the adverse effects of CO_2 on cell wall membrane it was suggested to study the effect of different gas-phases in primary AFB fermentation in an iGLR.

It is also very important to understand the oxygen supply in continuous fermentations of beer because it influences yeast cells metabolism and consequently the formation of active volatile and flavour compounds (HA, ES). The influence of the gas-phase in beer flavour was tested in order to understand how could the gas-phase influence the volatile compounds. For that several mixtures of air, CO_2 and N_2 were tested (20% CO_2 vs 80% air; 50% CO_2 vs 50% air;; 80% CO_2 vs 20% air; 100% CO_2; 50% CO_2 vs 50% N_2; 100% N_2). During these fermentations samples for HA and ES analysis were taken when steady state was achieved (section VIII.3.4). Parameters as reactor and wort barrel temperature (8 ºC) and residence time (14.3 h) were kept constant. Considering the differences in solubility of N_2 and CO_2 in the wort, and knowing that CO_2 decreases the pH in the bulk, a change in pH was expected, thus pH was monitored daily. **Figure VIII-5A** shows that when CO_2 was used the bulk pH was slighty below 4.5, even keeping the inflow pH constant at 4.5; the opposite was observed when pure N_2 was injected. In terms of free biomass it was detected an increase of 50% on free biomass concentration when pure N_2 was used. On the other hand immobilized biomass did not show real differences either in pure CO_2 or N_2. These differences can be explained by the CO_2 dissolution in the bulk medium. The effect of CO_2 on cells growth has been verified to reduce free and immobilized cell growth by 30% and 10% respectively (Shen et al., 2004). In our case the inexistence of changes in iBio concentration can be explainded by differences in the immobilization method and by the method use to determine immobilized cells mass, which has an error of 6.3% (section VII-3.6.3).

Sugar uptake and ethanol formation patterns show that when the ratio of CO_2 in CO_2/AIR mixture was increased (from the 15th day to the 25th day) sugar consumption decreases mainly the maltose uptake, which led to a decrease of ethanol production (**Figure VIII-6A/B**). By the analysis of **Figure VIII-5B** and **Figure VIII-6** it is possible to relate maltose consumption with free-cells concentration, under anaerobic conditions. Between the 31st day and the 35th day, when pure N_2 was injected, the increase on free-cells concentration was accompanied by

a simultaneous decrease of maltose concentration.

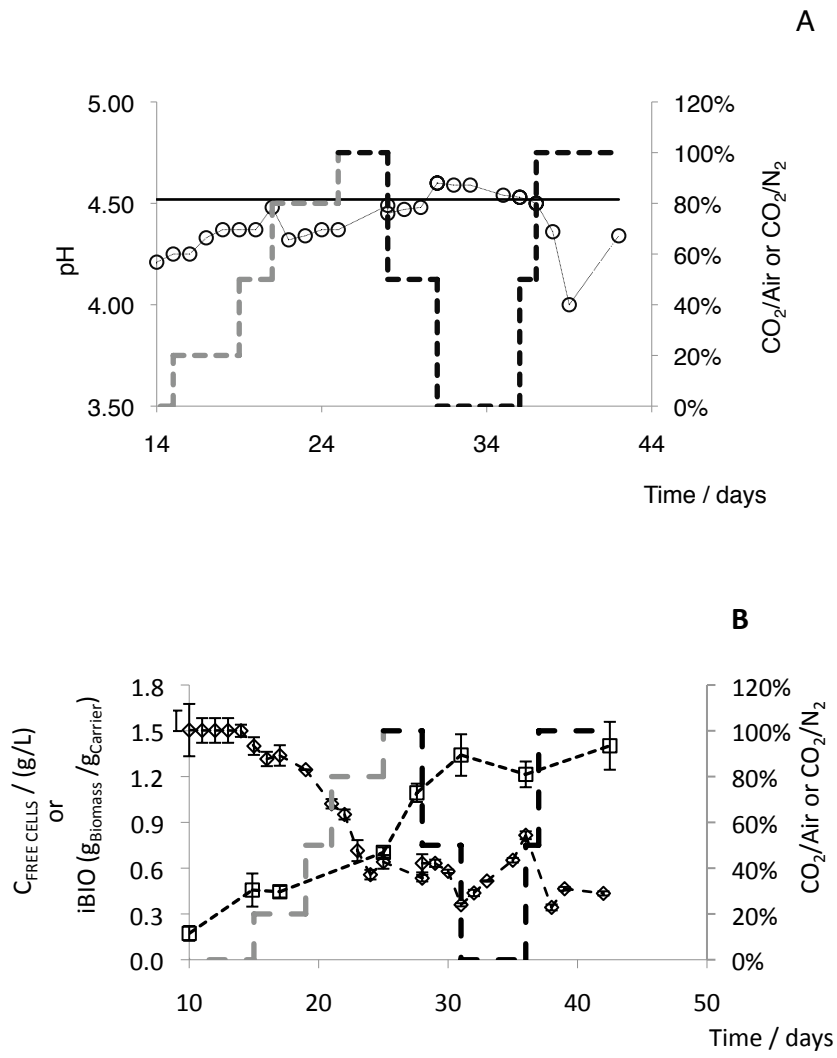

Figure VIII-5.A – pH evolution vs gas composition during primary AFB fermentation; B – Free and Immobilized biomass evolution vs gas-phase composition; ○ - pH; □ - iBIO ($g_{BIOMASS}/g_{DRY\ CARRIER}$); ◇ - Concenration of free cells (g/L); -- : CO_2/Air mixture; **--** : CO_2/N_2 mixture; ‑ : Wort barrel pH.

Maltotriose concentration was constant and around 5 g/L under anaerobic conditions. As for glucose concentration, a slight relation with immobilized biomass can be observed indicating that immobilized biomass consumes preferably glucose. Immobilized cells are reported to have changes in cell wall composition but these changes do not depend on the gas-phase (Shen et al., 2004). The gas-phase composition can affect the membrane solubility and selectivity to some

compounds, leading immobilized cells to consume glucose instead of maltose. However, this relation is not straightforward as it occurs for maltose and free cells and further studies must be undertaken.

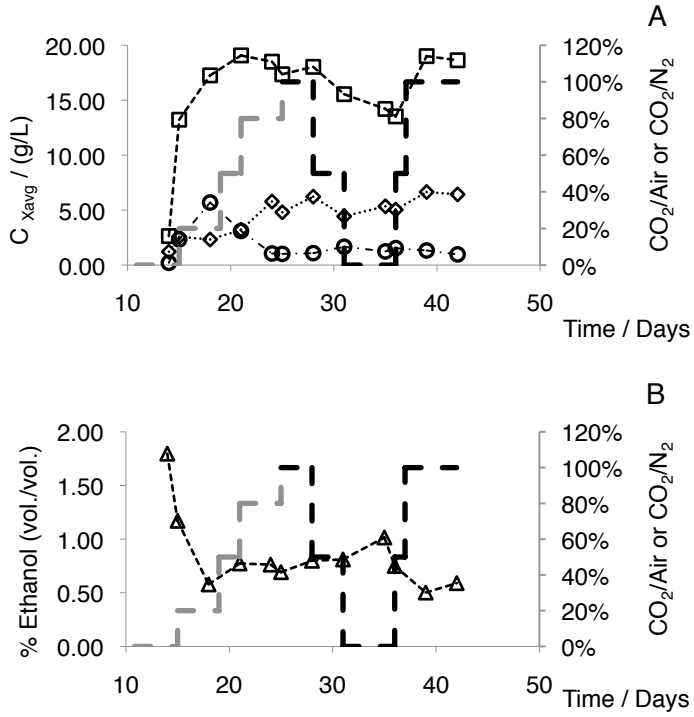

Figure VIII-6. A – Sugars evolution vs gas composition during primary AFB fermentation; B – Ethanol evolution vs gas-phase composition; ○ - Glucose; □ - Maltose; ◇ - Maltotriose;△ - Ethanol ; -- : CO_2/Air mixture; **--** : CO_2/N_2 mixture.

In addition, the evaluation of some volatile compounds was performed and is presented in **Table VIII-7**. As it was explained in section VII.3.7.3 the method used in this section is different from the method proposed by the European Brewery Convention (EBC, 1987). It is important to notice that the methods used are: (1) valid and reported by other authors; (2) all samples were analysed by the same procedure and therefore are perfectly comparable. Moreover the range of the values present in **Table VIII-7** for several compounds (e.g. 1-propanol and ethyl acetate) is similar to the values present in literature as displayed in **Table II -4** (Lehnert et al., 2008).

A first look at **Table VIII-7** shows that ethanol production exceeded

the maximum allowed in EU legislation for AFBs (CCE, 1992). In fact in brewing industry beers made in batch are not exactly equal in terms of ethanol content, and in order to obtain a standard final product some processes are applied. When, at the end of a batch fermentation, the final ethanol content of a traditional beer is higher than usual this beer can be diluted in sterilized water or mixed with other beer from other batch fermententation in order to obtain the required ethanol content. In our case, to achieve the legal ethanol content a dilution is required. The theoterical results from this dilution (considering for each compound the same factor as for ethanol) are presented in brackets in **Table VIII-7**. Therefore, this corrected values are the ones used to be compare with the literature and with the results obtained for the commercial Portuguese AFBs analysed (Comm1 and Comm2).

An analisys on **Table VIII-7** shows a strong influence of the conditions used (gas-phase change) on the final concentration of HA. The total production of HA is in the same range of commercial beers but below the treshold values (**Table II–4**). Generally, the total content of HA in continuous AFB produced is higher that Comm1 and lower than Comm2. In Comm1 the total HA content is mainly supported by the content of 2-phenylethanol (flavour treshold: 125 mg/L in Meilgaard (1975)), which is quite high even when it is compared with the content of this alcohol in commercial Czech AFBs (**Table VIII-6**).

Among the continuous AFB samples, as expected, the HA production is higher when air is present. This is similar to the experiments performed by Lehnert et al. (2008), who demonstrate an increase of HA with an increase of OTR. As explained, the OTR depends both from the initial oxygen on the inflow wort and the transfer from the gas-phase to the fermentation bulk. In our case the liquid flow in this situation was constant therefore only differences in the gas-phase are considered.

Comparing the two anaerobic gas-phases (pure N_2 with pure CO_2) it is possible to observe that with pure N_2 the amount of total HA is higher than with pure CO_2. Considering the high solubility of CO_2 and its adverse effects it is believed that yeast cells in the presence of high

amounts of dissolved CO_2 alter their metabolism to counter-balance such CO_2 adverse effects, leading to an underproduction of HA. Moreover the HA is related to yeast metabolism intensity, which was higher in pure N_2 than in pure CO_2 (**Figure VIII-5**). The values of total HA obtained when pure CO_2 (9.7 mg/L) was applied is similar to the values obtained previously (8.32 mg/L in **Table VIII-6**) when SG were used as carrier in an iGLR.

Concerning the ES content in **Table VIII-7** it can be observed that they are in the same range of commercial AFBs and below their threshold (**Table II 4**). As reported in chapter II (section II.4.2) ES prodution is influenced by oxygen content and the metbolism intensity (Lehnert et al., 2008; Shen et al., 2003; Van Iersel et al., 1999; Willaert and Nedovic, 2006). In our case low ES production occurs in the presence of air, being higher when in presence of N_2 or CO_2. When in the presence of air a dual effect occurs, which influences ES synthesis. In one hand yeasts' metabolism is higher (high HA produciton), but in the other hand the presence of oxygen represses the ATTase activity. In the presence of oxygen yeast cells metabolism is driven to repiratory metabolism and away from fermentative metabolism. Therefore the ideal situation is to achieve a condition where yeast metabolism is increased in anaerobic (or close to anaerobic) conditions. As showed before (**Figure VIII-5** and **Figure VIII-6**) in the presence of N_2 there was an increase of yeast cells in our iGLR (mainly free cells). This is an indicator that when N_2 is used as gas-phase in iGLR less stress is induced and yeast metabolism increases. In addition, as there is few oxygen available (only the dissolved oxygen from the inflow) the ATTase activity is not negatively influenced. Therefore it is not surprising that the best condition as far as ES production is concerned was achived when pure N_2 was injected in the iGLR. As found by Lehnert and co-workers (2008) it is important that some oxygen is present (for HA production and sterols synthesis) in continuous AFBs production. However it is also important to reduce the adverse effect of CO_2 in the fermentation performance and that was achieved with N_2. Nevertheless CO_2 is an important compound in beer flavour being considered one of

the primary flavour constituents (Briggs, et al. 2004). Therefore an AFB produced only in the presence of N_2 will lack the CO_2 influence in the final AFB flavour. In fact this was confirmed by the daily degustation test performed. However this was just a mere indication and of course at industrial scale CO_2 can always be added. Of course CO_2 is expensive but adding only CO_2 at the end of the process will reduce the costs to minimum values as its injection can be fully controlled. Observing the composition of the different analysed ES (**Table VIII-7**) it can be verified, as expected that ethyl acetate is in highest amount being followed by ethyl caprylate. If ethyl acetate is in the same range in continuous and commercial AFBs the opposite does not occur with ethyl caprylate. The synthesis of this specific ES is not yet fully understood, as well as their influence in AFB final flavour (Brányik et al., 2008; Verstrepen et al., 2003; Willaert and Nedovic, 2006). However it seems that immobilization induces its production. In the reactor used (iGLR) there are phenomena, such as gas stripping, that should be taken into account because they may reduce the amounts of volatile compounds in the final product. Macieira (2008) found that losses of volatile compounds by gas stripping mainly occur for aldehydes and diacetyl (higher than 60% for $D \leq 0.2\ h^{-1}$) while such losses are reduced for ES (around 30% in similar conditions). The exception in ES was ethyl caprylate, with losses by stripping of up to 50% ($D \leq 0.2\ h^{-1}$). Considering that the gas composition is not changing significantly the gas stripping, it can be concluded that ethyl caprylate formation is somehow induced in immobilized yeast in a continuous AFB production process using SG as carrier and an iGLR. However, and as ES synthesis is also strain specific, this result can also be a characteristic of the strain used in this section (see section VII.3.1).

Table VIII-7. Mean concentration and associated error (p=0.05) of volatile compounds during different stages of continuous fermentations.

Compound	100% Air	20% Air and 80% CO_2	50% CO_2 and 50%N_2	100% N_2	100% CO_2	Comm.1	Comm2.
Ethanol (g/L)	9.2 (3.9)	5.4 (3.9)	6.4 (3.9)	5.2 (3.9)	4.6 (3.9)	< 3.9	< 3.9
1-propanol (mg/L)	4.8±0.4 (2.0)	2.8±0.6 (2.0)	2.2±0.4 (1.3)	2.7±0.5 (2.0)	1.8±0.2 (1.5)	1.0±0.1	0.9±0.1
2-methyl-1-propanol (mg/L)	3.1±0.2 (1.3)	1.2±0.1 (0.9)	1.5±0.1 (0.9)	3.7±0.7 (2.8)	1.1±0.3 (0.9)	0.7±0.3	1.2±0.2
Amyl-alcohol (mg/L)	2.1±0.7 (0.9)	1.5±0.2 (1.1)	1.6±0.4 (1.0)	3.2±0.3 (2.4)	1.4±0.0 (1.2)	0.6±0.1	1.5±0.3
Isoamyl-alcohol (mg/L)	14.1±2.3 (6.0)	11.1±1.8 (8.0)	8.4±1.3 (5.1)	11.4±1.6 (8.6)	5.7±0.4 (4.8)	2.7±0.3	7±1.2
2-phenylethanol (mg/L)	3.9±0.6 (1.7)	2.8±0.9 (2.0)	2.2±0.4 (1.3)	2.9±0.9 (2.2)	1.4±0.8 (1.2)	0.9±0.4	25.4±2.5
tyrosol* (µg/L)	3.7±0.5 (1.6)	2.1±0.9 (1.5)	2.7±1.3 (1.6)	6.0±2.3 (4.5)	tr	tr	24.7±5.2
Total HA	28 (11.9)	19.4 (14.0)	15.9 (9.7)	23.9 (17.9)	11.4 (9.7)	5.9	36
ethyl acetate (mg/L)	1.6±0.7 (0.7)	1.2±0.3 (0.9)	2.1±0.6 (1.3)	5.2±0.5 (3.9)	0.9±0.3 (0.8)	1.5±0.2	4.0±1.1
Isoamyl acetate* (µg/L)	22.1±1.5 (9.4)	9.6±0.7 (6.9)	44.7±5.2 (27.2)	199.7±105.8 (149.8)	22.5±1.6 (19.1)	14.2±0.4	297.4±148.
Ethyl caprylate* (µg/L)	225.2±8.8 (95.5)	109.6±12.0 (79.2)	378.4±72.2 (230.6)	639.7±338.4 (479.8)	600.8±40.9 (509.4)	3.9±1.1	67.3±25.6
2-Phenylethyl acetate* (µg/L)	130.5±2.6 (55.3)	22.3±1.9 (16.1)	209.2±14.8 (127.5)	163.5±74.6 (122.6)	44.4±3.6 (37.6)	12.0±0.1	88.7±36.8
ethyl hexanoate* (µg/L)	67.1±5.2 (28.4)	32.9±1.5 (23.8)	66.4±6.8 (40.5)	134.5±71.5 (100.9)	78.0±5.0 (66.1)	3.4±0.2	52.3±28.2
ethyl decanoate* (µg/L)	41.9±4.5 (17.8)	11.8±2.6 (8.5)	134.2±27.2 (81.8)	252.8±153.2 (189.6)	270.8±16.2 (229.6)	4.7±1.4	8.0±3.8
Total ES	2.1 (0.9)	1.4 (1.0)	2.9 (1.8)	6.6 (4.9)	1.9 (1.6)	1.6	4.6
HA/ES	12.6	13.8	5.1	3.5	5.8	3.8	7.8
acetaldehyde (mg/L)	8.7±2.6 (3.7)	5.9±2.0 (4.3)	3.0±0.2 (1.8)	3.7±0.8 (2.8)	2.0±0.3 (1.7)	3.7±1.8	2.0±0.7
Total AL	8.7 (3.7)	5.9 (4.3)	3.0 (1.8)	3.7 (2.8)	2.0 (1.7)	3.7	2.0

Legend: In brackets are present the theoretically values obtained if a dilution of the fermented AFB was done to obtain an ethanol content of 0.5% (vol/vol) or 3.9 g/L; Comm1 and Comm2: Commercial Protugues AFBs.

Finally **Table VIII-7** also shows the amount of aldehydes. As expected in the presence of air (higher metabolism) the acetaldehyde concentration is higher. However, in the absence of air the values of total aldehydes are comparable with the commmercial beers and below the threshold. As in pure N_2 the yeast growth increased, an increase of acetaldehyde was also expected, which accordingly to the data in **Table VIII-7** was not observed. Aldehydes are responsible for the worty off-flavours and as their threshold is low (10 mg/L, see **Table II-4**), they contribute largely for AFBs off-flavours. Studies performed in iGLR by Lehnert and co-workers (2008) showed that aldheydes losses by gas stripping are very high for this reactor design (above 80%), which is one more advantage of using iGLR for continuous AFB production (Lehnert et al., 2008; Macieira, 2008).

VIII.4.6 Effect of ageing: preliminary studies

The continuous fermentation for testing ageing effect on fermentation performance and in yeast physiology was divided in two periods (**Figure VIII-7**):

A – In the first period carrier losses were replaced, maintaining the amount of carrier inside the reactor approximately constant;

B – In the second stage no carrier was added; this was considered as an ageing period.

This allowed comparing the two situations, being the first 33 days (Period A) described as a closed steady-state, while the subsequent 23 days (Period B) characterised by a gradual ageing of the immobilized biocatalyst. After the ageing period one litre of reactor contents (ca. 1/3 of the total reactor's volume), including spent grains (ca. 8% (vol./vol.) and medium was replaced (at the 56th day); this allowed to understand better the effect of carrier replacement that occurred during period A.

Figure VIII-7 shows the evolution of carrier inside the reactor and immobilized biomass at 8 ºC. Immobilized biomass accumulation finished after approximately 14 days, attaining a maximum concentration of approximately 1.7 $g_{biomass}/g_{dry\ carrier}$, followed by a gradual decrease to around 1.2 $g_{biomass}/g_{dry\ carrier}$, value at which an equilibrium was established (**Figure VIII-7**). The 1/3 of the reactor volume replaced by a suspension of clean carrier suspended in synthetic model medium led to a sudden decrease of the total immobilized biomass. However, this was subsequently followed by a gradual adhesion of cells onto the clean spent grain particles resulting in an increasing amount of immobilized biomass. The carrier losses that occur due to outflow losses (an average of 0.25 $g_{DRY\ CARRIER}$/day was considered) and immobilized biomass samples were monitored and controlled.

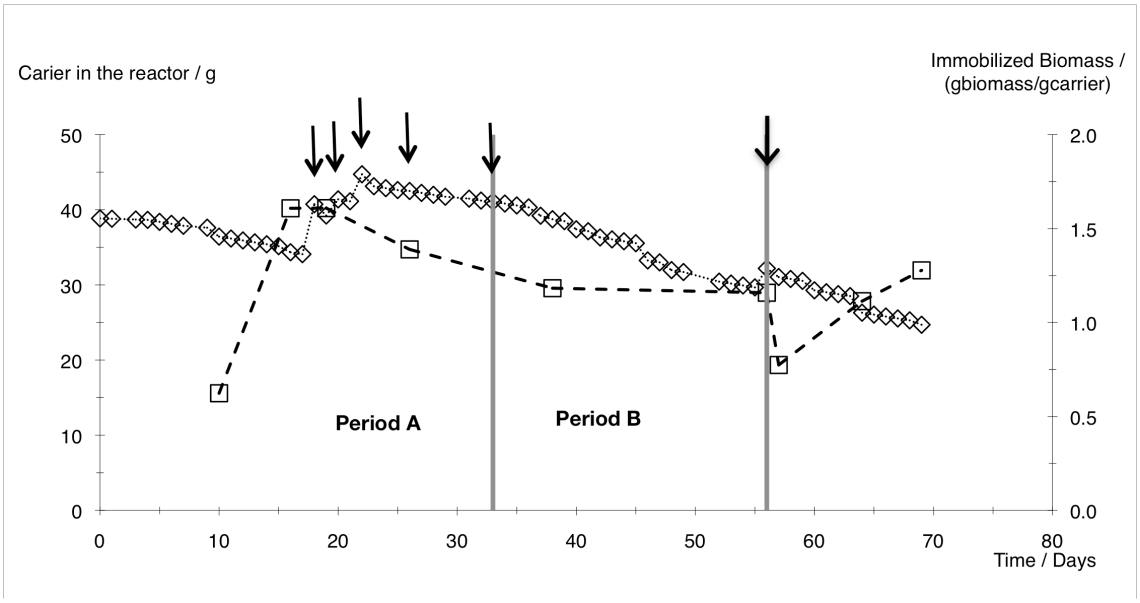

Figure VIII-7. Variation of immobilized biomass concentration (□) and carrier amount inside the reactor (◇) during the experiment. Black arrows identify carrier addition at fermentation days (left to right): 18th (6.9 g); 20th (2.4 g); 22nd (3.8 g); 26th (3.8 g); 33rd (2.9 g) and 56th (12.9 g).

During the whole continuous fermentation experiment the free cell viability remained relatively constant. A slight decrease was observed from approximately 92.5% to 88% viable free cells until the 17th day of

fermentation, remaining relatively constant around the last value for the rest of the time. This equilibrium results from the balance between yeast cell growth and yeas cells wash-out from the reactor. Regarding the viability of immobilized cells, it was observed that under the conditions of Period A the viability (± 85%) was relatively constant, however when the carrier replacement stopped during the second period (Period B), a decrease in immobilized cell viability was detected up to 77% of cell viability. After the carrier replacement, the immobilized biomass increased again to values similar to those existing at the end of Period B. This can be explained by the mechanism of adhesion of the new cells onto spent grain particles (Brányik et al., 2004a). When the free biomass adhesion to spent grains restored the maximum immobilized biomass concentration (69th day of fermentation) the viability of immobilized cells was similar to the obtained before (Period A).

Theoretically the immobilized cells in fully developed biofilm remain inside the reactor for long periods of time and naturally exceed their capability to grow reaching its Hayflick limit, which is finally leading them to die. The biocatalyst (carrier + cells) replacement occurred every time clean carrier was added, because non-colonized carrier surface was introduced into reactor allowing the adhesion of free cell population. Free cells have a higher viability that helped to maintain the high viability values of the cells immobilized onto the carrier. This keeps the immobilized cell viability similar to that of the free cells and as the total amount of immobilized cells is higher, the ethanol production was high with low glucose present **Table VIII-8**.

Table VIII-8. Ageing Fermentation performance parameters at different stages.

Stage	Concentration* (g/L)		$Y_{etanol/glucose}$	Total VDK's / (mg/L)
	Glucose	Ethanol		
Period A	3.51	9.29	0.50	0.06±0.007
Period B	5.69	5.18	0.49	0.04±0.001
End of Fermentation	2.33	7.23	0.46	0.06±0.009

* Values corrected considering maximum carrier load (8% (vol./vol.))

The addition of a larger amount of clean carrier (56th day) supports the previous idea. After 56th day of fermentation an increase of glucose consumption and ethanol formation was noted. The final amount of glucose and ethanol in the outflow at the end of the fermentation is similar to values obtained in the period of carrier addition (Period A – see **Figure VIII-7**). There is no significant decrease or a clear tendency of the ethanol/glucose yield. This result indicates that possibly no metabolic changes were present in immobilized cells; however, is expected that different results will occur if cell viability decreases further. **Table VIII-8** shows the values of total VDK's production; over every periods studied the total VDK's concentration is significantly below the taste threshold considered for lager beers (See **Table II-4**). A relationship between the increase of immobilized biomass with the increase of VDK's seems to be present both in Period A and after replacing 1/3 of reactor volume.

VIII.4.6.1 Yeast physiology and cell properties

The intracellular compounds of the immobilized biomass stained by fluorescent dyes during the continuous experiment were chitin rings, glycogen and neutral lipids. During Period A the values of these compounds seem to be near to steady state condition. On the contrary, in Period B an increase of the intensity of fluorescence of chitin rings (bud scars) and neutral lipids accompanied the decrease of viability.

The number of bud scars present on the cell surface is directly related to the number of times a cell has divided, and can represent a biomarker for replicative cell age estimation. The fact that the fluorescence bud scar signal increased before the increase of dead cell number means that it can be applied as an indicator of the immobilized biomass ageing with practical implications. This indicator (fluorescent bud scar signal) could be used for scheduling the replacement of aged biocatalyst during log term fermentations.

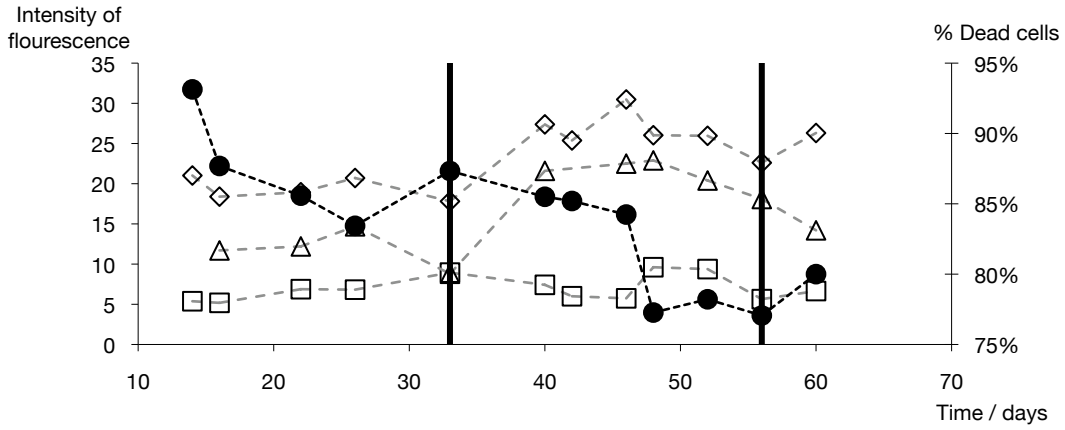

Figure VIII-8. Relationships between immobilized dead/non viable cells (●) and intracellular glycogen (□), neutral lipids (△), and bud scars (◇) during the course of the fermentation experiment.

Besides the bud scars an accumulation of neutral lipids (NL) was also observed in replicatively aged cells, which can also be used as an indicator to predict ageing. However, the physiological reason for lipid accumulation may not be entirely related with ageing and further research efforts will be required. Glycogen concentration did not show a significant variation over the studied periods.

Microbial adhesion tests to solvents (MATS) – **Figure VIII-9** – were carried out to evaluate the changes of relative cell surface hydrophobicity for free and immobilized cells during the different periods studied. Both free and immobilized yeast showed a significantly higher adhesion to chloroform, an electron acceptor solvent, suggesting thus a strong electron donor nature of the used yeast based on Lewis acid-base (electron donor/acceptor) interactions (**Figure VIII-9**).

Regarding free cells, the most significant change occurs during the immobilization process at the beginning of the experiment. Assuming that the yeast biofilm is in a dynamic equilibrium (adsorption/desorption) with the surrounding free cells, the increased adhesion to the hydrophobic solvents could be explained with the selection pressure inside the continuous reactor favouring the selection of hydrophobic cells able to either adhere to carrier and/or flocculate.

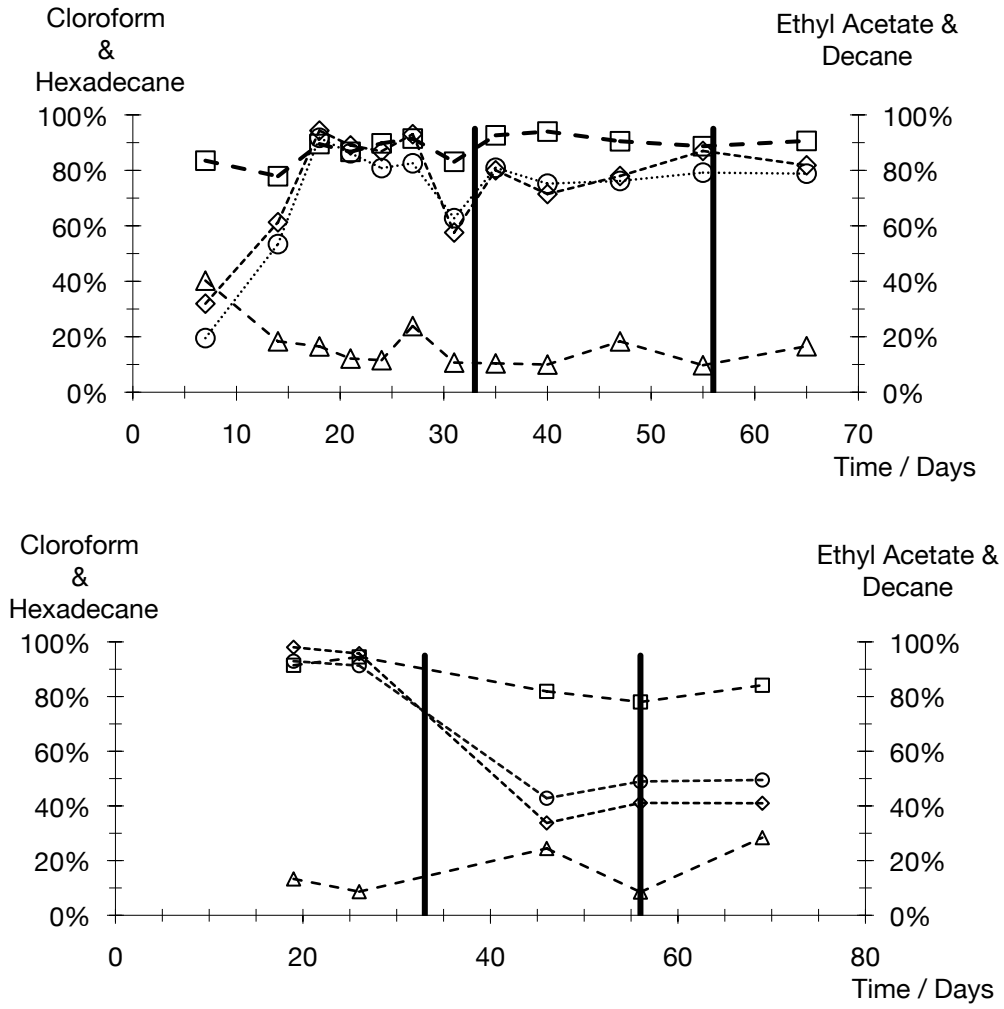

Figure VIII-9. MATS analysis results for free cells (Top) and immobilized cells (Bottom). Results are expressed as a percentage of cells adhered to a given solvent. Legend: Period A: up to 30th day; Period B: from 30th to 56th day; □ - Cloroform; ◇ - Hexane; ○ - Decane; △ - Ethyl Acetate.

Moreover, the adhesion properties of immobilized cells show, for the same fermentation time, the same values as free cells, suggesting thus the existence of a dynamic equilibrium between free and immobilized microbial populations. A significant decrease in adhesion of immobilized yeast to non-polar solvents (decane and hexadecane) was observed during the ageing period of the continuous experiment (**Figure VIII-9**). The nature of this phenomenon is not clear, but it can be most probably linked with the alteration of cell surface during yeast ageing. Further experiments will have to be carried out in order to elucidate this observation.

VIII.5 Conclusions

The production of AFB by limited fermentation, as compared to regular beer, has its own particularities that require either alteration in production procedure and/or the use of a special yeast strain. The same special approach is required for continuous fermentation with immobilized yeast in order to exploit its potential productivity combined with sufficient product quality.

It was shown that the laboratory yeast strain with disruption in the KGD2 (α-ketoglutarate dehydrogenase) gene had sufficient potential for volatiles formation (HA, ES), while it produced an amount of organic acids comparable to regular beer fermentation. In terms of flavour formation this genetically manipulated laboratory strain performed equally well in batch and continuous PBR. However, it was unable to form biofilm around spent grain particles and therefore its use was not possible in the iGLR.

Conversely the bottom fermenting strain *W96* adhered well to both of the solid supports, but the formation of flavour active compounds was insufficient with the exception of immobilization onto SG in iGLR. This system arrangement proved that even a strain that seems to be less suitable for AFB production can, under appropriate conditions, produce an acceptable final product.

The influence of the type of gas-phase in the iGLR showed to be more intense for free cells than for immobilized cells. Under anaerobic conditions with N_2 an increase in free cells concentration and in maltose consumption was verified. Moreover the results indicate that there is a relation between maltose uptake and free cells concentration. The results obtained with CO_2 and N_2 suggested that N_2 is a good subtitute as gas-phase in iGLR used for continuous AFB primary fermentation. The evaluation of flavour active compounds (HA,ES and AL) showed that in the presence of N_2 the formation of important falvour active compounds as ES was enhanced. Particulary the

formation of ethyl crapylate was higher in the continuous system tested (iGLR with SG).

The ageing effects experiments suggest that during carrier addition period conditions close to steady-state were achieved with almost constant (1) glucose and ethanol content in the outflow; (2) specific metabolic rates; (3) VDK formation; and (4) free and immobilized cells viability. The constant cell viability may be related to equilibrium between cell adhesion, growth and washout influenced by regular addition of clean, non-colonized carrier surface. It appears that regular replacement of small amounts of biocatalyst with clean carrier could be a suitable strategy to maintain a long-term viability and constant fermentation conditions inside of a bioreactor. On the other hand during ageing period a gradual decrease of immobilized cells viability occurred. A relationship between increase of bud scars and neutral lipids and decrease of immobilized cells viability was observed. These phenomena, especially for bud scars, could serve as an indicator for scheduling the biocatalyst replacement of long-term fermentations. The hidden effect of small biocatalyst additions was demonstrated by the replacement of 1/3 of reactor volume by a suspension of clean carrier particles. It was followed by a sudden decrease of immobilized biomass, which was subsequently gradually replaced by cell colonization of the available carrier surface. As regards dead cell number, the result was an improvement in immobilized cell viability.

VIII.6 References

ASBC, T. C. and the E. C. of. (**1996**). Microbiology, Yeast - 3. *Methods of Analysis of the American Society of Brewing Chemist* (p. 3).

Bezbradica, D., Obradovic, B., Leskosek-Cukalovic, I., Bugarski, B. and Nedovic, V. (**2007**). Immobilization of yeast cells in PVA particles for beer fermentation. *Process Biochemistry*, 42(9), 1348-1351.

Briggs, D. E., Boulton, C. A., Brookes, P. A. and Stevens, R. (**2004**). *Brewing Science and practice*.

Brányik, T., Vicente, A., Machado Cruz, J., and Teixeira, J. (**2001**). Spent grains–a new support for brewing yeast immobilisation. Biotechnology Letters, 23(13), 1073–1078.

Brányik, T., Vicente, A. A., Machado Cruz, J. M., and Teixeira, J. A. (**2002**). Continuous primary beer fermentation with brewing yeast immobilized on spent grains. Journal Of The Institute Of Brewing, 108(4), 410-415.

Brányik, T., Vicente, A. A., Kuncová, G., Podrazký, O., Dostálek, P., and Teixeira, J. A. (**2004a**). Growth model and metabolic activity of brewing yeast biofilm on the surface of spent grains: a biocatalyst for continuous beer fermentation. Biotechnology progress, 20(6), 1733-40.

Brányik, T., Vicente, A. A., Machado Cruz, J. M., and Teixeira, J. A. (**2004b**). Continuous Primary Fermentation of Beer with Yeast Immobilized on Spent Grains—The Effect of Operational Conditions. Journal of American Society of Brewing Chemist, 62(1), 29-34.

Brányik, Tomás, Vicente, A. A., Oliveira, R., and Teixeira, J. A. (**2004c**). Physicochemical surface properties of brewing yeast influencing their immobilization onto spent grains in a continuous reactor. Biotechnology and bioengineering, 88(1), 84-93.

Brányik, T., Vicente, A. A., Dostálek, P., and Teixeira, J. A. (**2005**). Continuous beer fermentation using immobilized yeast cell bioreactor systems. Biotechnology progress, 21(3), 653-63.

Brányik, Tomás, Silva, D. P., Vicente, A. A., Lehnert, R., Silva, J. B. A., Dostálek, P., and Teixeira, J. A. (**2006**). Continuous immobilized yeast reactor system for complete beer fermentation using spent grains and corncobs as carrier materials. Journal of Industrial Microbiology and Biotechnology, 33(12), 1010-8.

Decamps, C., Norton, S., Poncelet, D., and Neufeld, R. J. (**2004**). Continuous pilot plant-scale immobilization of yeast in κ-carrageenan gel beads. AIChE Journal, 50(7), 1599-1605.

Dömény, Z., Smogrovicová, D., Gemeiner, P., Sturdík, E., Pátková, J., and Malovíková, A. (**1998**). Continuous secondary fermentation using immobilized yeast. Biotechnology Letters, 20(11), 1041–1045.

EBC, A. (**1987**). Dimethyl Sulphide and Other Lower Boiling Point Volatile Compounds in Beer by Gas Chromatography. Analysis.

EBC, A. (**1999**). Vicinal Diketones in Beer: Gas Chromatographic Method.

Evellin, F., Perpète, P., and Collin, S. (**1999**). Yeast ADHI Disruption: A Way to Promote Carbonyl Compounds Reduction in Alcohol-Free Beer Production. Journal of American Society of Brewing Chemist, 57(3), 109-113.

Fonseca, M. M., and Teixeira, J. A. (**2007**). Reactores Biolóogicos (in Portuguese). Lidel-Edições Técnicas, p. 482.

Kourkoutas, Y., Bekatorou, A., Banat, I. M., Marchant, R., and Koutinas, A. A. (**2004**). Immobilization technologies and support materials suitable in alcohol beverages production: a review. Food Microbiology, 21(4), 377–397.

Kunze, W. (**2004**). Techology brewing and malting. (3rd ed., p. 939). Berlin: VBL Berlin.

Lehnert, R., Kurec, M., Brányik, T., and Teixeira, J. A. (**2008**). Effect of Oxygen Supply on Flavour Formation During Continuous Alcohol-free Beer Production: A Model Study. Journal of American Society of Brewing Chemist, 66(4), 233-238.

Lehnert, R., Novák, P., Macieira, F., Kurec, M., Teixeira, J. A., and Brányik, T. (**2009**). Optimisation of Lab-Scale Continuous Alcohol-Free Beer Production. Czech Journal of Food Science, 27(4), 267-275.

Levenspield, O. (**1999**). Chemical Reaction Engineering. (W. Anderson and K. Santor, Eds.)Distribution (3rd ed., p. 684). New York: John Wiley and Sons.

Macieira, F. F. (2008). Continuous fermentation of real alcohol- free beer.
IChem E, 77(Part C), 27–32.

Levenspield, O. (**1999**). Chemical Reaction Engineering. (W. Anderson and K. Santor, Eds.)Distribution (3rd ed., p. 684). New York: John Wiley and Sons.

Macieira, F. F. (**2008**). Continuous fermentation of real alcohol-free beer. MSc Thesis

Oliveira, M., Faria, M., Filomena, S., Barros, F., and Araújo, I. M. (**2006**). C6-alcohols as varietal markers for assessment of wine origin. Analytica Chimica Acta, 563, 300-309.

Perpète, P, and Collin, S. (**1999a**). Contribution of 3-methylthiopropionaldehyde to the worty flavour of alcohol-free beers. Journal of agricultural and food chemistry, 47(6), 2374-8.

Perpète, Philippe, and Collin, S. (**1999b**). Fate of the worty favours in a cold contact fermentation. Food Chemistry, 66, 359-363.

Pilkington, P., Margaritis, A., Mensour, N., and Russell, I. (**1998**). Fundamentals of immobilized yeast cells for continuous beer fermentation: a review. Journal of the Institute of Brewing, 104(1), 19–31. London: Harrison and Sons, 1904-.

Richardson, J. F., Harker, J. H., and Backhurst, J. R. (**2002**). Flow of Fluids through granular beds and packed bed columns. Vol. 2. Chemical Engineering. Particle Technology and Separation Processes (5th ed., pp. 191-236). Oxford: Butterworth-Heinemann.

Selecky, R., Smogrovicova, D., and Sulo, P. (**2008**). Beer with Reduced Ethanol Content Produced Using Saccharomyces cerevisiae Yeasts Deficient in Various Tricarboxylic Acid Cycle Enzymes. Journal Of The Institute Of Brewing, 114(2), 97-101.

Shen, H., Moonjai, N., Verstrepen, K., and Delvaux, F. (**2003**). Impact of attachment immobilization on yeast physiology and fermentation performance. Journal of the American Society of Brewing Chemists, 61(2), 79–87.

Shen, H.-Y., De Schrijver, S., Moonjai, N., Verstrepen, K. J., Delvaux, F., and Delvaux, F. R. (**2004**). Effects of CO2 on the formation of flavour volatiles during fermentation with immobilized brewer's yeast. Applied microbiology and biotechnology, 64(5), 636-43.

Smogrovicová, D., and Domény, Z. (**1999**). Beer volatile by-product formation at different fermentation temperature using immobilized yeasts. Process Biochemistry, 34(8), 785-794.

Van Iersel, M. F. M., Meersman, E., Swinkels, W., Abee, T., and Rombouts, F. M. (**1995**). Continuous production of non-alcohol beer by immobilized yeast at low temperature. Journal of Industrial Microbiology and Biotechnology, 14(6), 495–501.

Verbelen, P. J., De Schutter, D. P., Delvaux, F., Verstrepen, K. J., and Delvaux, F. R. (**2006**). Immobilized yeast cell systems for continuous fermentation applications. Biotechnology letters, 28(19), 1515–1525.

Virkajarvi, I., and Linko, M. (**1999**). Immobilization: A revolution in traditional brewing. Naturwissenschaften, 86(3), 112–122.

Virkajarvi, I., and Pohjala, N. (**2000**). Primary fermentation with immobilized yeast: some effects of carrier materials on the flavour of the beer. Journal of the Institute of Brewing, 106(5), 311–18.

Willaert, R., and Nedovic, V. (**2006**). Review Primary beer fermentation by immobilized yeast – a review on flavour formation and control strategies. Jounal of Chemical Technology and Biotechnology, 81, 1353-1367.

Yamauchi, Y., Okamoto, T., Murayama, H., Kajino, K., Nagara, A., and Noguchi, K. (**1995**). Rapid maturation of beer using an immobilized yeast bioreactor. 2. Balance of total diacetyl reduction and regeneration. Journal of Biotechnology, 38, 109-116.

IX. Chapter IX – Conclusions and Future Work

The main aim of this thesis was the development of a continuous AFB system that would overcome the industrial batch systems and the reported continuous methods. To reach these objectives, this thesis was divided in two main parts: AFB continuous fermentation and bioreactor hydrodynamics. Overall, the obtained results improved the existing knowledge on AFB production and pointed out for the work that needs to be done in order to deliver to the brewery industry a reliable and economically advantageous solution for continuous AFB production.

In the first part of the work, brewer´s yeast immobilization studies on corn cobs (Cc) and spent grains (SG) were followed by the characterization of the influence of several parameters in continuous primary AFB fermentation. The main conclusions were:

- Non-treated Cc and SG (see **Table III-4**) are efficient carriers for yeast immobilization;

- Chemical modification with DEC of these carriers does not improve its yeast immobilization capacity;

Yeast strain, reactor type and carrier are key parameters to be considered in the selection of the best continuous AFB process. Bottom yeast strains performed better in iGLR using SG as carrier, while mutant yeast strains allowed for better results in PBR with Cc as carrier. This, together with the use of bottom fermenting yeast strains by the Portuguese breweries and the EU laws concerning the use of genetically modified yeasts, allowed us to select the iGLR with SG as carrier as the most adequate system for continous AFB production.

In this system, the effect of introducing CO_2 and N_2 in the gas-phase was studied, being shown that N_2 has a positive influence in the formation of flavour active compounds.

Yeast ageing was also studied and in a long-term fermentation the constant adding of fresh carrier proved to be a suitable strategy for maintaining a steady performance of the continuous primary AFB fermentation. Moreover bud scars were determined as a suitable indicator of the loss of iBio viability in long term fermentations .

In the second part of the thesis, the hydrodynamic aspects related with the operation of immobilized cell systems were studied, starting from the influence of SG in BC regime flow stability followed by the global and local study of hydrodynamic parameters such as: mixing time, gas hold-up, liquid velocity, solids distribution. The main conclusions were:

- SG, a cellulose-based carrier, reduces HoR regime stability and a relation between the pseudo-viscosity induced by the presence of these particles and critical flow regime parameters was established;

- For the several iGLR configurations, the best mixing pattern was obtained for the highest A_d/A_r ratio (3.67) and riser length (1.4 m);

- An improved method using as an OP was developed and applied to measure gas-phase properties in g-l-s system with SG as solid-phase

- The effect of SG in iGLR hydrodynamics at used concentrations was negligible and the evaluation of its importance was only possible using advanced techniques such as OP and HSC;

- A hydrodynamic model for three-phase iGLR using SG was developed and good agreement with experimental data was obtained;

- The ethanol produced by the yeast was found to have a bigger effect than SG on gas-phase properties; SG loading up to 6% ($wt._{WET\ BASIS}$/vol.) is the adequate amount to be use for cells immobilization in alcoholic fermentation as it will not induce any relevant hydrodynamic modifications

- SG are a suitable carrier to perform alcoholic fermentation as it does not influence iGLR hydrodynamics under fermentation conditions.

- As a final appointment and considering that a lot has still to be done, some suggestions for future work are presented:

A systematic study to improve yeast attachement in SG should be done by modifying the conventional pre-treatment by a simpler and less costly one;

To perform a systematic study in order to understand the use of N_2 as the gas-phase in big industrial iGLRs and its effect on AFB properties. An economical evaluation comparing N_2 use as gas phase and CO_2 reutilization should be performed;

Long term fermentation strategies must be developed to tackle with yeast ageing effects and deal with the loss of iBio viability without the need of stop and start procedures;

For the OP measurements, to develop the injection system so that data acquisition may be performed a high gas flow rates and high acquisition rate.

To study the influence that yeast cells have in OP measurement mechanism as well as to develop a system that allows OP to be used online in order to obtain gas-phase properties evolution during fermentation.

X. Apendix I

Matlab program used to determined the gas-phase properties in *g-l-s* (SG) system using an OP.

```
clear all; close all
Solids='I:\Dados IBM\Resume\Data\0.25%\'; Gas_Flow='A - 250mLmin-1\';
Position='Central\'; Path=[Solids Gas_Flow Position]; fileList=dir([Path,'ASSAY*.*']);
nposition = numel(fileList); %number of files
for n=1:numel(fileList); Filename=[Path fileList(n).name];
% Aquisition board configuration
MaxVoltage_carte = 10; MinVoltage_carte=-MaxVoltage_carte; Precision_carte = 12;
Freq_ech = 0.01; % in MHz
%Reading the size and number of points in the file
info_fic = dir(Filename); nb_pt_fic = info_fic.bytes/4; nb_pt_bloc=Freq_ech*1E6*10*20;
nb_bloc = ceil(nb_pt_fic/nb_pt_bloc); duree_bloc = nb_pt_bloc/(Freq_ech*1E6);
% Range of aquisition board
du=(MaxVoltage_carte-MinVoltage_carte)/(2^Precision_carte); fid=fopen(Filename,'r');
for i = 1 : nb_bloc; %1
Data_Binaire = fread(fid,nb_pt_bloc,'int','b'); i_c = 1:2:nb_pt_bloc;
Data_Binaire_1=Data_Binaire(i_c); Data_Binaire_2 = Data_Binaire(i_c+1);
bloc(i).Data_Volt_1=Data_Binaire_1.*du; bloc(i).Data_Volt_2=Data_Binaire_2.*du;
end %1
% Assemble all blocks in two signals: optical probe and valve injections
Probe_array=[]; Valve_array=[];
for i = 1 : nb_bloc; %2
Probe_array=[Probe_array bloc(i).Data_Volt_1'];
Valve_array=[Valve_array bloc(i).Data_Volt_2'];
end %2
Final=[Probe_array' Valve_array' Time_array];
% Parameters
Spl_rate = Freq_ech*1E6; Inj_time = 0.5; dt=1/Spl_rate; Prb_volt=Final(:,1);
Inj_volt_0=Final(:,2); Zero_pos=find(Inj_volt_0<0); Inj_volt=[]; Inj_volt=Inj_volt_0;
Inj_volt(Zero_pos,1)=[0];
Zero_pos_1=find(Inj_volt>3); add0=Zero_pos_1-Inj_time*Spl_rate*0.375; add1=
union(Zero_pos_1,add0); % este artificio permite-me utilizar as frequencias de corte que
quiser. add2= Zero_pos_1+Inj_time*Spl_rate*0.75; Zero_pos_2= union(add1,add2);
neg_elements=find(Zero_pos_2<=0); Zero_pos_2(neg_elements)=[1]; Prb_volt_2=[];
Prb_volt_2=Prb_volt; Prb_volt_2(Zero_pos_2,1)=[0]; X=find(Prb_volt_2);
Prb_volt_3=Prb_volt_2(X); Time_array_2=Time_array(X); % time correction
clear Data_Binaire_1; clear Data_Binaire_2; clear Final; clear Prob_volt_2; clear Inj_volt_0;
clear Inj_volt;
%Gas level General and Plate level definition
noise=0.4; Overshoot_in_Prob_volt=find(Prb_volt_3>5);
First_max=find(Prb_volt_3>3,1,'first');
Prb_volt_3(Overshoot_in_Prob_volt,1)=[Prb_volt_3(First_max)];
InGasGeral=find(Prb_volt_3>(max(Prb_volt_3)-0.05*(max(Prb_volt_3)-min(Prb_volt_3))));
GasLevelGeral = mean(Prb_volt_3(InGasGeral)); NivPlat=GasLevelGeral-2*noise;
%Filter acquisition problems
Y=diff(X); end_block=find(Y>1)-1; begin_block=find(Y>1)+1;
begin_block=[X(1,1);begin_block]; number_block=numel(begin_block);
if number_block>numel(end_block); end_block=[end_block;numel(Prb_volt_3)]; end
% Erros in blocks due to acquisition issues
Blocks_diff=end_block-begin_block; Blocks_diff_pos=find(Blocks_diff>0);
end_block=end_block(Blocks_diff_pos); begin_block=begin_block(Blocks_diff_pos);
number_block_corr=numel(begin_block);
for i=1:number_block_corr; %3
bloc(i).Prb_volt_4=Prb_volt_3(begin_block(i):end_block(i));
bloc(i).Time_array_3=Time_array_2(begin_block(i):end_block(i)); noise=0.4;
bloc(i).InLiquid=find(bloc(i).Prb_volt_4<(min(bloc(i).Prb_volt_4)+0.025*(max(bloc(i).Prb_volt_4
)-min(bloc(i).Prb_volt_4))));
% Solving problems when block are too small
if numel(bloc(i).Prb_volt_4)<3; bloc(i).InLiquid =1; end
bloc(i).LiquidLevel = mean(bloc(i).Prb_volt_4(bloc(i).InLiquid));
bloc(i).treshold=bloc(i).LiquidLevel+noise; % treshold in Volts
% To determine when a block does not have bubbles
```

```
if max(bloc(i).Prb_volt_4)<2; bloc(i).treshold=[2]; end
Taq=[]; indexStart =[]; indexStop =[];
% Bubble Detection
try
Prb_Boolean = (bloc(i).Prb_volt_4>bloc(i).treshold); detectChange=xor(Prb_Boolean(1:end-1),
Prb_Boolean(2:end));          detectRise=detectChange          &          Prb_Boolean(2:end);
detectFall=detectChange&Prb_Boolean(1:end-1);                    indexStart=find(detectRise);
indexStop=find(detectFall);end
% calculate time of signal start/stop and bubble start/stop
bloc(i).Trise = bloc(i).Time_array_3(indexStart); bloc(i).Tfall=bloc(i).Time_array_3(indexStop);
if  numel(bloc(i).Trise)<numel(bloc(i).Tfall);  bloc(i).Tfall=bloc(i).Tfall(2:numel(bloc(i).Tfall),1);
end
if  numel(bloc(i).Tfall)<numel(bloc(i).Trise);  bloc(i).Trise=bloc(i).Tfall(1:numel(bloc(i).Trise)-
1,1); end
% Tm determination
nr_Bubbles_in_block=numel (bloc(i).Tfall-bloc(i).Trise);
for j=1:nr_Bubbles_in_block; %4
bloc(j).Prb_volt_5=bloc(i).Prb_volt_4(indexStart(j):indexStop(j)+1);
bloc(j).InGas=find(bloc(j).Prb_volt_5>(min(bloc(j).Prb_volt_5)+0.5*(max(bloc(j).Prb_volt_5)-
min(bloc(j).Prb_volt_5)))); bloc(j).GasLevel=mean(bloc(j).Prb_volt_5(bloc(j).InGas));
%Find Last Mounting point (2nd point for Tm determination)
bloc(j).Index_First_Gas_Point=find(bloc(j).Prb_volt_5>bloc(j).GasLevel*0.9,1,'first');
bloc(j).First_Gas_Point=bloc(j).Prb_volt_5(bloc(j).Index_First_Gas_Point);
%Tm for each bubble
bloc(j).Tm=numel(bloc(j).Prb_volt_5(1:                    bloc(j).Index_First_Gas_Point))*dt;
bloc(j).CC1=(bloc(i).Tfall(j)-
(bloc(i).Trise(j)+bloc(j).Index_First_Gas_Point*dt))/(bloc(i).Trise(j)+bloc(j).Index_First_Gas_Poi
nt*dt-bloc(i).Trise(j));
if nr_Bubbles_in_block<1; bloc(j).CC1=[2]; end
if bloc(j).Prb_volt_5(bloc(j).Index_First_Gas_Point)<NivPlat; bloc(j).Tm=[0]; end
if bloc(j).CC1<0.66; bloc(j).Tm=[0]; end
%Tg for each bubble
bloc(j).Tg=bloc(i).Tfall(j)-bloc(i).Trise(j); bloc(j).Ta=bloc(i).Trise(j); end %(j)4
% Voidage Determination
bloc(i).sumTg=sum(bloc(i).Tfall-bloc(i).Trise);          bloc(i).nrBubbles=numel(bloc(i).Tfall);
bloc(i).Taq=end_block(i)*dt-begin_block (i)*dt; bloc(i).voidage=bloc(i).sumTg/bloc(i).Taq*100;
% Assemble all Tm and Tg in an array of the main block (i)
bloc(i).Tg1=[]; bloc(i).Tm1=[]; bloc(i).Ta1=[];
for j=1:nr_Bubbles_in_block;
bloc(i).Tg1=[bloc(i).Tg1       bloc(j).Tg];       bloc(i).Tm1=[bloc(i).Tm1       bloc(j).Tm];
bloc(i).Ta1=[bloc(i).Ta1 bloc(j).Ta];
end; end %(i)3
bloc(n).Tg_assay=[]; bloc(n).Tg_assay=[bloc(n).Tg_assay bloc(1:number_block_corr).Tg1];
bloc(n).Tm_assay=[]; bloc(n).Tm_assay=[bloc(n).Tm_assay bloc(1:number_block_corr).Tm1];
bloc(n).Ta_assay=[]; bloc(n).Ta_assay=[bloc(n).Ta_assay bloc(1:number_block_corr).Ta1];
bloc(n).voidage_assay=[];
bloc(n).voidage_assay=[bloc(n).voidage_assay bloc(1:number_block_corr).voidage];
bloc(n).nrBubbles_assay=[];
bloc(n).nrBubbles_assay=[bloc(n).nrBubbles_assay bloc(1:number_block_corr).nrBubbles];
bloc(n).Taq_assay=[]; bloc(n).Taq_assay=[bloc(n).Taq_assay bloc(1:number_block_corr).Taq];
bloc(n).Sec_intital_time=[];
bloc(n).Sec_intital_time=[bloc(n).Sec_intital_time begin_block(1:number_block_corr).*(dt/0.57
5)];
bloc(n).Sec_final_time=[];
bloc(n).Sec_final_time=[bloc(n).Sec_final_time end_block(1:number_block_corr).*(dt/0.575)];
end %(n) 2
Sect_Results_C_A_250_mLmin_025_1=[bloc(1).voidage_assay'       bloc(1).nrBubbles_assay'
bloc(1).Taq_assay' bloc(1).Sec_intital_time bloc(1).Sec_final_time];
Sect_Results_C_A_250_mLmin_025_2=[bloc(2).voidage_assay'       bloc(2).nrBubbles_assay'
bloc(2).Taq_assay' bloc(2).Sec_intital_time bloc(2).Sec_final_time];
Sect_Results_C_A_250_mLmin_025_3=[bloc(3).voidage_assay'       bloc(3).nrBubbles_assay'
bloc(3).Taq_assay' bloc(3).Sec_intital_time bloc(3).Sec_final_time];
% Assemble all Tg,Tm and Ta
Center_A_250_mLmin_025_1=[bloc(1).Tg_assay' bloc(1).Tm_assay' bloc(1).Ta_assay'];
Center_A_250_mLmin_025_2=[bloc(2).Tg_assay' bloc(2).Tm_assay' bloc(2).Ta_assay'];
Center_A_250_mLmin_025_3=[bloc(3).Tg_assay' bloc(3).Tm_assay' bloc(3).Ta_assay'];
save('...\Center_A_250_mLmin_025%','Center_A_250_mLmin_025_1','Center_A_250_mLmin_0
25_2','Center_A_250_mLmin_025_3','Sect_Results_C_A_250_mLmin_025_1','Sect_Results_C_
A_250_mLmin_025_2','Sect_Results_C_A_250_mLmin_025_3');fclose(fid);
```